DOCTOR OF PHILOSOPHY

Pryolytic and kinetic study of Chlorella Vulgaris under isothermal and non-isothermal conditions

Neeranuch Phusunti

2013

Aston University

PYROLYTIC AND KINETIC STUDY OF *CHLORELLA VULGARIS* UNDER ISOTHERMAL AND NON-ISOTHERMAL CONDITIONS

NEERANUCH PHUSUNTI

Doctor of Philosophy

ASTON UNIVERSITY

November 2012

Aston University

Pyrolytic and kinetic study of *Chlorella vulgaris* under isothermal and non-isothermal conditions

Neeranuch Phusunti

Doctor of Philosophy, 2012

THESIS SUMMARY

Algae are a new potential biomass for energy production but there is limited information on their pyrolysis and kinetics. The main aim of this thesis is to investigate the pyrolytic behaviour and kinetics of *Chlorella vulgaris*, a green microalga. Under pyrolysis conditions, these microalgae show their comparable capabilities to terrestrial biomass for energy and chemicals production. Also, the evidence from a preliminary pyrolysis by the intermediate pilot-scale reactor supports the applicability of these microalgae in the existing pyrolysis reactor.

Thermal decomposition of *Chlorella vulgaris* occurs in a wide range of temperature (200-550°C) with multi-step reactions. To evaluate the kinetic parameters of their pyrolysis process, two approaches which are isothermal and non-isothermal experiments are applied in this work. New developed Pyrolysis-Mass Spectrometry (Py-MS) technique has the potential for isothermal measurements with a short run time and small sample size requirement. The equipment and procedure are assessed by the kinetic evaluation of thermal decomposition of polyethylene and lignocellulosic derived materials (cellulose, hemicellulose, and lignin). In the case of non-isothermal experiment, Thermogravimetry-Mass Spectrometry (TG-MS) technique is used in this work. Evolved gas analysis provides the information on the evolution of volatiles and these data lead to a multi-component model. Triplet kinetic values (apparent activation energy, pre-exponential factor, and apparent reaction order) from isothermal experiment are 57 (kJ/mol), 5.32 (log$A$, min^{-1}), 1.21-1.45; 9 (kJ/mol), 1.75 (log$A$, min^{-1}), 1.45 and 40 (kJ/mol), 3.88 (log$A$, min^{-1}), 1.45-1.15 for low, middle and high temperature region, respectively. The kinetic parameters from non-isothermal experiment are varied depending on the different fractions in algal biomass when the range of apparent activation energies are 73-207 (kJ/mol); pre-exponential factor are 5-16 (log$A$, min^{-1}); and apparent reaction orders are 1.32–2.00. The kinetic procedures reported in this thesis are able to be applied to other kinds of biomass and algae for future works.

Key words: Kinetics, Microalgae, Pyrolysis, Pyrolysis-Mass Spectrometry (Py-MS), Thermogravimetry-Mass Spectrometry (TG-MS), *Chlorella vulgaris*

ACKNOWLEDGEMENTS

I am heartily thankful to my supervisor, Professor Andreas Hornung, whose encouragement, guidance and support from the initial to the concluding level enabled me to develop an understanding of the subject. Also, I would like to express my sincere acknowledgement in the support and help on my thesis of my associated supervisor, Dr. Gareth Griffiths.

I would like to thank Professor István Marsi and Dr. Diar Nasiev who enlightened me through their knowledge of a computational programme, MATLAB, and their support on the software.

I offer my regards and blessing to members of European Bioenergy Research Institute (EBRI) who supported me in any respects during the completion of the project. Special thanks for Zsuzsa Mayer for sharing the knowledge, and Eduard Sperling and Dr. Andreas Apfelbacher for helping me to assemble the equipment.

Financial support from the Royal Thai Government under the program 'Strategic Scholarships for Frontier Research Network' of Thailand's Commission on Higher Education is gratefully acknowledged.

Last but not least, my deepest gratitude goes to my family and my boyfriend for their love and support throughout my study life in UK.

LIST OF CONTENTS

LIST OF TABLES

LIST OF FIGURES

NOMENCLATURE

Terms

Symbol	Description
A	pre-exponential factor
a, b, c	constant variables
α	fractional reaction or degree of conversion
β	constant heating rate
E_a	activation energy
$f(\alpha)$	kinetic model function or conversion function
G	Gaussian distribution value
H	intensity of peak
I_i	ion current of the ith ion fragment
$I(t)$	intensity or ion current of ion fragment at time t
m_0	initial mass
m_f	final mass
$m(t)$	mass at time t
m_{tot}	total evolved mass
M	number of data points
M_i	molecular mass of the ith ion fragment
$\overline{M}(t)$	mean molecular mass at time t
n	order of reaction or reaction order
N	number of ion fragments
p, q	partial orders of reaction
R	gas constant
R^2	coefficient of linear regression

k	reaction rate constant or rate coefficient
k_i	isokinetic constant
s	width of the peak
S	least square fitting value
t	time
T	absolute temperature
T_i	isokinetic temperature or compensation temperature
T_e	measured sample temperature
T_s	true sample temperature
T_{max}	peak temperature of a Gaussian curve
T_d	transfer time delay
ΔT_{TL}	thermal lag
V_i	yield of *i*th gas component
V_i^*	ultimate attainable yield for *i*th gas
$\dot{V}$	flow rate
V_R	reactor volume

Abbreviations

ATP	Adenosine Triphosphate
BSA	Bovine Serum Albumin
BtVB	Biothermal Valorisation of Biomass
CHP	Combined heat and power
DAEM	Distributed Activation Energy Model
DCM	Dichloromethane
DP	Degree of polymerization
DTA	Differential Thermal Analysis

DTG	Derivative of thermogravimetric curve
DSC	Differential Scanning Calorimetry
EGA	Evolved Gas Analysis
FID	Flame Ionization detector
FTIR	Fourier Transform Infrared Spectroscopy
FWO	Flynn-Wall-Ozawa method
GC	Gas Chromatography
HHV	High Heating Value
KAS	Kissinger-Akahira-Sunose method
KCE	Kinetic Compensation Effect
MID	Multiple Ion Detection
MS	Mass Spectrometry
MW	Molecular weight
NADPH	Nicotinamide Ademine Dinucleotide Phosphate
NDIR	Non-dispersive infrared photometer
PAH	Polyaromatic Hydrocarbon
Py-GC-MS	Pyrolysis-Gas Chromatography-Mass Spectrometry
Py-MS	Pyrolysis-Mass Spectrometry
RMSE	Root Mean Square Error
RT	Retention time
TCA	Trichloroacetic acid
TG	Thermogravimetry
TG-FTIR	Thermogravimetry-Fourier Transform Infrared Spectrometer
TG-MS	Thermogravimetry-Mass Spectrometry

Chapter 1

Introduction

'As far as the laws of mathematics refer to reality, they are not certain; and as far as they are certain, they do not refer to reality.'

Albert Einstein, 1921

1.1 Overview and Motivation

Climate change is a major problem concerning people around the world. Significant changes, including the increasing ocean and air temperatures, the melting of snow and ice, and the rising sea levels, are the discussed issues for many years. Both natural factors and human-made factors, such as the increase of population, the growth of industrialisation and human activities contribute to the climate change. Human activities, especially burning fossil fuels, increase the amount of greenhouse gases in the atmosphere. Generally, these gases trap heat in the atmosphere to keep the planet warm in a state of equilibrium but the excess human-made gases cause a shift in the earth's equilibrium. As the earth continues to warm, more changes are expected to occur and many effects will become more pronounced over time. For this reason, human-caused climate change gives a serious challenge to maintain the welfare, health, and productivity of society and the natural environment. A well-known collaboration, Kyoto Protocol, is an international agreement to reduce greenhouse gas emissions from industrialized countries and the European community. It seems like a first step toward the global emission reduction [1].

The environmental impacts from fossil fuels and the concern on the energy crisis around the world drive the interest on alternative energy supplies. From U.S. Energy Information Administration source [2] in Fig.1.1, the renewable energy consumption in US, including wind, solar, geothermal, hydroelectric and biomass, in total increases by 5.4 % in 2009.

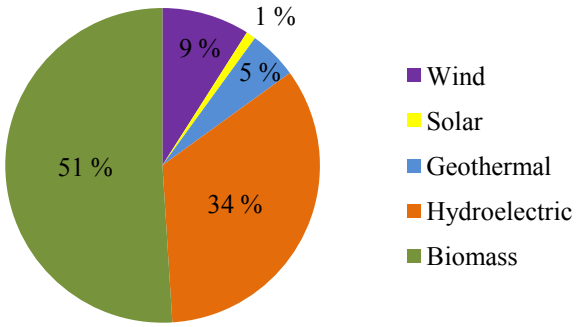

Fig. 1.1 Renewable energy consumption in the US's energy supply, 2009 (adjusted from [2])

One of alternative options is biomass which is a renewable and CO_2-neutral source. Biomass is not the solution for our total energy shortage but it offers the greatest potential for a major short-term contribution to national energy subject. In addition, there are several other benefits from using biomass to produce energy and fuels. Apart from the reduction of carbon dioxide and the improvement of environment, for the countries which depend on the imported fossil fuels, the production of indigenous energy crops can secure their energy supply. Moreover, the contribution of energy crops into energy industry creates many jobs to the society [3].

Unlike the direct usages of solar energy or wind power, biomass as a renewable energy carrier is always available and they can be used to provide three major forms of energy as electricity, heat and fuel, as well as a range of chemicals. Solid biomass and their liquid products are well recognized for the advantages of secure and harmless storage, and easy transportation [4]. Several choices of conversion process can be applied to transform biomass to energy, such as biological conversion, mechanical conversion and thermochemical conversion.

The thermochemical conversion (gasification, liquefaction, pyrolysis and combustion) offers high efficiency processes and scalable solutions. The existing commercial utilisation of thermochemical process on biomass has been developed and several new sites are on the investment plan in many countries [5-8]. Pyrolysis is an initial step of the thermal decomposition and it is carried out in the absence of oxygen at moderate temperature [9]. Three forms of product from pyrolysis are permanent gases (CH_4, CO, CO_2, and H_2), condensable volatiles (light hydrocarbon gases and tars) and solid residue, called bio-char.

The properties and proportion of each product depend on the operating condition, reactor design and also the nature of biomass materials [10, 11].

The challenge of bioenergy production growth against the attempt to secure a safe and inexpensive food supply is the keystone of this alternative energy development. Recently, there are some articles reporting the influence of biofuel production development on the food price [12-16]. To avoid a conflict with food production, aquatic biomass, both marine and freshwater algae become the potential biomass source. Also, they have high production yield and no demand on available arable soils. Moreover, the alternative application of microalgae to reduce the CO_2 emission for industrial processes or gas power plant offers more attractive opportunities. Interestingly, there are some reports which show that the bio-oils produced from microalgae have competitive potential as the fuels compared to bio-oil from lignocellulosic pyrolysis [17-19].

As a new biomass, algae are currently of research interest in many organizations. To develop algal biomass for commercial energy production, the understanding of their thermal behaviour and kinetics are necessary for the effective design and operation of the conversion units. Several pyrolysis kinetic models have been reported and they can be classified into three categories: global reaction models, multi-component models, and multi-step reactions models. The global reaction model describes the overall rate of devolatilization in a single step. Their kinetic parameters are the average values for the whole complex scheme. This single-step model fixes the mass ratio between pyrolysis products; therefore, the prediction of product yields based on process conditions is not feasible. Moreover, the pyrolysis process is too complicated to be described by a global apparent activation energy [20].

Some proposed models suggest that the thermal behaviour of the main components and their relative contribution in the initial biomass can present the primary decomposition rates of biomass [11, 21, 22]. For lignocellulosic material, their thermal degradation is contributed to hemicellulose, cellulose and lignin; although, in a few cases, the decomposition of components is involved more than one reaction step, especially hemicellulose and lignin [23]. The total devolatilization rate is calculated by linear summation of the individual volatilization rate for each component and the released volatiles from these concurrent reactions are lumped into several groups [20]. However, the overlapping between the different components in the measured weight loss curves and

the simultaneous participation of the other components cannot be avoided [23]. Most multi-component model can predict only the rate of weight loss. Thus, the additional measurements of the three product yields need to be taken into account in order to evaluate the related formation rates. Furthermore, some studies reported the multi-step reaction models which the formation rates of individual product species are measured [20]. Not only the different mathematic model evaluation, but also the nature of biomass and the experimental variables (i.e. the heating rate, the initial sample amount, particle size of the materials and the geometry of the apparatus) influence to the kinetic parameters [24, 25].

Thermogravimetry (TG) is the most common technique to determine the kinetic of thermal degradation. The measured weight loss of samples with time or temperature provides the global thermal behaviour [24, 26, 27]. Due to the complexity of pyrolysis, the reaction mechanism may change during the process. Hence, other analytical techniques must be employed to detect and analyse the changes that occur in the chemical composition. By coupling with Evolved Gas Analysis (EGA) techniques, such as Mass Spectrometry (MS), Gas Chromatrography (GC) and Fourier Transform Infrared Spectroscopy (FTIR), the proportion and evolution of volatile products can be monitored. These combined techniques provide more information on pyrolysis process which will lead to more understanding on the mechanism and kinetics.

Kinetic study can be carried out at two experimental methods, non-isothermal and isothermal method. In the former, the sample are heated up to a desired temperature at constant heating rate and in the later, the influence of temperature on the rate of weight loss is examined at several measurements at constant temperatures. The advantage of isothermal measurements over non-isothermal measurement is that isothermal measurement gives the homogeneous sample temperature, while under non-isothermal measurements; the presence of the temperature gradient is due to the non-stationary heating condition causes from the heat conductivity and sample size. Furthermore, the real sample temperature is very difficult to determine in non-isothermal measurements and also the rate equation from isothermal measurement is independent of temperature, as it gives opportunity to detect the change in reaction order or reaction mechanism [28-31]. However isothermal measurement requires several experiments at different temperatures which cause a longer experiment time and larger amount of sample. Another drawback is a certain extent degradation of samples before the system reaches a desired isothermal temperature [31]. To overcome the drawbacks, the reactor design or suitable analytical

equipment has to be optimized for effective isothermal kinetic study.

In last few decades, dynamic or non-isothermal kinetic study has gained more interest. This measurement does not require a sudden rise in temperature as the isothermal measurement does. The advantage of non-isothermal analysis is that only a single measurement can provide a sufficient data for the formal kinetic evaluation over an entire temperature range. However, the non-isothermal techniques have received pointed criticism and its increased sensitivity to experimental noise as compared to isothermal methods [20, 32].

Reaching to this point, the important of kinetics on the application of biomass for biofuel production was highlighted. Unlike woody biomass, the published kinetic parameters of microalgae samples are limited and different from species to species. It has been recognized that the thermal behaviour of microalgae is different from that of lignocellulosic materials because of the difference in basic compositions. Thus, more work on the kinetics of microalgae needs to be studied in both isothermal and non-isothermal measurement.

1.2 Research objectives

The main objective of this work is to study pyrolytic behaviour of *Chlorella vulgaris* and to explore the kinetic analysis methods of biomass and investigate the formal kinetic parameters in term of apparent activation energy, pre-exponential factor and apparent reaction order of *Chlorella vulgaris* in isothermal and non-isothermal conditions.

The pyrolytic behaviour of *Chlorella vulgaris* has been evaluated in order to assess their potential for bioenergy and as a supply of chemicals by a wide range of analytical instrument. A preliminary pyrolysis in a pilot-scale reactor is carried out to investigate the process performance and qualities of products.

New developed pyrolysis micro-reactor coupled with Mass Spectrometer (Py-MS) will be employed and assessed its potential as a technique for isothermal kinetic analysis. Isothermal analysis will be starting with the kinetic evaluation of polyethylene and lignocellulosic materials (cellulose, hemicellulose and lignin) to assess the equipment and procedure before applying them to *Chlorella vulgaris* sample.

In the case of non-isothermal kinetic analysis, an on-line Thermogravimetry coupled with Mass Spectrometry (TG-MS) is applied for *Chlorella vulgaris* pyrolysis. By assuming the overlapping of independent, pararell, *n*th-order reactions of several pseudo-components in the raw microalgae, a reaction model will be presented in a multi-component model. The model will take into account the different main components in microalgae sample, their thermal behaviour and individual evolved gases produced during pyrolysis process. Also, the developed procedure to utilize raw data from TG-MS data for kinetic evaluation is well demonstrated in this thesis.

Controversy from other authors who only report the kinetic data from non-isothermal conditions for the thermal decomposition of algae, this work might be the first report to present the isothermal kinetic results of microalgae. Moreover, there are no any accessible articles presenting the non-isothermal kinetic analysis of microalgae by multi-component approach before.

The objectives of this work can be summarized as:

1. To study pyrolytic behaviour of *Chlorella vulgaris* and to investigate the formal kinetic parameters in term of apparent activation energy, pre-exponential factor and apparent reaction order of *Chlorella vulgaris* under isothermal and non-isothermal conditions.
2. To assess the potential of *Chlorella vulgaris* as a biofuel and chemicals source by various analytical instrument and by a pilot–scale intermediate pyrolysis reactor in terms of applicability and qualities of products.
3. To evaluate the potential of a new developed Pyrolysis-Mass Spectrometry (Py-MS) technique for isothermal kinetic analysis.
4. To examine the formal kinetic parameters of polyethylene, cellulose, hemicellulose and lignin from isothermal measurements.
5. To demonstrate the developed procedure to employ raw TG-MS data for non-isothermal kinetic analysis.

1.3 Structure of the Thesis

The thesis is organised in nine chapters including this chapter. The following topics and contents are contained within the Chapters as set out below:

Chapter 1 This current chapter presents an overview and motivation for the work. The objectives and the outline of this thesis are also given in detail.

Chapter 2 The general information on biomass resource both lignocellulosic materials and microalgae biomass is presented in this chapter. Moreover, the chapter reviews the pyrolysis reactor which is available at European Bioenergy Research Institute (EBRI), together with the pyrolysis process and its products.

Chapter 3 The critical review on chemical kinetics, thermal degradation kinetics, isothermal and non-isothermal kinetic measurements, influences on kinetic measurement is detailed in this chapter. Also, the literature reviews on published kinetic parameters of lignocellulosic component (cellulose, hemicellulose and lignin) and algae are well presented.

Chapter 4 The description of lignocellulosic materials (cellulose, hemicellulose, and lignin) and the characterisation methods, together with their results and discussion are given in this chapter.

Chapter 5 The characteristics of *Chlorella vulgaris* as the selected microalgae sample for this work are described in term of basic components, proximate analysis, elemental analysis, functional groups and volatile products from lab-scale pyrolysis.

Chapter 6 The results and discussion of a preliminary experiment by a pilot-scale intermediate pyrolysis (Pyroformer) with *Chlorella vulgaris* pellets is presented here.

Chapter 7 This chapter presents the results and discussion of isothermal kinetic study of polyethylene, cellulose, hemicellulose, lignin, and *Chlorella vulgaris*. Also, there is the discussion on the potential of the experimental set-up for the isothermal kinetic measurements.

Chapter 8 Thermogravimetry-Mass Spectrometry (TG-MS) as the apparatus for non-isothermal kinetic study and the experimental conditions are presented. The results and discussion on non-isothermal kinetic study of *Chlorella vulgaris* are also well detailed. Furthermore, the discussion on the comparison of isothermal and non-isothermal kinetic parameters on *Chlorella vulgaris* pyrolysis is revealed.

Chapter 9 The final chapter of the thesis discusses the conclusions derived from this research and highlights the key achievements on kinetic analysis. Also, some recommendations for future works are given at this chapter.

Chapter 2

Biomass Pyrolysis

Thermochemical conversion includes a number of processes to produce useful fuels and chemicals at high temperatures from a wide range of bio-renewable feedstock. As one of these conversions, pyrolysis is simply defined as the chemical changes occurring when heat is applied to biomass in the absence of oxygen. Also, pyrolysis is viewed as the fundamental chemical reaction for gasification and combustion processes. With varied end-uses, the pyrolysis process can be carried out as slow, intermediate or fast pyrolysis. The products of biomass pyrolysis are a mixture of gaseous, liquid, and solid products depending on the operating conditions and the biomass feedstock.

2.1 Biomass resources

Around the world, the main energy supply for mankind, since the beginning of the industrial revolution, is based overwhelmingly on fossil fuels. The combustion of fossil resources such as mineral oil and coal has contributed to the increase in the proportion of carbon dioxide in the atmosphere which outweighs carbon dioxide uptake through the carbon cycle. The carbon is trapped in the carbon chain via photosynthesis in plants and released to the atmosphere when vegetable or animal biomasses decompose. The concept of utilising biomass as solid fuel is similar to the carbon cycle but the period of carbon dioxide release in the combustion of biomass is much shorter than that of the long geological periods required for gas, coal and oil formation. For this reason, the emission of carbon dioxide from burning of biomass is not considered to be relevant for the climate change and renewable fuels from plant sources are considered as 'CO_2 neutral'.

Biomass generally refers to the organic materials from plants or animals based on carbon, hydrogen, and oxygen, often nitrogen, sulphur and also small amount of other atoms, including alkali and heavy metals. Biomass is generated through photosynthesis in plants.

Photosynthesis, consisting of light and dark reaction, is the process to convert light energy to chemical energy in the form of sugar. These processes take place in the chloroplast (see Fig.2.1). The light reaction occurs on the thylakoid membrane which chlorophyll absorbs light energy and stores the energy in the form of ATP (Adenosine Triphosphate) and NADPH (the reduced form of Nicotinamide Adenine Dinucleotide Phosphate). Then, ATP and NADPH transfer to the dark reaction, which takes place in the stroma, to convert CO_2 to sugar molecule in the 'Calvin cycle'. The simple photosynthesis process may be presented by:

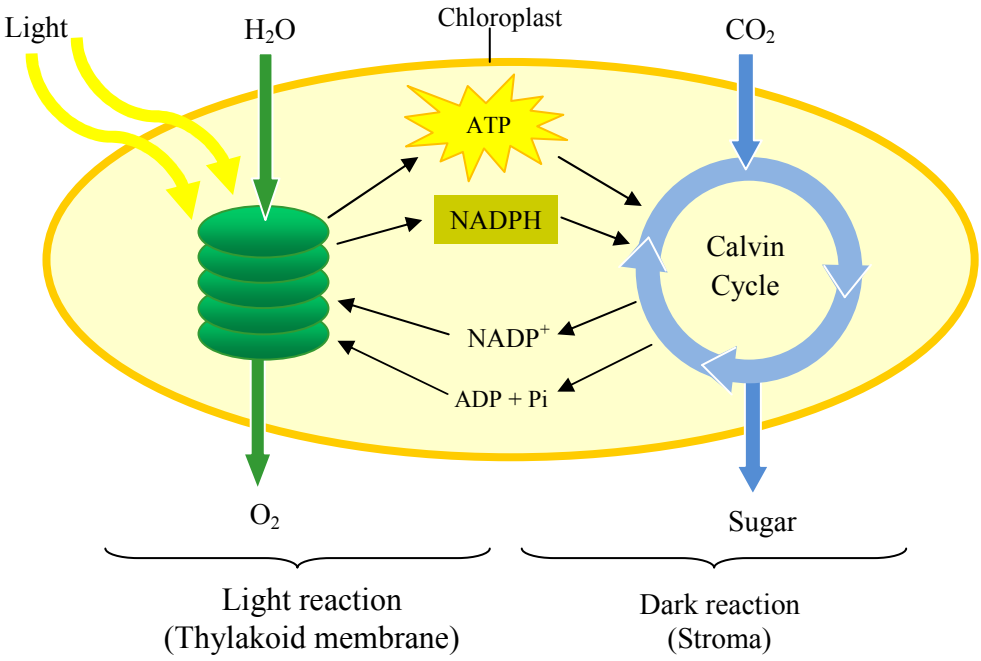

Fig. 2.1 Summary of photosynthesis process

Biomass in the form of wood is the oldest form of energy used by humans. Traditionally, biomass can be used directly by burning for heating and cooking or indirectly by converting through conversion technologies into gaseous and liquid fuels. Due to the various forms of fuel from biomass, they can be utilized for variety of needs, such as generating electricity, upgrading to fuel vehicles, and providing process heat for industrial facilities.

Biomass fuels are becoming a more common alternative fuel source to fossil fuels as the conventional energy prices rise. Sources of biomass can be forest biomass, energy crops (i.e. Rape, Willow, Switchgrass, Miscanthus, Poplar, Soybean and Sweet sorghum),

aquatic biomass, crop residues, animal wastes, municipal solid waste, wood and wood residues [33, 34].

2.2 Lignocellulosic materials

Lignocellulosic biomass refers to the plant biomass which consists of cellulose, hemicelluloses, and lignin. The proportion of these components depends on the biomass species and there are differences between hardwoods and softwoods. For example, different types of wood have different constituent proportions as shown in table 2.1 below.

Table 2.1 Chemical compositions (wt%) of some lignocellulosic biomass

	Cellulose	Hemicellulose	Lignin	Ref.
Hardwood$^{\Psi}$	43.0	35.5	21.7	[35]
Softwood$^{\Psi}$	43.1	27.7	29.2	[35]
Pine wood*	48.9	16.8	29.8	[36]
Beech wood*	46.4	22.4	25.3	[36]
Corn stover$^{\Omega}$	51.2	30.7	14.4	[37]

*on dry ash-free basis $^{\Psi}$on an extractive-free basis $^{\Omega}$on dry basis

2.2.1 Cellulose

Cellulose is the organic compound of which a primary structural compound is mixed with other polysaccharides and lignin on the cell wall in plants. Purity, the degree of polymerization (DP), and the moisture content influence the properties of cellulose samples [38]. The common chemical formula of cellulose is represented by $(C_6H_{10}O_5)_x$. Cellulose is a long linear chain polymer of homopolysaccharide consisting of β-D-glucose monomeric units linked together by (1→4)-glycosidic bonds. A compound of two glucose molecules called cellobiose is the basic building block (see Fig.2.2) of linear polymer of cellulose [35, 39]. The intra- and inter- molecular hydrogen bonds from the substituent (-OH and $-CH_2OH$) give cellulose high strength [33, 35, 40].

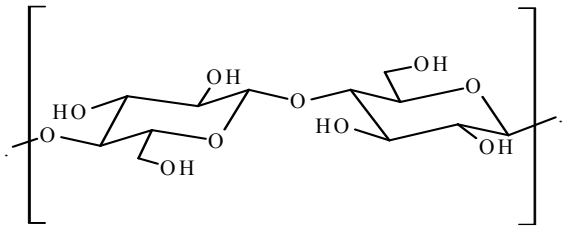

Fig. 2.2 The molecular structure of cellulose [41]

2.2.2 Hemicellulose

Hemicellulose is a complex heteropolysaccharides of hexoses (galacturonic, glucuronic, and methylglucuronic), pentoses (arabinose and xylose), and deoxyhexoses with low amount of uronic acid [40]. Hemicellulose is another component in the cell wall together with cellulose and lignin. Unlike cellulose, hemicellulose is a short chain about 50-200 monomeric units with branched structures. The low degree of polymerization and amorphous structure make hemicellulose have less strength than the crystalline structure of cellulose. The general formula of hemicellulose is $(C_5H_8O_4)_x$ [33]. Hemicellulose is soluble in weak alkaline solutions and it is decomposed during heating more readily than cellulose [42]. Hemicellulose consists of sugar units and the most abundant hemicelluloses are xylans and glucomannans. Softwood and hardwood are composed of xylan about 10% and 30% of the dry weight, respectively [43]. In hardwoods and grasses, the major hemicelluloses are xylan, while in softwood the major hemicelluloses are galactoglucomannans [39]. The chemical structure of xylan is shown in figure 2.3.

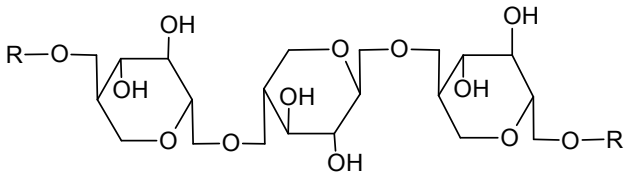

Fig. 2.3 The molecular structure of xylan [33]

2.2.3 Lignin

After cellulose, lignin is the most abundant component of wood and is the most abundant polymeric aromatic organic substance in the plant, making up 20-40% of its dry biomass [44]. Lignin interspersed with hemicellulose is located surrounding cellulose microfibrils, conferring mechanical strength to the secondary cell wall of plants and some algae [45].

Three-dimensional structure of lignin is predominant of three monolignol monomers, p-coumaryl alcohol, coniferyl alcohol, and sinapyl alcohol, which are shown in figure 2.4.

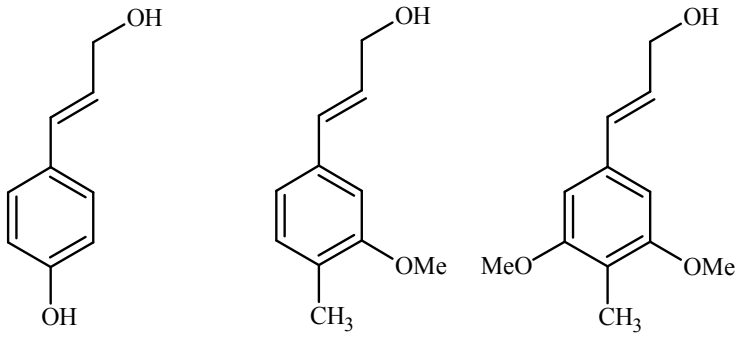

P-Coumaryl alcohol Coniferyl alcohol Sinapyl alcohol

Fig. 2.4 Three common monolignol monomers in lignin [46]

Lignin structure is complex and a highly cross-linked polyphenolic polymer via the β-alkyl aryl ether linkages mainly and also the carbon-carbon and carbon-oxygen bonds [45, 47]. Different proportion of three monolignol monomers [44] and the distribution of different linkages [48] depend on the source of original biomass and the isolation methods.

There are two procedures to obtain lignin which are given the conventional name after the method of separation. The first procedure is based on the removal of polysaccharides by hydrolysis and/or solubilisation and leaving lignin as a residue. Klason lignin or sulphuric acid lignin is obtained from the hydrolysis by 72% sulphuric acid. Hydrolytic lignin, Willsträller lignin, and cuproxam lignin are generated by dissolving cellulose with dilute acid, hydrochloric acid, and cuprammonium hydroxide, respectively. Another procedure is based on the solubilisation of lignin by specific solvents or reagents. For example, sodium hydroxide or a mixture of sodium hydroxide and sodium sulphide is used for the treatment of wood and produces the alkali lignin which is then precipitated with sulphuric acid. This lignin is known as Kraft lignin. Organosolve lignin is obtained from the organosolve process in which the lignin is dissolved in the organic solvent such as methanol or ethanol which hydrochloric acid as a catalyst [38, 45, 49].

2.3 Microalgae

Algae can be referred to as plant-like organisms that are usually photosynthetic and aquatic, but do not have true roots, stems, leaves, vascular tissue and have simple reproductive structures [50]. Algae can be grown in diverse habitats from permanent snow to deserts, such as snow banks, rock and soil, tree trunks [51] but commonly they are found in fresh water (i.e. lakes, rivers, ponds, pools) and in sea water. As algae have photosynthetic pigments, they are the producer of organic matter and oxygen in the sea as do land plants on land. Algae can be microscopic or macroscopic, motile or immotile, unicellular or multicellular plants which show a range in size from the very small about a micrometre to form of seaweeds which have size more than a metre [52]. While algae that can be observed by a microscope are known as 'microalgae', algae that are large or seaweed are known as 'macroalgae'. Algae are classified into many divisions by means of their pigmentation, life cycle and basic cellular structure [53]. The examples of algae classes and their cytological characteristics are presented in table 2.3.

2.3.1 Microalgal cell compositions

Generally, the cell compositions are not an intrinsically constant factor but they depend on environmental factors, particularly light, temperature and nutrient status. The compositions are often reported in terms of proteins, lipids, and carbohydrates as the major groups of compounds which are abundant in algal cells. Table 2.2 below shows some examples of chemical compositions of algae.

Table 2.2 The chemical compositions of some algae species

Microalgae	Chemical composition (wt%)*					Ref.
	Moisture	Ash	Protein	Lipid	Carbohydrate	
Spirulina platensis	3.76	10.38	61.32	8.03	15.81	[54]
Chlorella vulgaris	3.87	6.30	47.82	13.32	8.08	[54]
Isochrisis galbana	6.48	16.08	26.99	17.16	16.98	[54]
Nannochloropsis sp.	3.10	9.44	28.80	18.36	35.90	[55]
Phaeodactylum tricornutum	3.48	15.9	36.4	18.0	26.1	[56]
Porphyridium cruentum	4.87	20.0	34.1	6.53	32.1	[57]
Dunaliella tertiolecta	4.98	13.54	61.32$^{\Psi}$	2.87$^{\Psi}$	21.69$^{\Psi}$	[58]
Chaetoceros muelleri	N/A	40.40	27.20	19.70	11.46	[59]

* on dry basis $^{\Psi}$ on organic basis

Table 2.3 Cytological characteristics of some classes of algae [50-52, 60, 61]

Algae	Chromatophores	Nucleus	Pigments	Storage products	Cell wall
Cyanophyceae	Blue-green algae	×	Chlorophyll-a; phycocyanin; phycoerythrin	glycogen; glycoprotein; small granules of β-hydroxybutyrate polymer and lipid droplets in some species	peptidoglycan layer which is carbohydrate substance cross-linked by peptides, together with a lipopolysaccharide outside layer
Chlorophyceae	Green algae	✓	Chlorophyll-a, b, β- carotene, and lutein as the main pigments	Starch, stored in stroma	cellulose mainly
Phaeophyceae	Brown algae	✓	Chlorophyll a, c; β-carotene, violaxanthin; fucoxanthin as the dominant pigment	Manitol and laminaran, a β-1,3-glucan similar to the chrysolaminarin of other photosynthetic stramenopiles	alginic acid, cellulose, and sulfated polysaccharides
Rhodophyceae	Red algae	✓	Chlorophyll-a; carotetene; Phycoerythrin as the dominant pigment	Floridean starch	loose network of cellulose microfibrils filled in with an amorphous gel-like matrix of sulphated galactan polymers and mucilages.
Bacillariophyceae	Diatoms	✓	Chlorophyll-a, c; fucoxanthin; β, e-carotene, diatoxanthin, and diadinoxanthin as the dominent pigments	oils and fats	strongly silicified in two halves with characteristic structures and often markings
Euglenophyceae	Euglenoid algae	✓	Chlorophyll-a, b; β-carotene; neoxanthin; astaxanthin; antheroxanthin	paramylum and oil	no true wall but pellicle which may be flexible
Xanthophyceae	Yellow-green algae	✓	β-carotene, xanthophylls diatoxanthin and diadinoxanthin with low amounts of chlorophyll a	lipid in the form of cytoplasmic droplets, probably also presence of soluble polysaccharide chrysolaminarin	primarily, cellulose with silica sometimes also presents, and sometimes consists of two overlapping halves.

Carbohydrates

The main organic constituents of the cell walls of algae are carbohydrates with small quantities of lipids and proteins. Roughly the cell wall carbohydrates can be divided into water-soluble materials and water-insoluble materials. The former group have a less complicated molecular structure and the latter group is suitable as skeletal materials. The carbohydrates of algal cell walls include cellulose, mannan, xylan, alginic acid, fucinic acid and chitin [62]. Siddhanta, et al. [63, 64] reported the wide range of the crude cellulose extracted from several species of seaweed at 13.65 -1.2 %. Mannan and xylan have been found in red and green algae [65]. Alginic acid together with fucinic acid has been found as the major constituents of the cell walls of brown algae [66]. The amorphous or continuous matrix in the ultrastructure of cell wall is dissolved partly as the water-soluble fraction and partly in KOH solution as the hemicellulose fraction. Mucilages (D-glucose, D-mannose, D- and L-galactose, L-rhamnose, D-xylose, L-arabinose, D-glucuronic acid, D-galacturonic acid, L-fucose, D- and L-3, 6-anhydrogalactose, and 6-O-methyl-D- and L-galactose, sulphuric acid and pyruvic acid) are the mainly constituents of the continuous matrix of cell walls [62, 67]. Glucose is the principal sugar, while varying proportions of rhamnose, fucose, ribose, arabionose, xylose, mannose and galactose are detected [68].

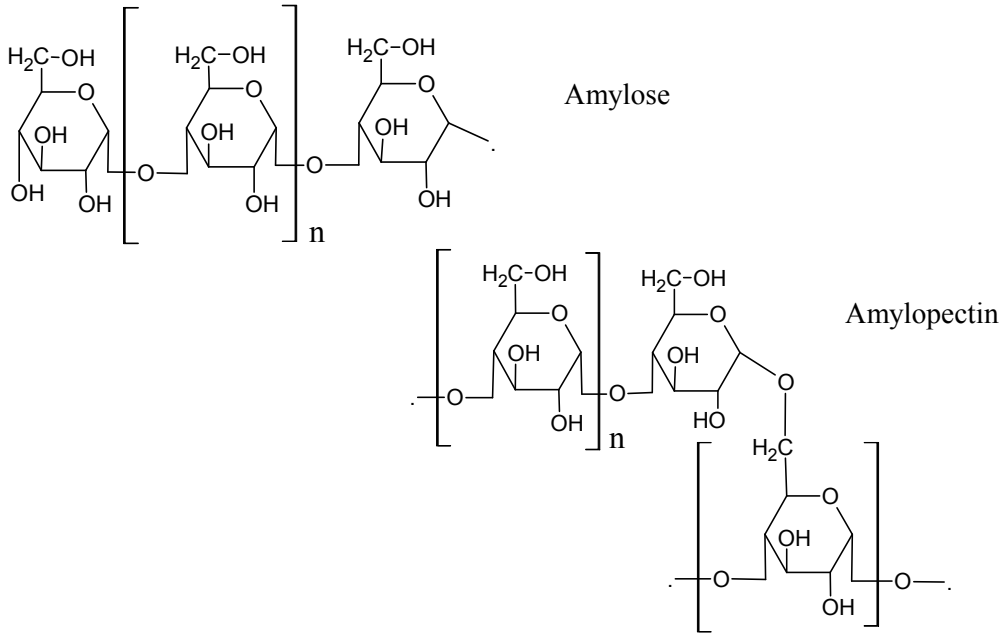

Fig. 2.5 Amylose and Amylopectin structures

As green algae have similar metabolism as that of land plant, the photosynthesis products are true starches, amylose and amylopectin (Fig.2.5). While brown algae have laminarin and manitol [69] and red algae have floridean starch as their main storage products [70].

Lipids

Lipid is another important component in algae cell. Non-polar lipid (monoglycerides, diglycerides, triglycerides, and free fatty acids) are available as storage products. The polar lipid (phospholipids and galactolipids), like those of chloroplast of higher plants, are largely surfactant molecules which function both as structural elements and as metabolites in the photosynthetic organelles.

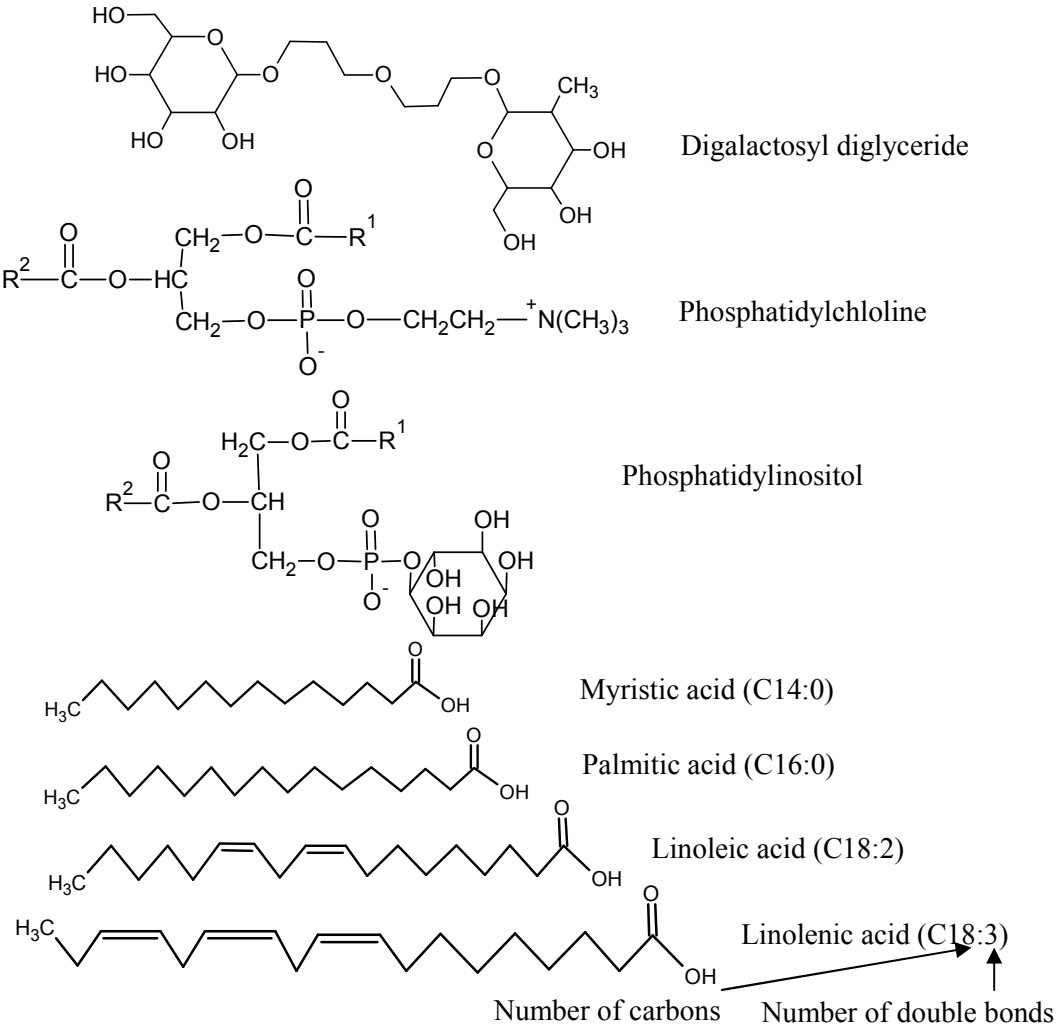

Fig. 2.6 Some structures of lipids and fatty acids which are available in *Chlorella vulgaris*

Most of algal oils have similar fatty acid constitutions to common vegetable oils. The fatty acids of algal storage occur in range from C12 to C24, thus the common saturated straight chain fatty acids of vegetable oils such as lauric (C12), myristic (C14), palmitic (C16) and stearic (C18) are found in algae. It is rare reported the appearance of branched-chain fatty acid.

For *Chlorella vulgaris*, the lipid compounds were found as Monogalactosyldiglyceride, Digalactosyldiglyceride, Phosphatidylethanolamine, Sulphoquinovosyldiglyceride, Phosphatidylglycerol, Phosphatidylcholine, and Phosphatidylinositol. Each of these lipid may consist of the fatty acids: C14:0, C16:0, C16:1, C16:2, C16:3, C18:0, C18:1, C18:2, C18:3 [71-73]. Yoo, Chan et al. [74] reported that palmitic acid (C16:0), oleic acid (C18:1) and linoleic acid (C18:2) were the main components; while palmatoleic acid (C16:1) and stearic acid (C18:0) were the minor fatty acids. The structure of some lipids and fatty acids available in *Chlorella vulgaris* are shown in Fig.2.6.

Proteins

Most of the figures in the literature on the content of algal proteins so-called 'crude protein' are based on the estimation by the method after Kjeldahl [75, 76]. The crude protein figure is obtained by hydrolysis of the algal biomass and estimation of the total nitrogen which results in an overestimation of the true protein content because proteins are not the only source of nitrogen. The cellular nitrogen include inorganic-, free α-amino-, free amino-, volatile-, and protein nitrogen. However, normally protein is the main component of nitrogen fraction. Other protein estimation procedures are the method after Lowry and Biuret method which based on colour reactions with defined protein content without reacting with other nitrogen-containing compounds [61].

2.3.2 Microalgal biomass production

Like terrestrial plants, the process of algal photosynthesis requires sunlight, carbon dioxide from the atmosphere and also several nutrients for their natural growth. Therefore, the mass cultivation of microalgae requires carefully controlled conditions to produce optimal yield.

The large-scale cultures are practically maintained outdoor because they have the advantage of available sunlight. However, the temperature and the intensity of sunlight are

the uncontrollable parameters due to the season dependence and circadian cycle in 24 hours of sunlight. These conditions are more appropriate for countries or regions with high solar radiation [61]. As the light source is the limiting factor, the artificial light sources like fluorescent lamps can be used in the pilot scale of microalgal cultivation [77]. For an efficient and economical photo-bioreactor, the selection of a light source as a key design challenge needs to consider both its spectral quality and intensity. The ability to absorb the solar energy of microalgae in mass cultivation is governed by several factors, including cell density, the length of the optical path of the system, the optical properties of the microalgal cells and rate of culture mixing [78].

Carbon dioxide fixation of microalgae is one of important factors for algae cultivation. Besides microalgae absorb free carbon dioxide from the atmosphere as a carbon source for photosynthesis from atmosphere, they can gain benefit from the fixation of CO_2 in discharge gases from industries and power plants [79]. Normally the ability of diffusion rate of CO_2 from the air into the water is too slow to replace the CO_2 assimilated by rapidly growing algae. Thus, the additional CO_2 must be applied to cultivation medium to ensure satisfactory growth [80].

Nutrients are another factor for natural growth of microalgae. The main nutrients are nitrogen, phosphorus, and also minor nutrients as silicon, potassium, sodium, iron, magnesium, calcium and some trace elements such as copper, manganese, zinc [50]. After carbon, nitrogen is the most important nutrient contributing to the biomass production. Some algae can fix nitrogen from the air in the form of nitrogen oxides [81]. Alternative sources of nitrogen can be applied as nitrate (NO^-_3), ammonia (NH^+_4) or urea into the medium [82]. Under nitrogen limitation or starvation, there is the discolouration of the cells because the decrease in chlorophylls and the increase in carotenoids, also there is the accumulation of organic carbon compounds such as lipids and carbohydrates depending on the algae species [83, 84]. Although phosphorus in algal biomass is in small amount, it plays an important role as a growth limiting factor.

Three main designs of mass cultivation of algae can be classified as the open system, the closed system and co-process system utilising the carbon source from industrial waste.

Open systems

Open systems can be the natural ponds as lakes, lagoons, ponds or artificial ponds, or specific designed containers. The most common design of open system is called 'raceway ponds' [85] which are made of a closed loop with circulation to stabilize algae growth and productivity (Fig.2.7(a)). The carbon dioxide fixation is mainly from the atmosphere but an external CO_2 supply can be installed to enhance the productivity. The advantages of open ponds over closed system are that they are easily to construct and are low cost. Also, they need less energy supply by using natural light energy from the sun [86]. However, open ponds have some limitations which influence the production. The low CO_2 diffusion, poor light utilization, and inefficient mixing cause lower productivity compared to the closed system. Moreover, due to the possibility of contamination or pollution from other algae and heterotrophs in open pond, suitable algal species should able to grow under highly selective environments [87].

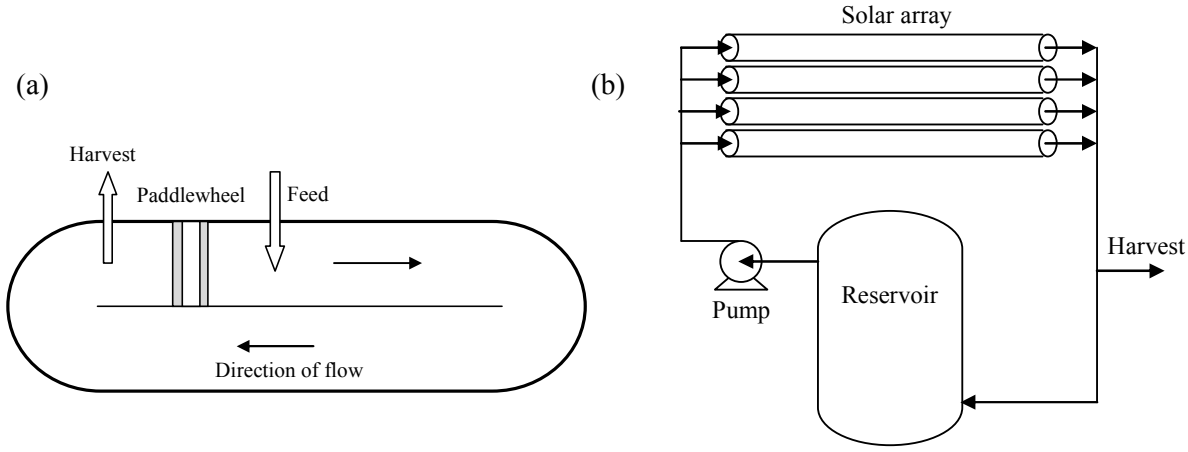

Fig. 2.7 (a) an open system (a raceway pond) and (b) photo-bioreactor for producing algae [88, 89]

Closed systems

The limitations of open ponds have driven the development of closed system which can be classified into outdoor closed systems and indoor closed systems. The typical design of a closed system is the 'tubular photo-bioreactor' [80]. The photo-bioreactor (Fig.2.7(b)) is suitable for some sensitive algal strains because the contamination is controlled easily. For indoor closed system, the artificial light sources are chosen at a suitable intensity.

Although the closed systems attain high cell mass productivities but the overall cost of closed systems are still higher than those of open systems.

Co-process with waste treatment

This system is to combine the algal cultivation with the carbon dioxide emission mitigation and wastewater treatments. The major driving forces of these designs are the removal of CO_2 from the atmosphere, capturing or utilizing the CO_2 from fossil fuel combustion, and reducing the cost of nutrients. This algal biomass can be converted efficiently into biofuels with high productivity and low-cost cultivation [90]. While the CO_2 fixation from the atmosphere is limited by low CO_2 concentration in air, the mitigation of CO_2 emissions from power plants achieves higher yield because of the higher CO_2 concentration [91].

The benefits from utilizing waste water treatment process to algae production are the saving of nutrients cost and the minimizing of the freshwater use for algae cultivation. Some preliminary growth studies indicated both fresh water and marine algae have a potential in waste waters treatment [92, 93]. Microalgae have potential to remove nitrogen, phosphorus, and metal ions from wastewater [79] and CO_2 from industrial exhaust gases; however these applications can only be achieved with a limited range of algae which are tolerant of the extreme conditions.

It is difficult to directly compare the performance characteristics of each mass cultivation system because they have different advantages and disadvantages. The choice of system depends on the production costs, value of the desired products, location and production quantity.

2.3.3 Potential role of biofuels from microalgae

Increased interest in the production of biofuels from algae has been achieved by several advantages.

(1) Microalgae have high energy efficiency to convert solar energy into chemical energy and they have rapid growth potential; some strains can be harvested daily [94]. Hence, the production yield of microalgae is higher in comparison to terrestrial plants [95].

(2) Although microalgae are grown in water media, as compared to terrestrial crops, microalgae require less freshwater demand [96].

(3) The microalgal biomass production is not seasonal and can be grown invariable climates (especially the closed system). Thus, they can be produced all year round [97]. Also, microalgae consist of 20-50% oil content [91] which leads to high oil productivity. Figure 2.8 is showing the comparison of oil yield for biodiesel production of several biomasses, including microalgae which are produced from photo-bioreactor. Biodiesel from algae oil has main characteristics quite similar to petroleum diesel [98].

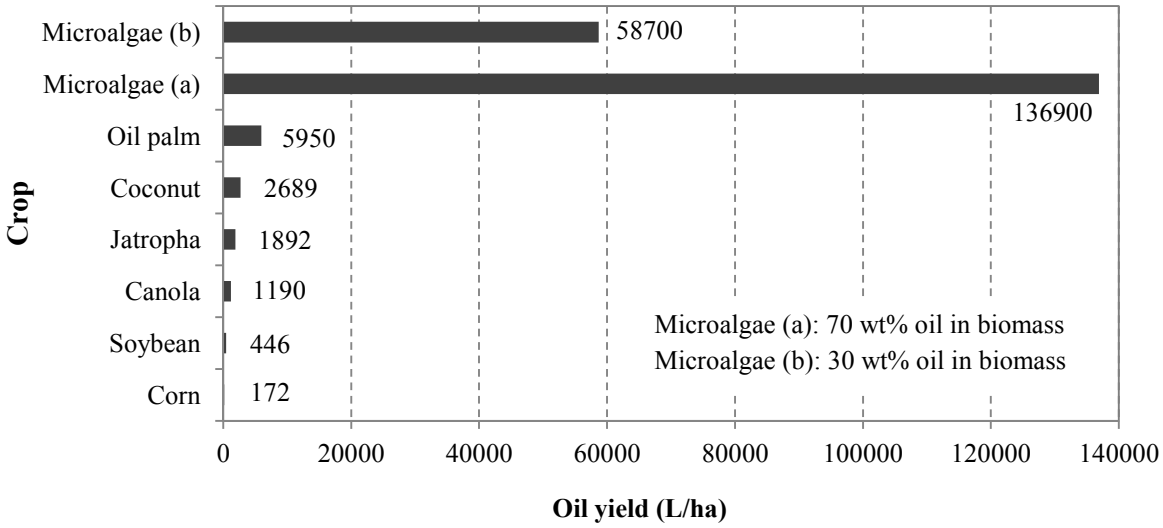

Fig. 2.8 The oil yield for biodiesel production from different biomass [99]

(4) Microaglae can be cultivated on non-arable land and marginal area which are not suitable for agricultural purposes, such as desert and seashore lands. Therefore, they do not compete with food production [97].

(5) For environmental and economic concerns, some microalgal cultivations are located next to the power plants or industries, for taking up CO_2 form flue gases and obtaining the nutrients, e.g. nitrogen and phosphorus from wastewater [100].

(6) Another environmental benefit of microalgal cultivation is that there are no herbicides or pesticides application requirements [97].

(7) Besides biofuel production, microalgae produce valuable co-products such as fertilizer [101] and materials for fermentation to produce ethanol or methane [91].

(8) Microalgal biomass can be utilized for a wide range of fuel production such as biodiesel [102], bioethanol [103], biomethane [104], and biohydrogen [105].

2.3.4 Biothermal Valorisation of Biomass (BtVB) process

Biothermal Valorisation of Biomass (BtVB) process is a patented process [106] which was developed at European Bioenergy Research Institute (EBRI), Aston University, UK. This process demonstrates an improved method for thermal conversion of ash-rich biomass as microalgal biomass and this process also presents the combination of microalgae into the bioenergy area effectively. It is the integration of different processes such as algal biomass production, biogas units, pyrolysis processes, gasification processes and heat and power generation plants. Pyrolysis vapours are high quality and highly energetic, dust and tar free which are suitable to combine with heat and power (CHP) use after a gasification step. Char produced from intermediate pyrolysis in BtVB process is suitable for further applications such as combustion, carbon sequestration and soil re-fertilisation. The varied sized feedstock can be applied into intermediate pyrolysis; char can be separated from vapour easily. Moreover, various types of biomass may be introduced to this process. Ash-rich biomass, like microalgae, is also possible for use in the intermediate reactor. Exhaust gases from biogas plants and from gas engines are transferred to algae plantation as a fertilizer. Apart from the raw microalgae biomass, algae with high oil content can be extracted by mechanical or solvent extraction for biodiesel production. Although microalgae biomass is main feed, other regional feedstocks can be used together with algae during the winter time, when algae production slows down. The diagram of Biothermal valorisation of Biomass (BtVB) process is shown in figure 2.9.

The BtVB process offers closed loops of fertiliser recycling. Residues from the biogas units may be used as a fertilizer in algae plantation. The high ash content microalgae are processed through thermal conversion techniques and yielded a by-product with high ash content solid phase. The mineral matter in pyrolysis char is used for the energy crops as fertilizer and at least part of char may be extracted with water to recover mineral elements such as potassium, phosphates, nitrates and silica and then feed this mineral solution into microalgae cultivation system as a growth fertilizer. The dried extracted solid residue may be used for coupled gasifier or as fertilizer to the energy crop field, so called ‘black earth’ which also brings carbon back into soil. Moreover, the aqueous phase of two-phase liquid products which is rich in inorganic matter may be added as a fertilizer to algae plantation and it can be considered as the closed water loop as well. In addition, the exhausts gases from engines are taken to algae medium as another source of fertilizer.

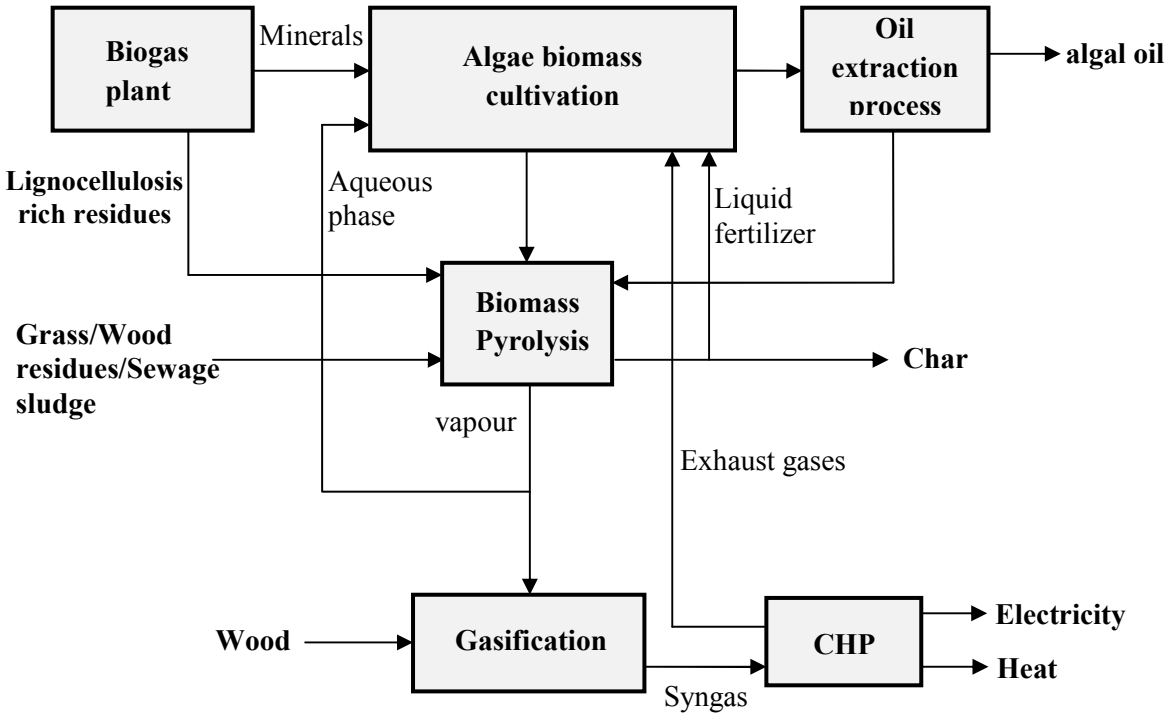

Fig. 2.9 The Biothermal valorisation of Biomass (BtVB) process [106, 107]

2.3.5 *Chlorella vulgaris*

Chlorella vulgaris is a species of green non-motile unicells in the Chlorophyceae class. They have a spherical shape with 2-15 μm diameter [108]. Sometimes it is called 'the green ball' as show in figure 2.10. *Chlorella vulgaris* have a simple life cycle with high reproductively rate. Their cells are divided into two or four non-motile daughter cells and enclosed for a little while within the parent cell wall [109]. When the parent cell wall breaks, daughter cells are released into the medium.

Fig. 2.10 The microscopic picture of *Chlorella vulgaris* [110]

Chlorella unicellular microalgae have been used as a model for biochemical and physiological works in many studies because their relatively simple structure and the close resemblance of photosynthesis and respiration systems with those in plants [111].

For decades, *Chlorella vulgaris* has been widely available in the food industry. They also show great potential for bioenergy applications due to their high growth rate and high oil content. They can be cultured under autotrophic and heterotrophic conditions [112]. The oil content (%) of *Chlorella*, compared to those of other microalgae is shown in table 2.4.

Table 2.4 The oil content of microalgae [99]

Microalgae	**Oil content (wt % dry)**
Schizochytrium sp.	50 - 77
Botryococcus braunii	25 - 75
Nanochloropsis sp.	31 - 68
Neochloris oleoabundans	35 - 54
Nitzschia sp.	45- 47
Cylindrotheca sp.	16 - 37
Nanochloris sp.	20 - 35
Isochrysis sp.	25 - 33
Chlorella sp.	**28 - 32**
Phaeodactylum tricornutum	20 - 30
Dunaliella primolecta	23
Tetraselmis sueica	15 - 23
Monallanthus salina	> 20
Crypthecodinium cohnii	20

The difference in oil content in microalgae depends on not only the species, but also the cultivation conditions. The carbon dioxide concentration, nitrogen depletion, harvesting time, and also the method of extraction are the influences to the lipid content and the lipid compositions. The lipid content in *Chlorella vulgaris* increases when the nitrogen concentration decreases and the CO_2 concentration increases [73, 113].

Moreover, there are several published works showing that *Chlorella vulgaris* has potential as a bio-sorbent for heavy metal removal, such as Cadmium (II), Nickel (II), Zinc (II), Lead (II), Chromium (VI), Iron (II), Iron (III), Copper (II) [114-121], phosphorus removal [122, 123], nitrogen removal in ammonia form [124, 125], and dyes removal from textile

wastewater [126, 127]. These proposed bio-sorption potentials of *Chlorella vulgaris* lead to their biomass production for biofuels combined with wastewater treatment as well as their solvent tolerance, acid tolerance and high CO_2 concentration tolerance [128-130] support their application to water treatments and CO_2 fixation.

2.4 Pyrolysis conversion process

Apart from the biochemical and physical conversion, thermochemical conversion has been currently attracting the most interest for biofuel production. It mainly consists of combustion, gasification, and pyrolysis process. Each gives a different range of products and uses different equipment configurations operating in different conditions. Combustion process is well-defined technology and generates environmental concerns. Pyrolysis becomes an interesting conversion technology because its efficient energy production, easily stored and transported products in the forms of liquid fuels and solid char, and the wide range of produced chemicals [43].

Pyrolysis is thermal degradation in the absence of oxygen and it is a fundamental step in combustion and gasification followed by total or partial oxidation of the primary products. Pyrolysis occurs at relatively lower temperatures about 300–800°C than those of gasification at 800–1100°C. High temperatures and long residence times are suitable for gas formation. The carbonisation process at low temperature and long residence times are the preferred conditions for char formation, whereas pyrolysis promoting the liquid production occurs at medium temperature with short residence times [131].

Based on the operating conditions, the pyrolysis can practically be divided roughly into three groups as conventional pyrolysis or slow pyrolysis, intermediate pyrolysis, and fast pyrolysis. The key parameter classifying them is the residence time of solid phase within the reactor. Gas phase residence time for fast and intermediate pyrolysis is kept below two seconds. The proportion of gas, liquid and char products are controlled by the heating temperature and vapour residence times. The process parameters as well as heating rate also influence the subsequent behaviour of the products by secondary reactions.

Conventional or slow pyrolysis is characterized by a slow heating rate which leads to significant portions of solid product. The vapour residence time is in the order of minutes

or longer. The residence time may last longer up to days at low temperature for producing charcoal or char mainly and is referred to a carbonization [33].

The characteristics of fast pyrolysis which are described by Bridgwater, et al. [132] are : (1) high heating rate and high heat transfer rate; (2) short vapour residence times less than 2 s; (3) well-controlled pyrolysis reaction temperature about 500°C and vapour phase temperature about 400–450°C; (4) rapid cooling of the vapour phase [132]. Chemical reaction kinetics, heat and mass transfer processes and phase transition play important roles in this complex conversion.

If the purpose of the pyrolysis process is to obtain high yield of liquid products, a fast pyrolysis is recommended. The main product is bio-oil which was reported up to 75 wt% on dry feed basis for woody biomass [131]. However the fast pyrolytic liquid products present in one phase include water, acids and tars. In the case of non-woody biomass (grasses, straws, industrial residues, and agricultural residues), their pyrolysis process and products are far more complicated than those of woody biomass. In addition, feedstock has to be well prepared with low moisture content.

To minimize the exposure period at low temperature, the fast pyrolysis technique uses small particle biomass in a fluidized bed and a very quick heating at the surface of the particle in ablative reactor [133]. These lead to the difficulties for separation solid phase from liquid and gas phases.

2.4.1 Intermediate pyrolysis

In the last few years, there has been a development of intermediate pyrolysis at European Bioenergy Research Institute (EBRI), Aston University as a part of Biothermal valorisation of Biomass (BtVB) process. The intermediate pyrolysis operated with coaxial conveyor screw reactor or 'Pyroformer' [134] in the parameter range of between slow and fast pyrolysis produces different product qualities. The operating temperature is in the range of 300–550°C depending on the biomass feed. The Pyroformer (length: 1810 mm; diameter: 220 mm) consist mainly of two screws which the inner screw (screw thread: 86 mm) transports the biomass feed from the feeder side to the other end of the reactor and the outer screw (screw thread: 90 mm), which moves in opposite direction, transports a fraction of the char produced during the run with the ratio by weight of biomass to char in

the range 1:1 to 1:20. The importance of char transporting with the outer screw as a heat carrier is to improve heat transfer and char also acts as a reforming agent during pyrolysis process. The figure 2.11 shows the design of Pyroformer as presented by Hornung and Apfelbacher [134].

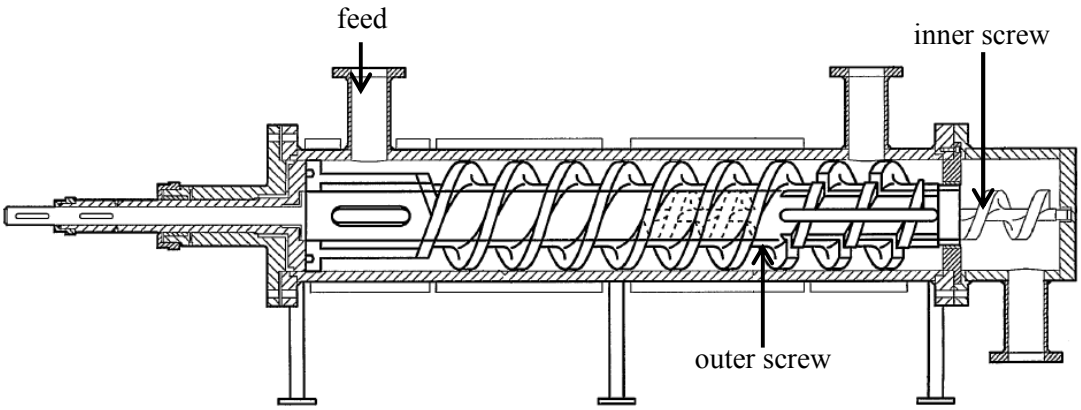

Fig 2.11 The longitudinal schematic view of Pyroformer (adjusted from [134])

Hornung and co-workers reported the product yields from intermediate pyrolysis as: liquids (40-60 wt%), char (15-25 wt%), and non-condensable gases (20-30 wt%) [107]. They also proposed the advantages of intermediate pyrolysis process in [107, 143, 135] that:

(1) Its operating conditions preventing the formation of high molecular tars and offer dry char which is suitable for fertilisation or combustion further applications.

(2) There are a wide range of feedstock which can be used with intermediate pyrolysis reactor, such as algae, residues from biogas plants, energy crops, wood residues, and sewage sludge.

(3) There is the flexibility in size of feedstock (in the forms of pellets, powdered, or chip) for intermediate pyrolysis, so the use of large size feedstock leads to separate solid phase from vapours phase easily.

(4) Pyrolysis liquids from intermediate pyrolysis present in two phases, aqueous phase and organic phase. The removal water from the pyrolysis liquids is easy and end up with low water content oily phase.

(5) Defined residence time can be adjusted flexibly by varying the speed of the screw. It is suitable for various feedstocks with different optimal residence time.

(6) This unit requires less sophisticated technology compared to slow and fast pyrolysis to get similar products, thus it is considered a low cost investment with the ability for scale up.

(7) Although the procedure to increase specific energy density of biomass as the intermediate for gasification and combustion has been investigated, there are some difficulties to apply pyrolysis liquids as direct fuel for engine or pyrolysis vapours into gasification system. The vapour phase from intermediate pyrolytic reactor has low ash content without dependence on ash content of starting biomass. This advantage offers the suitability of combining with a gasifier and also the applicability for ash-rich biomass such as microalgae biomass. Furthermore, the internal pressure in this reactor is above atmospheric pressure, typically at least 50 or 200-300 mbar over atmospheric pressure. This allows pumping pyrolytic vapour effectively into the gasifier.

2.4.2 Pyrolysis mechanism

Pyrolysis is a complex thermal degradation process composed of numerous reactions resulting in the production of a huge number of chemical compounds. However, basically the reaction products are often lumped into three groups: gas, pyrolytic liquid and char [136] or into two groups: volatile and char.

Based on thermogravimetry, the primary degradation of biomass start at about 227°C and is practically terminated at 427–477°C [23]. The weight loss of thermogravimetric analysis results from the overlapping of several reactions, thus they can be used for global mechanisms. The reaction mechanisms may be defined in three reactions which are (1) the primary pyrolysis or biomass devolatilization which is the main reaction to convert solid into permanent gas, condensable vapour and char; (2) secondary gas phase reaction of the release gas and tar species; and (3) heterogeneous reactions between solid and gas [137].

Moreover, typically the decomposition of lignocellulosic materials may be evaluated by two different models. The first approach is to consider separated competitive reactions to describe the product distribution independent of the chemical compositions [138]. The second approach is when the decomposition rates of biomass may be modelled by the

thermal behaviour of the main components in the biomass, namely cellulose, hemicellulose, and lignin, and also their relative contribution in the chemical composition [21, 27]. Each component decomposes at different rates and by different mechanisms. Several zones are reported in the weight loss curves which can be associated with the component decompositions; hemicellulose decomposes at 225–325°C, cellulose decomposes at 325–375°C and lignin decomposes in the wide temperature range at 250–500°C [23]. The volatile products from pyrolysis of biomass are mainly from the degradation of cellulose and hemicelluloses but lignin products dominate char yield [139].

When the heating rate increases, the weight loss region of each component will be merged to each other and shift to higher temperature. At fast heating rate or high temperature, all component degradation occurs simultaneously. However the overlap between the different compounds cannot be avoided, so the term 'pseudo-component' is more appropriate [23]. In addition, the thermal behaviour of each component cannot be applied directly to biomass due to the difference of separation procedure, the presence of mineral matter, and component interaction.

Hosaya, et al. [140] considered the interactions between lignocellulosic components. There were the significant interactions between cellulose and lignin. Lignin inhibited the thermal polymerization of levoglucosan but enhanced the formation of smaller molecules from cellulose. While cellulose reduced the secondary char formation from lignin and enhanced some lignin-derived product. On the other hand, the interaction between cellulose and hemicelluloses was described as a weak interaction.

Secondary reactions of primary tar vapours become active at high temperatures and sufficient long residence time. Primary tar is the product from primary pyrolysis and after leaving from the solid phase, the primary tar vapour is subjected to secondary tar reactions [141]. Tar is a very complex mixture of organic compounds such as phenolics, olefins and polyaromatic hydrocarbon (PAH) [142]. Tar formation can occur in the pores of the fuel particle as well as in the vapour phase and on surfaces of the fuel particles or other bed media. In addition primary volatiles may go through competitive pathways between char formation and cracking to form secondary volatiles [144]. Van de Velden, et al. mentioned that cracking and water-gas shift reaction are the important secondary reactions of pyrolysis [133]. Boroson, et al. (1989) [144] reported that at high severities, CO is the major by-product of tar conversion and the coke formation is negligible as well as the

decrease of tar molecular weight with increasing tar conversion [144]. Main factors which need to be concerned for supporting secondary reactions are particle size, temperature, gas dilution, residence time and amount of fuel [133, 145].

Although there is numerous weight loss measurements of biomass pyrolysis, there is a difficulty to compare these results because thermal characteristics depend on the biomass species, the geographical origin, age, operating parameters, and the thermal analysis instrument.

Pyrolysis mechanism of cellulose

Extensive studies on cellulose pyrolysis mechanism have been made over the past several decades. The early general mechanism for cellulose pyrolysis is 'Broido-Shafizadeh reaction scheme' [146] which is shown in figure 2.12. The initial reaction, involving no weight loss, is an induction or activation to form 'active cellulose' which is related to the nucleation process [147] and this step may be neglected at temperature above 300°C [146]. Following by a pair of competing reactions, one is the depolymerisation to yield levoglucosan and its breakdown products which are lumped together as 'volatiles'. Another pathway is char and gas formation.

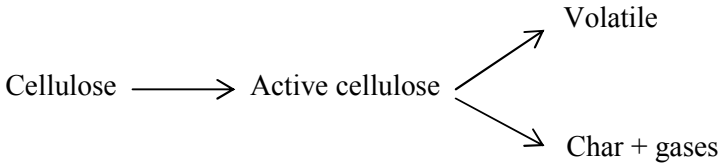

Fig. 2.12 Cellulose decomposition model by Bradbury, et al. [146]

Later, there were several studies aiming to improve the cellulose pyrolysis scheme. Mamleev, et al. [147] concluded that the char formation cannot occur in the same pathway as the gas formation because from the experiment result [147] showed the increase of light gases with heating rate but the Broido-Shafizadeh model predicts a decrease of gaseous and char yield. Thus, the gas formation competes with the char formation. Agrawal [148] proposed a modified version of the Broido-Shafizadeh model, assuming that cellulose decomposes into gas, char and tar products. Although the Broido-Shafizadeh model and its modified models have been widely applied, they do not describe the details of decomposition.

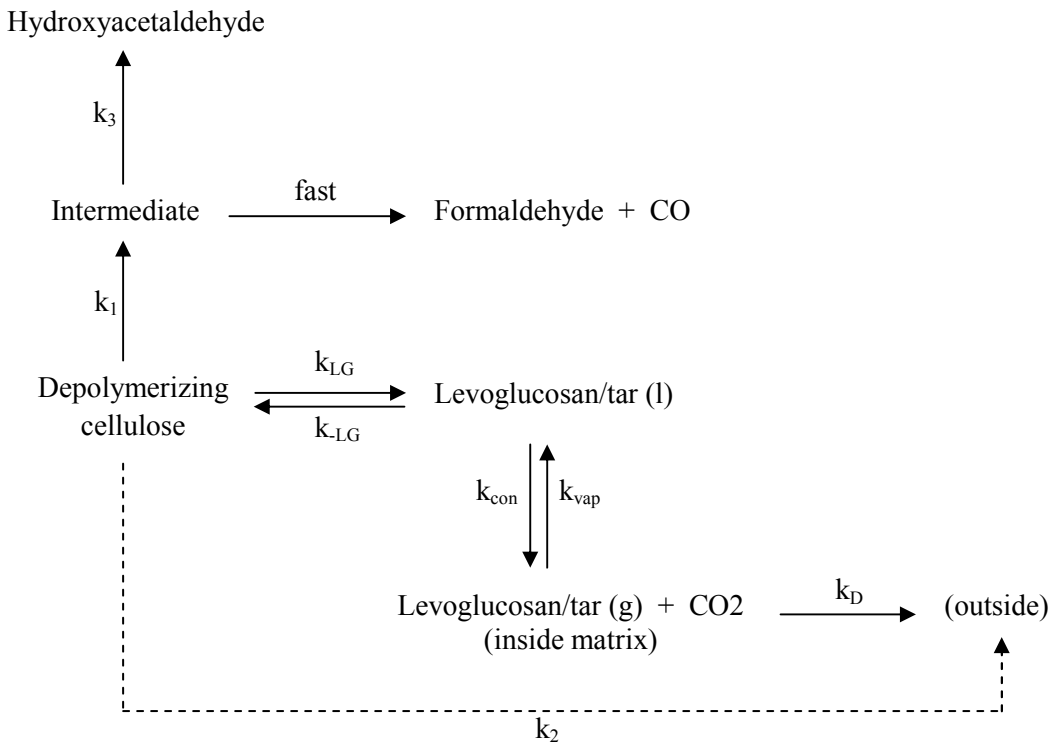

Fig. 2.13 Two coupling pathways of cellulose decomposition proposed by Banyasz, et al. [149]

Levoglucosan was considered as a main fraction of tar produced from the pyrolysis of cellulose. Later, the recognition of hydraxyacetaldehyde or glycoaldehyde as a major product led to the extension in detail of the cellulose mechanism [150, 151]. Recently, cellulose decomposition models have been suggested to be more complicated pathways. Banyasz, et al. [152] proposed a cellulose mechanism with hydroxylacetaldehyde, formaldehyde, CO_2, CO and levoglucosan as main products (see figure 2.13). This model consists of two main pathways (low temperature and high temperature pathway). Hydroxyacetaldehyde, formaldehyde and CO formation are token place at high temperature pathway involving an intermediate. While the formation of levoglucosan or tar at the low temperature pathway is reversible process.

Pyrolysis mechanism of Hemicellulose

Compared to cellulose studies, there are considerably fewer papers dealing with the decomposition of the various hemicellulosic materials. Xylan starts decomposing at a lower temperature (about 250°C) than that at which cellulose does and continues with slow degradation to the high temperature region [139]. The main products are attributed to

water, methanol, carbon monoxide, carbon dioxide, formaldehyde, formic acid, acetic acid, acetone, acrolein, 2-furaldehyde, and 3-hydroxy-2-pentono-1,5-lactone [153]. Due to the observed multi-peak of the derivative of the thermogram of hemicellulose decomposition, a three successive reaction chain model [27], a successive reactions model [154], and a semi-global reaction mechanism model [155] were proposed to describe the hemicellulose mechanism (see figure 2.14).

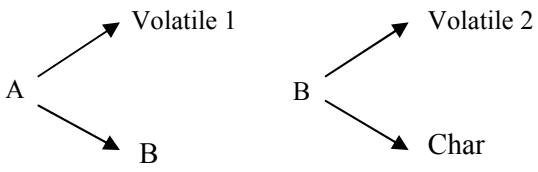

Fig. 2.14 Semi-global reaction mechanism for the thermal degradation of hemicelluloses; where the A is xylan and B is the intermediate reaction product (a reduced degree of polymerization intermediate).

From figure 2.14, the competition between volatile and solid formation is taken into account for both steps. The first stage is much faster than the second stage and the reaction time of these two stages decrease with temperature; while their ratio remains almost constant [155]. A large fraction of volatiles is produced in the first step due to the cleavage of the glycosidic bonds and the decomposition of side-chain structure. While the second slow degradation may be attributed to fragmentation of other depolymerised units [156].

Pyrolysis mechanism of Lignin

Due to the complexity of lignin and the difficulty in extraction, the study of pyrolysis mechanism of lignin is limited. Lignin decomposes over a wide range of temperatures starting from 200°C, a lower temperature than that of cellulose, and covers a rather wide temperature interval [139]. Lignin pyrolysis is a radical process of the competition between initiation, propagation and termination reactions. The initiation reactions are strongly related to the bond energies of lignin structure. While the termination reactions need to be concerned the diffusive limitations to the effective radical collisions and recombinations [44]. Main products from lignin pyrolysis are phenol and its derivatives–methoxyphenol, guaiacol and cresol. Also, methanol, formaldehyde, acetaldehyde, acetic acid and light hydrocarbons, as well as CO, CO_2 and H_2O are produced from pyrolysis of lignin [157].

Above 527°C, tar becomes the major pyrolysis products. The primary tar can occur the secondary cracking at the unsaturated side-chain and phenolic aromatic ring structure [158] to produce CO, CH_4, C_2H_4 and other light gaseous products [159]. Both gauiacols and catechols can undergo secondary reactions with relatively independent of the presence of other molecular species and the residual polymeric material [157, 158].

Sharma, et al. [45] studied char formation from lignin and reported that due to the highly cross-linked and refractory nature, lignin chars have lower reactivity than those of other biomass constituents. The yield and characteristics of lignin chars depend on the pyrolysis conditions. The presence of inorganic matter, such as Na and K, lead to high char yield. As the pyrolysis temperature increases, the aromaticity and the carbonaceous mature of the char increases and hydrogen, as well as oxygen content of the char decrease.

2.4.3 Pyrolysis products

The polymeric constituents of biomass are degraded into smaller units that can be liquids, gases, and solids. These products from the pyrolysis process can be used more readily and may be considerably more valuable than raw biomass. The primary products can be used directly or can be converted further into even higher quality and valuable fuel or chemical products. The compositions and properties of the biomass-derived products depend on the pyrolysis conditions, i.e. pyrolysis temperature and heating rate [160].

Liquid products

The present interest in liquid products from pyrolysis or other thermochemical conversion are driven by their high energy density which reduces the cost of storage and transport and their potential for further applications of heat and electricity generation and upgrading to premium-grade fuels. The dark brown organic liquids from pyrolysis are called bio-oil, pyrolysis oils, bio-crude oil, wood oil, pyrolysis liquids, wood liquids, or wood distillates. The pyrolysis oil is composed of a very complex mixture of both aliphatic and aromatic hydrocarbons together with high amount of oxygenated hydrocarbon [161, 162]. Five broad categories of hydrocarbons detected in pyrolysis oil are hydroxyaldehydes, hydroxyketones, sugars and dehydrosugars, carboxylic acids, and phenolic compounds [33]. The complexity arises from the degradation of lignin which gives a broad spectrum of phenolic compounds.

Although pyrolysis oil from biomass pyrolysis shows the opportunities for fossil fuel replacement, its properties are significantly different from those of petroleum-derived oils and the definition of oil quality may differ by applications. Table 2.5 shows the comparison between the properties of wood pyrolysis oil and heavy fuel oil. The properties of pyrolysis oil, such as poor volatility, high viscosity, coking, and corrosiveness are still the problems for using with the existing petroleum equipment and particularly in storage, there are some problems about phase separation, polymerization and corrosion of containers [163].

Table 2.5 The comparison between the properties of pyrolysis oil from wood pyrolysis and heavy fuel oil [163]

Physical property	**Heavy fuel oil**	**Bio-oil**
Elemental composition (wt%)		
C	85	54 - 58
H	11	5.5 - 7.0
O	1	35 - 40
N	0.3	0 - 0.2
Ash	0.1	0 - 0.2
HHV (MJ/kg)	40	16 - 19
Viscosity (at 50°C)	180	40 - 100
Moisture content (wt %)	0.1	15 - 30
pH	-	2.5
Specific gravity	0.94	1.2

Numerous compounds in pyrolysis oil are highly oxygenated (35-40 wt% oxygen content) depending on the type of biomass and process severity. The presence of a high content of oxygenated compounds in pyrolysis oil results in decreasing heating value, increasing uptake of water in the fuel, increasing the corrosiveness from acidic compounds [164, 165]. The moisture content of pyrolysis oil which is contributed from free water in original biomass and as a product of dehydration is much higher than that of fuel oil. This high water content causes the low heating value and affects viscosity and acidity as well as leading to phase separation and could affect subsequent upgrading processes. The low pH

value of pyrolysis oil as a result of the presence of organic acid, mainly acetic and formic acids [166] is the reason of corrosion of vessels, pipe lines and sealing materials.

The typical heating value of pyrolysis oil is about 16–19 MJ/kg, while some researchers reported higher heating values [167, 168]. To enable pyrolysis oil for industrial applications, the feedstock selection, pre-treatment, the improvement of pyrolysis unit, the upgrading of oil, the material selection and the ability to blend with other fuels should be taken into account [169, 170].

Solid products

Bio-char is a pyrolytic product which is a carbon-rich solid with some hydrogen and oxygen, and also alkali and alkaline earth matter. The operating conditions at a low temperature and low heating rate, the increasing particle size of the sample and the higher lignin content are promote the higher bio char yield [171]. Char can be activated by partial gasification with steam or CO_2 to increase their porosity or by chemical activation with zinc chloride or phosphoric acid [172]. When the pore structure and surface area of char are appropriate, they can be prepared for activated carbon applications. Activated carbon is widely used as an adsorbent in many applications such as toxic metal removal from water [173], taste- and odour-causing compound removal [174], removal or reduction of gaseous pollutants from the exhaust gas and removal of volatile organic compounds [175]. Besides absorbent applications, char can be used for catalyst support and base material for fertilizers [176]

Gaseous products

The main gases produced from pyrolysis are carbon monoxide, carbon dioxide and water. Other products are methane, ethylene, ethane, propylene, propane and methanol. The product yields and gas composition depend on temperature, residence time, and heating rate [177]. However, most of bio gas production is focused on the gasification process whose operating conditions support gas formation. The gaseous products with a low to medium heating value can be utilized into a combined heat and power (CHP) to produce electricity. Moreover, they can be upgraded to higher-value products such as methanol or gasoline but the conversion by gasification is more efficient.

Chapter 3

Formal kinetic parameters of pyrolysis process

3.1 Introduction to chemical kinetics

The rate of change in a quantity is defined as the derivative of that quantity with respect to time. The change of x at a time t_0 is $x(t_0+\delta t)-x(t_0)$; here δt is a very small time interval. From calculus, the rate of change of $x(t)$ at time t_0 is

$$\lim_{\delta t \to 0} \frac{x(t_0+\delta t)-x(t_0)}{\delta t} \equiv \left(\frac{dx(t)}{dt}\right)_{t=t_0} \quad \text{..... 3.1}$$

Chemical kinetics is the measurement and interpretation of the rates of chemical reaction. The study relates to following a reaction as a function of time with a suitable analytical technique by measuring the concentration of reactant or product during the progress of the reaction. The aims of chemical kinetics are not only to predict the rate of reaction from a function of state variables, but also to investigate reaction mechanism [178]. For benefits to industries, the kinetic data of the main reactions have been used for plant design since the reaction rates control the productivity, the cost of the product, and the profit of the plant [179].

During a chemical reaction, the concentration of reactants and products change in time. For example,

$$A + 3B \rightarrow 2C$$

The rate of the reaction above can be expressed as the change of the number of moles of each substance dividing by the stoichiometric coefficient.

$$Rate = \frac{-d[A]}{dt} = \frac{-d[B]}{3dt} = \frac{d[C]}{2dt} \quad \text{..... 3.2}$$

If the substance is a reactant, the expression shows with negative sign and with positive sign, if the substance is a product. In addition, the rate equation may take the form

$$Rate = k[A]^p[B]^q \quad \text{..... 3.3}$$

where k is the reaction rate constant and the exponents, p and q are the partial orders of the reaction. This relationship is based simply on the results of observation and experiment. The powers in the concentration terms of equation above are called the partial orders of reaction. While the overall order of reaction or reaction order (n) is defined as the sum of p and q.

$$n = p + q \quad \text{..... 3.4}$$

Most of kinetic studies are made under isothermal conditions to avoid any changes in the reaction rate due to temperature changes. Since Arrhenius discovered empirically that the rate constant is depending on temperature, the Arrhenius equation has been applied for kinetic studies [180].

$$k = A\exp(-E_a / RT) \quad \text{..... 3.5}$$

where A is the pre-exponential factor, E_a is the activation energy, T is the absolute temperature (K), and R is the gas constant.

3.2 Thermal degradation kinetics

The kinetics of thermal degradation processes have been widely studied via thermal analysis. It is referred to a group of techniques in which some physical properties of the sample are continuously measured as a function of temperature, whilst the sample is subjected to a controlled temperature change. By the nature of thermal analysis, the reactions are almost invariably heterogeneous reactions involving at least one initially solid reactant. For heterogeneous reaction, the concept of concentration of reactants or products does not play the significant role that it does in homogeneous reactions. Thus, the progress of reaction may be measured as the fractional reaction or degree of conversion (α). It is

defined in terms of the change in mass of the solid sample or equivalent definitions in terms of amounts of gas evolved or heat absorbed. If the change in sample mass is taken into account,

$$\alpha = \frac{m_0 - m(t)}{m_0 - m_f} \quad \text{.....} \quad 3.6$$

where m_0 is the initial mass; m_f is the mass of sample when reaction is completed; $m(t)$ is the mass at that stage.

Moreover thermal degradation kinetics of biomass can be carried out experimentally under either non-isothermal (dynamic) or isothermal (static) conditions [181]. These different conditions are achieved by the controlled reaction temperature. In the non-isothermal analysis, biomass samples are heated with time according to an assigned heating rate. On the other hand, under static analysis, the experiments are carried on at constant temperatures. Practically the measurement is either under very slow heating rate to prevent from the gradients of temperature, or under a condition of very fast external heat transfer rates [182]. The measurement at high heating rate reduces the non-isothermal stage of heating-up phase but it is affected from heat transfer limitations when the sample temperature is not controlled accurately. In the case of a slow-heating experiment, the weight loss during heating period cannot be neglected.

Isothermal measurements have several advantages in kinetic studies [28], which are: (i) changes in the mechanism are relatively easy to detect because decomposition rates are obtained for a single temperature and therefore a change in the order of reaction can be determined; (ii) the rate is possible to be calculated analytically; (iii) temperature of sample is exactly defined after attaining the isothermal temperature, the homogeneous sample temperature is reached [183]. However, some disadvantages of isothermal measurements need to be considered. Isothermal analysis requires a larger amount of sample for several experiments at varied reaction temperatures than that of non-isothermal measurement. This leads to the varied properties of sample [28]. In addition, during heating up period to reach a desired constant temperature, uncertainty arising from decomposition could occur.

Due to the drawbacks of isothermal measurements, non-isothermal or so-called dynamic measurements have been applied to kinetic studies. Non-isothermal analysis requires small sample size and small amount because the sample can be regarded as a fixed bed;

therefore, the heat transfer in the bed and the heat transfer within the particle are important. In addition, one measurement under non-isothermal conditions can give the data in a desired temperature range and it can be calculated to kinetic results quickly. However the non-stationary heat conduction causes the temperature gradient in the sample. The difficulties to determine the real sample temperature in non-isothermal measurement influence the accuracy in formal kinetic parameters evaluation [28, 29]. Also, it is difficult to maintain the high heating rates that are achieved in pyrolysis reactor.

In the last few decades non-isothermal methods have received more attention than isothermal methods. The main argument in favour of non-isothermal kinetic measurements compared with isothermal kinetic studies is their rapidity [32]. For fundamental studies, it was suggested that the non-isothermal kinetic data should be compared with the isothermal kinetic data for more accurate results [28]. The isothermal experiments are possible to separate unequivocally the temperature-dependent and concentration-dependent parts of a rate expression by experiments in which temperature and concentration are changing simultaneously. To enhance the ability of isothermal analysis, the improvement of measurement apparatus to overcome the drawbacks of isothermal method need to be considered.

The kinetic equation for solid-state reactions can be described as

$$d\alpha / dt = kf(\alpha) \quad \text{.......................................} \quad 3.7$$

where k is the reaction rate constant and α is the degree of conversion. The $f(\alpha)$ is the dependent kinetic model function or conversion function [31].

In thermal decomposition, the overall decomposition rate of a decomposing polymer can often be described by

$$d\alpha / dt = k(1-\alpha)^n \quad \text{.....................................} \quad 3.8$$

where n is the order of reaction. Hence, substituting equation (3.5) into equation (3.8), it becomes

$$d\alpha / dt = A\exp(-E_a / RT)(1-\alpha)^n \quad \text{...........................} \quad 3.9$$

For non-isothermal conditions, when the temperature varies with time as a constant heating rate $\beta = dT/dt$, the equation (3.9) is modified as

$$d\alpha / dT = (A / \beta)\exp(-E_a / RT)(1-\alpha)^n \quad \text{..... 3.10}$$

There are several methods for solving the kinetic equation. They can be classified roughly into the differential method and the integral method. The differential method requires the derivative of the measured mass-temperature curve with high signal to noise ratio. Smoothing can bias the calculation of kinetic parameters for a poor signal to noise ratio data. Integral methods overcome this disadvantage using the measured thermogravimetric data without differentiation. Nevertheless, these methods are not applicable at very low or very high degrees of conversion [31].

3.3 Techniques to study kinetics

Thermo-analytical techniques such as Thermogravimetry (TG) is based on the change in weight; while Differential Thermal Analysis (DTA) and Differential Scanning Calorimetry (DSC) are based on the change in energy of samples are the most common tools for kinetic studies of biomass pyrolysis. Although thermal analytical methods provide valuable information on pyrolytic kinetics, they cannot provide the nature and amount of volatile products formed during the thermal degradation of materials. For this reason, Evolved Gas Analysis (EGA) has been combined with the thermal analysis techniques to get more information on thermal degradation. Obtained evolutions of volatile products lead to the prediction on product formation and product yield. Apart from pyrolytic reactors in thermal analytic apparatus, several reactor designs have been developed for kinetic study at high heating rate and for eliminating the effects from operating condition and heat and mass transport phenomena.

3.3.1 Thermal analysis

Thermogravimetric analysers have been widely utilised in the study on thermal degradation of solid samples and a large literature is available. Measurement conditions of thermogravimetric analyser can be performed by non-isothermal and/or isothermal methods. In principle, TG curve from one heating rates is sufficient for these calculations but in practice, the experiment should include three or more different heating rates measurements for an accurate statistical manipulation and solving the compensation effect [184].

For the experimental set-up, the sample size should be sufficiently small to avoid a thermal difference between the sample and the thermogravimetric system. The feature of thermobalance should have the optimum position of a thermocouple to provide the actual temperature of the sample. Thus, its position should be located closed to sample. Also the temperature calibration is necessary to ensure that the equipment gives the actual temperature of the sample. The feature of a horizontal thermogravimetric analyser is shown in figure 3.1.

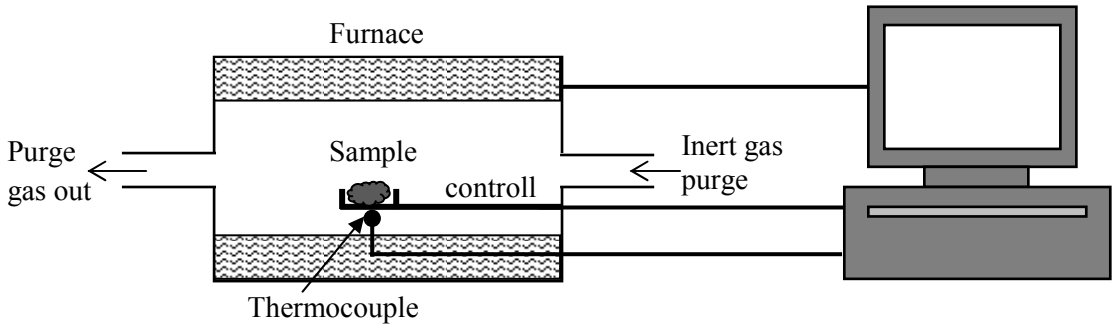

Fig. 3.1 The diagram of a horizontal Thermogravimetric analyser

The most relevant linear forms to solve the rate equation from TG data are the method of Freeman and Carrol [185], Coats and Redfern [186], Friedman [187]. Conesa, et al. [188] mentioned the general concerns of these methods, which are:

(i) The temperature is measured by the thermocouple; it is not the actual temperature.
(ii) These methods are appropriated for a single process.
(iii) The raw data from TG are very much manipulated
(iv) Most of these methods can solve the rate equation from one heating rate data

Furthermore, heat transport has been repeatedly cited as a limiting factor of the flash pyrolysis in TG. This could result in the apparent shift in biomass pyrolysis kinetics. Due to the low heat transfer, kinetic has been measured at relatively low operation temperature instead of the heating time of a particle. If the heat transfer effects cannot be neglected, the chemical kinetic model should be considered together with the heat transfer equations [184].

Differential Scanning Calorimetry (DSC) is another technique to apply to kinetic studies. DSC reflects the difference in the amount of heat added to a sample and reference is

plotted as a function of the temperature if the temperature is changed, or as a function of time for isothermal operation. The heat flow to or from the sample depend on whether the process is exothermic or endothermic. The integral or area of the DSC peak indicates the proportion of the transition heat for a particular reaction and the change in heat capacity involves the enthalpy change of the reaction [189-191]. The apparent activation energy can obtain from the DSC data at different heating rates [192].

3.3.2 Evolved gas analysis (EGA)

Evolved gas analysis becomes the most useful technique with two approaches: simultaneous analysis and combined analysis [193-196]. In the simultaneous analysis approach, two methods are employed to examine the materials at the same time. One of these methods can identify the volatile compound produced during the analysis simultaneously. The combinations for the simultaneous analysis are; for example, Thermogravimetric analyser coupled with a Fourier transform infrared spectrometer (TG-FTIR) [197, 198], Pyrolysis reactor coupled with a Mass Spectrometer (Py-MS) [199], and Thermogravimetric analyser coupled with a Mass Spectrometer (TG-MS) [200] on-line analysis. For combined analysis technique, more than one method is applied to analyse the sample and real time analysis is not possible. Trapped evolved gaseous species are then introduced into a detector for identification, such as a Thermogravimetric analyser coupled with Gas Chromatographer and Mass Spectrometer (TG-GC-MS) [201] or a Pyrolysis reactor coupled with Gas Chromatographer and Mass Spectrometer (Py-GC-MS) [202].

Radmanesh, et al. [203] measured the evolution of certain condensable vapours and non-condensable gases by gas chromatography technique. It was observed that the final total yield of gases increase but tar decrease by increasing the heating rate. A simple one step reaction had been used for the kinetic of each gas evolution during the pyrolysis:

$$dV_i / dt = A_i \exp(-E_{ai} / RT)(V_i^* - V_i) \quad \ldots\ldots\ldots\ldots\ldots\ldots\ldots\ldots\ldots\ldots 3.11$$

where, V_i is the yield of gas component at time *t* and V_i^* is the ultimate attainable yield for each gas. Then they proposed a kinetic model which can predict the change of the gases yield at different heating rates.

The utilisation of an evolved gas-FTIR apparatus for kinetic study in pyrolysis of biomass and coal have been published by Wójtowicz and co-workers [204-207]. They studied the

pyrolysis of both biomass and coal by TG-FTIR. Kinetic parameters were calculated based on parallel independent first-order reactions with a Gaussian distribution of activation energies. Each evolution peak was assumed to involve the respective precursor in the original biomass sample. Thus, each volatile species could evolve as one or more peaks independently. However, the model still needs further improvement by addressing the appropriate reaction mechanism, the mass influence, and the cross-linking competitive reactions. Moreover, Banyasz, J.L., et al. [149, 152] studied the mechanism and kinetic of cellulose pyrolysis by an evolved gas analysis-FTIR apparatus under non-isothermal condition with rapid heating rate from 400 to 800°C. The kinetic analysis was based on the peak areas and the peak temperatures of calculated evolution profiles of main produced volatiles (formaldehyde, hydroxyacetaldehyde, CO and CO_2).

Müller-Hagedorn, et al. [208] examined the pyrolysis of three different woods by TG-MS. Due to the difficulty to separate lignin from wood, they applied specific ion fragment range (105–212 u.) representing lignin-derived products under non-isothermal conditions. The degree of conversion (α) can be calculated as

$$\alpha(T) = \frac{\int_{T=100°C}^{T} \sum_{i=1}^{N} I_i(T) M_i(T) dT}{\int_{T=100°C}^{T=500°C} \sum_{i=1}^{N} I_i(T) M_i(T) dT} \quad \text{..... 3.12}$$

where N is the number of ion fragments, $I_i(T)$ is the ion current of the ith ion fragment, and $M_i(T)$ is the molecular mass of the ith ion fragment.

Bockhorn and co-workers [28, 30, 183] researched the thermal decomposition of polymers under isothermal condition by similar technique applied in this work. The evolved gas analysis by means of on-line mass spectrometry provided the evolution data for calculating the formal kinetic parameters. The degree of conversion at a time ($\alpha(t)$) can be expressed as

$$1 - \alpha(t) = m(t) / m_{tot} = 1 - \frac{\int_0^t I(t)\overline{M}(t)\dot{V}dt + I(t)\overline{M}(t)V_R}{\int_0^\infty I(t)\overline{M}(t)\dot{V}dt} \quad \text{..... 3.13}$$

where $m(t)$ is the actual mass at that stage and m_{tot} is the total evolved mass. $\overline{M}(t)$ is the mean molecular mass at time t, $I(t)$ is the intensity of ion fraction, $\dot{V}$ is the flow rate and

V_R is the reactor volume. A good agreement between the formal kinetic parameters from isothermal measurement and the ones from non-isothermal measurement by TG was reported [28]. In addition, an advantage from isothermal method is that the change in mechanism can be determined.

The Distributed Activation Energy Model (DAEM) has been used to model the evolution of individual pyrolysis product from different precursors in a set of simultaneous first-order reactions. Rostami, et al. [209] employed a DAEM to represent the complex reactions of biomass pyrolysis and the evolution of different volatile species with the input data from TG-FTIR or TG-MS analysis. Also, Várhegyi, et al. [210] described the overlapping curves from DTG and mass spectrometric intensity curves by DAEM, as well as the evolution of volatile products were well detailed.

3.3.3 Developed experimental reactors

In addition to the thermogravimetric analysis, heated grid experiments, drop tube experiments, and shock tube experiments, which are composed of a heating device and a mass loss recorder, can be used to study biomass reactivity under pyrolysis conditions. Thermogravimetry is appropriate for thermal decomposition of biomass at low heating rate but under flash pyrolysis at high temperature, drop tube, tubular reactors, screen heater, radiant heating techniques, and fluidized bed reactors are more suitable than TG.

Heated-grid reactor has been used for studying pyrolysis kinetics of solid fuel materials at high heating rate [211-214].The samples are placed on the wire mesh, which is electrically heated and is connected to a thermocouple for measuring its temperature. The mass loss can be recorded by gas analysis [215] or two measurements on a balance before and after the experiment [216]. Due to their operation at high heating rate, the weight loss during heating period can be minimized. Thus, the reactivity of sample is not changed before reaching a final temperature. The volatile products will be quenched at a cold gas phase to minimize secondary reactions. However this reactor needs to be used with some concerns. A fine powder is typically suitable as the particle size of sample should be small enough to avoid the temperature gradient and the amount of sample for each run is limited because of the restriction of the thermal load on the grid. Also sample particles should be applied over the grid with the same small thickness layer evenly.

Drop tube experiments heat the particles by convention and radiation at high temperature and high heating rate [217, 218]. Very small biomass particle about a few hundred micrometres are added together with inert gas stream or air to furnace at high temperatures. Hence these small particles are heated up rapidly and this causes a short heat-up time compared to the reaction times which it can be determined as the isothermal during the degradation process. Downstream of the drop tube reactor is quenched with N_2 and is collected and measured the weight [184, 219, 220]. This experiment is a time consuming procedure and introduces some errors from taking quenched products to the determination for the kinetic data. The large particle size of sample may cause a discontinuous feeding of the solid samples; while the small particle size may create a problematic pneumatic transport. The thermal profile from this reactor is very narrow of isothermal conditions at only the centre of the reactor and lower temperature than the oven value due to the thermal dispersion from extremities effects. Also the gas flow rate may influences to the thermal profile. The residence time can be measured only with a rough precision and at room temperature [221].

Over the last five decades, the shock tubes have been applied to the study of aerodynamic and high temperature kinetic studies in both homogeneous and heterogeneous systems [222]. The benefit on the kinetic study of the shock tube is the rate coefficient obtaining under diffusion free conditions because this reactor provides a nearly one-dimensional flow with instantaneous heating of reactants [223]. A shock tube consists of a uniform cross-section tube divided into a driver and driven sections. The driver section is high pressure with a low molecular weight gas and the driven section is filled with test gas at low pressure. The particle is heated using the energy contained in pressurized gas. The mass loss is recorded using gas analysis [224].

A tubular reactor is a simple flow reactor operating at constant pressure. This reactor is a cylindrical pipe of constant cross-section where the feed enters at one end and the product stream leaves at the other end. The lack of providing of stirring prevents complete mixing of the fluid in the tube which is the opposite assumption from that of the ideal stirred tank reactor. Composition is the same at all point in a given cross-section but changes along the axial coordinate of the tube. The literatures on using tubular or closed-tubular reactor [225] for thermal degradation and kinetic studies have been published in bioenergy research [226-230].

For the fluidized bed reactor, the biomass sample is injected in a pre-heated bed of inert particles. The progress of reactions can be measured from the withdrawn sample from the bed at different times. The feature of this reactor that biomass particles are mixing with bed material restricts the determination of decomposition rate at short residence times [184]. The produced gas flow can be analysed by evolved gas analysis connection, i.e. FTIR, FID (flame ionization detector), NDIR (non-dispersive infrared photometer) [231].

In addition, there are other types of reactor which have been facilitated in the thermal degradation researches, such as laminar entrained flow reactor [232-234], plasma pyrolysis [235, 236], closed loop-type reactor [28].

3.4 Influences on biomass reaction kinetics

The nature and rates of lignocellulosic decomposition reactions are affected by certain process variables, such as temperature, heating rate, particle size, and the presence of inorganic mineral content within the biomass material, and together with heat and mass transport limitations [20]. These factors on the thermal degradation kinetics are linked.

3.4.1 Heat and mass transport

When a solid particle of biomass is exposed to high temperature operation, external heat is transmitted to the particle surface by radiation and/or convection and then heat conduction takes place in the biomass particle from the surface to inside of the particle. At first in vaporization step, the flow of water vapour is controlled by diffusion and convective and diffusive transport. Then the chemical reactions of pyrolysis process occur. The heat changes from pyrolysis reactions and phase changes cause the temperature profile inside the particle. Volatile and gaseous products migrate from the solid across the heat-exposed surface and involve the heat transfer phenomena. Three combined mechanisms of heat transmission inside the pyrolyzing solid are the conduction through the solid particle, the radiation from the pore walls, and the transmission through the gas phase inside the particle pores. After volatiles leave the solid phase, char is formed by the change of physical structure of the reacting solid to develop a network of cracks, particle volume shrinkage, surface regression, and swelling [20, 23, 237]. Therefore, the model to describe

the thermal decomposition has been studies not only the reaction kinetics, but also including the effect from heat and mass transport phenomena [238-242].

3.4.2 Heating rate

Although there are some evidences supporting that heating rate has a small impact on the frequency factor, the dependence of biomass pyrolytic kinetics on heating rate is available [20]. Biagini, et al. [243] divided the activation energy into two sets of data, at low heating rate and high heating rate. For all materials and using all methods, the activation energy at low heating rate was found higher than that at high heating rate with respect to overall values. Haykiri-Acma, et al. [244] reported the effect of heating rate of the rate of mass loss that when the heating rate increases, the maximum rates of mass losses increase and heating rate also affects to the shape of the peaks from thermal analysis. Obviously, the higher heating rate shifted the main peak of DTG profile to the higher temperatures. It could be explained by the heat transfer inside the biomass particles. At low heating rate, a number of peaks can appear individually in small peaks. When heating rate go higher, some of them overlap and form a unique large peak.

3.4.3 Particle size

Particle size of biomass is fundamentally linked to heat and mass transfer. The induction period at the initial stage of the weight change data from isothermal measurements shows the low velocity of decomposition which is attributed to the heating of the particle. The large particle size prolongs the induction period due to the longer time of heat transfer from outside to particles and within particles. Jalan and Srivastava [245] observed that pyrolysis process was controlled by the primary pyrolysis reactions and external heat transfer for small particle size (<1mm); while large particle size (>1mm), the process was controlled by heat transfer, primary pyrolysis and secondary pyrolysis.

For small sample size, the large surface area improves heat and mass transfer. Thus, its fast heating rate causes more light gases and less char and condensate formation [246]. The uniform radial product distribution would result from the neglected temperature gradient between the surfaces and centres of the small biomass particle [247]. On the other hand, the large particle size prolong the resident time of volatile molecules from primary reactions inside the solid particles that enhances the secondary reaction [237].

3.4.4 Catalytic effect of inorganic material

Biomass contains various amounts of mineral matter. The mineral constituents of biomass can include Si, Ca, K, Na and Mg, with smaller amount of S, P, Fe, Mn and Al. These inorganic elements are available as oxides, silicates, carbonates, sulphates, chlorides and phosphates [248]. Some of these inorganic elements act as a catalyst affecting the rate of degradation [249]. Results from studies on the effect of catalyst informed the enhanced formation of char and gaseous products and inhibited formation of the volatile products. Also, inorganic contents promote secondary reactions which break down higher molecular compounds to smaller ones.

Several inorganic matter have been studied their catalytic effect on degradation. Potassium (K) was found to shift the pyrolysis to a lower temperature and lower activation energies [250]. In addition, sodium (Na) is another inorganic matter which was reported for its catalytic influence [251]. It is clear from Ayhan [252] that the different effects on pyrolysis between K_2CO_3 and Na_2CO_3 depended on the biomass species. Blasi, et al. [253] found that the pre-treatment to remove ash content shifted the initial degradation temperature slightly higher with a higher peak rate.

3.5 Variations in kinetic data

The widely scattered values of the activation energy and pre-exponential constant in the literature and the systematic temperature shift of data from thermogravimetric analyser called attention to the concern of the kinetics. The potential role of varied systematic errors in temperature measurement among the various thermobalances and the compensation effect are the reported explanations of these disagreements.

3.5.1 Compensation effect

The Arrhenius equation is widely used in heterogeneous kinetics because it has been well established in homogeneous kinetics and the constants in the equation can be calculated. A correlation between the observed values of the frequency factor and the activation energy, a change in one Arrhenius parameter is compensated by a correspondent change in the

other, is commonly called as the 'kinetic compensation effect' (KCE) [254]. This compensation is usually expressed as

$$\ln A = aE + b \quad \text{..... 3.14}$$

where a and b are constants. The linear relation showing kinetic compensation effect is also derived from the Arrhenius equation:

$$\ln A = \ln k_i + E_a / RT \quad \text{..... 3.15}$$

where k_i is called the isokinetic constant and T_i is called the isokinetic temperature or compensation temperature.

It has been recognized that different sets of kinetic parameters can describe similar conversion degree curves once a kinetic model has been selected but it is not necessarily that all of them have the same grade of accuracy [255]. Flynn [256] reviewed that either the result of scatter of the experimental data, misapplication of kinetic equations, or errors in the experimental procedures can be the reasons for the presence of kinetic compensation effect when studying identical specimens under the same conditions. Agrawal [257] also concluded that the inaccurate temperature measurement and large temperature gradients within the sample cause the compensation behaviour in the pyrolysis of cellulosic materials. Later, Narayan and Antal [258] revealed that as thermal lag increases, the ratio of E_a/log$A$ also increases.

Recently, Wang, et al. [259] reported the existence of kinetic compensation effect in their both low-and high-temperature stage of pyrolysis of seaweed. Várhegyi, et al. [260] reduced the compensation effect on their study by eliminating the number of unknown parameters. Moreover, [261], [262] and [206] reported evidence of compensation effect on their studies.

3.5.2 Thermal lag

In the design of furnaces or thermogravimetric analysers, the thermocouple is located closed to sample to reduce the thermal lag. Thermal lag (ΔT_{TL}) is the difference between the measured sample temperature (T_e) and the true sample temperature (T_s).

$$\Delta T_{TL} = T_e - T_s \quad \text{..... 3.16}$$

The pyrolysis reactions demand the reaction heat which increases sharply when the sample temperature rises. There is the competition between the reaction heat demand and the heat demand for the limited heat supply. The factors affect to the thermal lag problem are heating rate, the placement of the thermocouple, the size of the sample, the composition of the carrier gas, and the endothermicity of the reaction [258, 263]. As external heating rate increases or low heat-transfer coefficients, the measured temperature may slightly higher than actual temperature and the effect on thermal lag increases [264]. Grønli, et al. [265] reviewed the differences in kinetic parameters which were obtained from different heating rates could be attributed to thermal lag. They found that a small reduction of sample size led to the decreasing of the systematic error due to thermal lag but increased the values of E_a and log A, which agree with the hypothesis that 'thermal lag is largely responsible for the decrease in values of E_a and log A at higher heating rates.'

3.6 Literature review on kinetics of lignocellulosic components

3.6.1 Cellulose

The pyrolytic kinetics of cellulose, which is a main composition in biomass, has been widely studied for the past several years [31, 146, 147, 264-275]. Thermogravimetric analysis is the most widely used technique for the study of cellulose pyrolysis. The understanding of total mass loss for global pyrolytic kinetics is generally intended to predict the overall rate of volatiles release from the solid and it can be applied to mechanism study. The reported activation energy values of several cellulose samples, which depend on the sample origin and processing, the calculation method, the experimental conditions, vary from 48 to 282 kJ/mol [270].

Milosavljevic and Suuberg [276] concluded that the global kinetics of cellulose decomposition tends to cluster into two certain groups, depending on experimental setup and heating rates. The isothermal kinetic studies and high heating rate experiments showed the lower activation energy than the experiments with slow heating rates. Serious heat transfer limitations and associated temperature measurement problems were identified as the cause of this variation of kinetic parameters. Similarly, Grønli, et al. [265] studied kinetic pyrolysis of Avicel cellulose with thermogravimetric analysers at 5 and 40 °C/min. Kinetic analyses based on an irreversible, first-order reaction of the 40 °C/min data resulted in values of E_a range from 211 to 232 kJ/mol and values of $\log(A/s^{-1})$ between 16.1 and 17.9 which were somewhat lower than those obtained at 5 °C/min, the apparent activation energy was in the range from 234 to 263 kJ/mol and values of log (A/s^{-1}) lie between 17.8 and 21.1. The decrease of E_a and log A values at higher heating rate was attributed to the higher impact on thermal lag. Some studies suggest that inter-particle diffusion or evaporation limitations, as the latent heat of vaporization for pyrolysis tars (levoglucosan) is around 140 kJ/mol, cause the slower rate [277, 278].

Table 3.1 shows some published kinetic parameters of cellulose under thermal degradation experiments. More recently, Carpart, et al. [273] studied the pyrolysis of microcrystalline cellulose with TGA with two different modes of heating: non-isothermal and isothermal modes. From isothermal measurements, it showed the kinetics of nuclei-growth which was represented by the models of Avrami-Erofeev (A-E) and of Prout-Tompkins (P-T) type. From non-isothermal measurement, they simulated a model with two parallel reactions, one was related to the bulk decomposition of cellulose and another was related to the slower residual decomposition.

Table 3.1 Reported kinetic parameters of the pyrolysis of cellulose samples

Ref.	Sample	Experiment	Temperature	E_a (kJ/mol)	log$A$ (1/min)	n
[270]	Microcrystalline cellulose	TG/DSC	50-800°C	198	14.8	1.0
[279]	Cellulose	TG	350-400°C	282	24.9	2.0
[279]	Cellulose	TG	280-350°C	82.7	7.45	1.0
[264]	Cellulose (Whatman CF-11)	TG; 9 mg; 65°C/min	250–550°C	174	12.88	1.0
[264]	Cellulose (Whatman CF-11)	TG; 0.3 mg; 65°C/min	250–550°C	209	16.28	1.0
[264]	Cellulose (Whatman CF-11)	TG; 0.3 mg; 1°C/min	250–550°C	249	20.28	1.0
[280]	Cellolusic fabrics	TG, major stage	306-364°C	113-196	9.56-16.77	1.0
[273]	Microcrystalline cellulose	TG, bulk decomposition	25-700°C	202.65	17.07	1.0
[31]	Cellulose powder	TG, dynamic	25-700°C	156.5-166.5	8.69-9.99	1.0
[31]	Cellulose powder	TG, isothermal	305, 316, 326 & 343°C	150.6	11.64	0.39-0.49
[281]	Paper dunnage	Pyromat	25-700°C	168.0	13.73	1.0
[281]	Fibrous cellulose	Pyromat	25-700°C	180.6	14.48	1.0
[276]	Cellulose (Whatman CF-11)	TG, dynamic	> 330°C	140-155	11.78	0-1.0
[22]	Avicel cellulose	TG	25-900°C	201	16.8	1.0

3.6.2 Hemicellulose

Apparent kinetic parameters of the pyrolysis of hemicellulose have been analysed from its representative compound as xylan or from the subtraction from the pyrolysis of wood samples. Approximately the activation energy for the decomposition of hemicelluloses is lower than that of cellulose but it is higher than the activation energy of lignin [282]. Most of kinetic studies on hemicellulose pyrolysis carried on the non-isothermal condition by thermogravimetric analyser. The two-step process from TGA curves has been observed [208, 283]. Várhegyi, et al. [283] described the double peaks observed from hemicelluloses decomposition by a successive reaction model which led to a good fit to the experimental data. Müller-Hagedorn, et al. [208] determined the formal kinetic parameters of the main components in three different wood species by TG-MS pyrolysis. Hemicellulose presented two steps of decomposition. The difference in kinetic parameter values from different wood influences from the compositions of wood. The reported kinetic parameters of hemicelluloses as a main component in wood have been published from several researchers. Some published kinetic parameters of hemicellulose are presented in table 3.2. Cozzani, et al. [284] subtracted the hemicelluloses decomposition curve from the global curve of wood pyrolysis. A simple first-order kinetic model was applied to calculate its activation energy (72.8-103.2 kJ/mol).

The majority of the available kinetic studies point to a poor fit of simple reaction models in the whole range of conversion and the change in mechanism cannot be detected. The discrepancy in the reported activation energies of hemicelluloses can be explained by the difference in sample composition, experimental setting, the mathematical method to analyse data, and the possible interference of the lignin decomposition [285]. The kinetic parameters obtained from simple model tend to be lower than those from the complex models.

Table 3.2 Reported kinetic parameters of the pyrolysis of hemicellulose samples

Ref.	Sample	Experiment	Temperature	E_a (kJ/mol)	log$A$ (1/min)	n
[285]	Hemicellulose (bagasse)	TG	Up to 900°C	194	17.5	1.0
[286]	Xylan	TG/DSC-MS	200-400°C	168 104	17.18 9.08	1.0 1.0
[208]	Hemicellulose (Hornbeam)	TG-MS	150-450°C	163 257	14.6 20.4	1.7 0.8
[208]	Hemicellulose (Walnut)	TG-MS	150-450°C	175 262	15.8 20.9	1.8 0.8
[208]	Hemicellulose (Scots pine)	TG-MS	150-450°C	101 262	8.1 20.9	0.7 0.8
[282]	Hemicellulose (Rice hulls)	TG	230-350°C	154	13.9	1.0
[283]	Xylan	TG, 10 & 80°C/min	200-400°C	193-194 81-84	18.7-18.8 7.3-7.6	1.0 1.0
[24]	Hemicellulose (pinewood) Hemicellulose (Eucalyptus) Hemicellulose (pine bark)	Simulated isothermal curves from dynamic TG	450-700°C	89.0 80.4 49.3	7.60 6.82 3.49	1.0 1.0 1.0
[155]	Milled xylan	Radiant heating pyrolyzer	200-340°C	76.86 55.02	7.34 4.36	1.0 1.0

3.6.3 Lignin

There are widely different values for the activation energy of lignin pyrolysis: 35-65 [283], 18-20 [287], or 34-36 kJ/mol [282]. In the review of Ferdous, et al. [288], the kinetic parameters of lignin have been calculated by static and dynamic measurements under assuming first-order reaction. The activation energy was mostly reported in the range that lowers than 50-80 kJ/mol. However there are some articles presenting the lower activation energy values at 30-65 kJ/mol [282, 283]. Recently, Murugan, et al. [289] reported the wide range of activation energy between 33-285 kJ/mol. The causes of this wide range of reported activation energy are operating conditions (temperature, heating rate, and the nature of carrier gas) and the nature of lignin (composition, functional groups, and separation method) [49, 288]. Table 3.3 shows some kinetic parameters from literature. In addition, Jiang, et al. [49] indicated that the reaction order strongly depended on the separation method but slightly on the plant source of lignin but the frequency factor was independent from both factors.

Pasquali and Herrera [290] studied several lignins in isothermal pyrolysis in the temperature range between 226 and 435 °C and they applied the Avrami-Erofeev equation for solid state reactions. They found activation energies of lignins were in the range of 12.49-42.60 kJ/mol. Ferdous, et al. [288] carried out the pyrolysis experiments in a fixed-bed reactor and in a thermogravimetric analyser (TGA). The complex process of lignin pyrolysis was analysed by the distributed activation energy model (DAEM). The kinetic analysis of lignin pyrolysis in a fixed-bed reactor gave the activation energy for Kraft lignin in the range of 17-89 kJ/mol; while the activation energy calculated from DAEM was in the range of 80-158 kJ/mol. The small activation energy obtained from the fixed-bed reactor indicated the presence of mass and heat transfers effect.

Table 3.3 Reported kinetic parameters of the pyrolysis of lignin samples

Ref.	Sample	Experiment	Temperature	E_a (kJ/mol)	log$A$ (1/min)	n
[279]	Lignin	TG, dynamic	300-390°C	67	6.51	1.0
	Lignin	TG, dynamic	390-500°C	70.7	7.10	2.0
[282]	Lignin (rice hull)	TG, dynamic	150- 900°C	34	1.7	1.0
[288]	Kraft lignin	TG, dynamic, DEAM	234-503°C	80-158	7.5-9.3	1.0
[291]	Ligin (organosolv)	TG, dynamic	30-900°C	18.86-42.47	n/a	0.30-0.74
[290]	Lignin (Klason)	TG, isothermal	226-435°C	12.49-42.60	n/a	0.5
[292]	Alcell lignin	TG, dynamic	25-700°C	83-195	n/a	1.0
[293]	Lignin (Milled wood)	Microreactor(fixed bed)	500-1000°C	82.0	7.30	1.0
[294]	Lignin (birch)	Microreactor (fixed bed)	300-600°C	75	6.16	1.0
[295]	Kraft lignin(pine)	Microwave reactor (isothermal)	160-680°C	25.2	2.67	1.0

3.7 Literature review on kinetics of algae

Compared to the literature on kinetics of lignocellulosic materials, there is a limited literature concerning the pyrolytic kinetics of algae (microalgae and macroalgae). The proper understanding of their thermal properties and reaction kinetics are crucial for the efficient design, operation, and modelling of the pyrolysis, and related thermochemical conversion systems for algae. Like the kinetic studies of lignocellulosic materials, most of kinetic studies in algae are based on the non-isothermal condition assessed by thermogravimetric analysers. The pyrolysis of algae is a multi-step process and the reported activation energy of algae pyrolysis vary and the reaction orders are higher than n=1 (see Table 3.4).

Peng, et al. [296] studied the kinetic characteristics of heterotrophic *Chlorella protothecoides* by a thermogravimetric analyser. They observed that the devolatilization consists of two main temperature zones, lipid decomposition and other main components (i.e. protein) decomposition. The activation energy for the devolatilization stage was in the range of 113–127 kJ/mol; while that of the high temperature zone was in the range of 126-158 kJ/mol. The microalgae were devolatilized at lower temperature range than those of lignocellulosic materials, which was economically feasible. Also, Peng, et al [297] compared the kinetics of *Spirulina platensis* and *Chlorella protothecoides* microalgae. As the heating rate increased, the reaction rate in the devolatilization stage increased but the activation energy decreased. The reported activation energy for *Chlorella protothecoides* was 42.2-52.5 kJ/mol, which was lower than that of *Spirulina platensis* (76.2–97.0 kJ/mol).

Shuping, et al. [298] determined the pyrolysis of *Dunaliella tertiolecta* in a thermogravimetric analyser. The iso-conversional method and the master-plots method were used for kinetic analysis. The master-plots method gave an *Fn* model (*n*th-order) as the most probable reaction mechanism. While Li, et al. [299] described the pyrolytic mechanism by Avramic-Erofeev equation for the pyrolysis of three kinds of red algae; *Pophyra yezoensis*, *Plocamium telfairiae* Harv and *Corallina pilulifera*. In both of these articles, researchers suggested that the thermal behaviour was influenced by compositions of biomass. The relationship between the apparent activation energy and pre-exponential factor could be explained by the kinetic compensation effect.

Table 3.4 Reported kinetic parameters of the pyrolysis of algae

Ref.	Sample	Experiment	Temperature	E_a (kJ/mol)	Log$A$ (1/min)	n
[296]	*Chlorella protothecoides* (heterotrophic)	TG; 15, 40, 60, 80°C/min	160-340°C 340-520°C	113-124 127-150	9.7-10.5 10.2-12.2	1.37-1.57 1.01-1.61
[297]	*Chlorella protothecoides*	TG; 15, 40, 60, 80°C/min; Freeman-Carroll method	150-540°C	42.2-52.5	6.3-8.0	1.55-1.98
[297]	*Spirulina platensis*	TG; 15, 40, 60, 80°C/min; Freeman-Carroll method	190-560°C	76.2-97.0	3.5-4.0	1.25-1.88
[300]	*Enteromorpha prolifera*	TG; 10, 20, 50°C/min; Freeman-Carroll method	174-551°C	228.1	21.7-27.5	2.2-3.7
[298]	*Dunaliella tertiolecta*	TG; 5, 10, 20, 40 °C/min; isoconversional & master-plots methods	155-299°C	146.1	13.36	2.4
[299]	*Porphyra yezoensis*	TG/DSC; 10,30,50°C/min; Popescu method	170-400°C	163.7	11.7-15.8	3.0
[299]	*Plocamium telfairiae* Harv	TG/DSC; 10,30,50°C/min; Popescu method	180-380°C	261.2	17.3-28.5	3.0
[299]	*Corallina pilulifera*	TG/DSC; 10,30,50°C/min; Popescu method	170-390°C	245.7	17.5-29.2	3.0
[259]	*Enteromorpha clathrata*	DTG -Thermal analyzer; 20, 30, 40, 50 °C/min; Coats-Redfern method	170-330°C 290-580°C	228.7-245.3 85.90-96.48	21.66-22.53 6.57-7.48	A 2.0
[301]	*Laminaria jajponica*	TG/DSC; 10, 30, 50°C/min; Popescu, FWO & KAS methods	190-370°C	207.7	14.72-21.27	3.0 (B)

[301]	*Sargassum pallidum*	TG/DSC; 10, 30, 50°C/min; Popescu, FWO & KAS methods	170-420°C	202.9	13.70-29.94	3.0 (*B*)
[302]	Floating *Enteromorpha clathrata*	TGA; 5,10,15,20,25°C/min; Coats-Redfern method	227-273°C 273-504°C	165.32 27.49	15.18 3.88	*B* 2.0
[302]	*Ulva lactuca L.*	TGA; 5,10,15,20,25°C/min; Coats-Redfern method	211-260°C 260-571°C	192.26 27.22	17.38 3.65	*B* 2.0
[302]	*Zosterae Marinae L.*	TGA; 5,10,15,20,25°C/min; Coats-Redfern method	218-260°C 260-620°C	50.29 35.46	2.53 4.49	*B* 2.0
[302]	*Thallus Laminariae*	TGA; 5,10,15,20,25°C/min; Coats-Redfern method	220-290°C 290-561°C	215.96 28.49	19.90 3.98	*B* 2.0
[302]	*Asparagus schoberioides kunth*	TGA; 5,10,15,20,25°C/min; Coats-Redfern method	227-281°C 281-560°C	205.60 32.81	20.23 4.20	*B* 2.0
[302]	*Undaria pinnatifida (*Harv.*)*	TGA; 5,10,15,20,25°C/min; Coats-Redfern method	235-270°C 270-527°C	214.91 30.18	21.70 4.07	*B* 2.0
[303]	*Chlorococcum numicola*	Thermobalance; 5,10,20°C/min; distributed activation energy model	200-525°C	189.15-190.02	17.83-18.19	6.63-7.88

A : three dimensional diffusion; *B* : Avrami-Erofeev

The wide range of reported kinetic parameters can be related to several aspects. It is often expected to describe a solid state decomposition by a single set of kinetic parameters and the isothermal and non-isothermal values are expected to be equal. However, the nature of solid state processes is the multi-step reactions which contribute to the overall reaction rate that can be measured in thermal analysis. The complexity of thermal decomposition in solid samples is a cause of the variation in reported data. Moreover, there are several approaches to evaluate kinetic data. The model-fitting approach from a single heating rate is considered to give highly uncertain values due to its dependence on both the temperature and the reaction model. Apart from the difference in computational methods, the kinetic parameter depends strongly on the experimental conditions, such as the inert flow rate, temperatures, atmosphere, and sample size. The difficulty to measure a real sample temperatures and heating rates also cause the discrepancy in kinetic values. Thus, the kinetic study should be carried out at kinetically controlled conditions to minimize the uncertainty from experimental conditions and also the evaluation should be taken into account the multi-step mechanisms of the solid state decomposition.

Chapter 4

Characteristics of Lignocellulosic components

In this chapter, the experimental, as well as the result and discussion on the characteristics of lignocellulosic main components (cellulose, hemicelluloses and lignin) are presented in detail. Proximate and ultimate analysis together with the thermal behaviour analysed by thermogravimetric technique of these three materials are given and discussed based on their application in thermo-chemical conversion process.

4.1 Materials

The samples used in this study were three commercial products: Whatman filter paper, Xylan, and Alkali lignin which represent cellulose, hemicellulose and lignin, respectively (see figure 4.1). Whatman No.44 filter paper (Whatman International England) is 0.007 % of ash with content of at least 98% alpha cellulose and has a thickness of 176 μm. Filter paper was cut into rectangular (less than 1×1 mm^2) to minimize the effect from particle size. It is difficult to obtain a commercial hemicelluloses sample, thus xylan has been widely used as a representative of hemicelluloses of hardwood in pyrolysis study [156, 286, 304, 305]; although different physical and chemical properties have been found depending on the source material and production method. In this study, xylan (poly (β-D-xylopyranose [1→4]) powder as the commercial product extracted from birch wood (Sigma Chemical Co.) with xylose residues at least 90% was used. An alkali lignin powder (Sigma Chemical Co.) was used as a source of lignin in this study which has a low sulphonate content and molecular weight of 10,000 u. All samples without further treatments were stored in desiccators until use.

Fig. 4.1 Filter paper, Xylan and Alkali lignin samples representing cellulose, hemicellulose and lignin, respectively, used in this work

4.2 Proximate and Ultimate analysis

4.2.1 Experimental

Proximate analysis for filter paper, xylan and lignin was conducted using a thermogravimetric analyser (TGA/DSC1 STAR^e system, Mettler Toledo). Ten milligrams of sample were used for each measurement. All measurement comprised three different steps which were the drying and the devolatilization in helium atmosphere and the combustion in air atmosphere at gas flow rate 100 ml/min. Moisture content was considered as the mass loss when the sample was heated till 105°C and this temperature was maintained for 10 minutes. Then the devolatilization stage was measured at 600°C by heating rate at 20°C/min. The combustion process of the remaining solid samples was carried out under air atmosphere at 20°C/min to 900°C. The fixed carbon fraction was calculated by subtracting the percentages of volatile matter, moisture content and ash from 100%. Each measurement was repeated three times to check the reproducibility.

The elemental compositions of filter paper, xylan and lignin were analysed by Medac Ltd where the C, H, S and N analysis was carried out by the combustion analysis with ± 0.30% accuracy. The oxygen content was obtained by subtracting from 100% of the sum of (C, H,

N and S) contents in percentage. The results of proximate and ultimate analyses of three lignocellulose derived materials are given in table 4.1.

4.2.2 Results and discussion

Table 4.1 Proximate and ultimate analysis of lignocellulosic components (as received)

	Cellulose	**Hemicellulose**	**Lignin**
Proximate Analysis (wt%)			
Moisture	3.53 ± 0.25	9.42 ± 0.11	8.05 ± 0.18
Volatile	92.35 ±1.49	74.15 ± 1.05	33.56 ± 0.37
Fixed Carbon[(a)]	4.11 ± 1.24	6.63 ± 0.19	4.49 ± 0.90
Ash	0.007	9.80 ± 0.74	53.91 ± 0.71
Ultimate analysis (wt%)			
C	43.01	37.50	46.85
H	6.55	6.24	5.10
O[(a)]	50.25	56.03	44.28
N	< 0.10	< 0.10	0.16
S	< 0.10	< 0.10	3.61
C/H	6.57	6.01	9.19
C/O	0.86	0.67	1.06

[(a)] by difference

At 600°C, the volatile content produced from cellulose was higher than hemicellulose and lignin, while lignin showed the highest solid residue after combustion process. This lignin sample was identified as alkali lignin which was isolated with alkali and precipitated by mean of mineral acids. Thus, ash content in this kind of lignin is at high level. As these three materials are the main components in the biomass, the bio-char obtained from pyrolysis at 600°C would be high with the solid residue mainly from lignin but this temperature; however, cellulose and hemicelluloses produced considerable amount of volatiles. From elemental analysis, the lignin structure consists of a high level of carbon and low oxygen content compared to those of cellulose and hemicelluloses. According to their chemical structures, cellulose and hemicellulose have large amount of hydroxyl groups along the backbone, while lignin structure contains considerable methyl groups as

well as hydroxyl groups. All samples contain very low nitrogen content which leads to low nitrogen oxide gases produced. Lignin was the only material showing the sulphur content which was considered from the production process.

4.3 Thermal behaviour by Thermogravimetry (TG)

4.3.1 Experimental

Thermogravimetric analyser (TGA/DSC1 STAR^e system, Mettler Toledo) was used to investigate the weight loss stages of biomass components (cellulose, hemicellulose and lignin). In the TG experiment, the samples were heated from ambient temperature to 600°C at heating rate of 10-40°C/min under helium atmosphere. During the experiment the cell of TG was flushed with 100 ml/min of helium to maintain the inert atmosphere for pyrolysis process and remove the gaseous and condensable products to prevent any secondary vapour phase interactions. Small amount of sample (~10 mg) were applied for each measurement to eliminate the heat and mass transfer influences. Sample and furnace temperature detectors of TG were calibrated by three standard metals (Indium, Zinc and Aluminium) before starting experiment to minimize the error from thermal lag. The measurements of each sample were checked for the reproducibility by repeating three times. The thermogravimetric data of cellulose, hemicelluloses and lignin obtained by recording the history of weight loss of the samples as well as their derivative curves at different heating rates are presented in Fig.4.2 (a)–(c). Moreover, Fig.4.3 shows the comparison of TG and DTG curves of these three lignocellulosic derived materials at heating rate of 20°C/min.

4.3.2 Results and discussion

From Fig.4.2, unlike that of lignin, the major weight loss of the cellulose and hemicellulose were completed below 400°C. The thermal degradation above 400°C could be considered as an aromatization process [286]. Thus, with limited aromaticity the secondary reactions of cellulose and hemicellulose at high temperature could be negligible, while the aromatic structure in lignin continued to degrade up to 600°C.

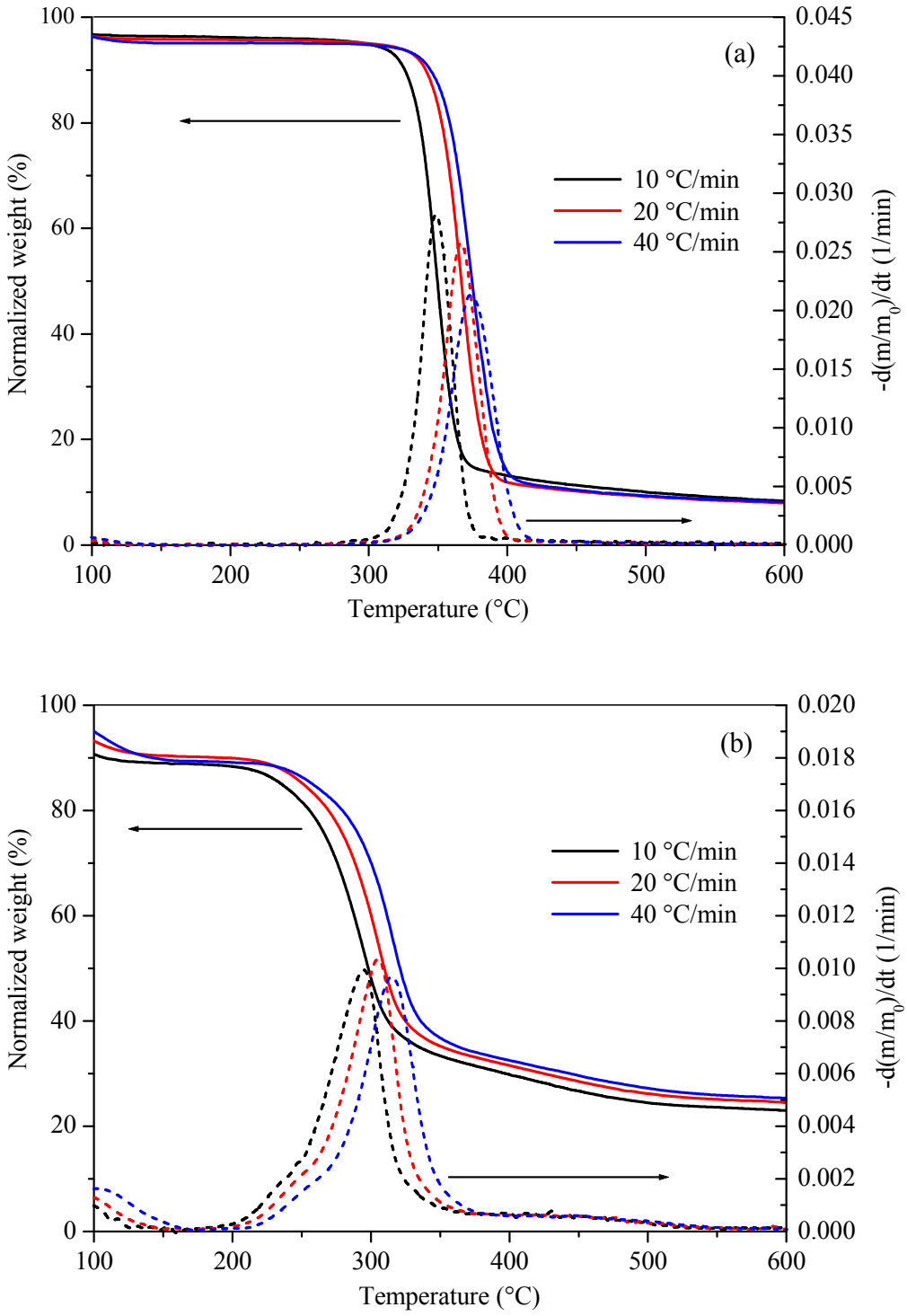

Fig. 4.2 The TG and DTG curves of (a) cellulose, (b) hemicellulose, and (c) lignin at heating rate 10, 20, and 40°C/min; the solid lines represent the TG curves and the dotted lines represent the DTG curves.

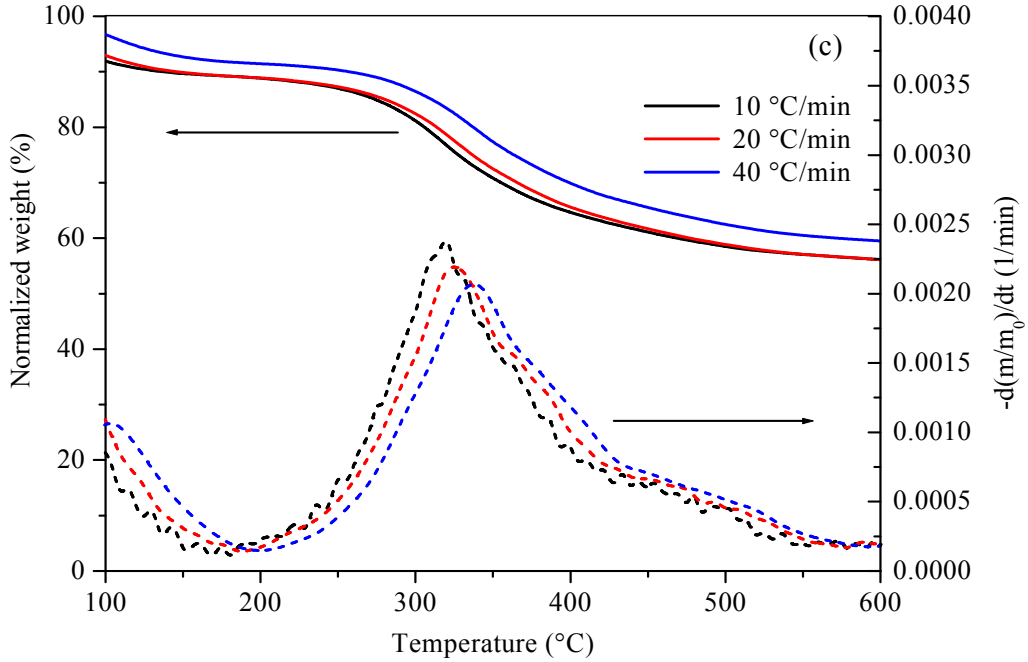

Fig. 4.2 The TG and DTG curves of (a) cellulose, (b) hemicellulose, and (c) lignin at heating rate 10, 20 and 40°C/min; the solid lines represent the TG curves and the dotted lines represent the DTG curves (continued).

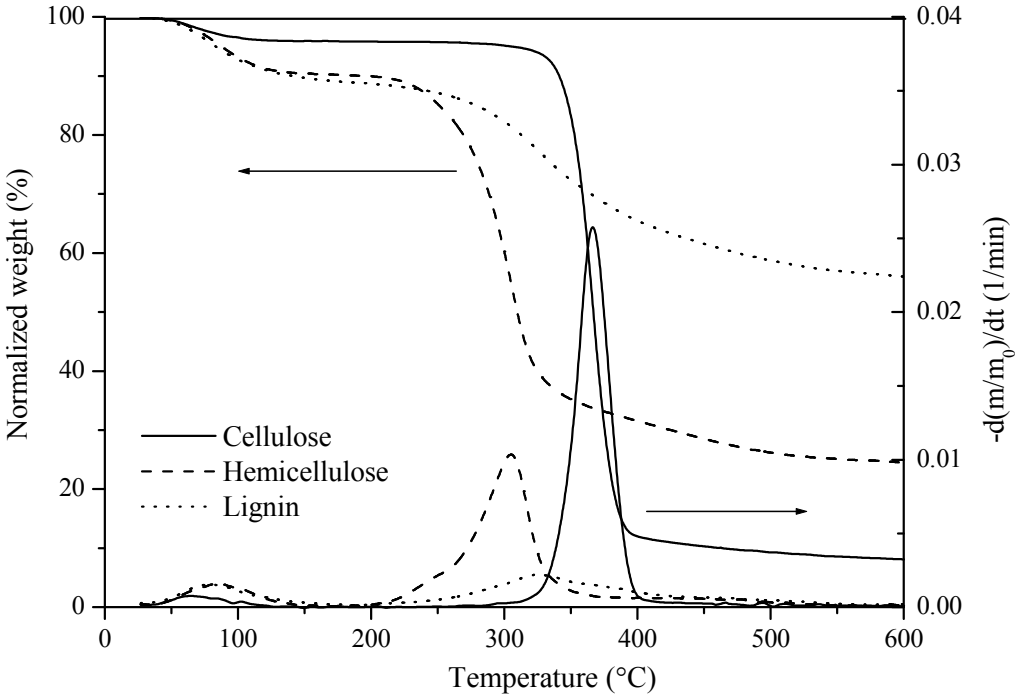

Fig. 4.3 The comparison of thermogravimetric, TG and the derivative of thermogravimetric, DTG curves of three lignocellulosic components at 20°C/min

The thermogravimetric curves show that the heating rate influences the residue (char) at the end of the experiment. This effect is mostly related to the difference in heat and mass transfer of the sample particles externally and internally. At lower heating rates, sample particles were heated slowly, leading to a better and more effective heat transfer to the inside of the particles. As a result of the more effective heat transfer, the sample decomposes promptly, enhancing the weight loss. Hence, at lower heating rates, more volatiles were produced than at higher heating rates. On the other hand, at higher heating rates, the temperature difference inside a sample particle is enhanced and then the residue at the end of the pyrolysis increased.

The shift of thermograms toward high temperature as the heating rate increases can be observed clearly in every sample. Table 4.2 shows data from the thermograms, in particular, the initial reaction temperature ($T_{initial}$), the temperature at the maximum mass loss rate (T_{max}) and the end temperature (T_{end}) of devolatilization step as well as the reaction rate at different heating rates. The increase of reaction rates were at the same ratio with the increase of heating rates. The reason for this shift is also from heat transfer effect at high heating rate, the minimum heat required for depolymerisation is reached at higher temperature because of the less effective heat transfer than the low heating rate does.

Fig. 4.3 shows the comparison among the measured thermogravimetric (TG) curves and the derivative of the thermogravimetric curves (DTG) of cellulose, hemicellulose and lignin at heating rate 20°C/min. At low temperature less than 200°C, there was the water evaporation region in all samples. The decomposition of cellulose occurred in a narrow range of temperature and focused at a temperature range of 320–400°C with the maximum mass loss rate at 365°C. Hemicellulose started decomposing at a lower temperature but the temperature range on decomposition was wider than did cellulose. The pyrolysis of hemicellulose started at 190°C and its mass loss rate increased greatly with increasing temperature and obtained its maximum value at 305°C. After 350°C the degradation rate of hemicellulose was slow for solid residue decomposition until finishing the degradation at 550°C. Lignin started decomposing at low temperature as hemicelluloses did and reached the maximum rate at 325°C but its pyrolysis occurred in an extensive temperature range (190–580°C) with relatively low rates.

Table 4.2 Temperature characteristics and reaction rates for the pyrolysis of three lignocellulosic compounds by Thermogravimetry

Samples	Heating rate (°C/min)	Instantaneous maximum reaction rate (1/min)	Temperature (°C) of devolatilization		
			$T_{(initial)}$	$T_{(max)}$	$T_{(end)}$
Cellulose	10	0.281	300	350	380
	20	0.502	320	365	400
	40	0.802	320	375	420
Hemicellulose	10	0.100	180	295	360
	20	0.208	190	305	370
	40	0.430	210	315	380
Lignin	10	0.024	180	320	560
	20	0.044	190	325	580
	40	0.085	200	340	590

Due to the difference in structure and compositions of each component, during non-isothermal pyrolysis these three materials would undergo different reaction pathways. Hemicellulose has the highest reactivity for thermal decomposition because its structure is random and amorphous with less strength. In contrast, cellulose is a crystalline, long chain polymer of glucose units without any branches supporting the hydrogen bonding. Thus, more energy is required for depolymerisation of cellulose polymer as the main mass loss stage of cellulose comes later than that of hemicellulose. Lignin has heavily cross-linked structure of three basic kinds of benzene-propane units. Hence, the structure of lignin results in high thermal stability and is difficult to decompose. Volatiles produced from lignin occurred from the breaking down of different functional groups with different thermal stabilities. This difference leaded to a broad range of decomposition in lignin [283].

As cellulose, hemicellulose and lignin are the three main components of a biomass, the biomass pyrolysis process can be divided into four temperature regions: lower than 200°C (moisture removal), 200-330°C (predominately hemicellulose decomposition), 330-400°C

(predominately cellulose decomposition) and higher than 400°C (predominately lignin decomposition).

4.4 Summary and recommendation

Whatman filter paper, Xylan and alkali lignin showed as the promising representatives for cellulose, hemicelluloses and lignin, respectively. Alkali lignin had a high ash content which influences its pyrolytic behaviour. These three main components in biomass showed different reactivity which could be summarized that the reactivity of hemicellulose > cellulose > lignin. This difference is influenced from their different chemical structures. The thermal decomposition characters of each sample can explain the multi-step decomposition in biomass. Characteristics of these basic materials influence the mechanisms and kinetics of biomass decomposition. To understand the very complex pyrolytic behaviour of biomass, those of cellulose, hemicellulose and lignin are fundamental and important. Further in this present study, these promising representatives of lignocellulosic main components will be used to analyse their formal kinetic parameter of pyrolysis process in Chapter 7.

Chapter 5

Pyrolytic Characteristics of *Chlorella vulgaris*

Unlike the woody biomass, the studies on pyrolysis of either microalgae or macroalgae are limited. It is well-established that the main components lignocellulosic biomass are cellulose, hemicelluloses and lignin, while those of algae can be classified simply as protein, carbohydrate and lipid which present at various proportion depending on species, cultivation condition and harvesting process. For effective utilization of algae in energy industry, more researches on the pyrolytic behaviour and kinetics are required. In this work, *Chlorella vulgaris*, freshwater green algae, are selected due to its fast growth rate, high environmental tolerance and easy to cultivate.

This chapter will give the methods and results on characteristics of *Chlorella vulgaris*. Proximate, ultimate and mineral analyses, together with main components analysis are presented here. The thermal behaviour of *Chlorella vulgaris* will be analysed by Thermogravimetry coupling to Mass Spectrometry (TG/MS) to gain more information on gaseous product evolutions. Moreover the functional groups available in these algae will be investigated by Fourier Transform Infrared Spectrometry (FTIR). Pyrolytic volatiles of *Chlorella vulgaris* at different reaction temperatures studied by Pyrolysis-Gas Chromatographic/Mass Spectrometry (Py-GC/MS) will also be presented in this chapter.

5.1 Materials

Chlorella vulgaris was provided by IngrePro B.V., Netherland in the form of dry powder (Fig. 5.1). The strain is *Chlorella vulgaris* Beijerinck CCAP211/11B, cultured in F/2 (F2P) medium ($NaNO_3$, $NaH_2PO_4 \cdot H_2O$, $Na_2SiO_3 \cdot 9H_2O$ and Trace metals) [306] at a pH of 8.0 in

a photo bioreactor in a greenhouse (20-35°C) under Dutch spring conditions. For harvesting, a stacked disk centrifuge (Alfa Laval Clara 80) was used, after which the paste (5-7% dry matter content) was stored in (milk) cooling tanks until drying. The latter was done using a dual drum dryer (GMF Gouda). Delivered microalgae powder was grounded in a mortar to get into the 90% at size less than 0.066 mm diameter and stored in a sealed container at low temperature until use.

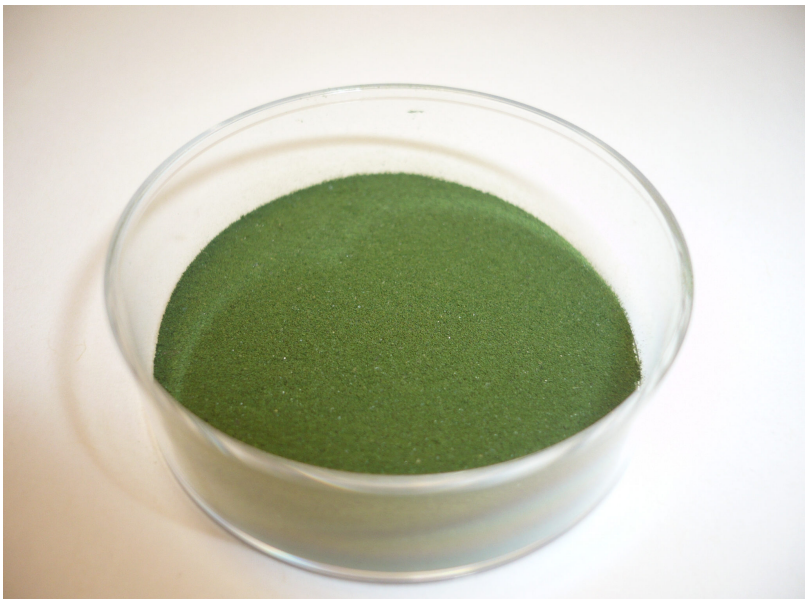

Fig. 5.1 *Chlorella vulgaris* powder

5.2 Proximate and Ultimate analysis

5.2.1 Experimental

The proximate analysis of the microalgal samples were carried out in accordance with ASTM standards. The moisture content in test samples was determined according to ASTM E1756-01. Biomass samples were dried in a convection oven at 105°C until constant weight was recorded. Moisture content was calculated from the weight loss and represented water that may be physically present or chemically bound in the biomass. The volatile content was determined by the mass loss excepting water removal from TG measurements at heating rate 20°C/min up to 575°C under helium atmosphere. Determination of the ash content in the test samples were carried out according to ASTM E1755-01. The ash content was determined by burning 1.0 g of sample in a crucible in an

electric muffle furnace at 575°C until the weight was constant. The fixed carbon content of the test samples was calculated by difference.

The heating value of the microalgal sample was determined by microprocessor controlled oxygen Bomb calorimeter (Parr 6100 Calorimeter) with sample weights ranging from 0.5 to 1.0 g. The bulk density of microalgae powder was analysed according to ASTM D1895B. All analyses were done in triplicates. The organic and metal elemental compositions were analysed by Medac Ltd where the C, H, S, O and N analysis were carried out by combustion analysis with ± 0.30 % accuracy. Metals were analysed by using Varian Vista MPX ICP-OES system. The analysis results in this section are shown in Table 5.1.

5.2.2 Results and discussion

The proximate, ultimate and mineral analyses together with main component contents of *Chlorella vulgaris* are listed in Table 5.1. Microalgae have high water content after harvesting but they can achieve low moisture content by drying. The dried *Chlorella vulgaris* used in this study had low moisture content about 5.8 wt%. However the ash content in the microalgae is higher than land crops [307] due to the accumulation of inorganic matter from growing medium. This inorganic content can act as catalysts on pyrolysis process as it is well established for terrestrial biomass that the presence of alkali metals affects the mechanism of pyrolysis, pyrolysis oil quality and increase char yields. The mineral analysis indicated a large quantity of Ca, Na and K. Some trace heavy metals such as Cr, Pb and Cd (< 10 ppm) were concentrated in microalgae due to its biosorption properties. It could be seen that the calcium ion was the most abundant ion in this sample. However the calorific value on dry basis of *Chlorella vulgaris* which was comparable to other plant species (17-21 MJ/kg) [308] together with their lower oxygen content than woody biomass [309] makes *Chlorella* a promising feedstock for bio-oil production via pyrolysis.

Table 5.1 Proximate, ultimate and mineral components analysis of *Chlorella vulgaris*

Analysis	***Chlorella vulgaris*** (as received)
Proximate analysis	
Moisture (wt%)	5.80 ± 0.08
Volatile (wt%)	61.57 ± 1.83
Fixed carbon (wt%)[(a)]	15.68 ± 1.83
Ash (wt%)	16.95 ± 0.13
Heating value (MJ/kg)[(b)]	20.34 ± 0.05
Bulk density (g/ml)	0.59 ± 0.01
Ultimate analysis (wt%)	
C	44.56
H	6.18
O[(a)]	30.71
N	6.76
S	0.79
Mineral analysis (wt%)	
Ca	4.62
Na	1.24
K	1.09
P	0.67
Mg	0.33
Fe	0.25
Al	0.03

[(a)] by difference [(b)] on dry basis

5.3 Main components analysis

5.3.1 Experimental

Total lipids of samples were extracted by a modified version of the Bligh and Dyer method [310]. In this method, 0.25 g of dry microalgae was acidified with 0.15M acetic acid 1mL followed by the addition of chloroform/methanol (1:2 v/v) 7.5 mL. The test tube was filled with nitrogen gas and the solution was stirred at low temperature for 2 hours, followed by

the addition of 2.25 mL distilled water and 2.25 mL of chloroform. The phase was well mixed by vortexing for 1 minute. Phase separation was achieved by leaving at -20°C overnight and the lower chloroform phase containing the lipids was removed and evaporated under N_2. The extracted lipid was weighed and calculated based on algae power weight. The extraction was repeated 3 times to assess the variation in lipid content.

Crude protein was determined by TCA-acetone extraction. *Chlorella vulgaris* (0.25 g) powder was put into a homogenisation tube and then added 10% trichloroacetic acid (TCA). Algal cells were broken by homogenization for 1 min and then the homogenate was centrifuged to precipitate the protein. The protein fraction was washed five times in ice-cold acetone and dried under nitrogen atmosphere at 80°C. Protein pellets were weighted to calculate the protein content. Carbohydrate content was calculated from the difference of 100% and the sum of crude protein, lipid, moisture and ash content. The content of these main components are summarized in table 5.2.

5.3.2 Results and discussion

Table 5.2 Main components analysis of *Chlorella vulgaris*

Analysis (wt%)	***Chlorella vulgaris*** (as received)
Protein	42.88 ± 4.15
Carbohydrate[(a)]	22.06 ± 2.85
Lipids	12.31 ± 1.30
Moisture	5.80 ± 0.08
Ash	16.95 ± 0.13

[(a)] by difference

Unlike the main components (cellulose, hemicellulose and lignin) in lignocellulosic biomass, microalgae contains relatively high amount of proteins, carbohydrates and lipids. Due to the high protein content (42.88 wt%), nitrogen content in *Chlorella vulgaris* was high. The lipid content in microalgae depended on growing conditions and species. Lipid content was reported in a broad range from 14 up to 22 wt% [311]. The high lipid levels in algae are usually favourable for bio-diesel production. Carbohydrates in algae largely represent cellulose from cell walls and starch granules as a photosynthetic product.

5.4 Thermal behaviour by Thermogravimetry-Mass Spectrometry (TG-MS)

5.4.1 Experimental

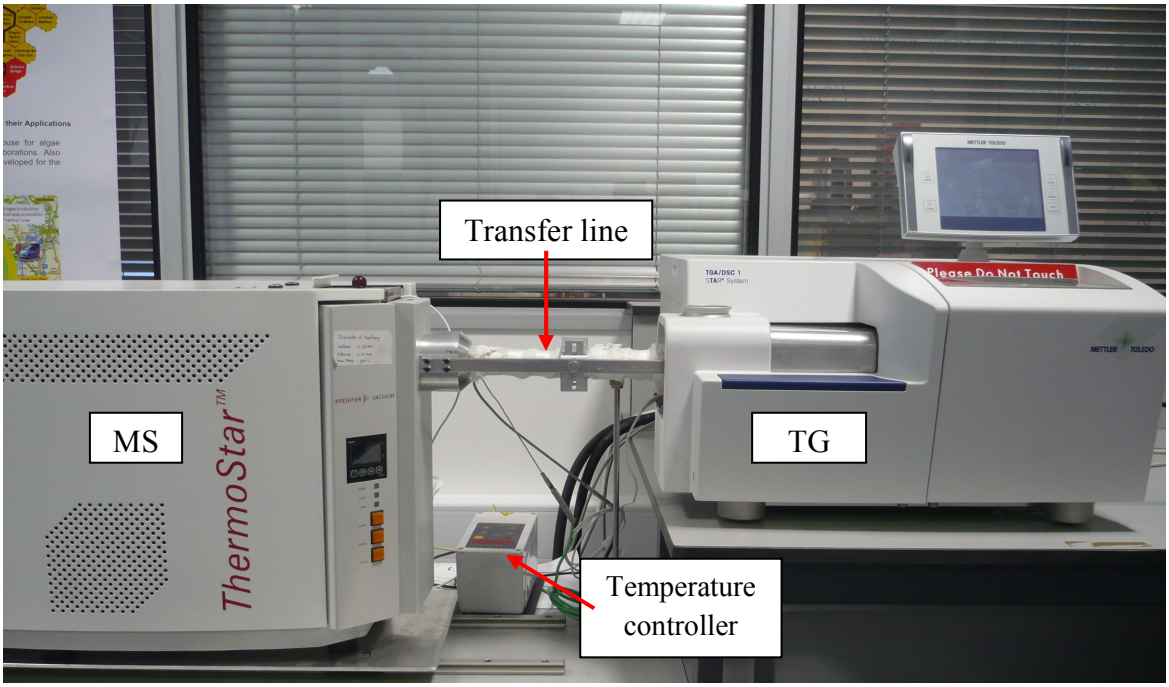

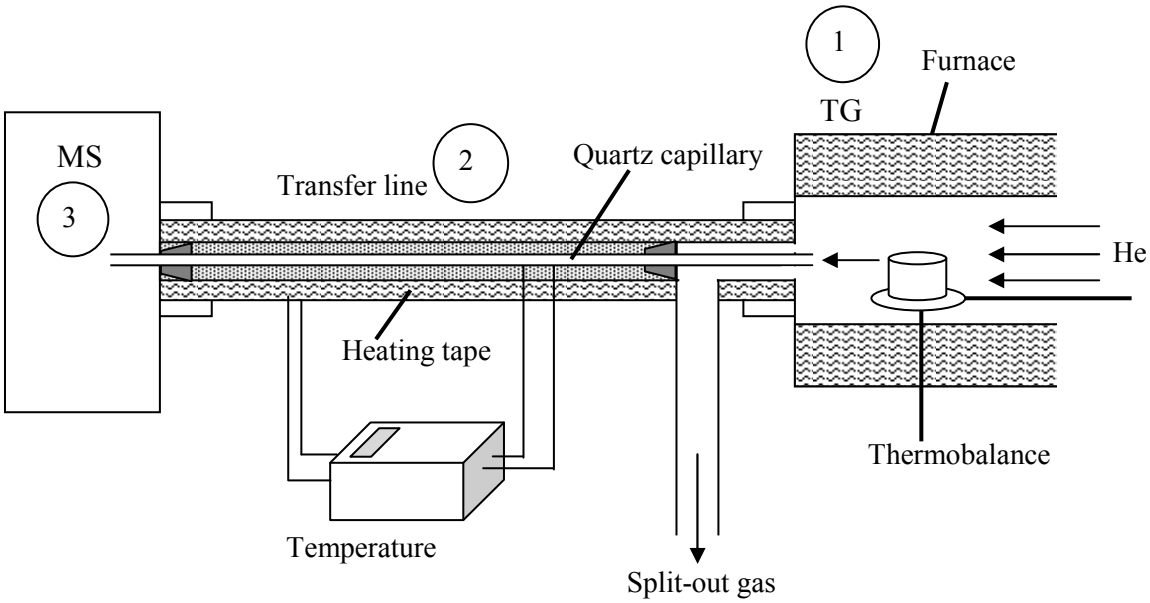

Fig. 5.2 Thermogravimetric analyser coupling with Quadrapole Mass Spectrometer (TG-MS)

An in-house built coupling (Fig.5.2) of Thermogravimetric analyser (TGA/DSC1 STAR^e System, Mettler Toledo) with Quadrapole Mass Spectrometer (ThermoStarTM Pfeiffer vacuum with QMS200) was used to investigate the pyrolytic characteristics of *Chlorella vulgaris*. TG-MS is comprised of the following components: (1) Thermogravimetric analyser (TGA/DSC1 STAR^e System, Mettler Toledo); (2) Transfer line with a deactivated quartz column (5 m×150 μm/220 μm); (3) Evolved gas analysis by Quadrapole Mass Spectrometry (ThermoStarTM Pfeiffer vacuum with QMS200). TG-MS allowed the simultaneous measurements of weight loss and mass spectra data as a function of temperature or time. Calibration experiments were performed with calcium oxalate monohydrate ($CaC_2O_4 \cdot H_2O$) presented in Appendix A. In the TG experiment, the samples were heated from ambient temperature to 600°C at heating rate of 5-20°C/min under the inert atmosphere. The mass of *Chlorella vulgaris* was weighed about ~10 mg. The small sample size minimized the limitation of heat and mass transfer. During the experiment the cell of TG was flushed with 100 ml/min helium to maintain the inert atmosphere for pyrolysis of the sample and purged the gaseous products to mass spectrometer inlet. The molar fractions of evolved gaseous products from TG experiments passed to the mass detector through a heated deactivated column. The transfer line between TG and MS was heated at 300°C to avoid the condensation of volatile compounds and the tip of coupling column was placed closed to the sample crucible in TG in the direction of the gas flow.

5.4.2 Results and discussion

The weight loss curves (TG) and their derivative curves (DTG) of *Chlorella vulgaris* in helium atmosphere at different heating rates (5, 10, 20°C/min) are shown in Fig. 5.3. They revealed that three stages existed in the pyrolysis process. The first stage at temperature lower than 110°C, there was a small change in weight attributing to evaporation of water which was absorbed on the surface of the samples. The second and third stages together could be considered as the devolatilization of pyrolysis process. The devolatilization region started at about 200°C and was completed at 550°C with temperature peaks around 290-310°C for the lower temperature peak and around 430-450°C for the higher temperature peak. The reaction rate, the temperature at maximum rate and the total weight loss under pyrolysis conditions at different heating rates is reported in table.5.3.

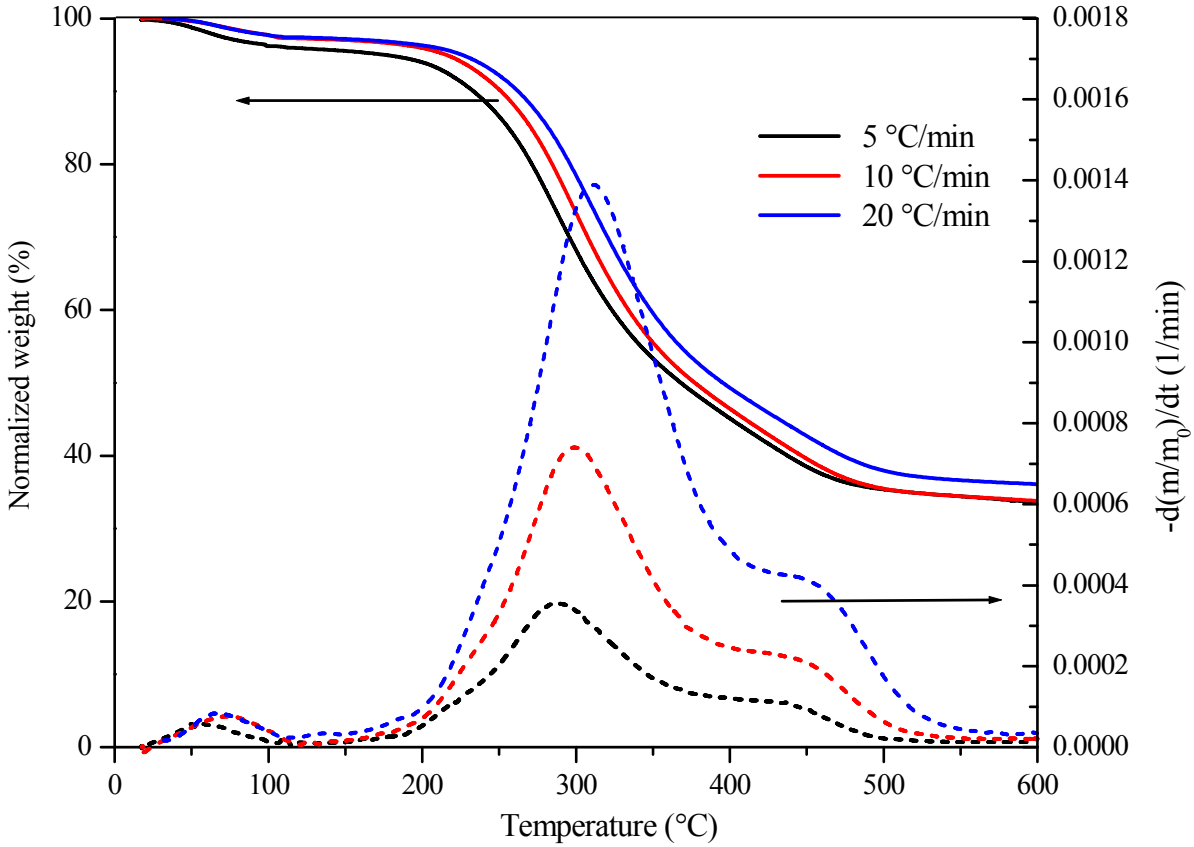

Fig. 5.3 The thermogravimetric (solid lines) and derivative of thermogravimetric (dotted lines) curves of the pyrolysis of *Chlorella vulgaris* samples at heating rate 5-20°C/min.

The influence of heating rate on the volatile content could be explained by the difference in heat and mass transfer of the sample particles. When sample particles are heated slowly, the heat transfer to the inner of particles is more effective. As the sample particle decomposes promptly, leading to increased volatile production. On the other hand, the temperature gradient inside a sample particle is larger at high heating rates and this cause higher char residue production. The shift toward high temperature of higher heating rate was also the result from the effect of the heat transfer at different heating rates.

Table 5.3 Temperature characteristics and reaction rates in the devolatilization stage

Heating rate (°C/min)	Instantaneous maximum reaction rate (%/min)		Devolatilization		
			T_{max}(°C)		Volatile content (wt%)
	$T_{(lower)}$	$T_{(higher)}$	$T_{(lower)}$	$T_{(higher)}$	
5	0.024	0.007	290	430	62.34
10	0.044	0.014	300	440	62.14
20	0.085	0.027	310	450	60.23

From DTG curves, the devolatilization was presented by the overlapping of two main peaks. The different decomposition regions could be considered as the degradation of different main algal components. The weight changes at 200-380°C reflected the decomposition of mainly proteins and carbohydrates [296, 298]. The remaining carbohydrates and lipids were decomposed above 400°C. Due to the lipid content in this algal sample was relatively low compared to protein and carbohydrate contents, the height of lipid decomposition peak at higher temperature peak is lower than the first peak around 300°C [312]. At temperatures higher than 500°C, the slow further decomposition of the solid residue occurs.

The evolved gases emitted from decomposition in TG were monitored by coupled Mass Spectrometry. The molecular masses reported as *m/z* were 2, 18, 28, 44, 34, 64 and light hydrocarbons which have molecular mass less than 100 u. The identification of each *m/z* can be observed in table 5.4. The evolution curves of ion-fragments of various released gases are shown as ion current versus temperature curves in Fig. 5.4. Evolution curves of H_2S and SO_2 were much lower than the major gaseous products. The evolved gas profile of nitrogen containing gases would not be presented because these gases evolution were interrupted from the evolution of other major gases profiles.

The main products of this sample are H_2O, CO, CO_2, CH_4, NH_3 and H_2. Helium was used as a purge gas, instead of nitrogen gas, because nitrogen gas has the same molecular mass as the molecular mass of carbon monoxide gas.

Table 5.4 Relation between mass per charge ratio (*m/z*), fragment and probable molecule

m/z	fragment	probable molecule
2	H_2^+	H_2
18	H_2O^+	H_2O
28	CO^+	CO
44	CO_2^+	CO_2
34	H_2S^+	H_2S
64	SO_2^+	SO_2
Light hydrocarbons (less than *m/z* =100)		

The molecular ions of water (H_2O^+; *m/z* =18) were found at two different temperatures, indicating the presence of two types of water in samples, one was the water which was physical absorbed on sample was evolved around 80°C. At the first stage of the process, there was confirmed with MS evolution data that it was the water removal only. Another kind of water which was the products of chemical reactions, starting from 200°C to high temperature with a maximum peak temperature at about 300°C corresponded with the main mass loss region observed from TG curves. The bulk of water in the bio-oil was generated at this stage due to the presence of oxygenated compounds.

The ion current curve for the evolved gas of CO_2^+ (*m/z* = 44) gained at about 325°C attributed to the devolatilization reaction. A significant amount of CO^+ (*m/z* =28) evolved throughout the whole temperature range of devolatilization. However the detected CO^+ could be considered as overestimated value because not all the signals for mass number of 28 are from CO^+. Some of them were also from $C_2H_4^+$. Also there was no change of H_2 (*m/z* = 2) at low temperature. At temperatures higher than 500°C which was considered as a charring process, the evolved ion current of H_2 could be observed. While low molecular weight hydrocarbons were produced mainly at the temperature of main devolatilization with two stages around 200°C to 550°C. It appeared that water and hydrocarbons were mainly evolved during the devolatilization step. Small amount of H_2S gas could be detected at 200-400°C, while SO_2 was released after 250°C. Moreover, the features of evolved gases detected by Mass Spectrometer were correlated to TG curves from Thermogravimetric analyzer. This shows the ability of coupled TG-MS for analysis of real-time detection of evolved gases applied to lab-scale pyrolysis study.

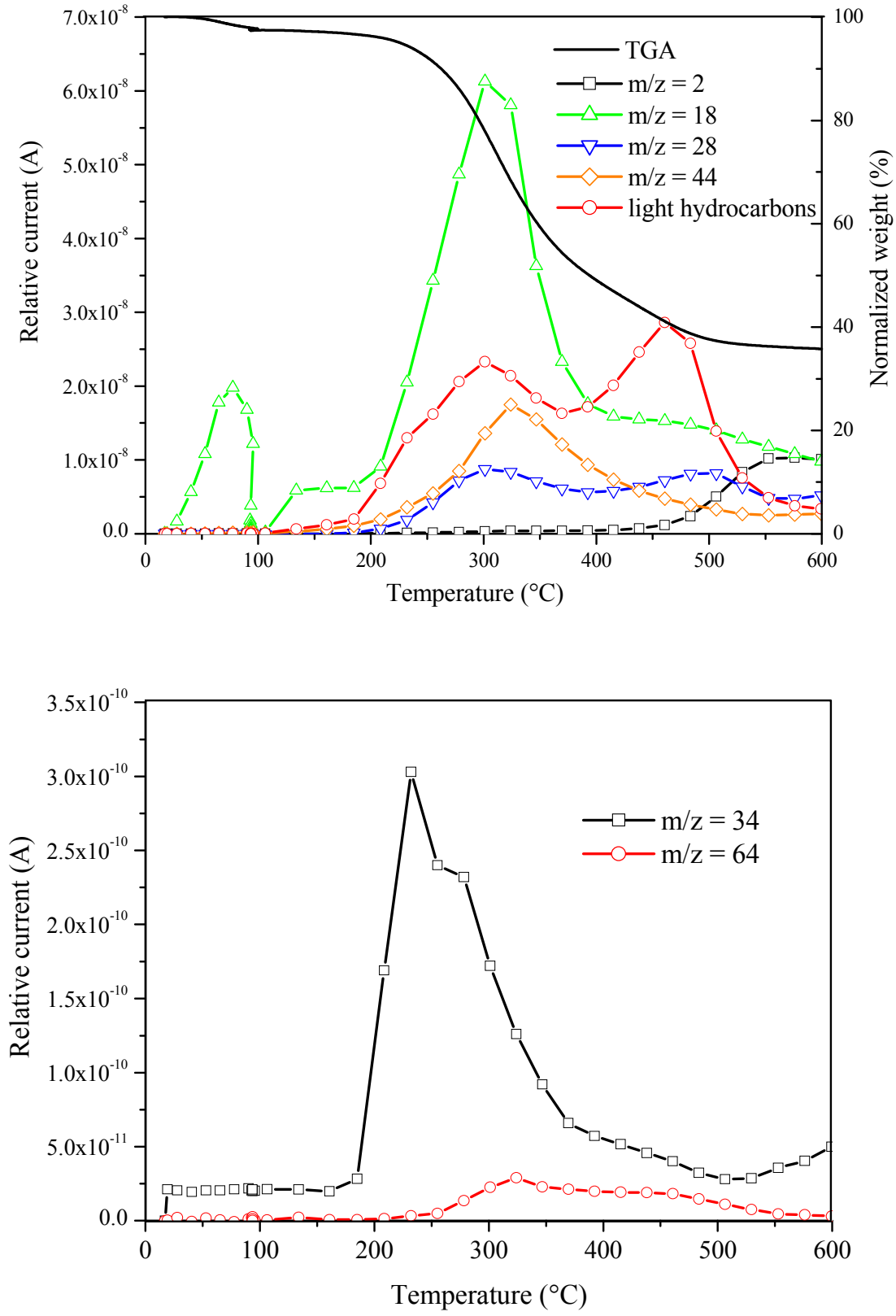

Fig. 5.4 Evolution of gaseous products during the pyrolysis of *Chlorella vulgaris* by TG-MS at heating rate 20°C/min

5.5 Functional group analysis by Fourier Transform Infrared Spectroscopy (FTIR)

5.5.1 Experimental

The functional groups of *Chlorella vulgaris* samples were investigated by using Fourier Transform Infrared Spectroscopy (FTIR) (Perkin Elmer Spectrum 100) with a resolution of 4 cm^{-1} in the range of 400-4000 cm^{-1} by averaging 16 scans with KBr background subtraction. One milligram of each powder sample was mixed with 200 mg of oven-dried KBr powder as reference material and subjected to a pressure of 10 tons on a thin disc.

5.5.2 Results and discussion

The FTIR spectrum of dried *Chlorella vulgaris* in wavenumber range of 400–4000 cm^{-1} at room temperature is shown in Fig.5.5. Table 5.5 shows spectral peaks which could be assigned to distinct functional groups belonged to different classes of bio-molecules. Band assignments were based on IR spectrum database [313] and previous studies on algae. The study of Giordano, M., et al. [314] shows the significant peaks around 3000-2800, 1800-1500, and 1200-1000 cm^{-1} for palmitic acid, BSA (Bovine serum albumin) and starch, respectively.

The broad band at high wave number (3300 cm^{-1}) showed the presence of hydroxy (-OH) functional group in sample which was from the structures of three main components (protein, carbohydrate and lipid) and also absorbed water in algae. Between 3000 and 2800 cm^{-1}, it was the characteristic region of C-H asymmetric stretching of aliphatic groups (-CH_3 and –CH_2-) which was primarily from lipid molecules. The existence of protein could be identified from the bands at 1656, 1545 and 1239 cm^{-1} as the amide I, II and III band, respectively. A lipid band (C=O) around 1800-1700 cm^{-1} was not clearly presented in the sample since the content of lipids was low and the obscuration from protein character band. In the range of 1390-1460 cm^{-1}, there were the asymmetric and symmetric deformations of –CH_3 and –CH_2- in protein molecules. These bands were assigned in literature at various wavenumbers. The C-O-C and C-O stretching of polysaccharides molecules showed at 1154 and 1030 cm^{-1}, respectively. Most spectrum between 1200 and 900 cm^{-1}, which was mainly represents the polysaccharides molecules functional groups, were obscured by the intense band of silicate from culture medium [83]. There was a

difficulty to identify the raw spectrum between 1800-800 cm^{-1} due to the overlapping of bands from various bio-molecules, mainly proteins and carbohydrates.

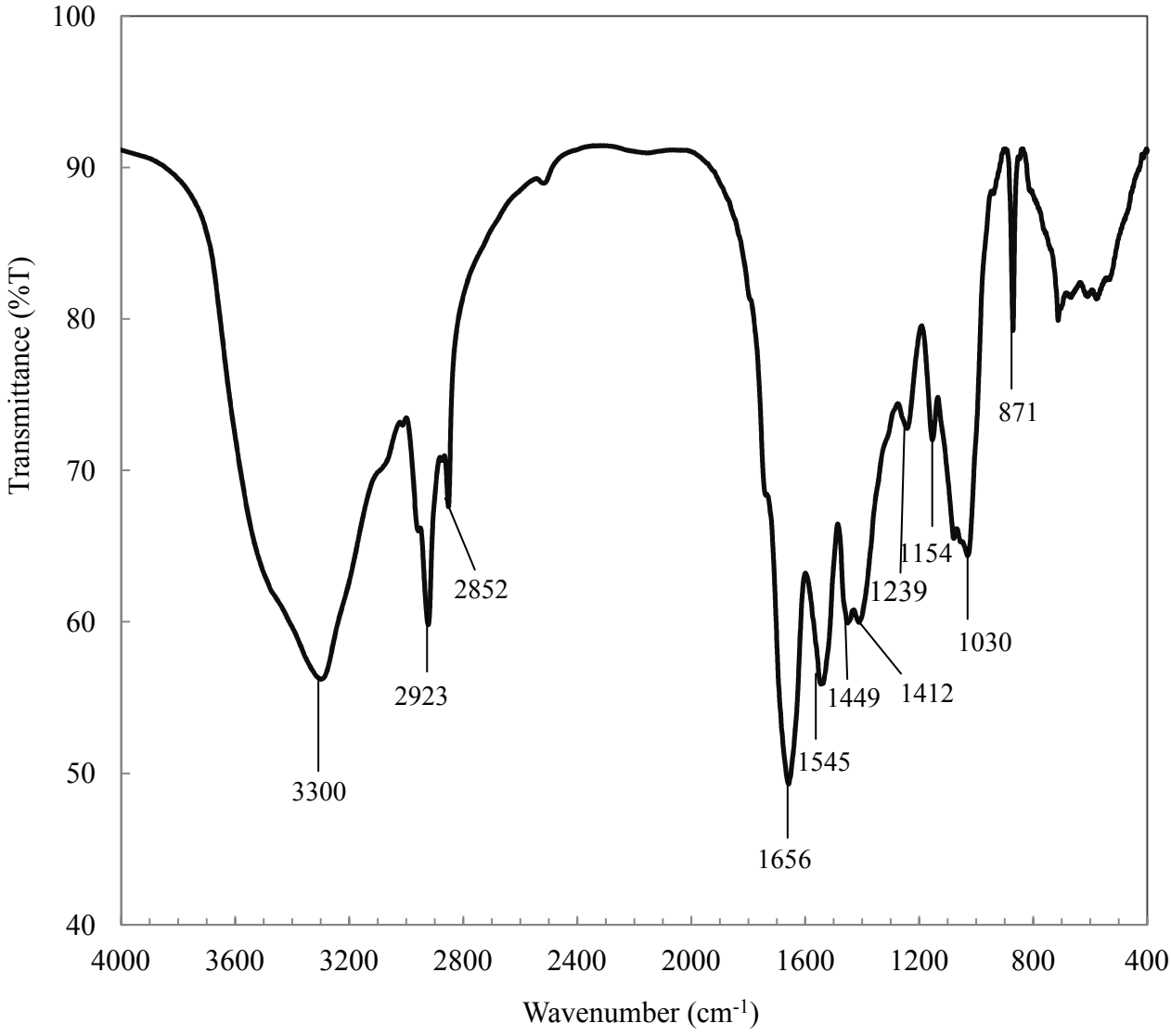

Fig. 5.5 The FTIR spectrum in wavenumber range of 400–4000 cm^{-1} of dried *Chlorella vulgaris* at room temperature

Table 5.5 The present functional groups in *Chlorella vulgaris* sample

Wavenumber (cm^{-1})	Functional group	Bio-molecules/source	Ref.
3300	-OH stretching	Carbohydrates, proteins, lipids, water	[315]
2923	$-CH_3$ stretching	Aliphatic groups of lipids primarily	[314, 315]
2852	$-CH_2-$ stretching	Aliphatic groups of lipids primarily	[314, 315]
1656	C=O stretching	Proteins (Amide I band)	[315]
1545	H-N stretching	Protein (Amide II band)	[83]
1449	$-CH_3$ and $-CH_2-$ bending (asym)	Proteins	[314]
1412	$-CH_3$ and $-CH_2-$ bending (sym)	Proteins	[314]
1239	P=O and H-N bending	Phospholipids of nucleic acids and proteins (Amide III band)	[313, 315]
1154	C-O-C stretching	Carbohydrates as polysaccharides	[315]
1030	C-O stretching	Aliphatic groups in carbohydrates	[313]
	Si-O stretching	Silicate from culture medium	[314]
871	$-CH_2$ bending	Carbohydrate as polysaccharides	[83, 313]

5.6 Pyrolytic products by Pyrolysis-Gas Chromatographic/Mass Spectrometry (Py-GC/MS)

5.6.1 Experimental

To investigate gaseous products from *Chlorella vulgaris* in lab-scale pyrolysis, experiments were performed on a Double-short pyrolyser (Model Py-2020iD) interfaced to a Gas Chromatograph (Hewlett 5890 Packard Series II) and Mass Selective detector (Hewlett Packard 5972 series). Grounded algal powder (0.3 mg) was inserted into the micro-reactor and pyrolysed at 300, 400, 500 and 600°C. The released volatiles passed through an injection port at 300°C of 150 kPa and were separated on a DB-1701 column (60 m × 0.250 mm diameter × 0.25 μm thickness). The temperature program for the GC operation was initiated at 40°C and increased at the rate of 3°C/min until 290°C with a hold time of 25 min. Helium was used as the carrier gas at a flow rate of 0.8 ml/min,

followed by a split injection at the ratio of 25:1. The mass spectra of compounds were measured in the range from 20 to 600 u. The identification of the peaks was based on standard mass spectral databases (NIST) and standard chemicals spectrum collected by EBRI researchers.

5.6.2 Results and discussion

The chromatogram from Py-GC/MS analysis of *Chlorella vulgaris* at 600°C are shown in Fig.5.6. The main compounds are listed in table 5.6. These identifications were based on the combination of standard mass spectral databases and retention data of standard chemicals. The main compounds found in this Py-GC/MS chromatogram were 3, 7, 11, 15-tetramethyl-2-hexadecen-1-ol, toluene, indole and 9-octadecenamide. Most chemicals could be detected at long retention time after 30 min. Analytical pyrolysis indicated the production of a range of aromatic, nitrogen-containing and long chain compounds. The aromatic compounds included toluene, phenol, indole, benzeneacetonitrile and benzenepropanenitrile. Nitrogen-containing compounds were pyrrole, indole, benzeneacetonitrile, benzenepropanenitrile and 9-octadecenamide. While 1-tridecene, heptadecane, 3, 7, 11, 15-tetramethyl-2-hexadecen-1-ol and 9-octadecenamide have a long chain hydrocarbon in their molecular structures. Nitrogen-containing compounds were produced from protein and chlorophyll components in microalgae. The presence of aromatic compounds could be considered from amino acids. Also, it can be linked to the existence of lignin-like components in *Chlorella vulgaris*. There are few studies reporting the presence of lignin or lignin-like compounds in aquatic algae, especially in red algae [316-318]. However the true lignin in green microalgae has not been confirmed and also the comparison of the results of Py-GC/MS technique applied to microalgae to those obtained in other studies is limited by the relatively few published reports.

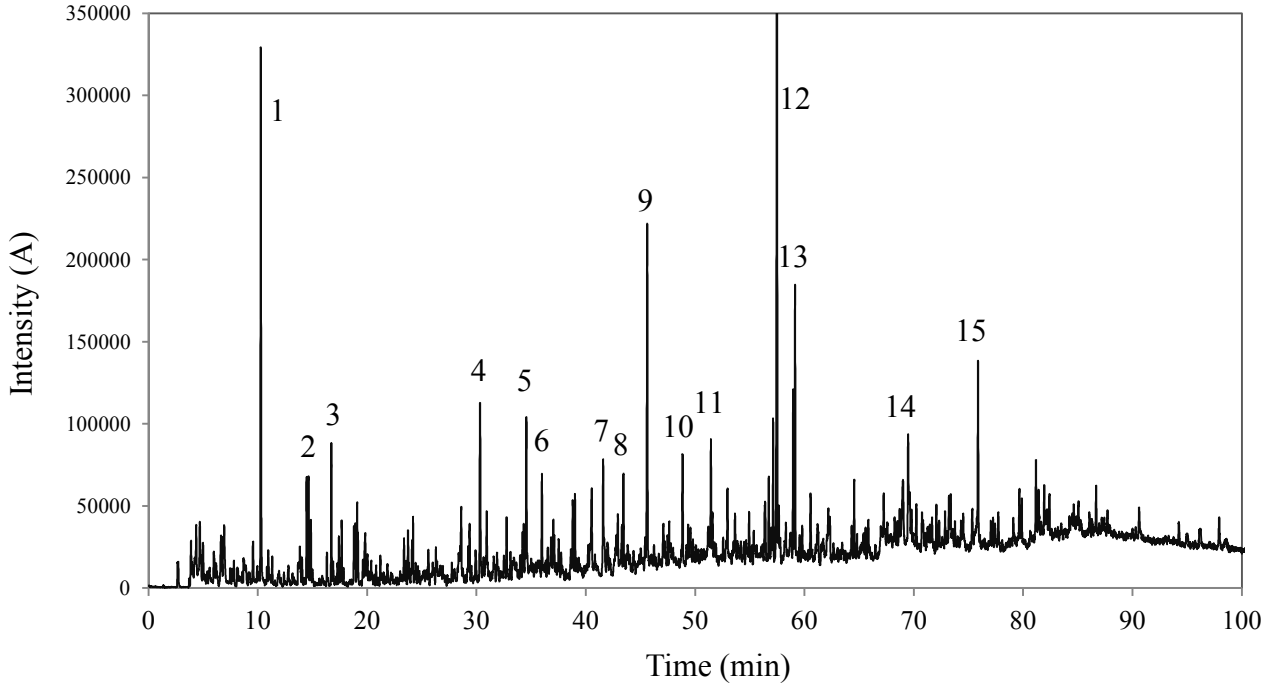

Fig. 5.6 Py-GC/MS chromatogram from pyrolysis of *Chlorella vulgaris* at 600°C.

Table 5.6 Organic compounds produced from *Chlorella vulgaris* by Py-GC/MS at 600°C

No.	RT (min)	MW	Compounds
1	10.26	92.14	Toluene
2	14.63	67.09	1H-Pyrrole
3	16.72	104.15	1,3,5,7-cyclooctatetraene
4	30.32	94.11	Phenol
5	34.56	108.14	Phenol, 3-methyl-
6	35.98	117.15	Benzeneacetonitrile
7	41.58	131.17	Benzenepropanenitrile
8	43.41	182.35	1-Tridecene
9	45.61	117.15	1H-Indole
10	48.84	131.17	1H-Indole, 3-methyl
11	51.44	240.47	Heptadecane
12	57.49	296.53	3,7,11,15-tetramethyl-2-hexadecen-1-ol
13	59.13	296.53	3,7,11,15-tetramethyl-2-hexadecen-1-ol
14	69.47	296.53	3,7,11,15-tetramethyl-2-hexadecen-1-ol
15	75.86	281.48	9-Octadecenamide

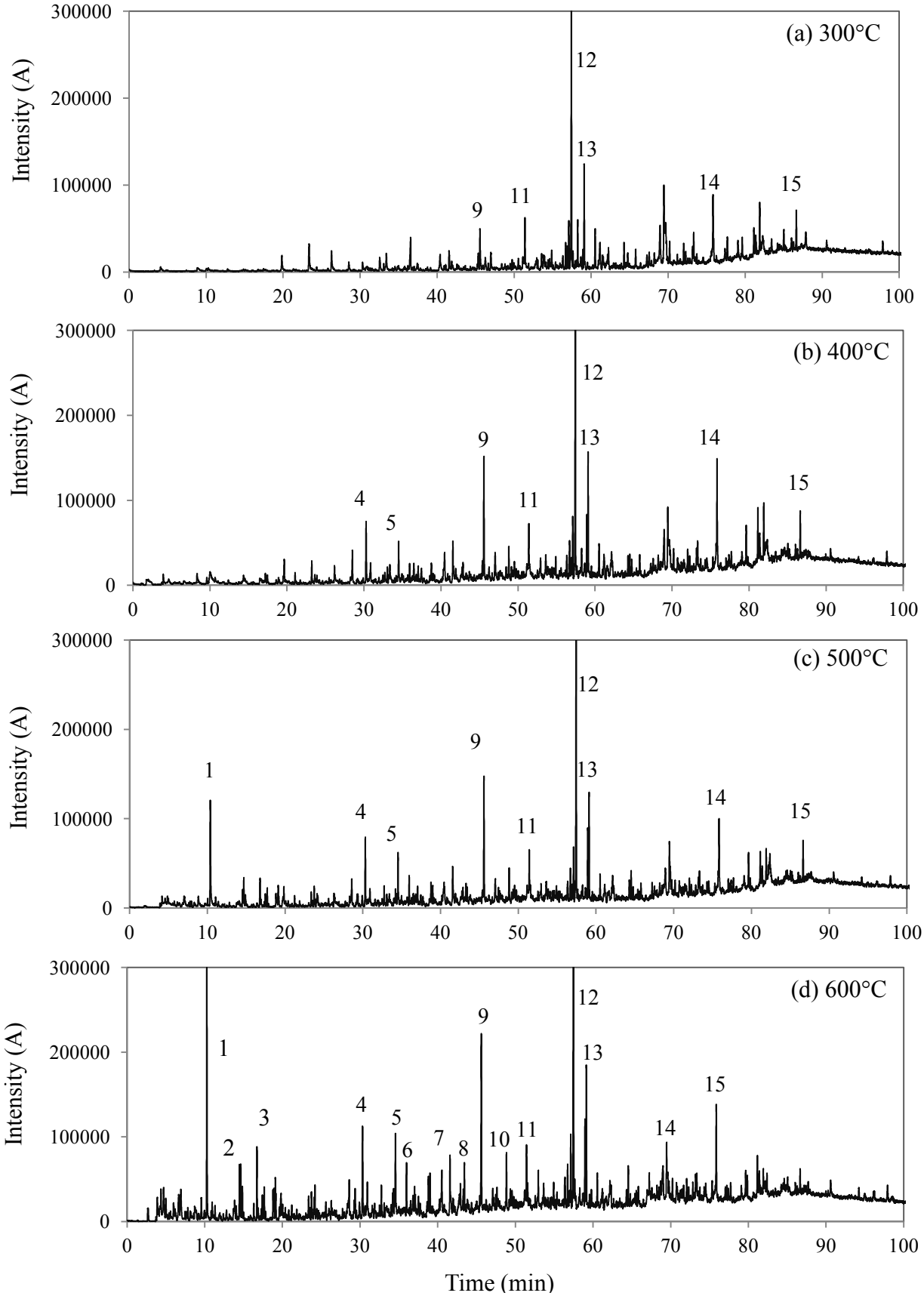

Fig. 5.7 Chromatograms from Py-GC/MS of *Chlorella vulgaris* at different temperatures

The comparison of Py-GC/MS chromatograms at different temperatures in Fig.5.7 shows that there were no peaks at retention time lower than 20 min at temperature 300 and 400°C. 3, 7, 11, 15-tetramethyl-2-hexadecen-1-ol and 9-octadecenamide were detected at whole range of the pyrolytic temperature. The presence of toluene, pyrrole and 1, 3, 5, 7-cyclooctatetraene was observed at temperatures of 500 and 600°C only. The above results suggested that these products were favoured at high temperature pathways. Unlike heptadecane peak, the intensity of phenol, phenol, 3-methyl- and indole increased as the increase of temperature. While some compounds at long retention time were reduced in the peak intensity at higher temperatures.

5.7 Summary and recommendation

Microalgae have the potential to be a resource for energy production due to their high productivity and no food competition. *Chlorella vulgaris* has promising characteristics which can be compared to woody biomass. These microalgae had heating value in the similar range of those from plant biomass and it had low oxygen content which result in a higher stability of bio-oil. Although high ash content was found in microalgae sample, pre-treatment by washing with water could be considered as a method to remove inorganic and metal compounds from algae. The thermal behaviour of *Chlorella vulgaris* depended on the compositions of biomass. Protein content was the most abundance in these algae. Its chemical structures were inferred by FTIR technique. Thermal decomposition started from low temperature at 200°C and finished around 500°C, depending on heating rate. The gaseous production could be monitored by Thermogravimetric-Mass Spectrometry (TG-MS) to gain more information of thermal decomposition of the sample. Most of major gaseous products were evolved in the devolatization temperature range but hydrogen gas started to be produced after the main mass loss region according to charring process. The volatile products from analytical pyrolysis in Py-GC/MS showed complexity of produced compounds which can be classified into aromatic compounds, long chain hydrocarbons and nitrogen-containing compounds.

Chapter 6

A preliminary investigation on the pilot scale pyrolysis of *Chlorella vulgaris*

Aquatic plants have become more interesting as an alternative source of biomass for thermo-chemical conversion to generate energy. Unlike woody biomass which has been employed successfully in commercial scale, there are limited studies for non-analytical scale pyrolysis of microalgae. Most existing pyrolysis reactors have been developed to optimize the production from wood materials. Hence, the applicability and performance of these reactors with microalgae feedstock will be the important information to achieve the development toward the demand on microalgae applications. In this work, *Chlorella vulgaris* will be carried out only a preliminary experiment with a pilot-scale intermediate pyrolyser (Pyroformer) at EBRI, Aston University to monitor its performance and produce bio-oil and bio-char for their properties investigation. This chapter will explain the reactor feature, how to set up the experiment and analyse the pyrolytic products and the potential of *Chlorella vulgaris* for the bioenergy applications.

6.1 Pilot scale intermediate pyrolysis system

The pilot scale pyrolysis experiment was carried out with a 'Pyroformer', a patent twin screws reactor [134], located at European Bioenergy Research Institute (EBRI) at Aston University, United Kingdom (Fig.6.1). This unit can be used to perform intermediate pyrolysis process with various biomass materials from terrestrial biomass such as energy crops and wood residues to algae and sewage sludge. This pyrolyser allows various forms of feed to apply into such as pellet, ship, or lump of sewage sludge.

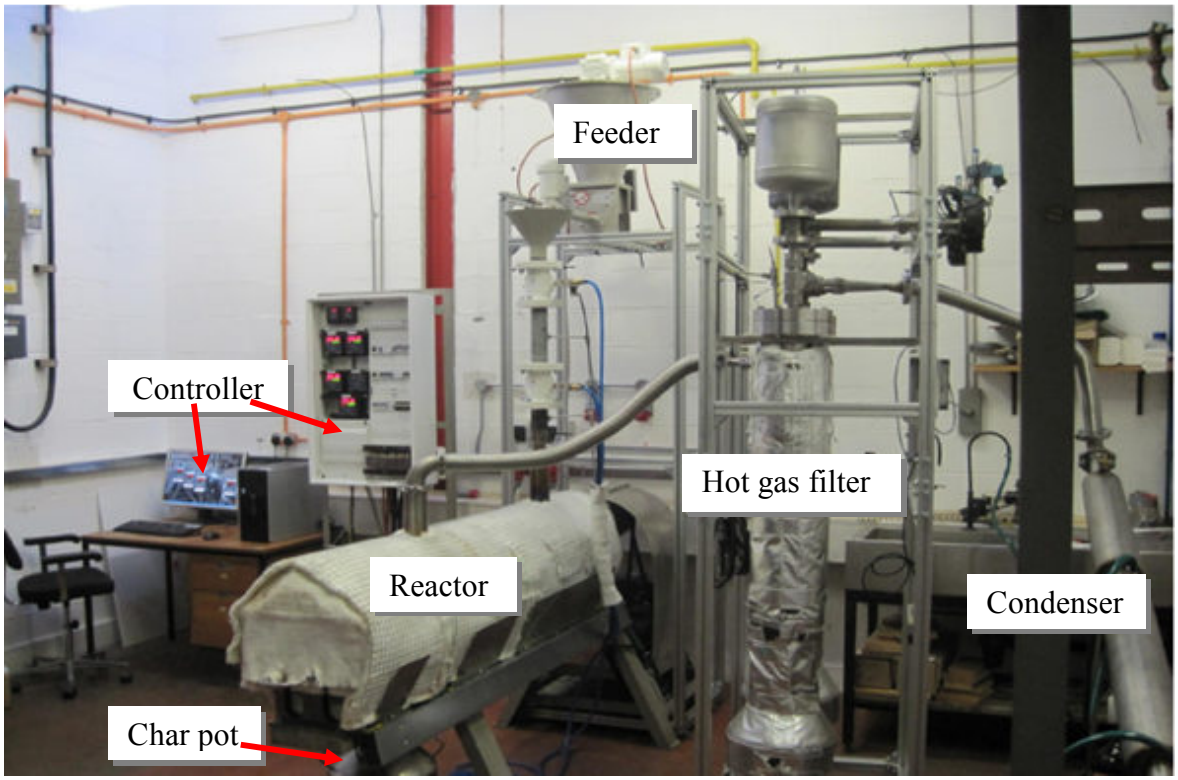

Fig. 6.1 Intermediate pyrolysis unit (Pyroformer) set-up at EBRI, Aston University

Fig.6.2 shows the diagram of pilot scale intermediate pyrolysis unit which consists of seven sections (feeding system, pyrolysis reactor, hot gas filter, vapour-condenser, electrostatic precipitator, char pot and controller). The feeding system is located at the top of reactor and allows feed transfer into reactor with controlled rates. Feed goes to reactor at a side of reactor and moves along the reactor by means of two screws with opposite movements. The residence time of solid phase (~ 5 min) can be controlled by the rate of these screws, while the vapour residence time is in few seconds. Nitrogen gas (~ 50 l/h) is flushed inside the reactor during the experiment to remove oxygen gas from the system and carries volatiles to hot gas filter to remove solid particles from volatile gases. The solid residue or bio-char will be collected at the char pot at the bottom below the reactor. The cleaned pyrolytic gases progress a long tube of condenser which is cooled by water flow. The condensed liquid products are collected in bottles beneath the condenser and the incondensable gases go to the electrostatic precipitator. Some pyrolysis oil will be recovered in electrostatic precipitator and the permanent gases will go through a venting duct.

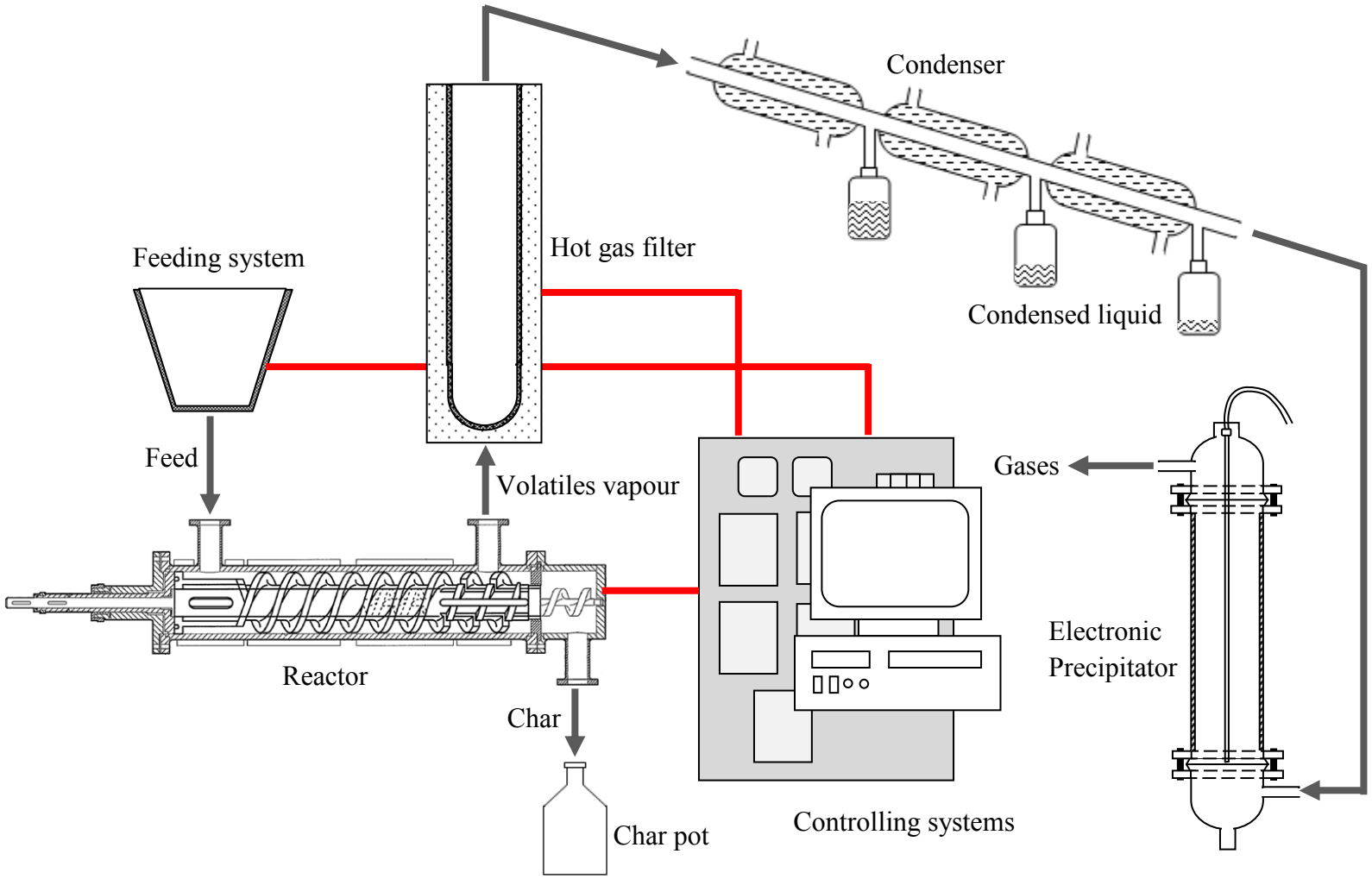

Fig. 6.2 Diagram of Pyroformer set up at EBRI, Aston University

6.2 Experimental

6.2.1 Pyrolysis experimental set-up

Chlorella vulgaris was pelletized to 0.5-1.2 cm length by a Pellet Press/Pelletiser-Flat Die at temperature 70-80°C and then was tested with intermediate Pyroformer reactor. The nitrogen gas (0.2 MPa pressure) was used as the sweeping gas to remove oxygen from the reactor and purge the gas phase out of reactor. Reactor was externally heated from ambient temperature by 100°C steps with holding time 45 min until reaching 500°C and this temperature was kept throughout the experiment. The 10 kg of sample was fed into reactor at constant temperature of 500°C with 3.3 kg/hr of feeding rate. After the gas phase was filtered through a hot-gas filter, most of condensable compounds were collected at the condensers. The bio-char was collected in the char pot at the bottom of the reactor. Char pot and liquid bottles were left to cool down before taking products for measuring product yields and further analysis.

6.2.2 Liquid product analysis

Condensed liquids separated into two phases which were the organic phase in the top called bio-oil or pyrolytic oil and the aqueous phase at the bottom (Fig.6.3). The organic phase was separated easily from the aqueous phase by using gravity separation in a separatory funnel and this separated oily phase would be further analysed.

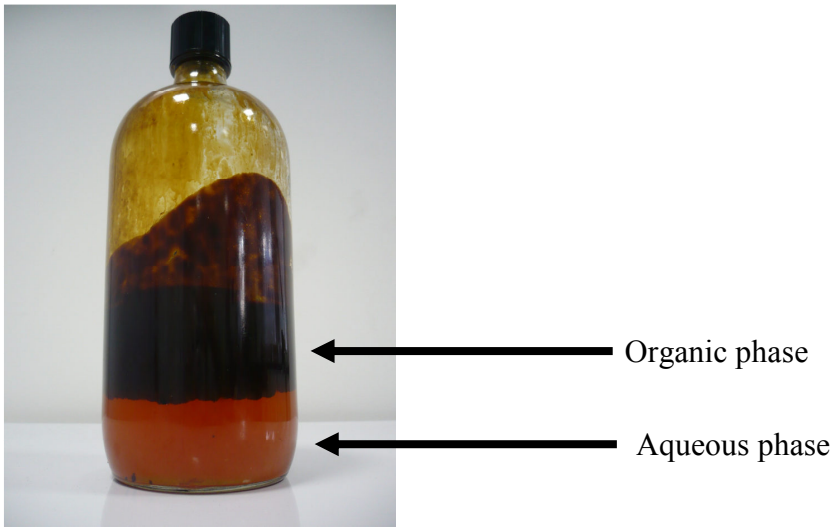

Fig. 6.3 Liquid products from intermediate pyrolysis of *Chlorella vulgaris* at 500°C

The organic phase, a dark brown liquid, was determined its calorific value by Parr 6100 Bomb Calorimeter. The water content was determined by Karl-Fisher Titration (V2-Volumetric KF Titration, Mettler Toledo). The elemental analysis results were obtained from MEDAC Ltd. Moreover, the key chemical compounds presenting in bio-oil sample were identified by Gas Chromatographic Mass Spectrometry (GC/MS). GC/MS analyses were performed by a Hewlett-Packard (Series II 5890) gas chromatograph and a Hewlett-Packard mass spectrometer 5972 series with a mass selective detector and a 60 m length × 0.25 mm film thickness DB 1701 column. The pyrolytic liquid was dissolved in dichloromethane (DCM) in the ratio 1:100 and filtered by microfilter. The sample was injected into a GC at 310°C with helium gas as a carrier gas at 30 mL/min. The oven temperature was increased from 40°C to 290°C by a ramp at 3°C/min and held for 20 min. The mass spectrometer scan range was from 50 to 550 mass units and chemical compounds corresponding to each peak in bio-oil chromatogram were identified by using the mass spectral library (NIST) and chromatogram database of standard chemicals.

6.2.3 Solid product analysis

Fig. 6.4 Bio-char from intermediate pyrolysis of *Chlorella vulgaris* at 500°C

Solid residue or bio-char (Fig.6.4) collected from char pot was ground and analysed by mean of ultimate and mineral analyses, proximate analysis by thermogravimetry (TG) technique and Fourier transform Infrared Spectrometry (FTIR). The ultimate and mineral

analysis results were obtained from MEDAC Ltd. The proximate analysis of bio-char was studied by TG (TGA-DSC1, Mettler Tolledo) in helium atmosphere at 100 mL/min flow rate. Samples of 10 mg were pyrolyzed from ambient temperature to 900°C with heating rate of 20°C/min. FTIR measurements of the bio-char samples was performed using a Perkin Elmer Spectrum 100 FTIR Spectrometer to identify the chemical structure. Solid samples were analysed using KBr as transparent pellets and measured with 16 scans in the range 4000-400 cm^{-1} with background subtraction.

6.3 Results and discussion

6.3.1 Product yields and the performance of pyrolysis set-up

Products from pyrolysis can be classified into three phases: solid, liquid, and gaseous phase. Their produced yields are shown in table 6.1.

Table 6.1 Product yields from the intermediate pyrolysis at 500°C of *Chlorella vulgaris*

Products	Liquid		Solid	Gas*
	Organic phase	Aqueous phase		
Yield (wt%)	14.11	11.55	26.44	47.90

* by difference

The product yields of bio-char and pyrolytic liquid were in similar amounts. The yield of liquid products (25.66 %) of *Chlorella vulgaris* was in the range of those (~17-55 %) from literature [17, 18, 312, 319]. However the product yields depend on many factors such as kind of microalgae, reaction temperature, residence time, features of reactor. From the observation of this preliminary run, some of the microalgae powder adhered to the wall of the feeding line probably because of electrostatic forces and the adhesive oil produced at the feeding line. Therefore, they could not react completely and could block the feeding line. Moreover, the bio-char regarding from the algal feed in powder form was quite difficult to be removed from the reactor into char pot. As well as some tars recovered in the electrostatic precipitator could not be removed completely from the precipitator wall. Due to these reasons the liquid product yield from the preliminary run was low. As gaseous

product was obtained from the difference, the high gaseous product yield could be considered from the error of liquid product yield determination.

6.3.2 Bio-oil characteristics

The main components of microalgae and the complexity of pyrolysis process lead to difference in the properties of algal bio-oil compared to bio-oil from wood and fossil oil. To investigate the potential of bio-oil produced from *Chlorella vulgaris*, their properties are presented and discussed below.

Table 6.2 Comparison of bio-oil from *Chlorella vulgaris*, wood[17] and fossil oil[17]

Properties	Bio-oil/Oil (wt%)		
	Wood	*C.vulgaris**	Fossil
C	56.4	57.25	83.0-87.0
H	6.2	10.02	10.0-14.0
O	37.3	25.04	0.05-1.5
N	0.1	8.32	0.01-0.7
HHV (MJ/kg)	21	37.42	42
Density (kg/L)	1.2	0.95	0.75-1.0
Water content	15-30[163]	3.25	0.1[163]

* organic phase

The properties of *Chlorella vulgaris* bio-oil, woody bio-oil and fossil fuels [17] are presented in table 6.2 for comparison. The calorific value (HHV) of the organic phase was high at 37.42 MJ/kg, corresponding to their low water content at 3.25%. From elemental analysis, the organic phase of the microalgae had a carbon content value similar to woody bio-oil but it had higher hydrogen content. The lower oxygen content of organic phase bio-oil (25.04 wt%) caused the considerably high HHV and more stable than woody bio-oil. Usually, pyrolytic oil from biomass contains higher oxygen content than that of fossil oil and this lead to the instability of bio-oils. Their characteristics change during condensation and under storage. Their high nitrogen content could result from the high protein and chlorophyll content in microalgae, led to the concern about the formation of NOx during combustion. Hence for using of bio-oil as fuels or chemical sources, upgrading is required;

for example, to improve their storage stability and to reduce nitrogen content before applying to combustion process. Overall the characteristics of bio-oil derived from *Chlorella vulgaris* were comparable to that from woody biomass. They had higher heating value, lower density, and lower water content and were more stable than woody bio-oils.

To gain chemical information on bio-oil, the GC-MS peaks were assigned by reference compounds and the standards NIST Mass Spectra database. In Fig.6.5 the GC-MS spectra of organic phase dissolved in dichloromethane are shown. The results of GC/MS analysis revealed that algal bio-oil is a complex mixture of numerous compounds. The major compounds presenting in bio-oil are listed in table 6.3 which give about 14 different main products. The most abundant peak in this sample was toluene. Toluene, indole, hexadecanenitrile, phenol and 3, 7, 11, 15-tetramethyl-2-hexadecen-1-ol presented the high abundance in this bio-oil sample. Main classified groups of these compounds were aromatic, aliphatic and nitrogen-containing compounds. The GC-MS results identified some nitrogen-containing compounds such as pyrrol, pentanenitrile, 4-methyl-, indole, benzenepropanenitrile, and hexadecanenitrile. These compounds led to the high nitrogen content in bio-oil of *Chlorella vulgaris* pyrolysis and they could be considered deriving from protein and chlorophyll macromolecules. Microalgal bio-oil generally reported fewer oxygenated compounds than bio-oils obtained from lignocellulosic biomass [202, 320, 321].

Tetradecane and pentadecane found in this bio-oil sample are the straight-chain alkanes which are similarly found in diesel and aviation fuels. Like diesel, bio-oil also comprises of aromatic hydrocarbons such as toluene, ethylbenzene, styrene, phenol. Toluene is used as an octane booster in gasoline fuel used in internal combustion engines and also used as a solvent. Ethylbenzene is an important chemical in the petrochemical industry of the production of styrene which is a precursor for polystyrene and several copolymers. Indole is a popular compound in fragrances manufacturer and also a precursor for many pharmaceuticals. Overall, the building blocks for liquid transport fuel and chemical production are presented in this bio-oil sample. Many chemicals in this pyrolytic oil could be upgraded or isolated to high-value products. Compounds detected in bio-oil were correlated to the volatile products which could be detected from Py-GC/MS technique presented in table 5.6 of Chapter 5.

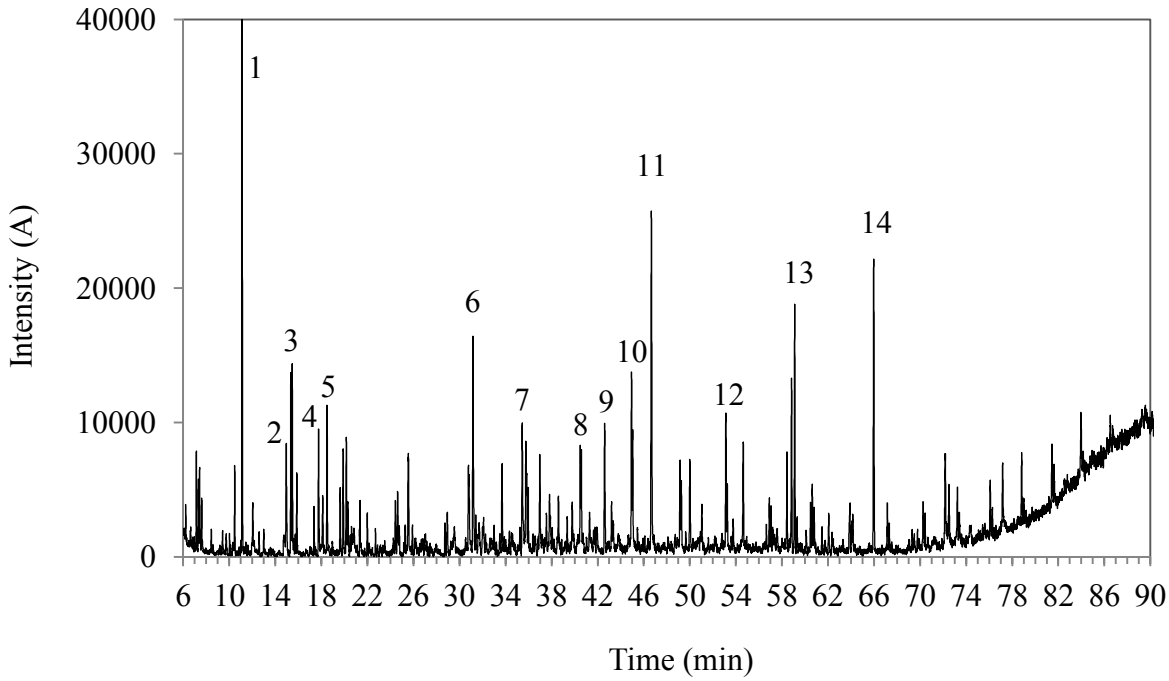

Fig. 6.5 GC-MS chromatogram of the organic phase of *Chlorella vulgaris* pyrolysis liquid products at 500°C with dichloromethane as the solvent

Table 6.3 Major chemical compositions of bio-oil from the pyrolysis of *Chlorella vulgaris* at 500°C with dichloromethane as the solvent

No.	RT (min)	Compound	MW
1	11.11	Toluene	92
2	15.34	Pyrrole	67
3	15.47	Ethylbenzene	106
4	17.76	Styrene	104
5	18.48	Pentanenitrile, 4-methyl-	97
6	31.17	Phenol	94
7	35.44	Phenol, 4-mehtyl-	108
8	40.48	Tetradecane	198
9	42.59	Benzenepropanenitrile	131
10	44.94	Pentadecane	212
11	46.66	Indole	117
12	53.13	Octadecane	254
13	59.1	3, 7, 11, 15-tetramethyl-2-hexadecen-1-ol	296
14	65.97	Hexadecanenitrile	237

6.3.3 Bio-char characteristics

Solid residue or bio-char from intermediate pyrolysis of *Chlorella vulgaris* at 500°C was dry and brittle with high porosity. The proximate, ultimate and mineral analysis results of this bio-char sample are shown in table 6.4.

Table 6.4 The Proximate, Ultimate and Mineral analysis of bio-char from pyrolylsis at 500°C compared to algal biomass

Analysis	*Chlorella vulgaris*	Algal bio-char
Proximate analysis (wt%)		
Moisture	5.80	0.61
Volatile	61.57	11.26
Fixed carbon*	15.95	46.51
Ash	16.68	41.62
Ultimate analysis (wt%)		
C	44.56	42.83
H	6.18	2.54
O	30.71	15.75
N	6.76	5.2
S	0.79	0.55
Mineral analysis (wt%)		
Ca	4.62	9.56
Na	1.24	2.69
K	1.09	2.70
P	0.67	1.83
Mg	0.33	0.61
Fe	0.25	0.78
Al	0.03	0.35

* by difference

Moisture content in algal char was very low at 0.61% and the volatile matter decreased from 62% for the raw microalgae to 11% for the bio-char, while the fixed carbon and ash content were significantly increased. The elemental analysis showed that in bio-char there were some oxygen and nitrogen remaining in char structure. The high oxygen remaining in

bio-char can be considered as the bound oxygen in metal oxides. The main mineral matter in bio-char from *Chlorella vulgaris* were calcium, sodium, potassium and phosphorus. Most of the mineral matter was concentrated in the char although some of metal may be volatilised during pyrolysis process. The high ash content remaining in bio-char can be considered for the application of bio-char as a fertilizer or catalyst. Bio-char can be put into ground to improve the productivity of soil and enhance crop yields [322]. Also bio-char can be extracted by suitable solvent to recover useful nutrients.

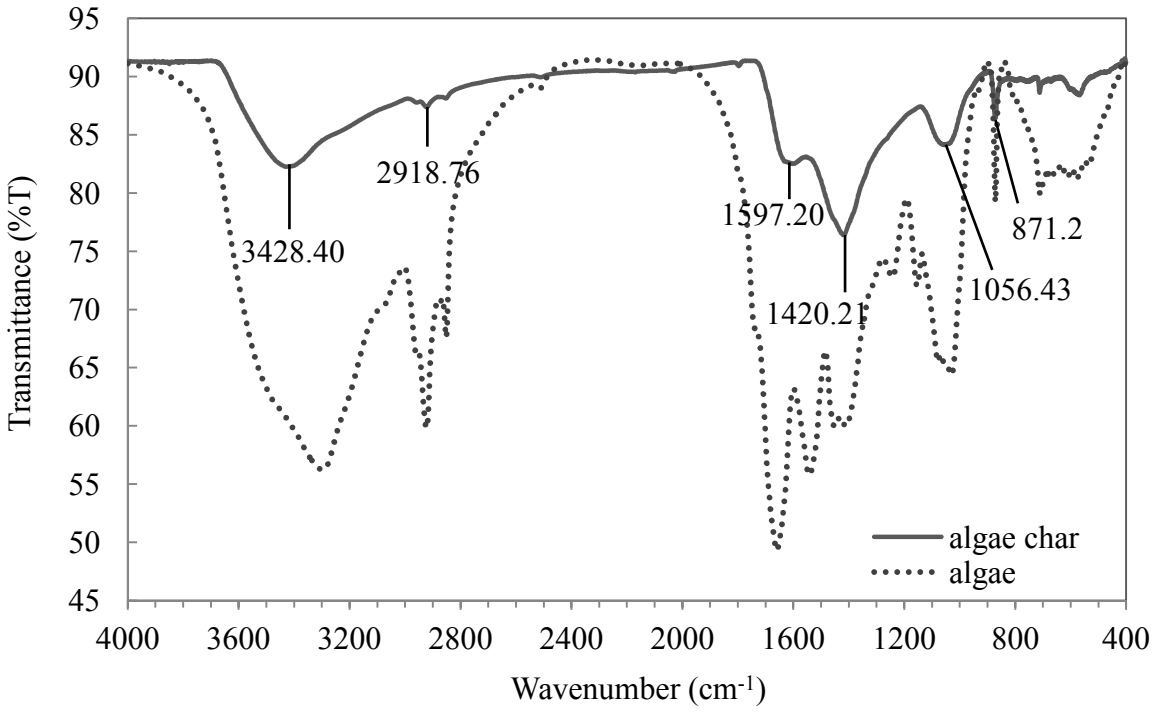

Fig. 6.6 FTIR chromatograms of *Chlorella vulgaris* and bio-char samples from intermediate pyrolysis at 500°C

To examine the chemical structure of bio-char, the chromatogram of *Chlorella vulgaris* char measured by FTIR technique is presented in Fig.6.6. The chromatogram showed the presence of some functional groups in bio-char. The band around 2900 cm^{-1} representing the aliphatic $–CH_3$ and $–CH_2$- stretching had dramatically reduced after pyrolysis at 500°C, while CH_2 bending at 1420 cm^{-1} was still significant high. This can be interpreted that most of acyl chains/lipids were decomposed at temperature 500°C but the protein polymers were higher reactivity than lipids and there were proteins remaining after pyrolysis at 500°C. According to the observation above, the decease of the band at 3300-3500 cm^{-1} can be considered as the decrease of –OH group and the remain intensity of this band in bio-char

can be identified as the remaining of mainly –NH groups of protein and also related to the presence of 1597 cm^{-1} band which is representing another N-H stretching in protein. The band at 1056 and 871 cm^{-1} were reduced after pyrolysis which show that the decomposition of carbohydrate polymers. Moreover it can imply that the inside of sample pellets is not completely pyrolyzed because there is the presence of active functional groups in bio-char sample.

6.4 Summary and recommendation

Information on both laboratory and pilot scale pyrolysis of algal biomass is not as much as the extensive reports on the pyrolysis of a wide variety of lignocellulosic biomass in literature. The reported bio-oil yields from algae are in a wide range from 17–55 wt% which depends on the nature of conversion process and reactor, as well as the algae species. However, most of published results claimed the more promising properties of bio-oil from algae over woody bio-oil.

The Pyroformer, pilot scale intermediate pyrolytic reactor produced promising product yields and qualities. Bio-char is dry, brittle and contain high mineral content which is suitable to application as a fertilizer. Bio-oil produced from this pyrolysis unit contains several chemicals which can be upgraded as fuels and high-value chemicals. However, there are some aspects which are needed to be taken into account for further experiments with this reactor. First, the microalgae feed needs to be pelletized before feeding to reactor to reduce the blocking and uncompleted reaction of microalgae in powder form. Second, the condenser should be kept at lower temperature to improve the condensation of volatile products. Third, to gain more yield of pyrolytic liquid, tars captured at the electrostatic precipitator wall should be collected and take into the determination of yields.

The preliminary properties of bio-oil suggested that *Chlorella vulgaris* has potential to be utilized in the thermo-chemical conversion process although the competition with other sources due to its high ash content and high nitrogen content in bio-oil are concerned. The higher stability for storage, higher heating value, lower density and lower water content offer the better application for fuels than those of lignocellulosic bio-oil. Furthermore, bio-oil contains several useful chemicals, thus with suitable separation processes, these chemical can be recovered for utilization in other industries. However, to enhance yield

and product properties from microalgae, the reactor needs to be optimal designed based on the information of characteristics and kinetics which are important for the challenge to scale up into commercial production. Moreover the upgrading process and correlating applications should be taken into account, such as fertilizer aspect of bio-char or combination the pyrolyzer with a gasifier to recover energy from produced gaseous products.

Chapter 7

Isothermal Kinetic Analysis

To determine the formal kinetic parameters of pyrolysis process, two conditions of measurement can be carried out; isothermal and non-isothermal (dynamic) experiment. Each of them has both advantages and disadvantages. Firstly, this chapter is focused on the isothermal conditions, while the non-isothermal study is discussed in next chapter (chapter 8). The new developed Pyrolysis Mass Spectrometry (Py-MS) technique is chosen as an effective apparatus for isothermal measurements. The Py-MS operating conditions and also its potentials for isothermal study are presented here. Polyethylene, as a standard polymer, is studied under isothermal conditions to evaluate the instrument and methodology. In addition, isothermal kinetic analysis is applied to lignocellulosic materials for evaluating the instrument and evaluation procedure with typical biomass before employing to microalgae sample. The formal kinetic parameters are reported in form of apparent activation energy, pre-exponential factor and apparent reaction order.

7.1 Experimental set-up

A schematic of the rapid evolved gas analysis by the Mass spectrometry apparatus used in this study is shown in Fig.7.1. This effective micro reactor enables the determination of global kinetic parameters of thermal degradation reactions of solid and liquid samples by means of mass spectrometric data under isothermal conditions. The apparatus is comprised of the following components: (1) A Double-Shot Pyrolyzer, a vertical micro-furnace, is able to heat sample from ambient to furnace temperatures in less than a second. This rapid heating avoids uncontrolled decomposition and side reactions within the sample matrix. Helium gas is purged through reactor vertically at 20 ml/min. The sample holder allow to insert sample immediately into the constant temperature reaction zone (2) A stainless steel column as a transfer line with 2.5 m length and 0.15 mm inner diameter is kept at 300°C to

avoid the condensation throughout experiments. (3) A quadruple Mass Spectrometer (Hewlett Packard 5972 series) measures the fraction of produced volatile compounds.

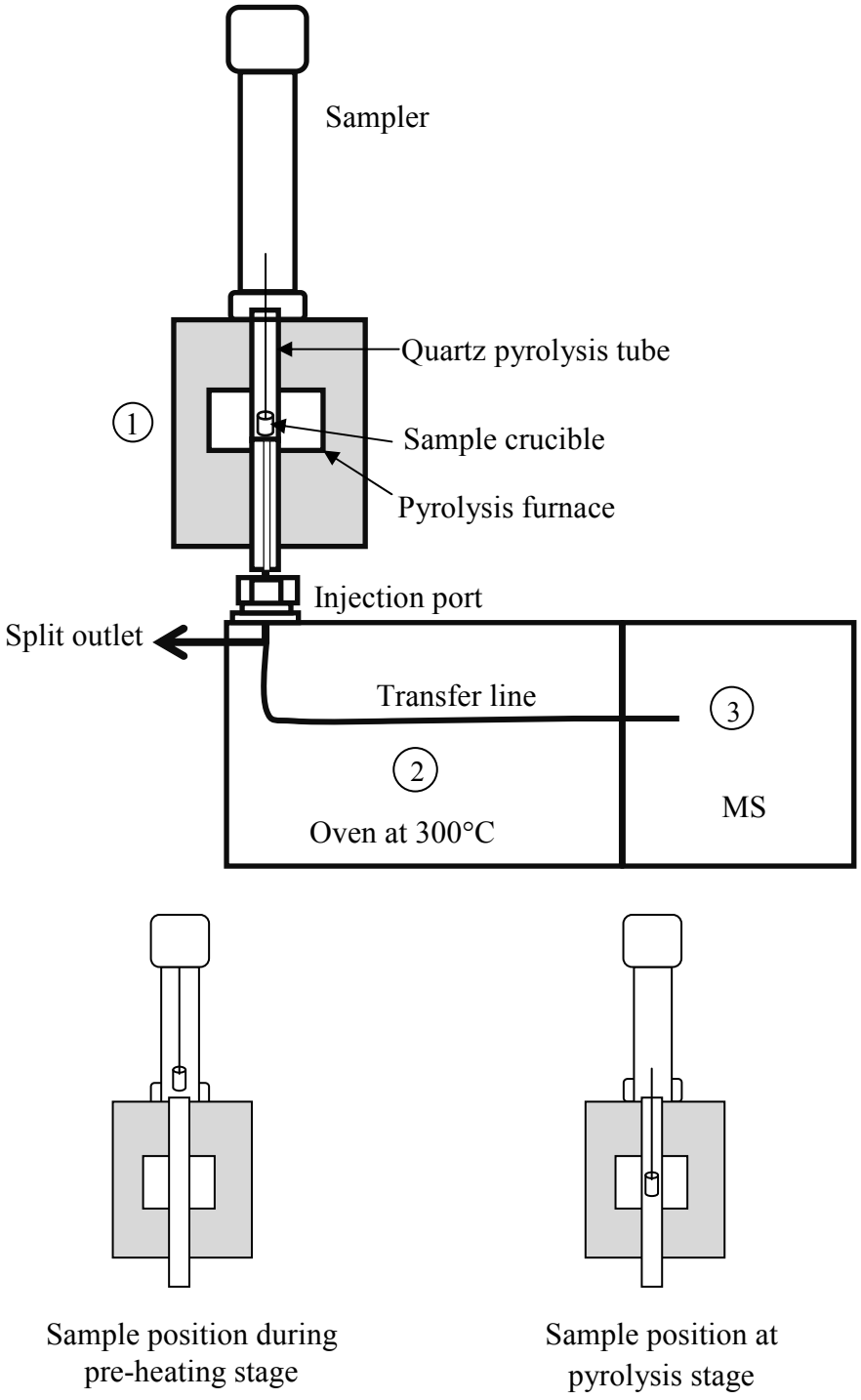

Fig 7.1 Diagram of the Double-Shot Pyrolyzer coupled with Mass Spectrometer for isothermal measurements

Measurements were performed with small sample size of 0.05-0.2 mg to minimize the effect from heat transfer phenomena. The reactor was purged to remove oxygen from the atmosphere for three minutes before sample crucible was dropped down into the furnace. The studied temperature ranges (Table 7.1) for each sample were selected according to their weight loss temperature range in dynamic thermal decomposition. Pyrolytic gases were injected continuously into transfer line at 300°C and were kept at this temperature along the way to the MS. The split ratio of the outlet products and carrier gas before going into mass spectrometer was set between 1:20 and 1:25. The fraction of produced gases was measured from 10 to 300 u. The measurement was considered to be finish when the evolution curve reaches its baseline, as no more decomposition taking place. Every experiment was repeated three times for reproductive results.

Table 7.1 Temperature ranges for isothermal measurements of each studied materials

Materials	**Polyethylene**	**Cellulose**	**Hemicellulose**	**Lignin**	***C. vulgaris***
Temperature(°C)	450-550	350-400	280-340	320-500	250-600

7.2 Evaluation of formal kinetic parameters from isothermal measurements

The single step kinetics for solid state decomposition with assuming of *n*th-order model ($f(\alpha) = (1-\alpha)^n$) is shown in equation (3.8). The degree of conversion for isothermal degradation obtained by integration of this equation

for $n = 1$ is

$$\alpha(t) = 1 - e^{-k(T)t} \quad \text{..... 7.1}$$

The degree of conversion is given by $n \neq 1$

$$\alpha(t) = 1 - (k(T)t(n-1)+1)^{1/(1-n)} \quad \text{..... 7.2}$$

where k is the rate coefficient and n is the apparent order of the overall decomposition reaction.

In the case of on-line gas analysis data by means of mass spectrometry for kinetic study, the ion currents in relationship with time *I(t)* are detected to follow the progression of thermal decomposition of solid or liquid samples. The degree of conversion is equivalent to the mass having already left the reactor $\int_0^t I(t)\overline{M}(t)\dot{V}dt$ plus the actual mass of products in the gas phase $I(t)\overline{M}(t)V_R$ normalized by the total evolved mass of products.

$$\alpha_{\exp}(t) = \left(\int_0^t I(t)\overline{M}(t)\dot{V}dt + I(t)\overline{M}(t)V_R \right) / \int_0^\infty I(t)\overline{M}(t)\dot{V}dt \quad \ldots\ldots\ldots\ldots \quad 7.3$$

where $\overline{M}(t)$ is the mean molecular mass at time *t* (calculated from the single ion currents), $\dot{V}$ is the flow rate and V_R is the reactor volume.

To evaluate the rate coefficient (*k*) and apparent order of reaction (*n*), the degree of conversion given by equation (7.2) is fitted by means of least square fitting in equation (7.4) to the experimental degree of conversion (equation (7.3)) from $\alpha_{exp}(t)$ by variation of *k* and *n*.

$$S = \frac{1}{N}\sum_{i=1}^{N}(\alpha_{\exp} - \alpha_{cal})^2 \equiv \min \ldots\ldots\ldots\ldots\ldots\ldots\ldots\ldots \quad 7.4$$

To determine the apparent kinetic parameters, the linear regression of $-\ln k(T)$ versus $1/T$ from the linear form of Arrhenius equation

$$\ln k(T) = \ln A - E_a / RT \quad \ldots\ldots\ldots\ldots\ldots\ldots\ldots\ldots \quad 7.5$$

can provide the apparent activation energy (E_a) and the pre-exponential factor (A) from linear slope and interception at Y-axis.

7.3 Isothermal kinetic analysis of polyethylene

Due to its less complicated structure and more published information on its thermal decomposition than biomass materials, polyethylene was used as a standard material to evaluate the instrument and experimental set-up, as well as the analysis process of isothermal kinetic study. Polyethylene which was used in this work is a small granule high-density polyethylene (Lupolen PE/HD 5261); mp.: 134°C.

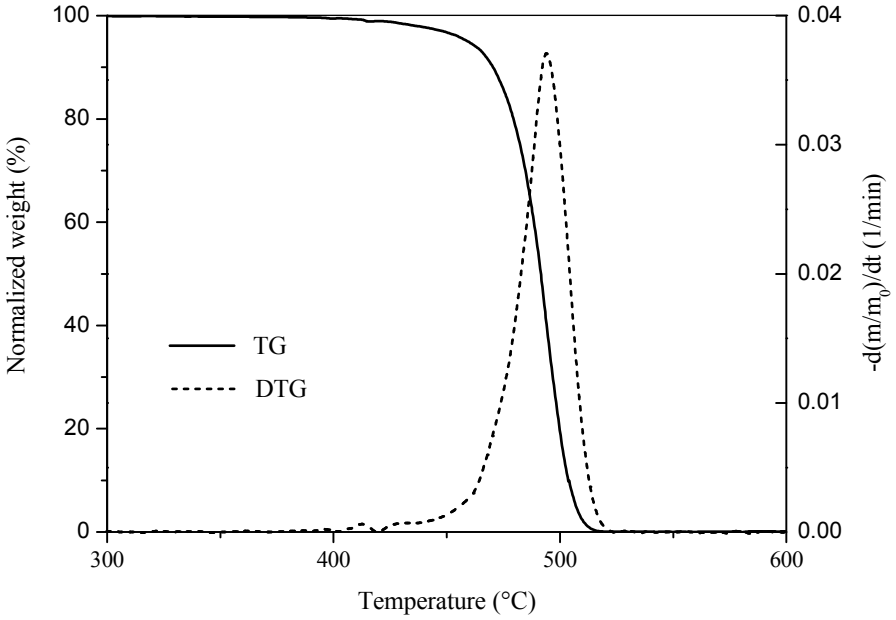

Fig. 7.2 The mass loss (TG) and its derivative (DTG) curves of polyethylene by thermogravimetry at heating rate 20°C/min

To identify studied isothermal temperature range, non-isothermal experiment of polyethylene by Thermogravimetry (TGA/DSC1 Mettler Tolledo) at heating rate 20°C/min with helium (100 ml/min) atmosphere showed that its thermal decomposition occurred in the temperature range of 450–520°C. The weight loss and derivative curves are shown in Fig.7.2. Thus, the different temperatures of isothermal experiments were chosen in the decomposition temperature range or higher. Eleven different temperatures from 450°C to 550°C with interval of 10°C were applied for the isothermal kinetic analysis. It is important to notice the difference between the product evolutions for temperature below and above 450°C. For temperature lower than 450°C, the evolution curves have the high noise to signal ratio and the low maximum sample conversion which will influence to the accurate kinetic analysis. The evolution profiles for different pyrolytic temperatures are presented at Appendix B.

Evolved gases from isothermal pyrolysis process were detected as the fraction of produced gases on the relationship with time. Degree of conversion (α) curves obtained from equation (7.3) show three different sections on their thermal decomposition behaviour. Fig. 7.3 is an example of the degree of conversion curve measured at temperature 500°C. At the first section (1), it is an initial induction period with a low velocity of decomposition

which can be attributed to the heating of the sample particles to reach a set temperature. In addition, this degree of conversion curve came from the measured signal by evolved gas analysis, thus the induction time can also include the transfer time between pyrolyzer and MS detector. The induction time reflecting heat transfer effect depends on reaction temperature and particle size; as the set temperature increases or particle size decrease, induction time is shortened. Next section (2) is the period with a rapid weight loss of the sample or the rapid production. Several reactions take place in parallel or series producing complex products until reaching section (3). There is a relatively long period of time with a reduced weight loss rate before the particles go to its final weight.

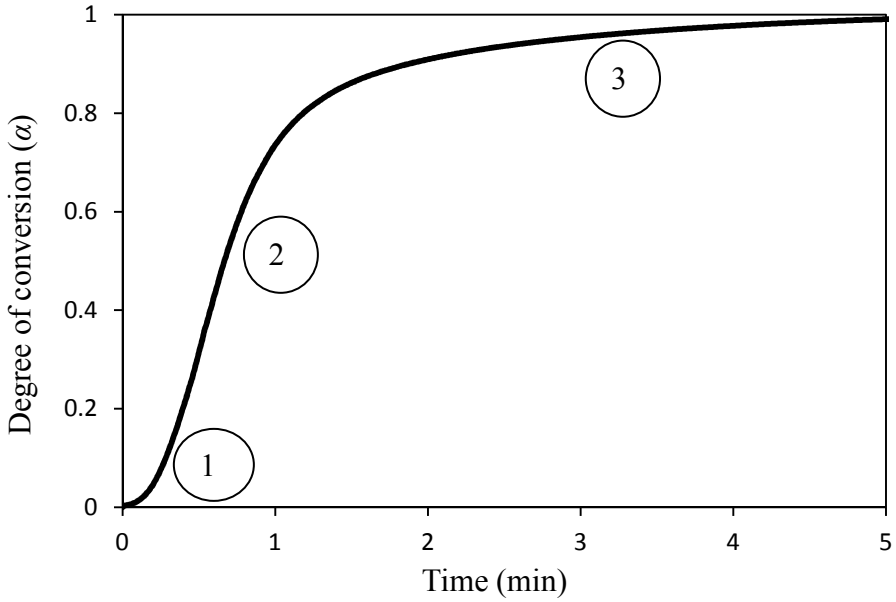

Fig. 7.3 The degree of conversion of polyethylene decomposition at temperature 500°C

Fig.7.4 shows the extent of reaction which fraction of the initial polyethylene mass converted to gas phase products at different isothermal temperatures. A very quick mass loss (90%) of polyethylene was observed within a time least than 1 minute at high temperatures and 10 minutes for 450°C. After this rapid decomposition, polyethylene continued mass loss slowly to the end of experiment. The long induction time of thermal decomposition of polyethylene can be considered as a melting process. Polyethylene has a melting point at 134°C which is lower than every isothermal temperature in this study. At the initial time of experiment, polyethylene particle not only is heated up to reach the set temperature, but also the absorbed heat is used for melting.

In addition, it shows evidence that the experimental set-up has high sensitivity. It could provide the promising degree of conversion curves of isothermal temperatures which are different in the small interval (10°C). In addition, the measurement time for each temperature is in the short period level. For polyethylene, each run could be finished in 25 minutes at 450°C and could be finished in a short time about 2 minutes at 550°C. Although the measurement time depends on reaction temperature and the type of studied material, this experimental set-up clearly reduces the time consumption which is a drawback found in isothermal kinetic study.

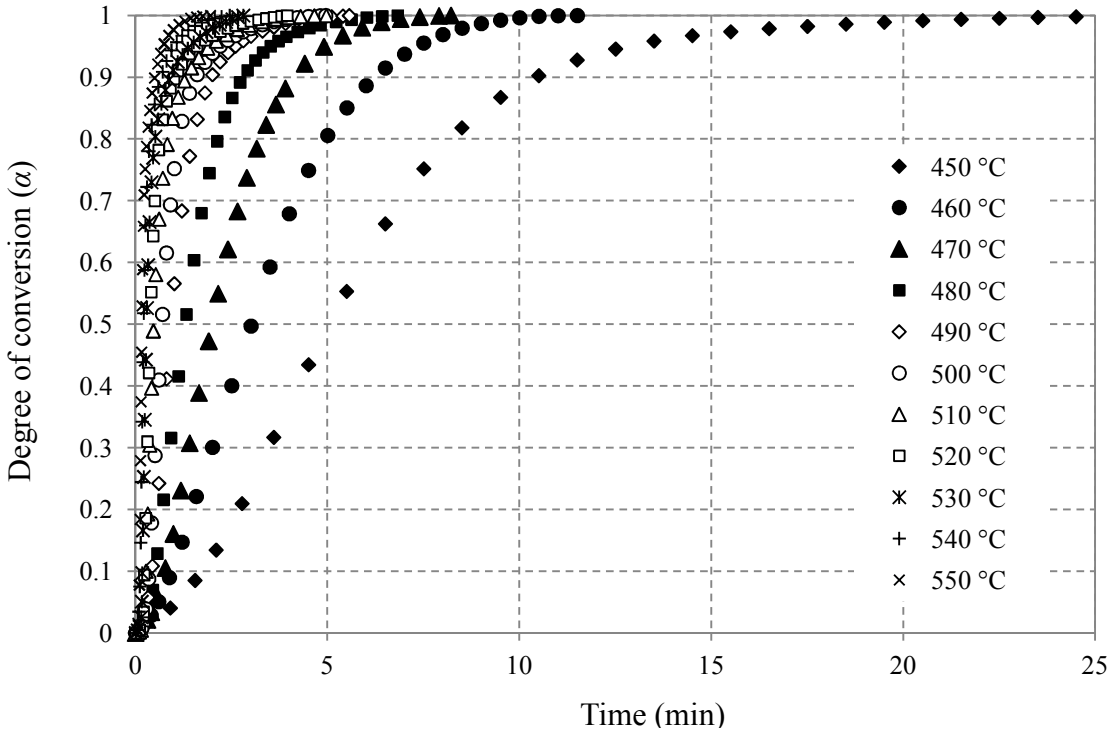

Fig. 7.4 Degree of conversion for the decomposition of polyethylene as a function of time at isothermal temperature range from 450 to 550°C

The degree of conversion curves from isothermal experiments were analysed for the rate coefficient (k) and apparent reaction order (n) by least square fitting (equation (7.4)). Apparent activation energy of thermal degradation of polyethylene (216 ± 9 kJ/mol) and a log of pre-exponential factor (14.89 ± 1.34 min^{-1}) were obtained from the linear regression of $-\ln k$ and $1/T$ in Arrhenius plot within 95% confidential interval (Fig.7.5). The coefficient of linear regression (R^2) is 0.9958. One of advantage of isothermal analysis over non-isothermal analysis is that the reaction order can be measured in dependence on

temperature, while non-isothermal analysis gives an average value of reaction order in the whole temperature range. Thus, the change of mechanism can be detected in isothermal measurement. For polyethylene thermal decomposition in the studied temperature range, the apparent reaction order (Fig.7.6) is constant at 0.7 at temperature range 450-470°C and then increases up to 1.6. This increase was also observed in literature which it was involved the alkane formation at longer reaction times and higher temperature [28]. Despite the varying reaction order, the activation energy is constant throughout the temperature range. This can be considered that the rate determining step is remaining the same reaction.

The comparison between the experimental degree of conversion curves and the model degree of conversion curves are shown in Fig.7.7. The model thermal decomposition can represent the measured thermal decomposition of polyethylene in a wide range of temperature with the small deviation range of activation energy at 9 kJ/mol and of log pre-exponential factor at 1.34 min^{-1}. The deviation between model and experimental data is caused by the melting process at the initial time of thermal decomposition of polyethylene. However at high degree of conversion the influence of melting disappears, the fitting becomes more promising.

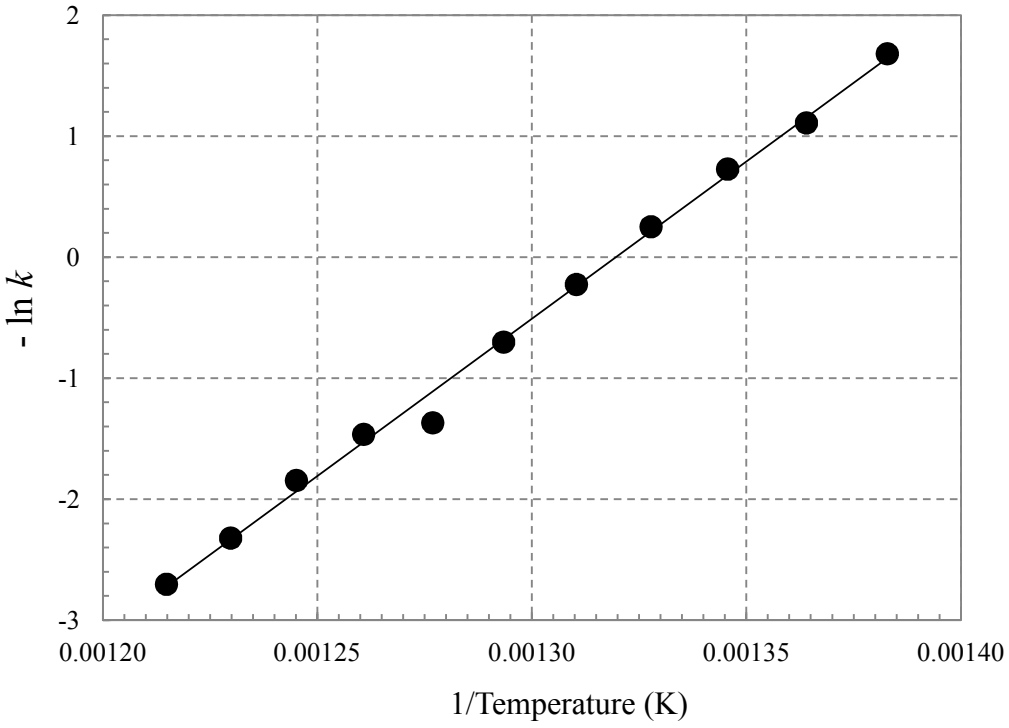

Fig. 7.5 Arrhenius plot for the isothermal decomposition of polyethylene from 450 to 550°C

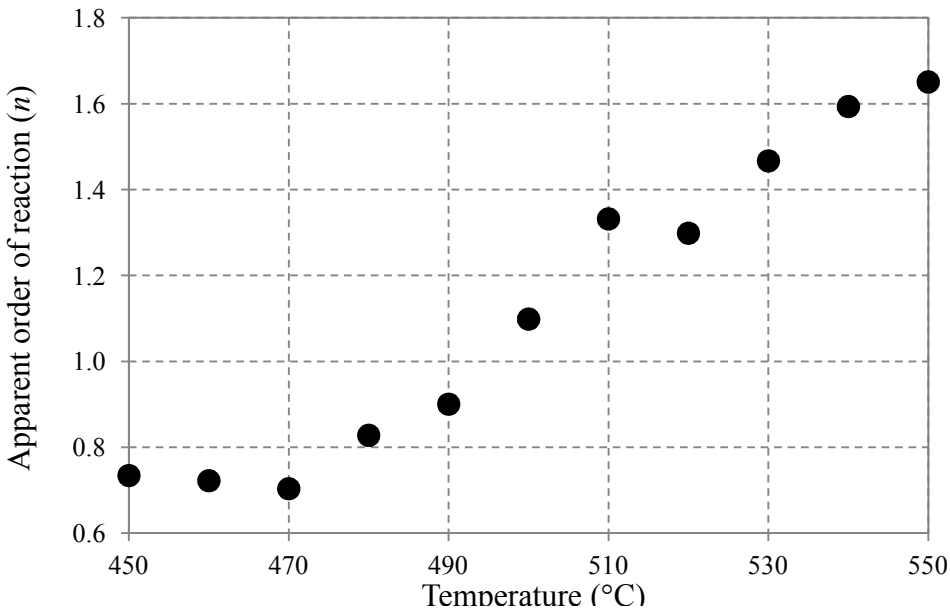

Fig. 7.6 Apparent order of reaction in dependence on temperature of polyethylene

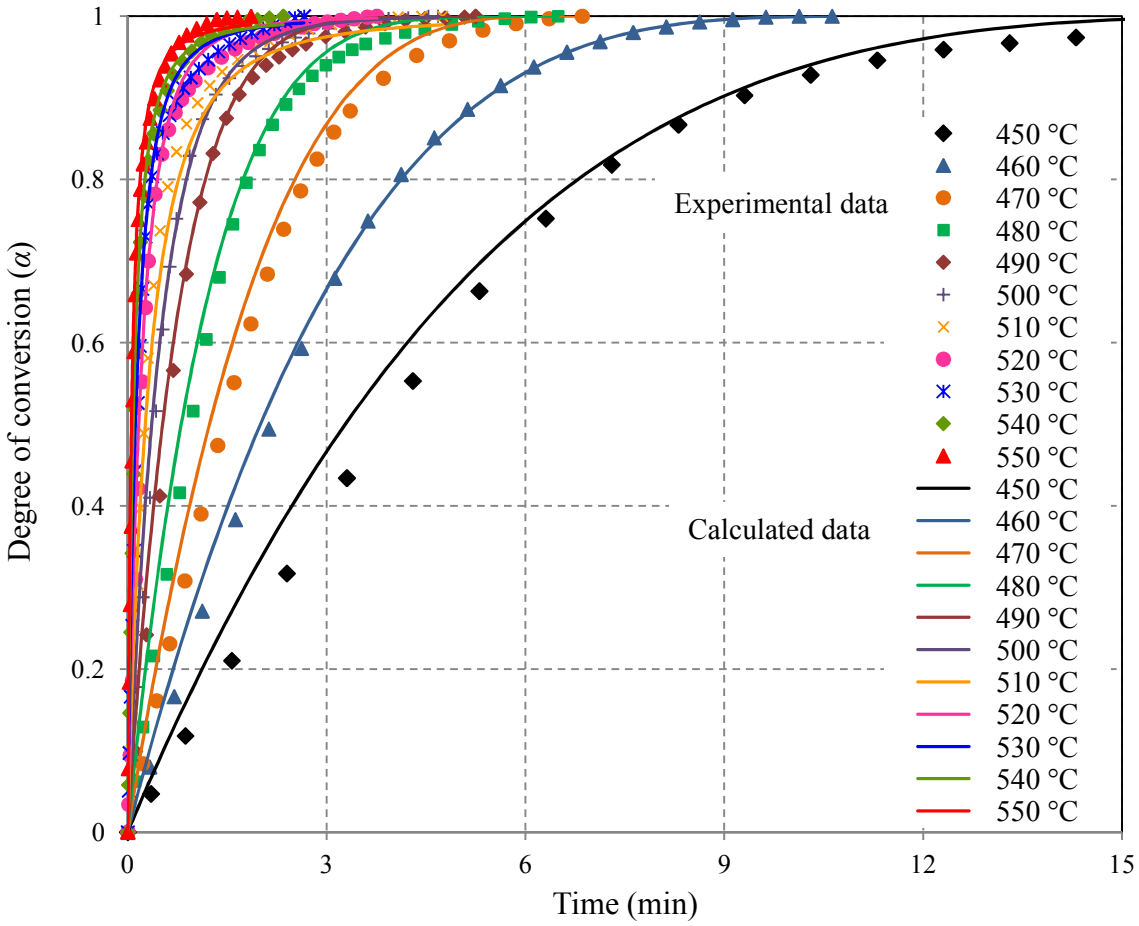

Fig. 7.7 The comparison of degree of conversion from experiments and from calculation (dots for experimental curves and solid line for calculated curves)

Moreover, the formal kinetic parameters of polyethylene have been compared to those obtained by other researchers considering under different operating conditions (Table 7.2). Although the results have been obtained considering different reaction orders and even diverse experimental conditions, a very acceptable agreement is observed. There is a kinetic compensation effect between log A and E_a among the reported data (Fig.7.8) which has been considered to be the result of mathematical, physicochemical and experimental causes [258]. The relationship of the compensation effect (based on data in table 7.2) can be derived in a form:

$$\log A = 0.0743\ E_a - 1.6175$$

Table 7.2 Reported kinetic parameters of thermal degradation of high density polyethylene

Ref.	**Analysis**	E_a **(kJ/mol)**	**log** A **(min^{-1})**	n
[30]	isothermal (440-480°C), Closed loop-type reactor	268	17.78	0.8-1.4
[323]	isothermal (445-460°C), custom-made thermobalance	192	12.59	0.5
[324]	isothermal (390-470°C), TG-DTA	249*	17.24*	0.86-1.0
[325]	isothermal (400-450°C), TGA	220	15.06	1.0
[324]	dynamic (5-50°C/min), TG-DTA	347	24.4	1.0
[326]	dynamic (5-20°C/min), TGA	214 -269	15.16-22.39	0.6
This work		216	14.89	0.7 – 1.6

* obtained at n = 1

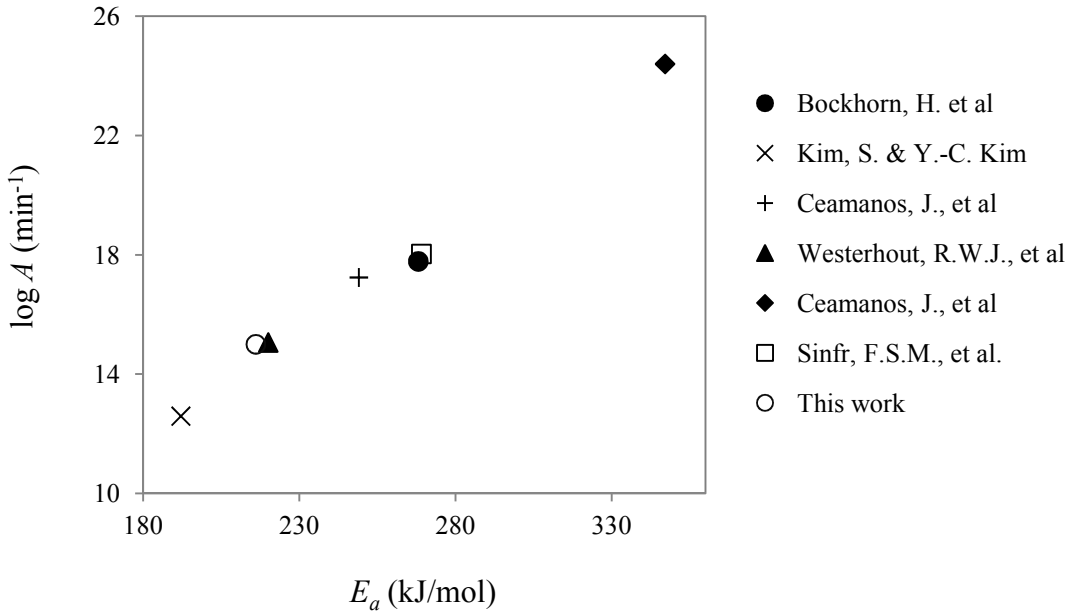

Fig. 7.8 The relationship of log A and E_a obtained from literature in table 7.2 (*Ref. Bockhorm, H. et al [30]; Ceamanos, J. et al. [324]; Kim, S. [323]; Sinfr, F.S.M., et al. [326]; Westerhout, R.W.J., et al. [325]*)

Most of researchers have used thermogravimetry for kinetic study in both isothermal and non-isothermal condition. Different operating system (i.e. reactor design, reaction temperature, heating rate, atmosphere and inert gas flow rate) and sample size can be the important causes of the discrepancy. For example, the isothermal measurements with thermogravimetry technique need to heat up samples with slow heating rate to reach the desired temperatures. Thus, there are some decompositions already taking place during heating period. Heating rate is an important factor to the diversity in reported kinetic data according to heat transfer phenomena. Also some reactors require a large amount of sample which is different from sample size (0.05-0.2 mg) required for the reactor used in the present work.

To summarize, the isothermal kinetic analysis of polyethylene as a standard material can lead to some conclusions and recommendations as:

(1) The experimental set-up by micro reactor coupled to a mass spectrometer which was used in this present study has a potential to monitor the progression of pyrolysis process and to be an apparatus for isothermal kinetic study.

(2) The amount of sample per measurement is very small which minimizes the effect from heat and mass transfer. Also this experimental set-up is suitable for the analysis in the case of limited amount of samples.

(3) Each measurement takes a very short period, thus the drawback of isothermal study, which is time-consuming, can be reduced by this experimental method.

(4) Most isothermal kinetic measurements have suffered from uncertainty arising from decomposition that could occur during the course of the temperature rise to the target values. In this work, sample was inserted into the furnace at a constant temperature. The decomposition during heating period can be eliminated. Although there is a detectable induction time, it is very small comparing to the whole measurement time.

(5) The model of thermal decomposition of polyethylene can represent the experimental data for every studied temperature. However at these temperatures polyethylene go through a melting process which causes the diversity between the measured data and the model data at low degree of conversion.

(6) A restriction of this experimental set-up is that the lowest isothermal temperature should keep in the temperature range of mass loss in non-isothermal measurement. Due to this system is applied with very small amount of sample, at low temperature the high noise to signal ratio of evolution curves and low maximum solid conversion will affect to kinetic analysis.

(7) The obtained formal kinetic parameters of polyethylene as apparent activation energy (216 ± 9 kJ/mol), the log of pre-exponential factor (14.89 ± 1.34 min^{-1}) and order of reaction (0.7-1.6) are acceptable with literature data; although there is a compensation effect and the difference among reported data.

The kinetic evaluation of polyethylene decomposition shows that this instrument and the procedure have potential for isothermal analysis. Then, this new technique and evaluation procedure are employed to the typical wood based materials (cellulose, hemicellulose, and lignin) to demonstrate that the unit is capable to assess the formal kinetic parameters from biomass components before applying to algae sample.

7.4 Isothermal kinetic analysis of cellulose

Isothermal measurements for Whatman filter paper as a representative for cellulose were carried out at 350, 360, 370, 380, 390 and 400°C under helium atmosphere. Complex products were detected by mass spectrometer from 10 to 300 mass units and normalized amount of each mass product is shown in Fig.7.9. The most abundant product is levoglucosan (*m/z* = 60). Also hydroxyacetaldehyde (*m/z* = 31), formaldehyde (*m/z* = 29), water (*m/z* = 18), carbon dioxide (*m/z* = 44), carbon monoxide (*m/z* = 28) and several tars are the relevant products of thermal decomposition of cellulose.

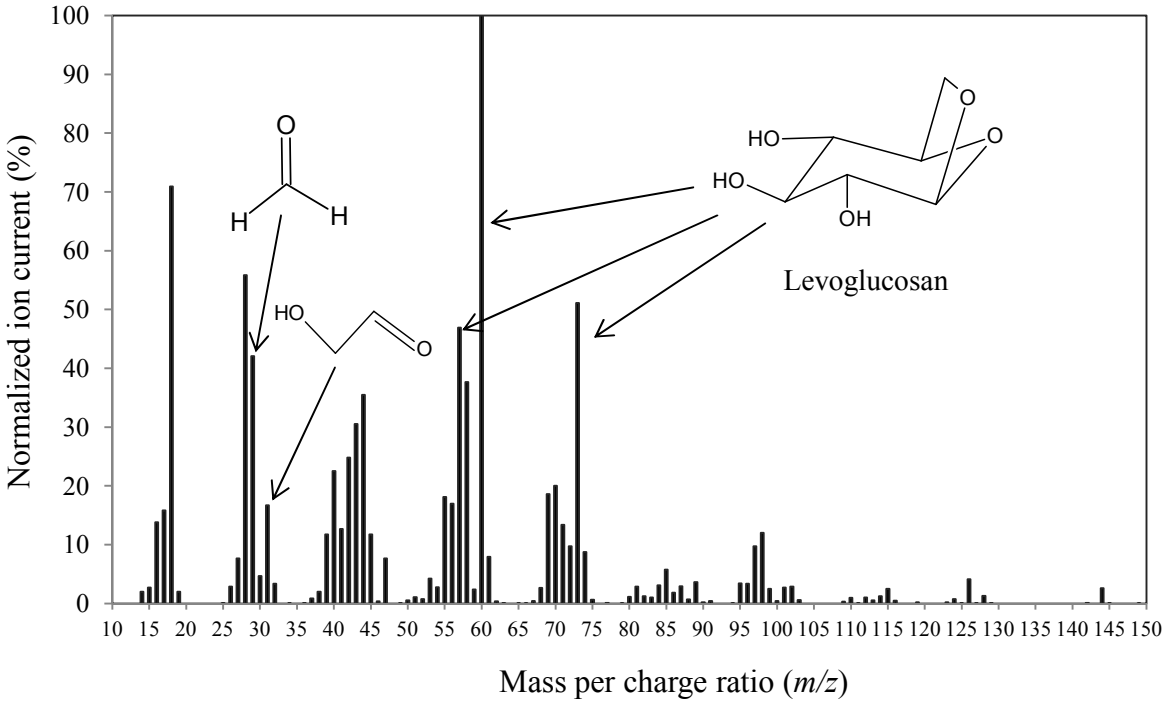

Fig. 7.9 Mass spectrum obtained by isothermal degradation of cellulose at 350°C

The typical fraction decomposition reaction (α) versus time (t) curves at different temperatures of cellulose is presented in Fig.7.10. In this temperature range, the 90% decomposition of cellulose was obtained at less than 4 minutes. Short induction periods (~6 s) refer to the heating of sample particles for all measurement (350-400°C).

For evaluation of the kinetic data, the degree of conversion equation is fitted by means of least squares fitting by variation of k and n to the experimental degree of conversions. Apparent activation energy (E_a) obtained from the Arrhenius plot in Fig.7.11 with 95%

confidential interval is 131 ± 6 kJ/mol and the log of pre-exponential factor is 10.89 ± 1.19 min^{-1} with a coefficient of linear regression (R^2) at 0.9928. The temperature-dependent reaction order (Fig.7.12) of cellulose thermal degradation is considered to be constant at 1.06 for temperature between 350 and 400°C. The degree of conversion curves from obtained kinetic parameters is compared with the experimental curves in Fig.7.13. A good fitting can be observed at the whole range of temperature; although at higher temperatures the discrepancy becomes larger.

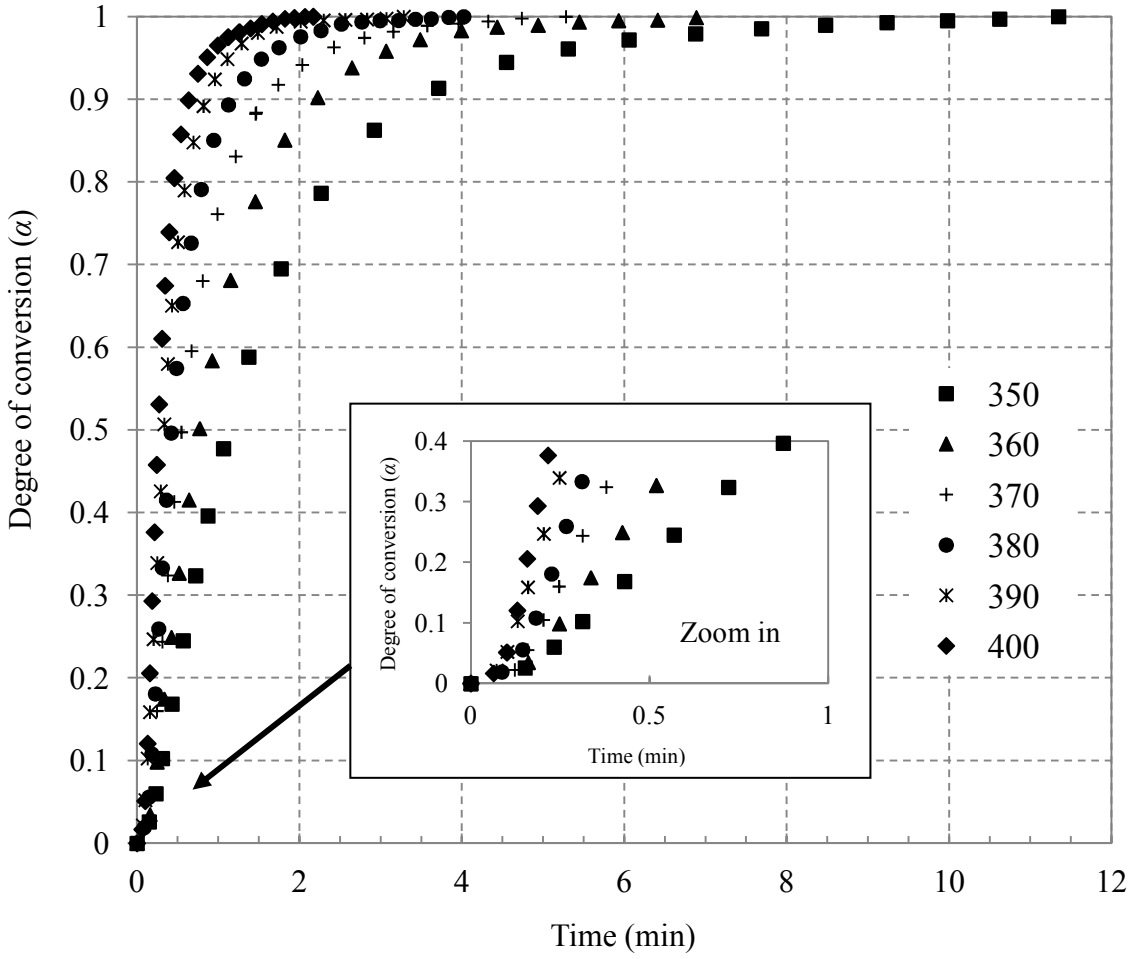

Fig. 7.10 Degree of conversion for thermal decomposition of cellulose as a function of time for temperatures at 350-400°C

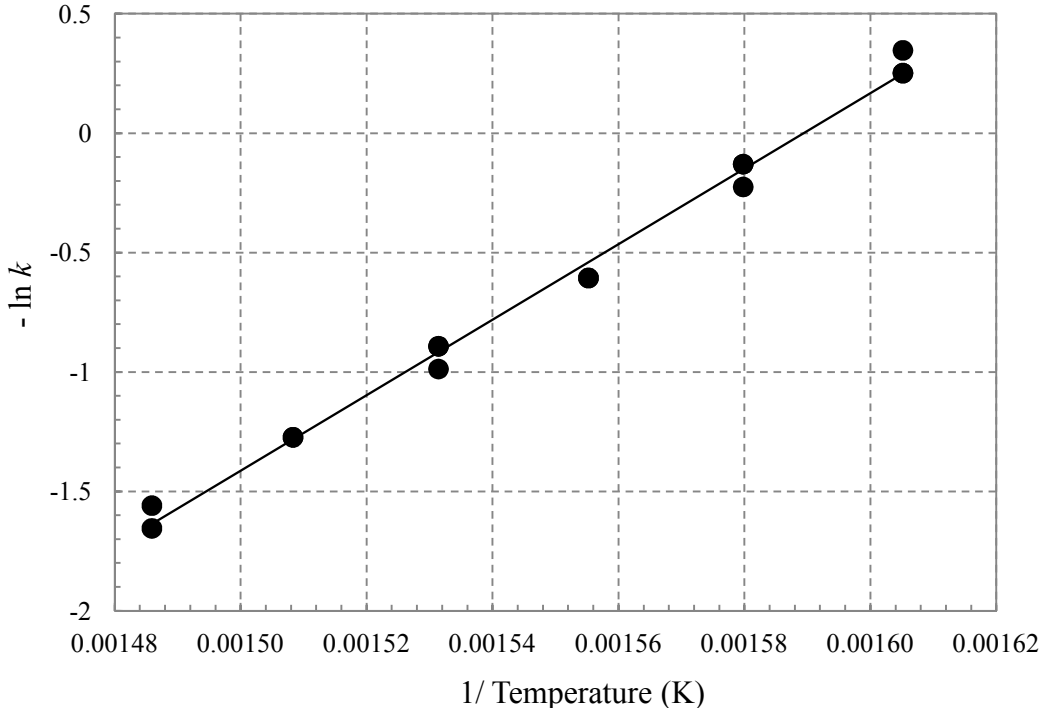

Fig. 7.11 Arrhenius plot for the decomposition of cellulose

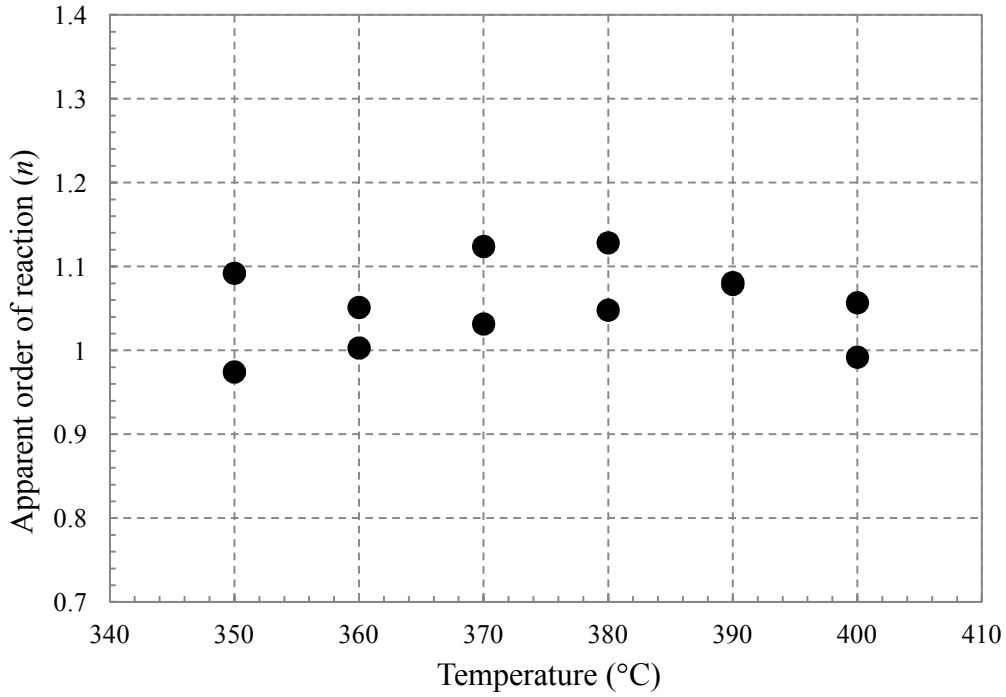

Fig. 7.12 Apparent order of reaction in dependence on temperature of cellulose

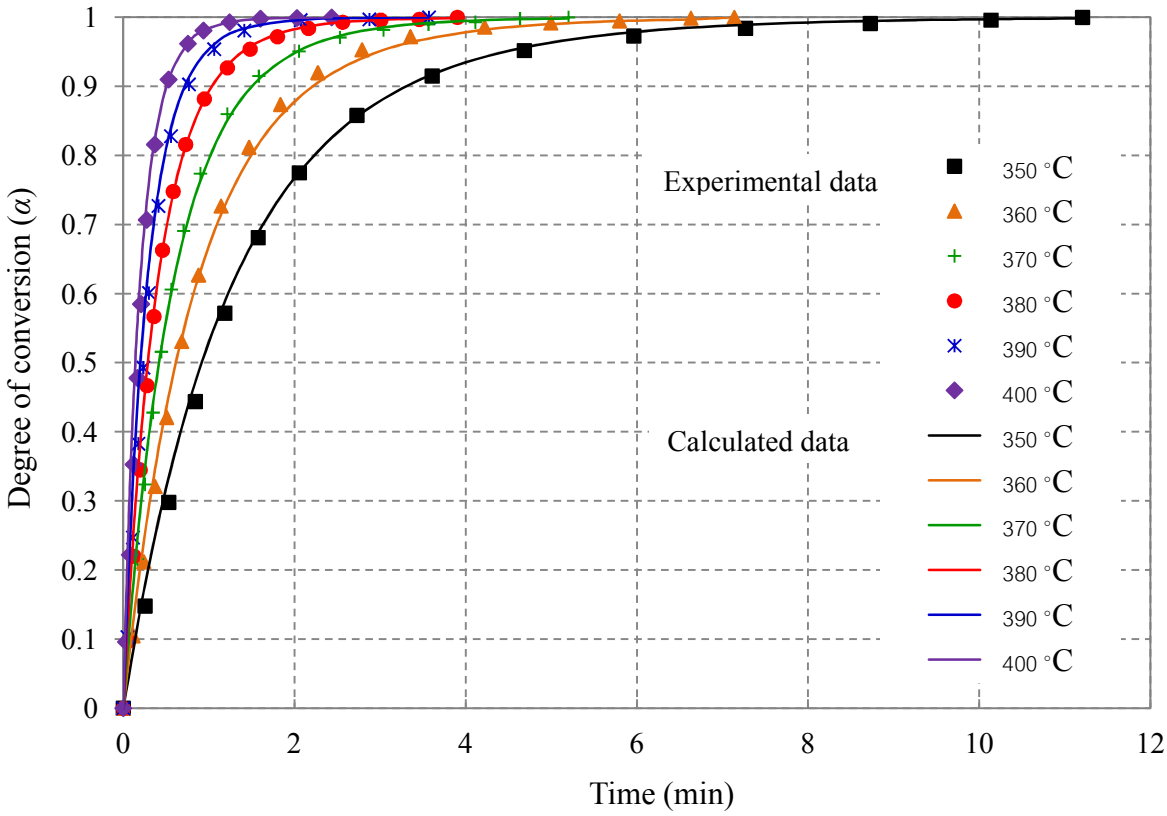

Fig. 7.13 The comparison of the degree of conversion from experiments and from calculation of cellulose (dots for experimental curves and solid line for calculated curves)

Fig.7.14 compares the apparent kinetic parameters of this present study (O) with those reported in literature. Most of kinetics of cellulose decomposition is based on a single reaction, expressed in term of total mass conversion (α). Also it is often that the reaction model is considered as n =1 reaction. Conesa, J.A., et al. [327] had tested several functions for cellulose decomposition and they reported a first-order rate model and a Prout-Tompleins type model giving the best fitting. While Dollimore, D. and Holt, B. [328] reported a good fit to weight loss data with Avrami-Erofeev rate equation.

The compensation effect among reported kinetic parameters in Fig.7.14 for cellulose thermal degradation is existent with a relationship as

$$\log A = 0.0708\, E_a + 1.4055; \quad R^2 = 0.9599$$

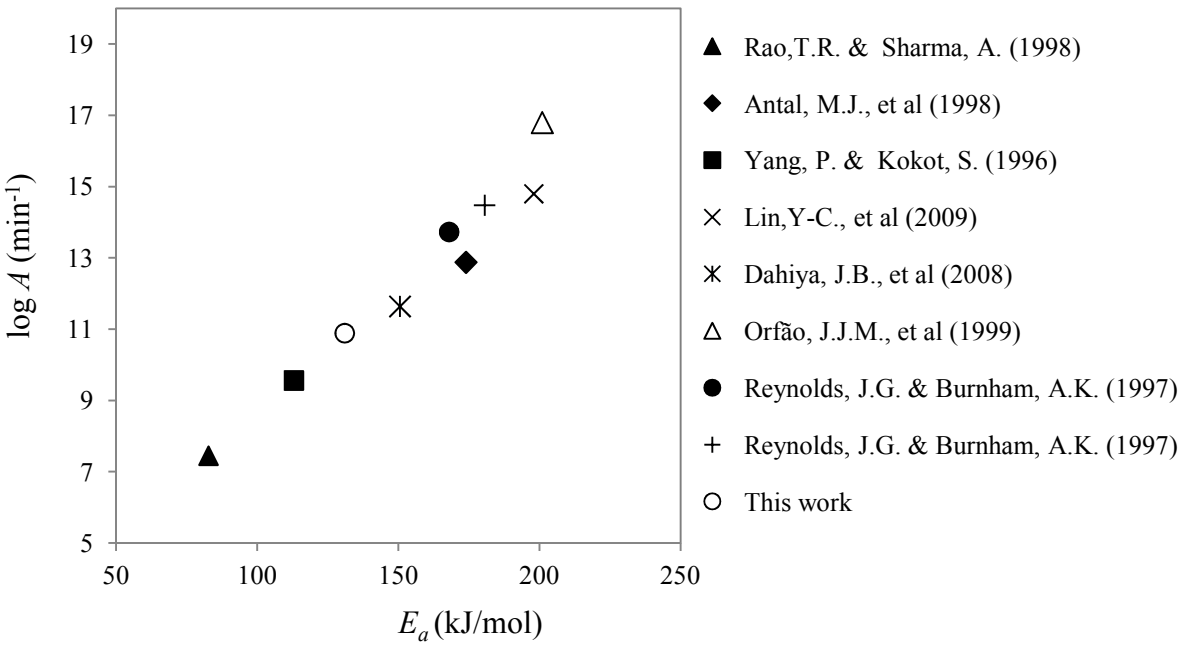

Fig. 7.14 The relationship of log A and E_a obtained from literature of cellulose decomposition and this work

(*Reference: Lin, Y.-C., et al. [270], Teng, H. & Y.-C. Wei [282], Antal, M.J., et al. [264], Yang, P. & S. Kokot [280], Capart, R., et al [273], Dahiya, J.B., et al. [31]*)

The varying of parameters is caused by the different types of cellulose, the heating rate, the sample mass and the evaluation of sample temperature during thermal decomposition. Moreover the published activation energy values and pre-exponential factors are valid for the certain temperature range.

7.5 Isothermal kinetic analysis of hemicellulose

Xylan as a representative of hemicellulose was pyrolyzed at 280, 290, 300, 310, 320, 330 and 340°C. Due to its lower reactivity than cellulose, the selected isothermal temperature range was lower than that of cellulose. These selected temperatures range is kept in the devolatilization region which was observed from non-isothermal weight loss data and these range is low enough to minimize the interrupting from char formation. At 300°C, the produced compounds from xylan decomposition are mainly the permanent gases as carbon dioxide, water, and carbon monoxide, as well as ketones, furans, carboxylic acids, and alcohols as shown in Fig.7.15. Tars can be detected up to m/z = 283.

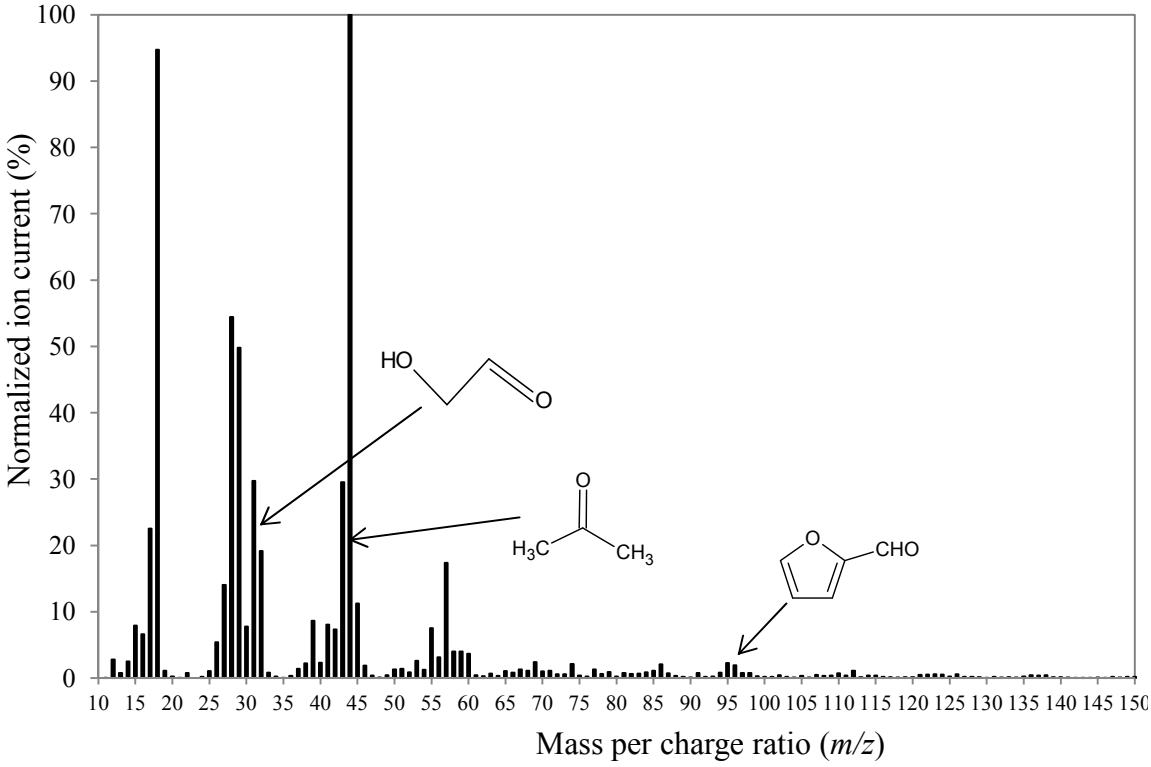

Fig. 7.15 Mass spectrum obtained by isothermal degradation of hemicellulose at 300°C

The degree of conversion curves of hemicellulose thermal decomposition are shown in Fig. 7.16 at various temperatures. Even though the reaction temperature is low (280°C), the degradation occur rapidly. The average induction period was about 3 second and the conversions at 90% were reached in 6 minutes.

Fig.7.17 shows the Arrhenius plot of hemicellulose at various temperatures. A linear regression at a coefficient of linear regression (R^2) of 0.9956 provides the apparent activation energy of 125 ± 5 kJ/mol and the log of pre-exponential factor of 11.53 ± 0.93 with 95% confidential interval. The order of reaction presented in Fig.7.18 shows an average order ($\bar{n}$ = 1.10). Due to the constant order of reaction, it can be implied that here is no mechanism change at temperature 280–340°C. The comparison between the experimental curves and the model curves (Fig.7.19) shows a good fit. It can be notified that at higher temperature the diversity of model from measurement data becomes greater. This model parameter can be applied with high accuracy for the whole range of studied temperatures.

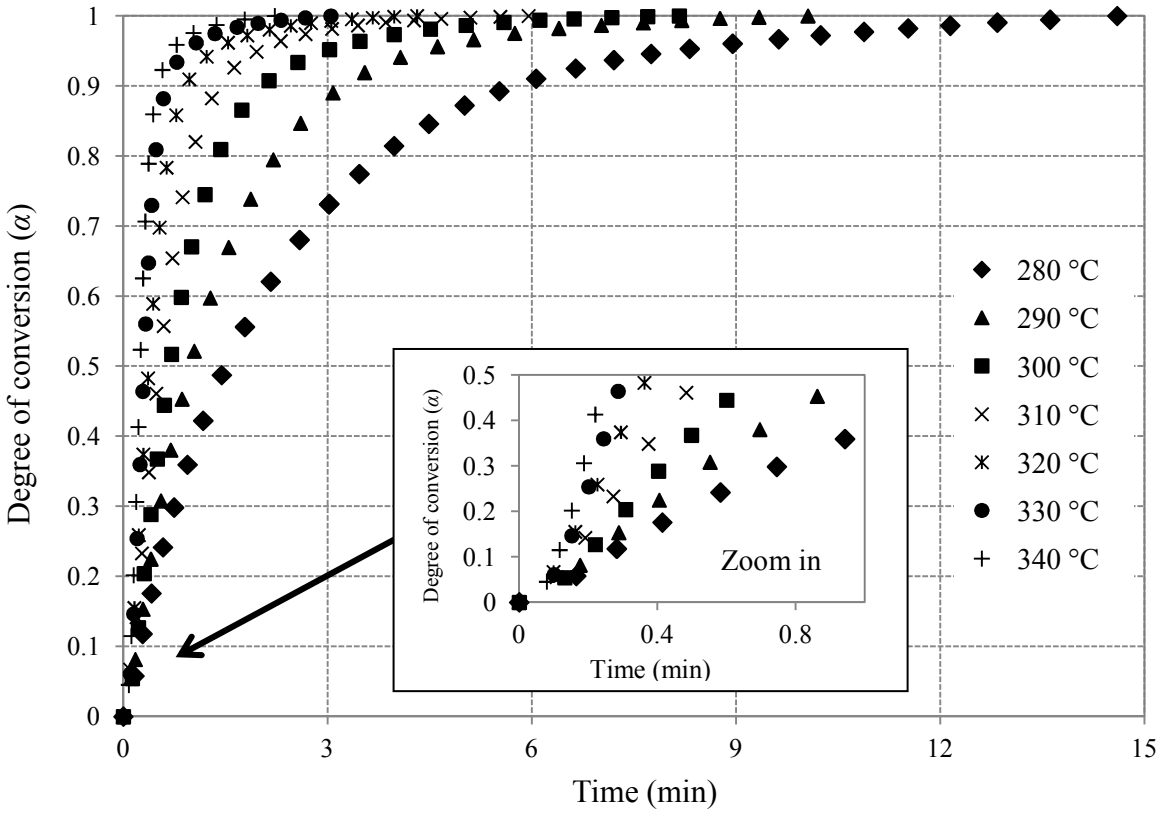

Fig.7.16. Degree of conversion for thermal decomposition of hemicellulose as a function of time for temperatures 280-340°C

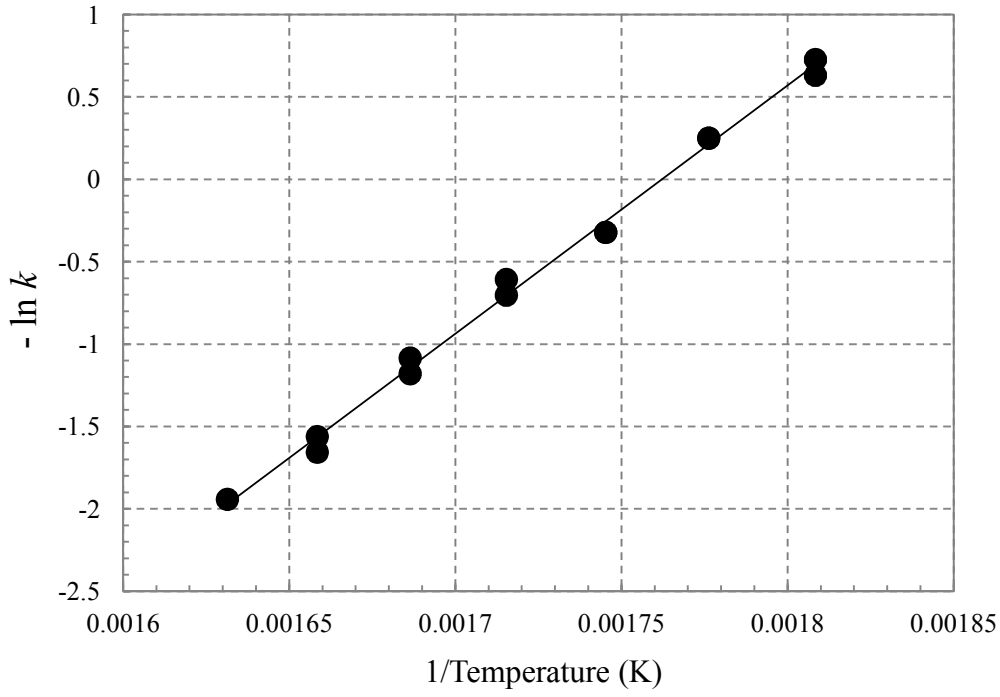

Fig. 7.17 Arrhenius plot for the decomposition of hemicellulose

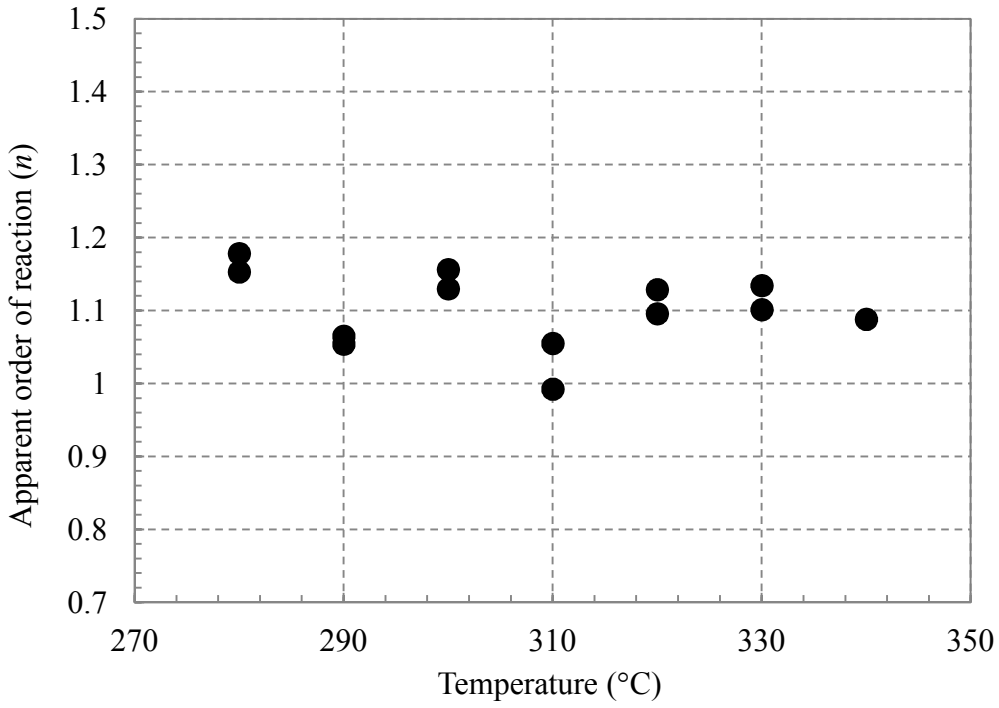

Fig.7.18 Apparent order of reaction in dependence on temperature of hemicellulose

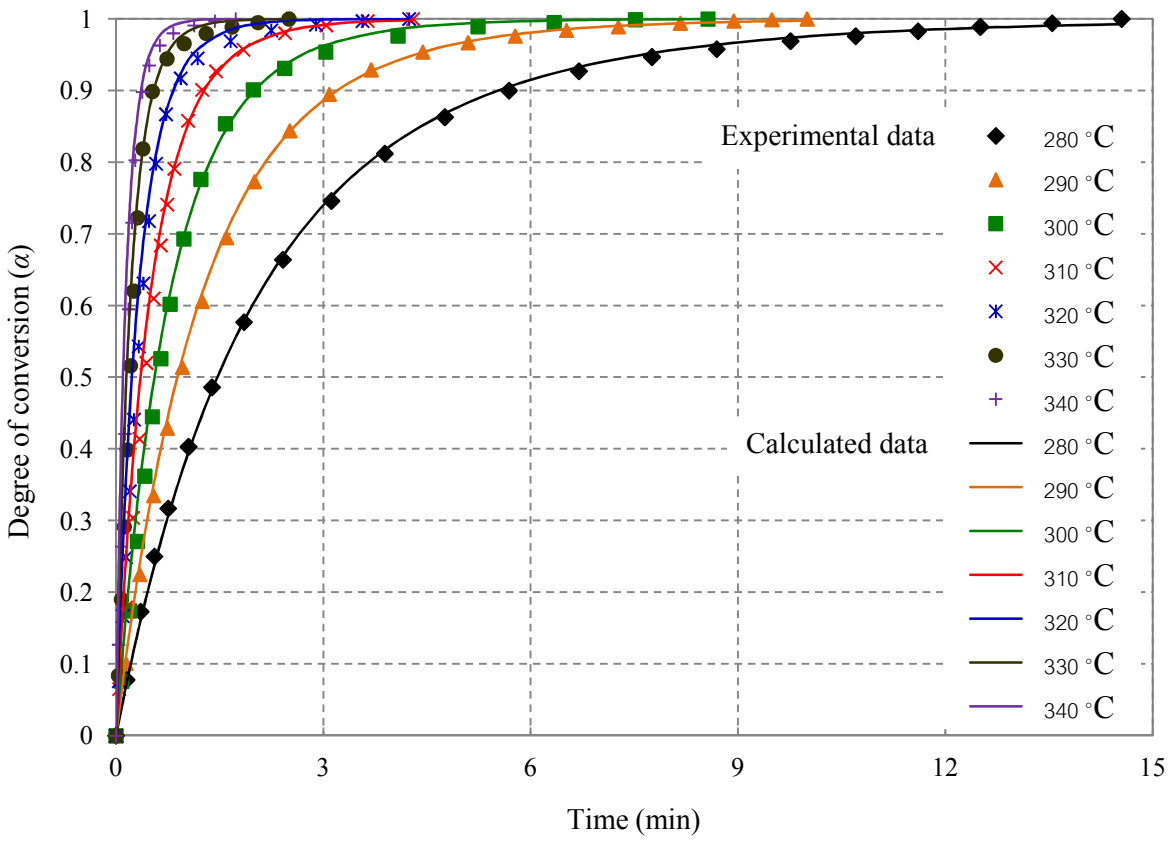

Fig. 7.19 The comparison of degree of conversion from experiments and from calculation of hemicellulose (dotted lines for experimental curves and solid lines for calculated curves)

There are few studies compared to those of cellulose have been carried out on the thermal decomposition of hemicellulose. Reported kinetic models can be classified into one-step mechanism and multi-step mechanism. The obtained kinetic parameters from this work based on one-step reaction shows comparable values for the data in literature. There is a compensation effect among the reported kinetic parameters of hemicelluloses as shown in Fig.7.20. From this range of data, the relationship of activation energy and pre-exponential factor can be derived in a linear form ($R^2 = 0.9554$) as

$$\log A = 0.0708E_a + 1.4644$$

The diversity of kinetic data for hemicellulose decomposition is due to the different experimental conditions and reaction model. In addition, kinetic data have been evaluated by assuming the temperature of the sample is equal and no temperature gradients at different heating system. However the kinetically controlling conditions are difficult to achieve and the heat transfer phenomena can cause a large error in thermal decomposition of solid samples.

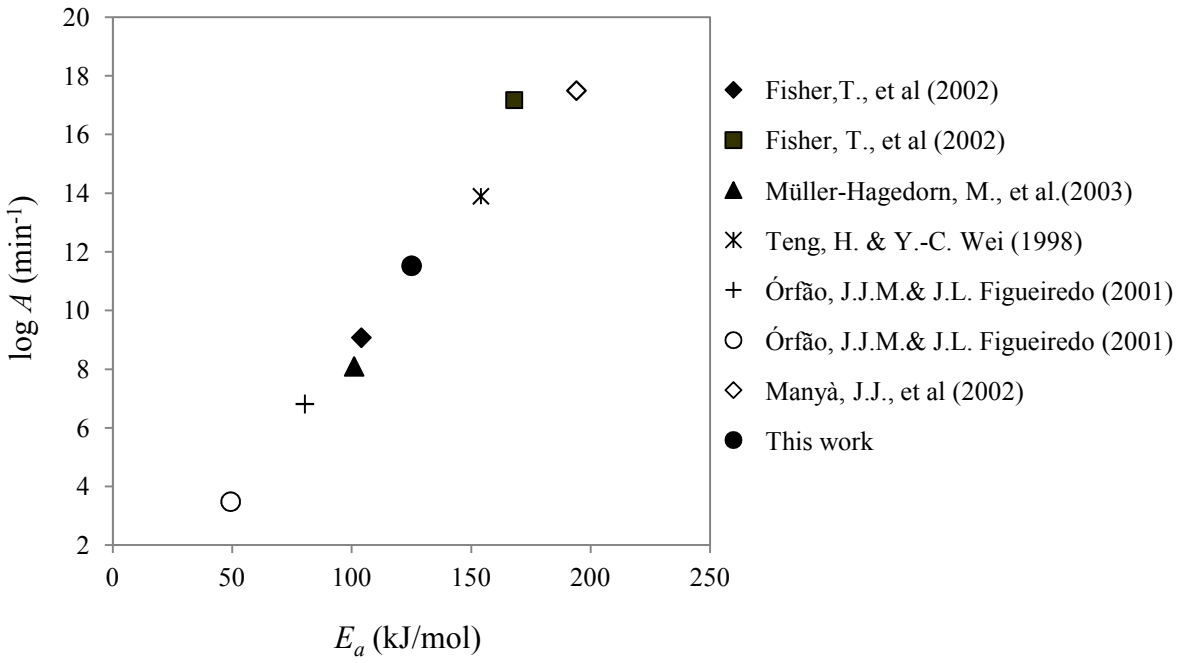

Fig. 7.20 The relationship of log A and E_a for one-step model evaluation of hemicellulose decomposition

(*Ref: Fisher, T., et al. [286]; Müller-Hagedorn, M., et al. [208]; Teng, H. & Y.-C. Wei [282]; Órfão, J.J.M.& J.L. Figueiredo [24]; Manyà, J.J., et al. [285])*

7.6 Isothermal kinetic analysis of Lignin

Alkali lignin was used in this study as a representative for lignin. The small lignin samples (0.1 mg) were pyrolyzed at isothermal temperatures from 320 to 500°C with 20°C intervals. The degree of conversion curves at isothermal temperatures is presented in Fig.7.21. Lignin decomposes at rapid rate at the beginning and then the rate becomes much lower at higher degree of conversion, especially at higher than 95% conversion. The induction period (~1 s) is shorter than those of cellulose and hemicellulose. This correlates to the dynamic thermal degradation of lignin from chapter 4 showed clearly that lignin degrades in a wide range of temperature but it starts decomposition at low temperature as that of hemicellulose.

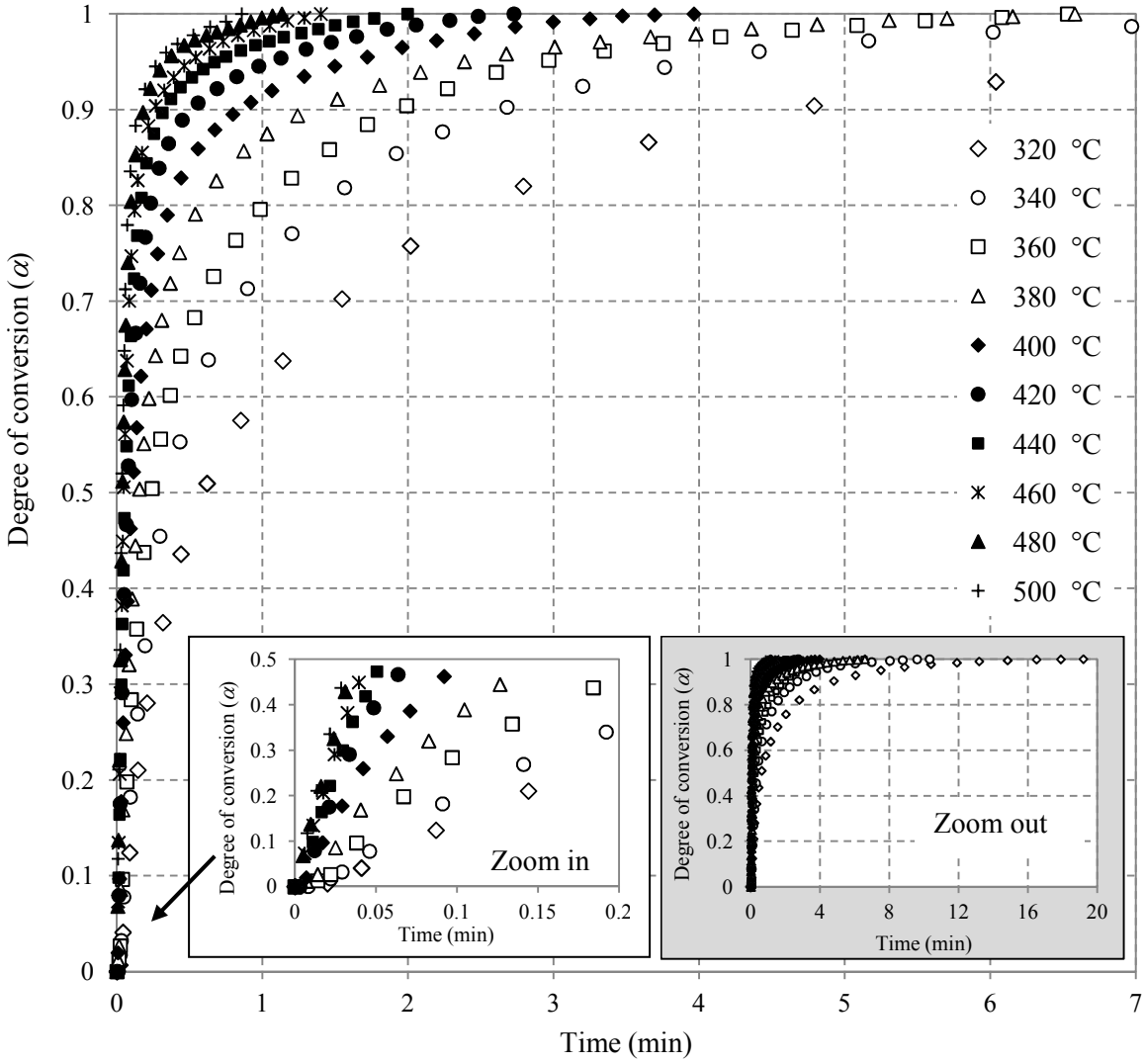

Fig. 7.21 Degree of conversion for thermal decomposition of lignin as a function of time for temperatures at 320-500°C

Apparent activation energy and the log of pre-exponential factor obtained from the Arrhenius plot (95% confidential interval) in Fig.7.22 is 72 ± 4 kJ/mol and 6.51 ± 0.73 min^{-1} with a coefficient of linear regression (R^2) of 0.9924. The order of reaction (Fig.7.23) shows a quite inconstant value. At low temperatures (<380°C) the reaction order is around 1.75 and then the order increase to about 1.88 at 380°C. After that the reaction order slightly decreases until around 1.64 at 500°C. This can be explained that at low temperatures, only small molecules such as carbon monoxide, carbon dioxide, water and light hydrocarbons production play an important role but at high temperatures, the tars production becomes predominant. That can see clearly from mass spectrometric result in Fig.7.24 (a-b). At temperature 340°C, there are no compounds with mass per ratio higher than 100 can be detected. On the other hand, there is several tar products, which are mainly aromatic compounds, can be detected up to *m/z* = 300 at temperature 500°C. Comparing to the non-isothermal thermal decomposition, temperature around 400°C is the starting temperature of slow solid decomposition.

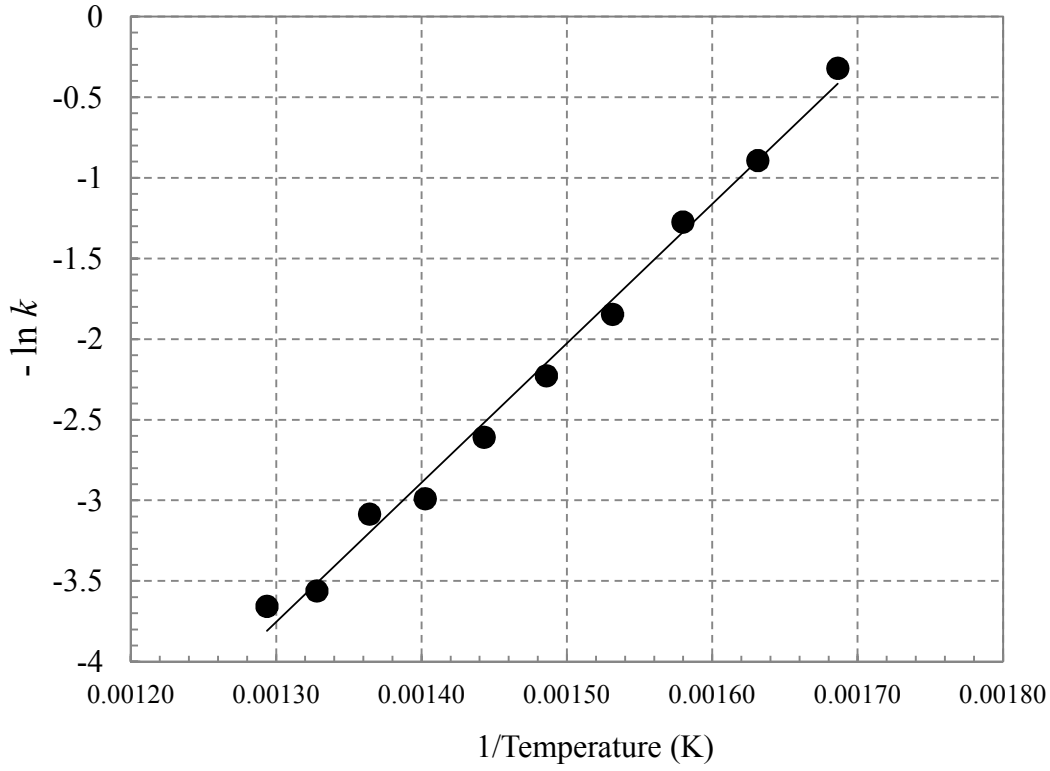

Fig. 7.22 Arrhenius plot for thermal decomposition of lignin

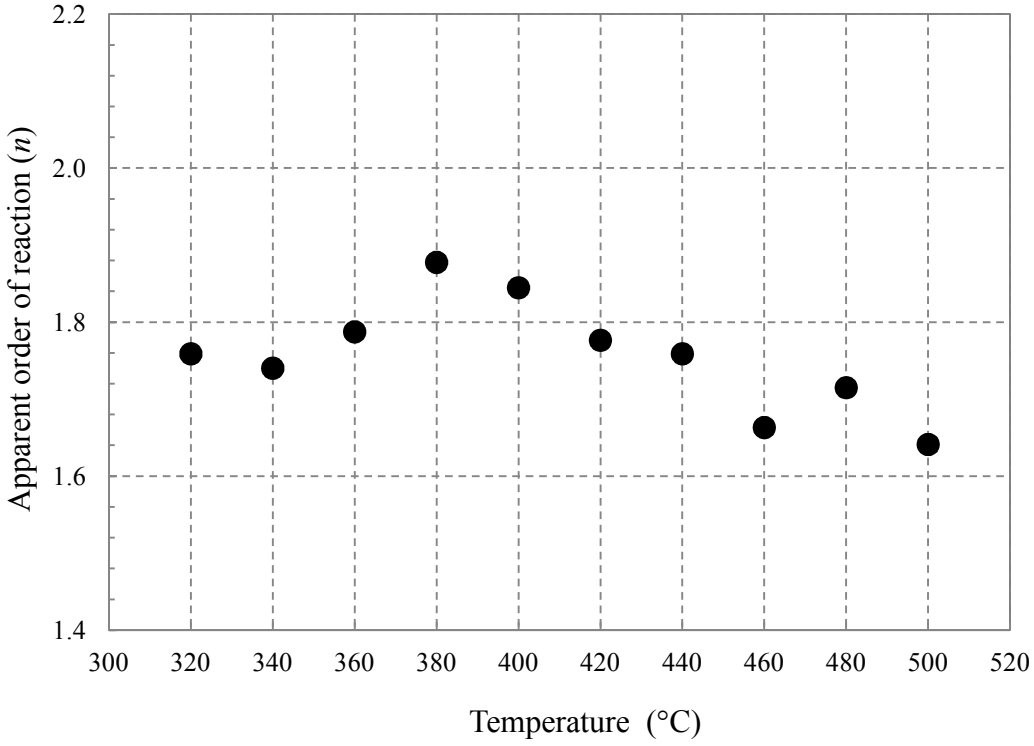

Fig. 7.23 Apparent order of reaction in dependence on temperature of lignin

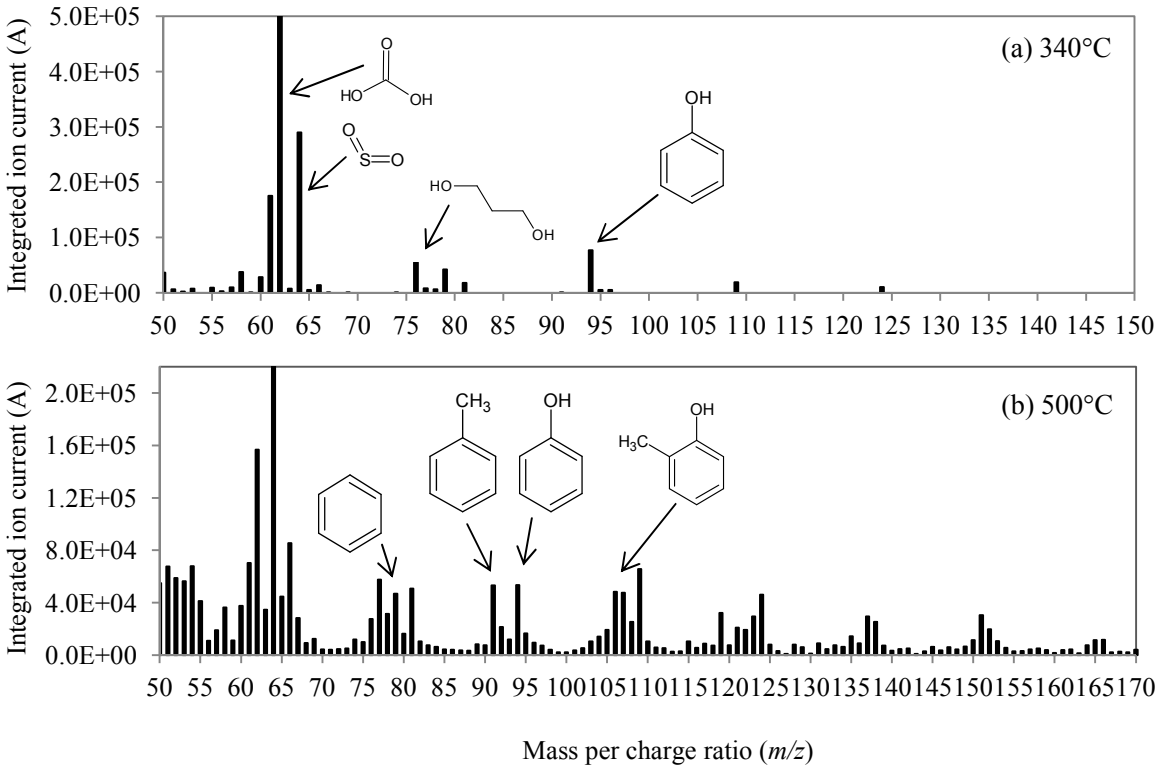

Fig. 7.24 Mass spectra of thermal decomposition of lignin at 340 and 500°C

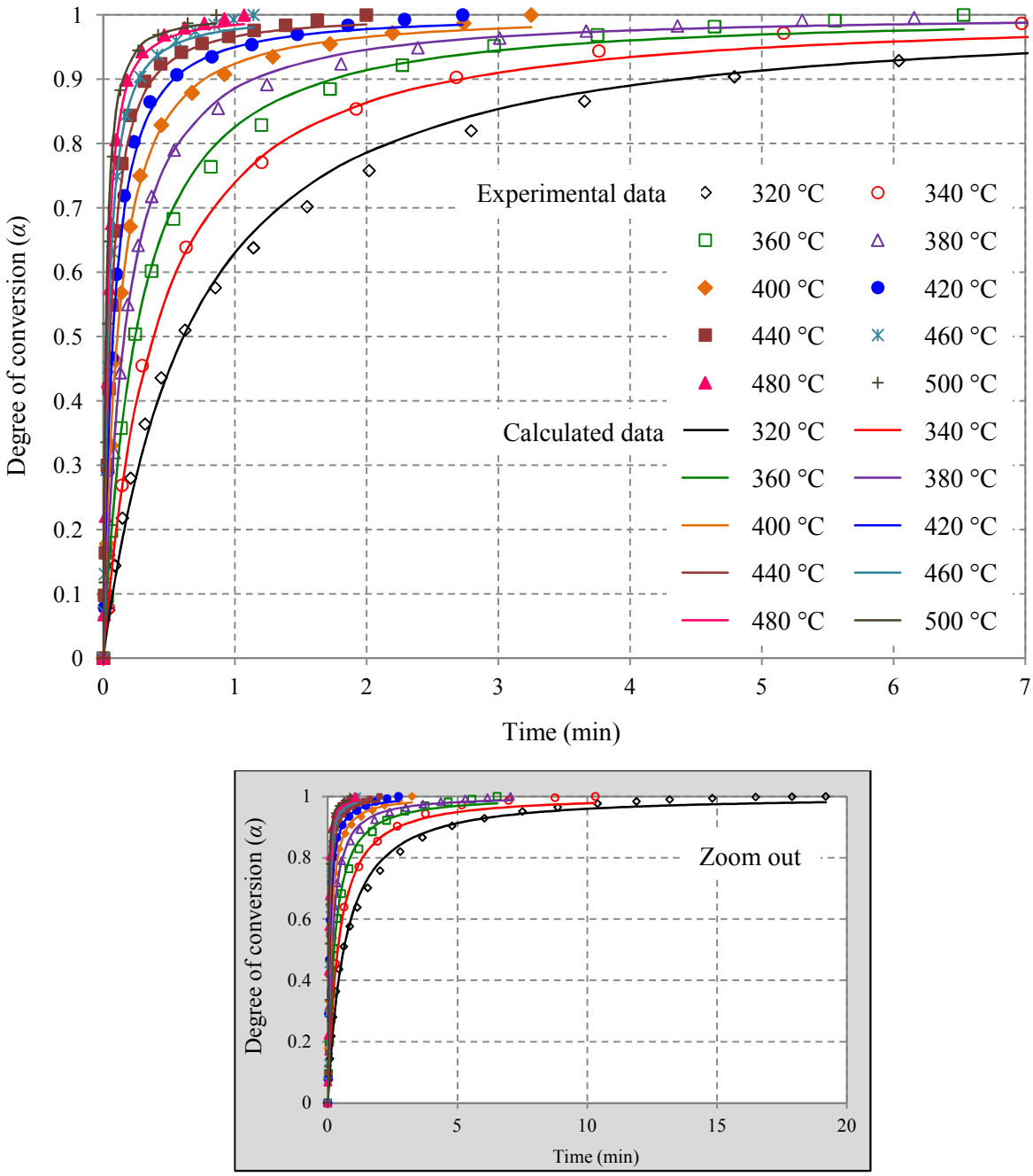

Fig. 7.25 The comparison of degree of conversion from experiments and from calculation of lignin (dots for experimental curves and solid lines for calculated curves)

The comparison of the model conversion curves with the measured curves at various temperatures is shown in Fig.7.25. Good fitting is obtained at the conversion degree up to 95%. After their rapid decomposition, they turn to very slow weight loss until reach the constant weight. This very slow rate will give a long extension of the degree of conversion

curve toward longer time with small weight change. This change made it difficult to identify the final time of thermal decomposition of lignin to reach the constant weight. Thus, the model curves show the possibly long tail of degree of conversion curves.

The discrepancy at some points between the measured and model curves can be caused from the complex mechanism of lignin which decomposes in a wide range of temperatures. In this range, there can be several series and parallel reactions occur as it can be observed from the inconstant order of reaction plot. Moreover, at low temperatures, the thermal decomposition may be affected from the melting process of lignin which causes the discrepancy at low temperature curves.

The obtained kinetic data in this present work are similar to those in literature of which activation energy of lignin decomposition is in the range of 60–80 kJ/mol and the pre-exponential factor is in the range of 6–8 min^{-1} [279, 288, 293, 294]. However there are some works reporting the higher value up to 195 kJ/mol [292] and some reported very low activation energy value at 12.49-42.60 kJ/mol [290]. This wide range of value causes by the different type of lignin, the experimental conditions and also the evaluation method.

Section 7.4-7.6 showed that this new developed instrument and the kinetic evaluation procedure applied in this work are capable to apply to typical biomass materials (cellulose, hemicelluloses and lignin). Also, the calculated kinetic parameters are in good quality after comparing with literature data and also comparing with measured data from this work.

7.7 Isothermal kinetic analysis of *Chlorella vulgaris*

Chlorella vulgaris was decomposed in the absence of oxygen at various isothermal temperatures from 250 to 600°C. These temperatures were chosen from the main weight loss region detected in non-isothermal thermogravimetric measurements. Products from thermal decomposition of *Chlorella vulgaris* are complicated because microalgae are composed of several biopolymers, such as protein, soluble polysaccharide, insoluble polysaccharide and lipid. The mass spectrum of volatile products from *Chlorella vulgaris* decomposition, such as phenol, pyrrole, toluene, and indole, at 600°C is shown in Fig.7.26.

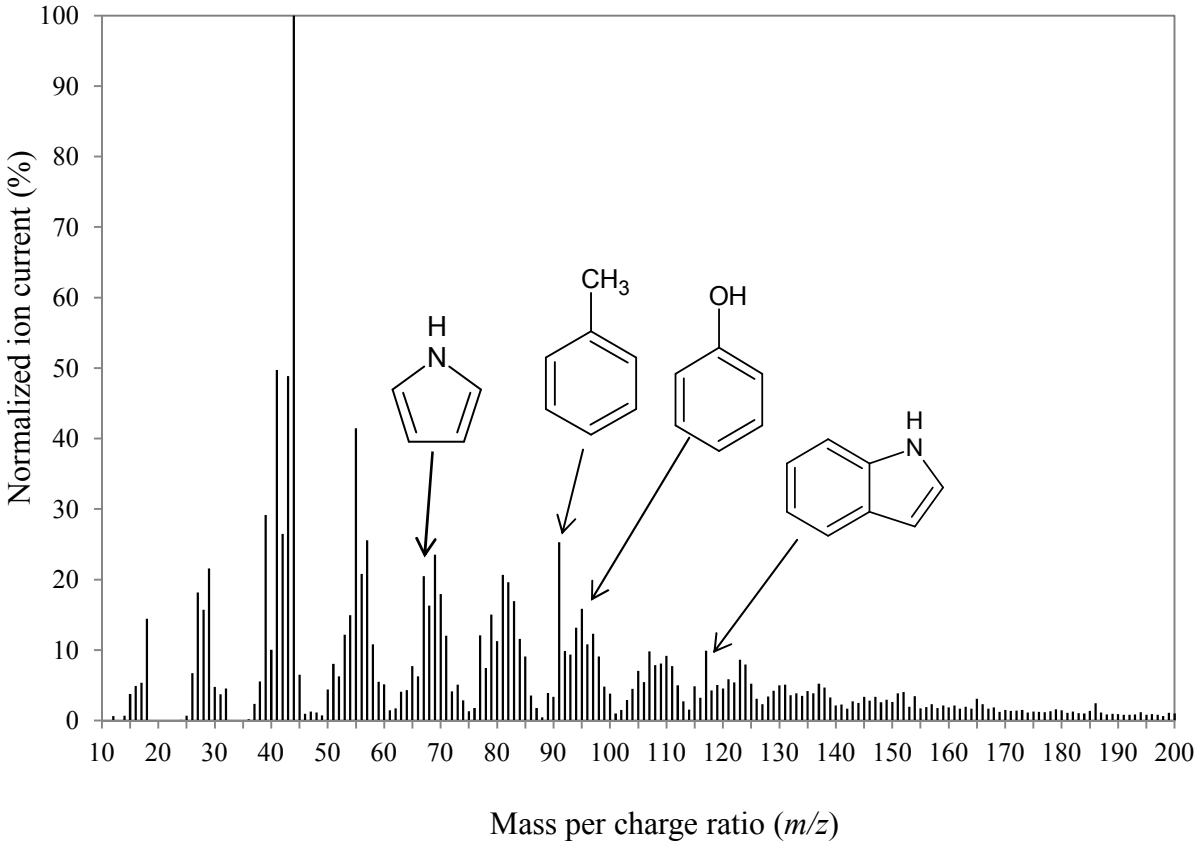

Fig. 7.26 Mass spectrum of decomposition products of *Chlorella vulgaris* at 600°C

Large number of products can be detected up to around 300 mass units. These include permanent gases, carbon dioxide which is the most abundant gas in this pyrolysis, carbon monoxide and water. A wide range of light hydrocarbons and tars at high molecular weight are important for liquid-phase products.

From the isothermal measurements, the degree of conversion curves (α) at various temperatures from 250 to 600°C with 50°C intervals are plotted in Fig.7.27. The conversion at 90% can be achieved in 10 minutes for 250°C and in 0.15 min for 600°C, while the whole measurement is completed at 23 min and 0.5 min for 250°C and 600°C, respectively. The short induction period at the beginning of decomposition is less than 6 seconds which is negligible comparing to the whole measurement time. At high temperatures, their induction periods are constant around 2 seconds which refers to the transfer time and the time gap between inserting sample into furnace and starting the detection of MS.

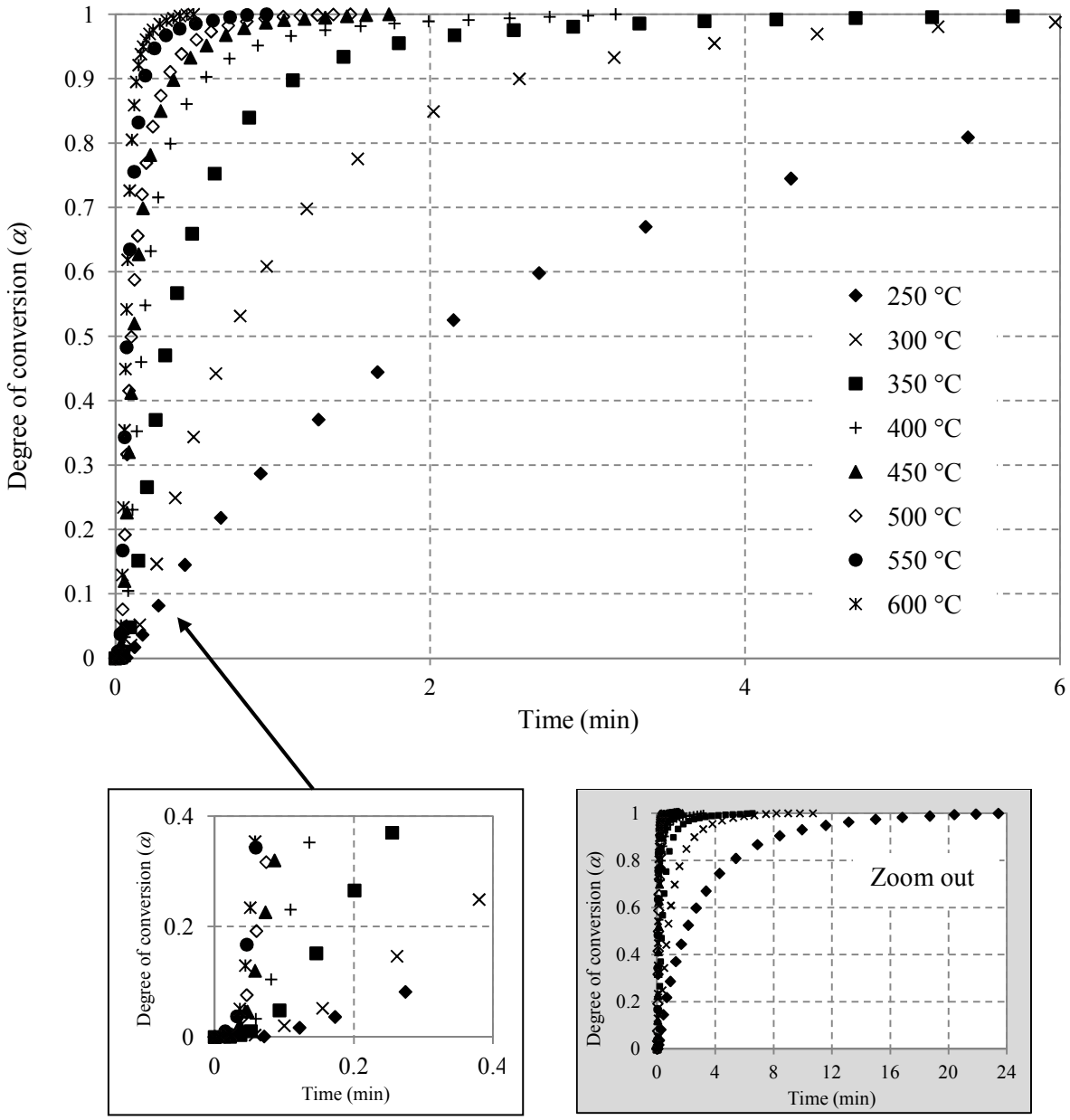

Fig. 7.27 The degree of conversion (α) for thermal degradation of *Chlorella vulgaris* as a function of time for temperature 250–600°C

To evaluate apparent kinetic parameters, the rate coefficient (k) and apparent order of reaction (n) were calculated by means of least square fitting (equation (7.4)) and then the apparent activation energy and pre-exponential factor were obtained from linear regression of Arrhenius equation (equation (7.5)). Arrhenius plot and the order of reaction plot are shown in Fig.7.28 and Fig.7.29, respectively.

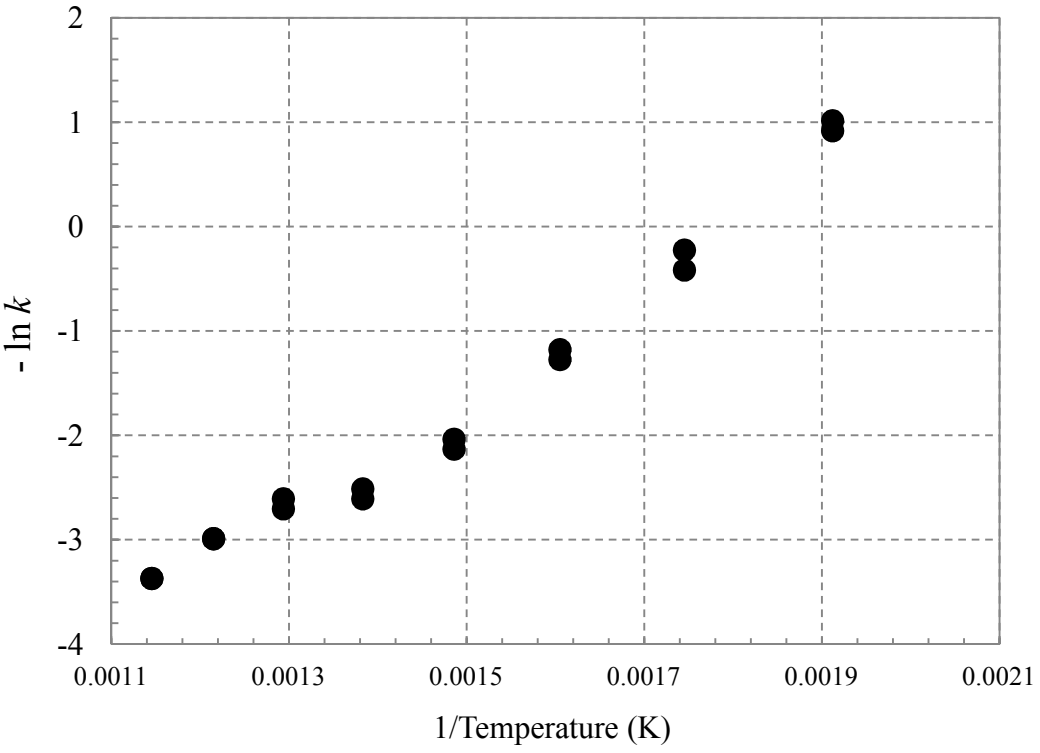

Fig. 7.28 Arrhenius plot for thermal decomposition of *Chlorella vulgaris* at 250–600°C

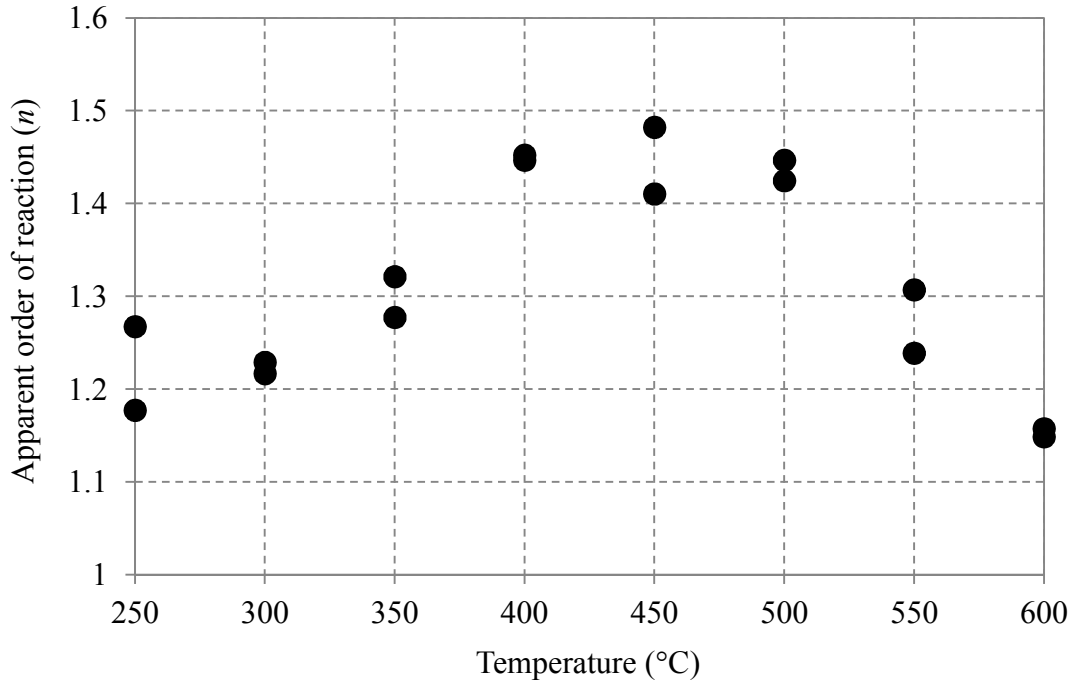

Fig. 7.29 Apparent order of reaction for thermal decomposition of *Chlorella vulgaris* at 250–600°C

From the Arrhenius plot in Fig.7.28, there are the changes in slope of Arrhenius plot after 400°C and at 500°C. However, due to the inconstant of Arrhenius slope within 400-600°C compared to the slope in the range of 250-400°C, more experimental results were added to Fig.7.28 at temperatures of 420, 470, 520, and 570°C to clarify the trend of this plotting. The Arrhenius plot including the additional results is showing in Fig.7.30. It can be seen that the first change after 400°C can be approximated the change temperature around 430°C. Hence, the Arrhenius plot from this experiment can be separated into three sections as (I.) 250-430°C; (II.) 430-500°C; (III.) 500-600°C.

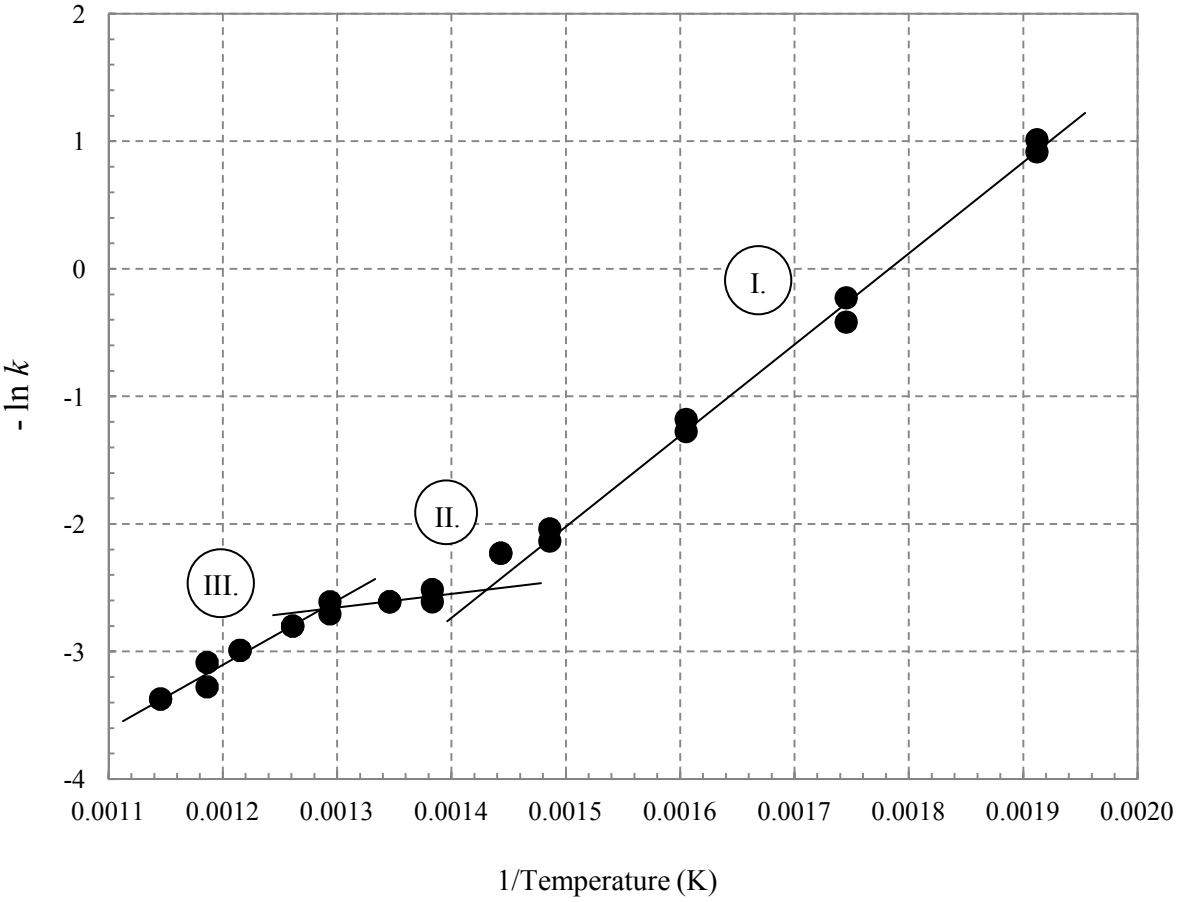

Fig. 7.30 Arrhenius plot for thermal decomposition of *Chlorella vulgaris* at 250–600°C when including the additional data at 420, 470, 520 and 570°C

Based on the change in Arrhenius plot, the order of reaction plot (Fig.7.29) can also be separated into three sections. At temperature 250-430°C, the order of reaction value increases from 1.21 to 1.45 and between temperatures 430-500°C, the order of reaction trends to be constant at 1.45. After 500°C, the order of reaction value decreases from 1.45

to 1.15. The apparent activation energy, pre-exponential factor and apparent order of reaction values for the whole range of temperature (250-600°C) are summarized in Table 7.3. The R^2 for temperature 430-500°C is low because the number of data is small in a narrow range of temperature.

Table 7.3 Apparent activation energy, apparent order of reaction and pre-exponential factor for isothermal decomposition of *Chlorella vulgaris*

Temperature (°C)	E_a **(kJ/mol)***	**log** A **(min^{-1})***	R^2	n
250 - 430	57.2 ± 2.8	5.32 ± 0.55	0.9957	1.21-1.45
430 - 500	8.8 ± 9.4	1.75 ± 1.52	0.4950	1.45
500 - 600	40.4 ± 5.3	3.88 ± 0.78	0.9616	1.45-1.15

* at 95% confidence interval

The model plotting from the obtained kinetic parameters are compared with the measured data in Fig.7.31. It needs to be noted here that the calculated kinetic parameters depend on the related temperature ranges. These calculated or model plots show a good fitting with experimental data in the wide range of temperature with considering the mechanism change.

The change of reaction order observed from thermal degradation of *Chlorella vulgaris* between 430°C and 500°C suggests the complex mechanism which depends on temperature. It is well established that microalgae comprise of several biopolymers and they have different thermal reactivity. Thus, at different reaction temperatures, decomposition pathway of *Chlorella vulgaris* is dominant by favoured components. However, within middle temperature region (430-500°C), the apparent activation energy of *Chlorella vulgaris* under isothermal conditions is lower than the other regions. Therefore, this can be suggested that the pyrolysis of these microalgae sample should be carried out at temperature between 430°C and 500°C because of requiring less energy than other reaction temperatures.

The literature on kinetics of both microalgae and macroalgae has a limited number compared to the lignocellulosic biomass. All accessible reports up to now are based on the

non-isothermal kinetic analysis by thermal analysis techniques. The reported kinetic parameters from non-isothermal studies are the overall values of complex mechanism.

A very wide range of reported activation energy for algae is in the range of 27.2–261.2 kJ/mol [259, 296-303, 329]. The reasons that make a large diversity in kinetic parameters of algae are:

1. Studied temperature range: The kinetic parameters depend on the temperatures. For kinetic studies on algae, there are some studies showing the different kinetic parameters at low and high temperatures. The higher activation energies were found at low temperatures than those at high temperatures [259, 329] as the same trend in this present work.
2. Different type of algae: The kinetic parameters of microalgae and of macroalgae and also among different species of microalgae show the varying in reported values because of the difference of cell components.
3. Evaluation method: In non-isothermal kinetic analysis, researchers applied different method to evaluate kinetic data, such as Freeman-Carroll method, Popescu method, Isoconversional method and Coats-Redfern method.
4. Reaction model: There is a varying in order of reaction or reaction model in literature. Most of works, the orders of reaction are higher than 2.0. Avramic-Erofeev model (n =3) are often applied for low temperature region.
5. Complexity of microalgae reaction: Many reactions with various activation energies occur during thermal decomposition of microalgae. If the low activation energies steps dominate in the studied temperature range, the apparent activation energy in this range may present at a low value. In addition, in the case of simulated overlapping decomposition curves, the apparent kinetic values of overall process are closed to kinetic values of the low activation energy curve [330].

The apparent kinetic parameters of this work are at the low value comparing to other reports. These can be affected by all reason mentioned above. The *n*th-order model is applied into the kinetic analysis in this study. Although this model is appropriated for other materials (polyethylene and lignocellulosic main compounds), in the case of *Chlorella vulgaris*, other reaction models should be considered in the future studies for thermal decomposition of these microalgae.

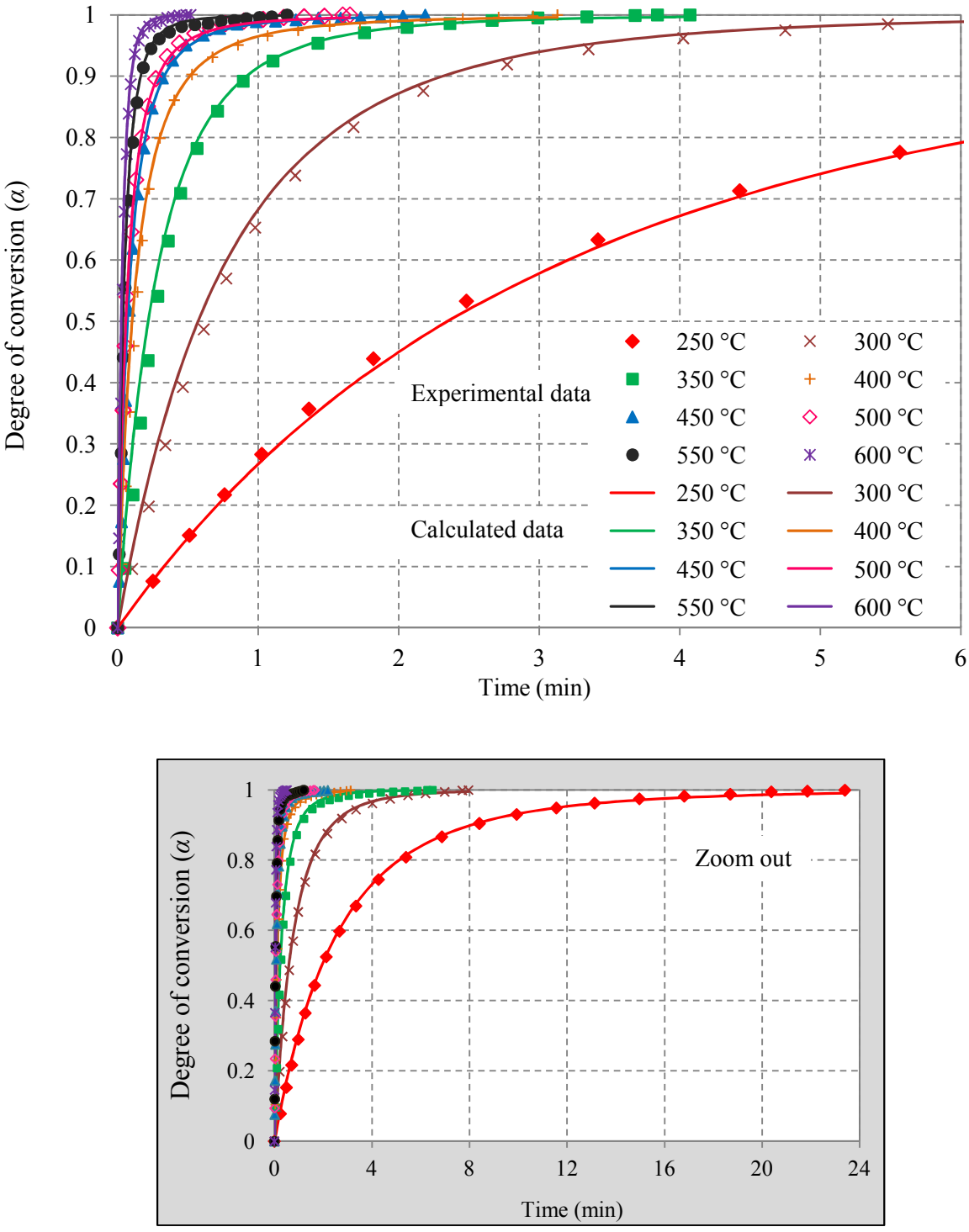

Fig. 7.31 The comparison between the experimental degrees of conversion curves and the calculated curves from applying three kinetic parameter sets of *Chlorella vulgaris* decomposition (dots for experimental curves and solid lines for calculated curves)

7.8 Summary of isothermal study

In the last few decades the kinetic study of the thermal decomposition of biomass tends to be carried out under non-isothermal conditions due to its rapidity. Unlike isothermal condition, the change of temperature and concentration occur simultaneously in non-isothermal measurement, thus the rate expression is affected from both temperature-dependent and concentration-dependent factors. Although the important benefit from isothermal analysis is that the change of reaction mechanism can be detected, while the non-isothermal analysis gives the overall value of the process, its time consumption and limitations of analytical instrument reduce the kinetic interest in isothermal conditions.

The new developed microreactor with evolved gas analysis used in this work shows the potential for kinetic study for polymers and biomass materials. This experimental set-up minimizes the requirement of sample size and experimental time without temperature overshooting. These lead to the kinetic study of limited amount of sample and it makes isothermal analysis comparable to the rapidity of non-isothermal analysis. Moreover, the small sample size leads to the reduction of heat transfer effect. In addition, not only had the monitoring the progress of reaction but also the information on products can be detected by means of evolved gas analysis via mass spectrometer. The apparent kinetic parameters for every material in this isothermal study are listed in table 7.4 below.

Table 7.4 Summary of apparent kinetic parameters of every studied material (at 95% confidence interval)

Sample	***T* (°C)**	***E*$_a$ (kJ/mol)**	**log *A* (min^{-1})**	***n***	**R^2**
Polyethylene	450 - 550	216 ± 9	14.89 ± 1.34	0.7-1.6	0.9958
Cellulose	350 - 400	131 ± 6	10.89 ± 1.19	1.06	0.9928
Hemicellulose	280 - 340	125 ± 5	11.53 ± 0.93	1.1	0.9956
Lignin	320 - 500	72 ± 4	6.51 ± 0.73	1.64 - 1.88	0.9924
C.vulgaris	250 - 430	57 ± 3	5.32 ± 0.55	1.21-1.45	0.9940
	430 - 500	9 ± 9	1.75 ± 1.52	1.45	0.4950
	500 - 600	40 ± 5	3.88 ± 0.78	1.45-1.15	0.9616

The kinetic parameters from isothermal conditions are much less available in the literature compared to those from non-isothermal conditions. Especially in the case of algae, there are no accessible reports which study kinetics in isothermal conditions so far. The obtained kinetic values in this present study can be considered to be in the range of other reported values. In addition, the compensation effect is observed in the activation energy and pre-exponential factor of this range of samples. The comparison of kinetic parameters needs to consider different experimental conditions, such as sample size, heating rate, reaction temperatures and atmosphere.

In the case of polyethylene, since its melting point is lower than the reaction temperature, the heat of adsorption for phase transition in sample particles need to take into account the thermal decomposition process, as biomass materials cannot detect the phase transition at the initial experimental time. It has been observed that the experiments in which samples are rapidly heated or isothermal measurements give the apparently lower activation energies than the values from the slow heating rate experiments. The heat transfer phenomena inside the sample and between the experimental system and the sample, the complex mechanism of thermal decomposition and the mathematical analysis are the main causes for the discrepancy in the results of kinetic parameter from pyrolysis.

Due to the limited reported information on thermal decomposition of algae and the unavailability of their isothermal kinetic parameters, it is difficult to compare the kinetic result of *Chlorella vulgaris*. However the existence of the mechanism change in decomposition and the temperature dependence of kinetic data are presented for microalgae in the present work alongside some literatures data. The change can be explained by the influence of thermal decomposition of different fragments/biopolymers in microalgae. The low activation energy of *Chlorella vulgaris* can be affected from the selected reaction model and the complicated of thermal decomposition process.

Chapter 8

Non-isothermal Kinetic Analysis

From the result of the isothermal analysis of *Chlorella vulgaris* in chapter 7, the apparent kinetic parameters are separated into three sections. It is mainly because the multi-component in this microalgae sample. While lignocellulosic materials have three well-identified main components (cellulose, hemicellulose and lignin) and these materials are also available commercially. Therefore, it is possible to reduce the complexity of the decomposition of lignocellulosic biomass by studying from the decomposition of their main components instead. On the other hand, the knowledge of the main components of algae is still on studying and it is not able to identify the specific materials to represent this microalgae sample. Thus, the non-isothermal kinetic analysis in this chapter is applied to *Chlorella vulgaris* to present a procedure for analysing the complex reaction by evolved gas analysis technique and together with the deconvolution method by Gaussian distribution.

8.1 Experimental set-up

Non-isothermal experiments were studied by an in-house built coupling of Thermogravimetry and Mass Spectrometry (TG-MS) which was given its detail in section 5.4.1 (see Fig.5.2). The quadrupole mass spectrometer was employed to record the gas evolution profiles at total pressure of 1×10^{-6} - 5×10^{-6} mbar. Maximum 64 channels were set in Multiple Ion Detection (MID) mode to detect the selected masses in the range from 1 to 100 mass per charge ratio (*m/z*), including H_2 (*m/z* = 2), CO_2 (*m/z* = 44), CO (*m/z* = 28), H_2O (*m/z* = 18), NH3 (*m/z* = 17) and various hydrocarbons.

Due to the limitation of MS channels in TG-MS measurements, the evolution profile of tars with mass range between 100-300 mass unit was obtained from the dynamic Pyrolysis (A Double-Shot pyrolyzer)-Mass Spectrometry (Hewlett Packard 5972 series) (Py-MS). Temperature profile for pyrolyzer was set the same as those of Thermogravimetry in TG-

MS. The sample size 0.5-1.0 mg was inserted into furnace in helium atmosphere with flow rate 20 ml/min. The metal transfer line was kept at 300°C to minimize the condensation.

8.2 Evaluation of formal kinetic parameters from non-isothermal measurements

For non-isothermal measurements, temperature increases constantly with a ramp rate (β) and the kinetic equation is described by equation (3.10). Thermal decomposition of solid resulting in gaseous product can be interpreted by assuming that the measured product concentration of gaseous mixture leaving the system at any time reflects the rate of decomposition of solid sample at that time.

Since the measured mass per charge ratios are limited over the range of temperature due to the limited detection channels of mass detector (64 channels). The production rate of volatiles can be detected as a function of ion current time or pyrolytic temperature. The degree of conversion is adapted from [208] in equation (3.12) and expressed in the form of

$$\alpha(T) = \frac{\int_{T_0}^{T} \sum_{i=1}^{N} I_i(T) M_i dT}{\int_{T_0}^{T_\infty} \sum_{i=1}^{N} I_i(T) M_i dT} \quad \text{..... 8.1}$$

where N is the different volatile product, M_i is the molecular weight of each ion fragment and $I_i(T)$ is the ion current of each ion fragment at temperature T.

A model based on parallel, independent, *n*th-order reactions will be applied to thermal decomposition of *Chlorella vulgaris*. This model simply assumes that solid sample consists of several fractions which decompose at different rates and temperatures. The reactions are kinetically controlled and there are no secondary reactions among the released gaseous products. The evolved gas profiles show the overlapping of many peaks and shoulder(s). Each peak or shoulder will be treated as a single reaction from a separating fraction presenting in sample. Thus, the deconvolution method is required to enable the kinetic evaluation for every single peak.

For deconvolution method, simple derivative of weight loss curve of a single reaction can be presented in the form of Gaussian distribution. As the complexity of biomass pyrolysis,

there are many overlapping single reactions during the reaction temperature range. For a single reaction, a Gaussian curve represents its weight loss behaviour. The Gaussian distribution or normal distribution is a continuous probability distribution that has a bell-shaped probability density function which can be generally written as

$$f(x) = a\exp\left(-\frac{(x-b)^2}{2c^2}\right) \quad \text{..... 8.2}$$

Making equation more applicable for experimental data, the Gaussian distribution is adjusted to

$$G = H\exp(-(T - T_{\max})^2 / s^2) \quad \text{..... 8.3}$$

where $T_{\max}$ is the peak temperature of a Gaussian curve, *s* is the width of the peak and *H* is the intensity of peaks. The relationship in equation (8.3) is used to describe the evolved gas profiles by optimization the parameter *H*, T_{max} and *s* with measured data by using MATLAB programme.

A single expression can be used for a single reaction or a single peak in any MS profile. The expression can be adjusted to:

$$d\alpha_j / dT = (A_j / \beta)\exp(-E_{aj} / RT)(1-\alpha_j)^{n_j} \quad \text{..... 8.4}$$

Hence, the whole kinetic description of the sample pyrolysis relates to several kinetic parameter sets. Then, the overall mass loss rate for parallel reactions is a linear combination of $d\alpha_j / dT$ rates:

$$-d\alpha_{cal} / dT = \sum_{j=1}^{M} d\alpha_j / dT \quad \text{..... 8.5}$$

where α_{cal} is the simulated degree of conversion and *M* is number of data points.

To evaluate the apparent kinetic parameters of a single reaction, the direct model fitting by minimizing the deviation between the measured data and model curve. The deviation is presented in form of 'Root Mean Square Error (RMSE)' between the approximation $\alpha_{cal}(t)$ and the measured values $\alpha_{\exp}(t)$ by

$$RMSE = \sqrt{\frac{1}{n-1}\sum_{i=1}^{n}(\alpha_{\exp} - \alpha_{cal})^2} \quad \text{..... 8.6}$$

8.3 Weight loss curves and evolution profiles of volatile products

The weight loss of *Chlorella vulgaris* during thermal decomposition from 100°C to 600°C at 20°C/min is presented in the form of its derivative (DTG) in Fig.8.1 (a). It shows that *Chlorella vulgaris* decomposes into two main peaks at 200-400°C and 400-550°C.

The lack of information on product evolution from thermogravimetry leads to the combination with evolved gas analysis technique. In this work, mass spectrometry is selected to monitor the products from pyrolysis of *Chlorella vulgaris* samples. Simultaneous total evolved gas profile or total ion current (TIC is presented in Fig.8.1 (b). The ion current in y-axis of TIC represents a fractional intensity of the evolved gas mass with respect to the carrier gas. At lower temperatures, the permanent gases and water are the dominant products and at higher temperatures, there are several light hydrocarbons and tars are produced. The well correlation between DTG and TIC curve can be observed. However, the ratio of peak height between two decomposition regions in TIC is different from that of the weight loss curve. This difference can be explained by the absence of tars evolution in TIC due to the limitation of MS detector. If the total ion current includes evolved tars profile, it is assumed that the height ratio between both peaks of TIC will be similar to DTG curve. The rate of the produced tars can be obtained by Pyrolysis-Mass spectrometer (Py-MS) for evolved gases mass up to 300 u. In addition, the increase of baseline and the transfer time delay in TIC curve are observed.

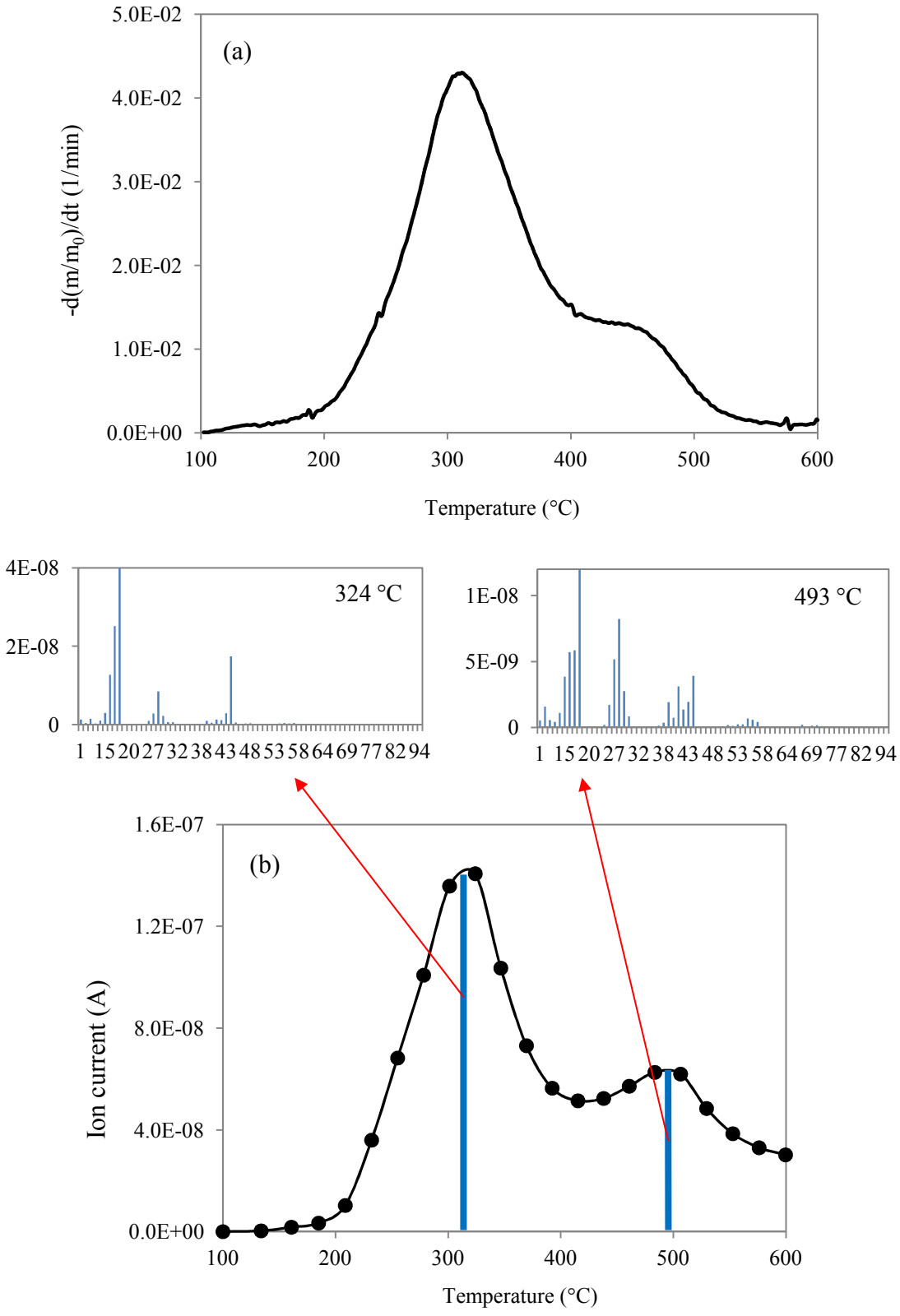

Fig. 8.1 (a) The derivative of thermogravimetric curve at 20°C/min and the produced gases evolved at peak temperatures, as well as (b) the total ion current (TIC) curve.

8.4 Evolved-gas Data treatments

From the observed differences between DTG curve and TIC curve (Fig.8.1), it is necessary to treat all evolution profile before further evaluation. There are four issues which are the volumetric flow, the estimated response factors, tars evolution from pyrolysis-mass spectrometry (Py-MS), and evolved-gas transfer delay are considered in this data treatments section.

8.4.1 The volumetric flow

Volumetric flow from the TG to the MS detector depends on the temperature and pressure of the system [331]. The vacuum pump inside mass spectrometer reduces the total pressure of the system to 1 - 5 × 10^{-6} mbar which is suitable for the operation of the MS detector. Moreover, the carrier gas flow rate, the temperature of transfer line, the length and inner diameter of capillary influence the total pressure. Thus, at the same operating conditions, the pressure and temperature is constant. Then the volumetric flow should be stable.

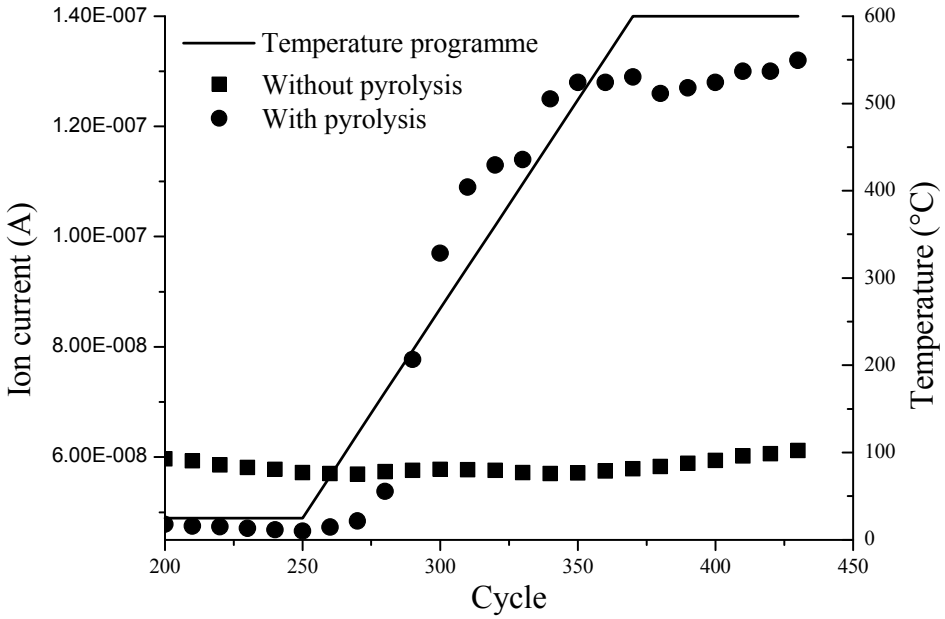

Fig. 8.2 The plotting of helium ion intensity when there is a pyrolysis of biomass (●) and when there is no pyrolysis of biomass (■) taking place in TG chamber and the temperature programme (——).

However, the volumetric flow in this experiment was found unstable which can be explained by the increased capillary diameter. For every measurement, the total pressure before starting pyrolysis reached at a constant value. When thermal decomposition of sample takes place in TG chamber, samples absorbs heat to breakdown into smaller compounds and leave the TG through transfer line, so that every produced compound, especially the high boiling point compounds, which move passed the transfer line carry a certain heat capacity. When they reach the capillary in transfer line, they cause the expansion of the capillary diameter. That means the change of capillary size which allows more volume of evolved gas can go to mass spectrometric detector. The volumetric flow of gases; therefore, increases as the temperature of pyrolysis increases. It can be seen in Fig.8.2 that when solid sample is pyrolyzed, the intensity of helium as an inert gas increases. Whereas the flow rate of helium gas remains stable, the intensity of helium becomes higher. That means more helium gas can go through the capillary. On the other hand, an experiment with the same operating conditions but there is no sample applied inside TG chamber shows a constant level of helium throughout the whole range of temperature. Thus, this phenomenon will be taken into account for baseline correction of evolved gas data.

8.4.2 The estimated response factors

The applications of evolved gas analysis by mass spectrometry have been employed for both qualitative and quantitative analysis. Since each ion detected in the MS has its own response factor, only the shape and the characteristic temperatures of the peak can be compared in the case of the intensities of different ions [332]. To compare the quantity of different species, calibrations need to be done by either injecting some gases with known concentration into the system or pyrolyzing some chemicals with well-known stoichiometric reaction and measure their intensities from mass spectrometer. Due to the complex mass spectrometric fragmentation of the volatiles produced from biomass pyrolysis and the limitation of calibration data, there are no absolute responses factors from calibration which can be employed for every fragment.

In this work, the semi-quantitative analysis was applied for the attempt to compare the proportion of each evolved gas profile in total ion current. There are several factors controlling the total ion current curve, such as carrier gas flow rate, raw material size, temperature and heating rate. The influences from these factors on different species were

assumed to be negligible because they were kept at the same values for every measurement and the evidence from a report [333] showing similar response factors at different temperature and heating rates. The important factor which will be taken into account in this present work is relative molecular weight of each fragment as the 'simplified response factors'.

Based on the concept of mass spectrometry, the measured ion current reflects the concentration or number of particles at different mass per charge ratio (*m/z*). At standard electron energy (70 eV), the fragments with double (X^{++}) or triple (X^{+++}) charges are negligible [334], the mass per charge ratio values (*m/z*, X^{+}); thereby, represent the mass of fragment. To compare with weight loss from TG, these concentrations of fragments need to be simply converted to weight basis by multiply with their molecular weight.

The evaluation of the ability to compare between total ion current and DTG curve after applying the simplified response factors is demonstrated by the experiment with calcium oxalate monohydrate ($CaC_2O_4 \cdot H_2O$) in Fig.8.3. Calcium oxalate monohydrate is widely used [335-339] on TG-MS system due to its well-known stoichiometric thermal decomposition reaction for three steps of reaction to produce H_2O, CO and CO_2 at different temperatures.

$$CaC_2O_4 \cdot H_2O \rightarrow CaC_2O_4 + H_2O$$

$$CaC_2O_4 \rightarrow CaCO_3 + CO$$

$$CaCO_3 \rightarrow CaO + CO_2$$

From Fig.8.3 (a), calcium oxalate monohydrate decomposes in three steps to produce H_2O, CO and CO_2, respectively. The evolved gas profile (Fig.8.3 (b)) of these gases from MS detector shows the different intensity ratio from DTG curve but when multiplying with the simplified response factors or molecular weights (Fig.8.3 (c)), the better correlation between DTG and relative signal from mass spectrometry can be observed.

Based on the possibility to use the molecular weight as simplified response factors, the ion current at every mass per charge ratio (*m/z*) value will be changed to relative ion current or relative ion intensity by applying these factors to enhance the ability of the comparison between DTG and MS signals in this work.

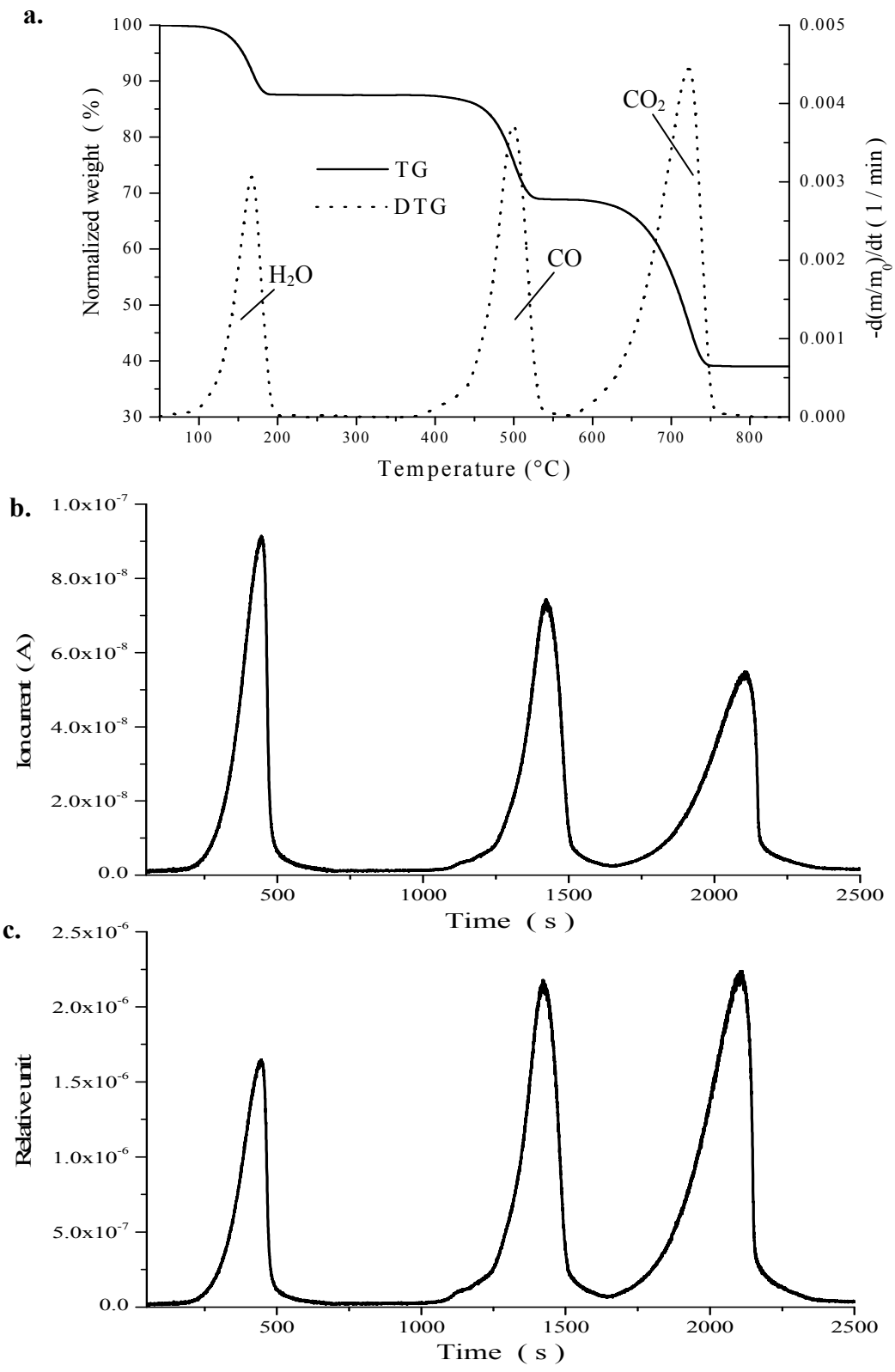

Fig. 8.3 (a.) the weight loss and its derivative of calcium oxalate monohydrate decomposition at 20°C/min, (b.) the total ion current measured by mass spectrometer and (c.) the relative signal on weight basis by applying the simplified response factors

8.4.3 Tars evolution from Pyrolysis-Mass Spectrometry (Py-MS)

The limitation of the TG-MS used in this work is that the fragments which have mass higher than 100 u. (tars) cannot be detected. Thus, the total ion currents from mass spectrometer of TG-MS measurements do not include tars evolution. However, the weight loss from thermogravimetry links the overall decomposition. For accurate comparison between TG/DTG curves and evolution profiles, the tars (100-300 u) evolved profile obtained from the Pyrolysis-Mass Spectrometry (Py-MS) technique at the same conditions as those of TG-MS is included in the total ion current.

8.4.4 Evolved-gas transfer delay

The transfer time is the total time required for the produced gases to transfer from the TG sample crucible to the MS ion detector. It depends on the capillary length and inner diameter, temperature, the pressure at the entrance of the capillary, the dynamic viscosity of evolved gases and evolved gas properties [331, 340].

A transfer time delay between the DTG signal from thermogravimetry and the evolved gas profile from mass spectrometry in this work was observed. An estimation of the time delay can be calculated from the difference of the time at the maximum of the DTG peaks and the time at the maximum of the MS signal peaks.

$$t_d = t_{(MS)} - t_{(DTG)} \quad \text{.....8.7}$$

t_d is the transfer time delay, $t_{(MS)}$ is the time at the maximum of the MS signal and $t_{(DTG)}$ is the time at the maximum of the DTG peaks.

A thermogravimetric analyzer is primarily designed for optimum response to temperature and mass changes rather than the provision for evolved gas analysis. Therefore, the combination with mass spectrometer may introduce dead volumes and cold spots [334]. The large dead volume leads to the back diffusion of evolved gas. The influence of convective and diffusional mass transfer causes the time lag and the deviation of curve shapes between the measured DTG and MS signals [341]. In addition, in gas-solid system, the physical adsorption caused by molecular interaction forces leads to the condensation of vapour to liquid form [342,343]. Especially at cold spots, the evolved gases with high boiling point trend to take longer time in capillary or to condense [340]. Unlike

hydrocarbon compounds, permanent gases can transfer immediately to mass spectrometric detector. The cold spot in TG-MS causes the shifting and broadening of the evolved gas profiles of condensable volatile organic compounds. The presence of cold spots also affects the profile of water evolution and small influence for permanent gases [334].

Based on this information, the evolved gas profiles of hydrocarbons will be shifted toward lower temperature or shorter time with a step of the transfer time delay value (t_d).

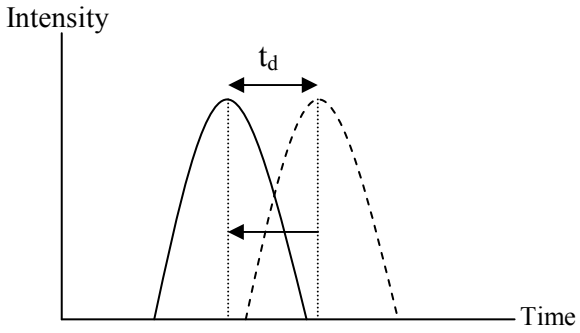

8.5 Lumped-product evolution

The pyrolysis of biomass is complicated involving several reactions and producing a large number of products. There are 64 evolution profiles of pyrolysis products from the *Chlorella vulgaris* sample. To condense the complex products into more easily manageable system, all volatiles are lumped into six groups. The similarity of each evolved gas profile in case of the peak temperatures and shape, the fragmentation in mass spectrometer, as well as the general main products from pyrolysis are the key points to classify into these groups. For example, if the evolution profiles of *m/z* = M and *m/z*=N have similar pattern in term of shape and peak temperature, together with their fragmentation background are from the same fragment chemically. Thus, they are considered to produce via a similar process. Then *m/z*=M and *m/z*=N are classified in the same group. These six groups are (1) the water and ammonia gas evolution; (2) carbon dioxide evolution; (3) carbon monoxide and methane evolution; (4) the light hydrocarbons evolution with single peak of decomposition; (5) the light hydrocarbons evolution with double peaks of decomposition and (6) tars evolution (Fig.8.4 and Fig.8.5). Although H_2O and NH_3 are different chemicals, their evolution temperatures and shape of profiles are the same which can

consider that these products are produced from the same fragment in initial sample, such as the high reactive side chains. Thus, H_2O and NH_3 were classified in the same group. In this evaluation the evolution profile of H_2 was not be included because for this pyrolysis of *Chlorella vulgaris*, H_2 was released after the devolatilization temperature (see Fig.5.4) which is outside of the studied temperature of this work.

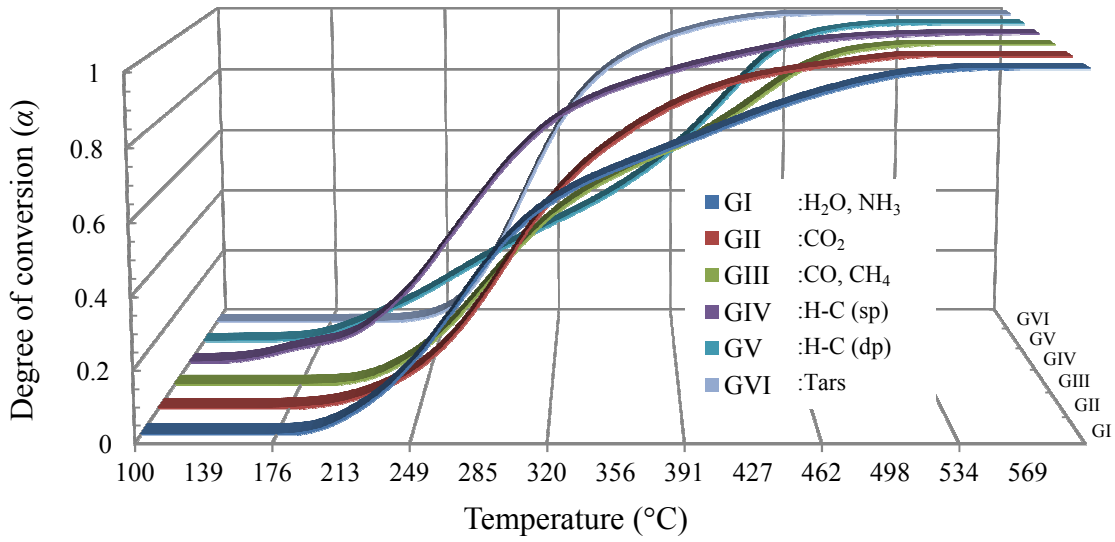

Fig.8.4. Degree of conversion (α) curves of six evolved gas profiles (Group I-VI) of *Chlorella vulgaris* pyrolysis from 100°C to 600°C

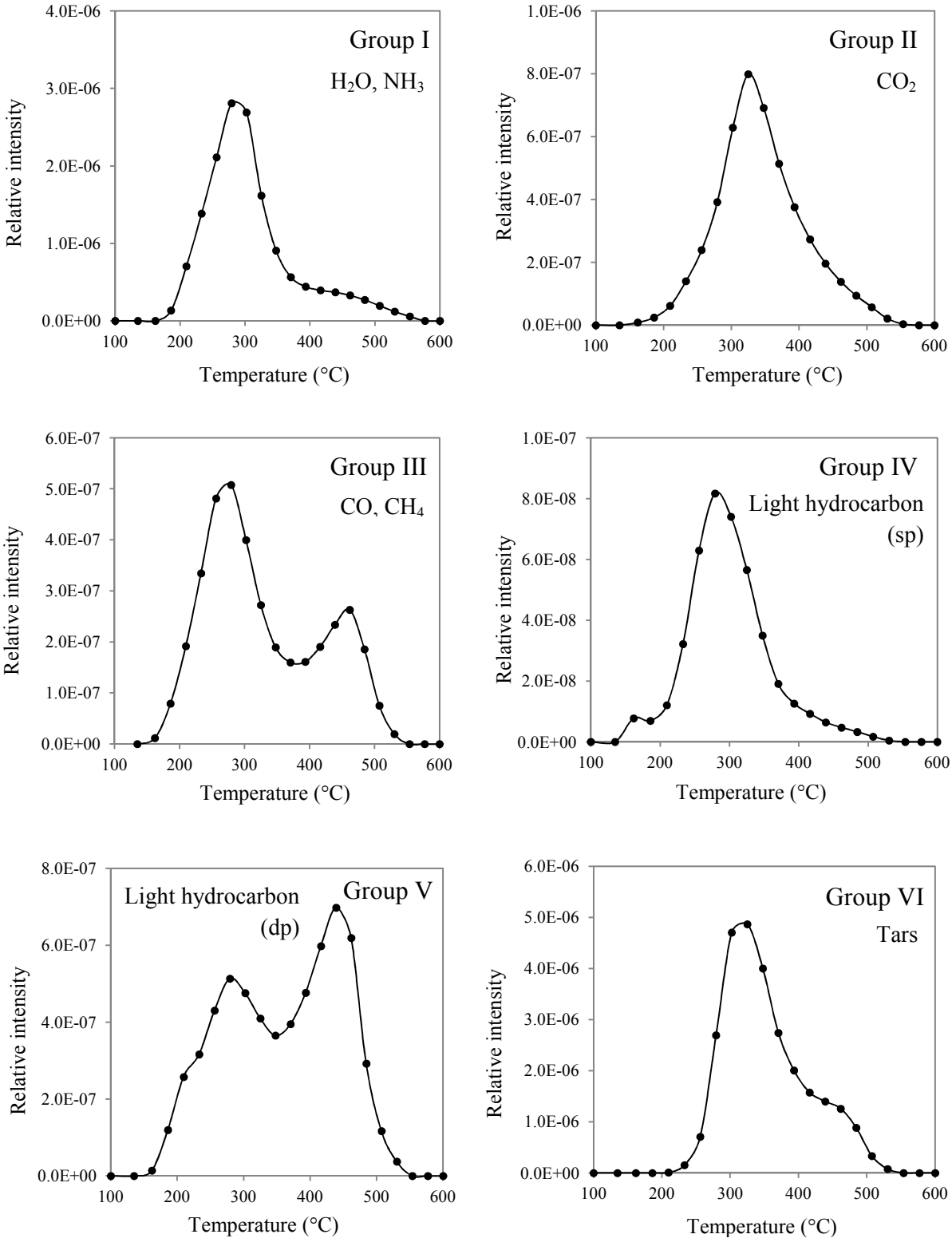

Fig. 8.5. Six lumped gas profiles for volatiles produced from *Chlorella vulgaris* pyrolysis at 20°C/min

8.6 Deconvolution method applied to evolved gas profiles

The evolved profiles represent the sum total of many overlapping individual peaks which are from different respective fractions in original biomass sample. These overlap of several peaks can be seen in every gas profile. Each peak and shoulder, called a 'pool', represents a single reaction. In order to determine precisely the position of the peaks, the evolved gas profiles are deconvoluted by means of the Gaussian distribution (equation (8.2-8.3)).

The size of pools for individual species are determined by adjusting the simulated peak temperature (T_{max}), peak height or peak intensity (H) and peak width (s) to fit the evolved gas profile with the trial and error approach. Then optimization tool in MATLAB programme (R2011a) is applied to gain the optimal Gaussian distribution parameters for the MS gas profiles at 95% confidential interval. The list of Gaussian distribution parameters of every evolved gas profile obtained from the MATLAB optimization tool is presented in Appendix C and the figures of the Gaussian distribution curve fitting for the evolved gas profiles are presented in Fig.8.6. The Gaussian distribution shows the good fitting to the measured profile of every volatile with R^2 values of 0.99, excepting the value of 0.97-0.99 for group IV. This lower value is due to the low intensity of group IV profile.

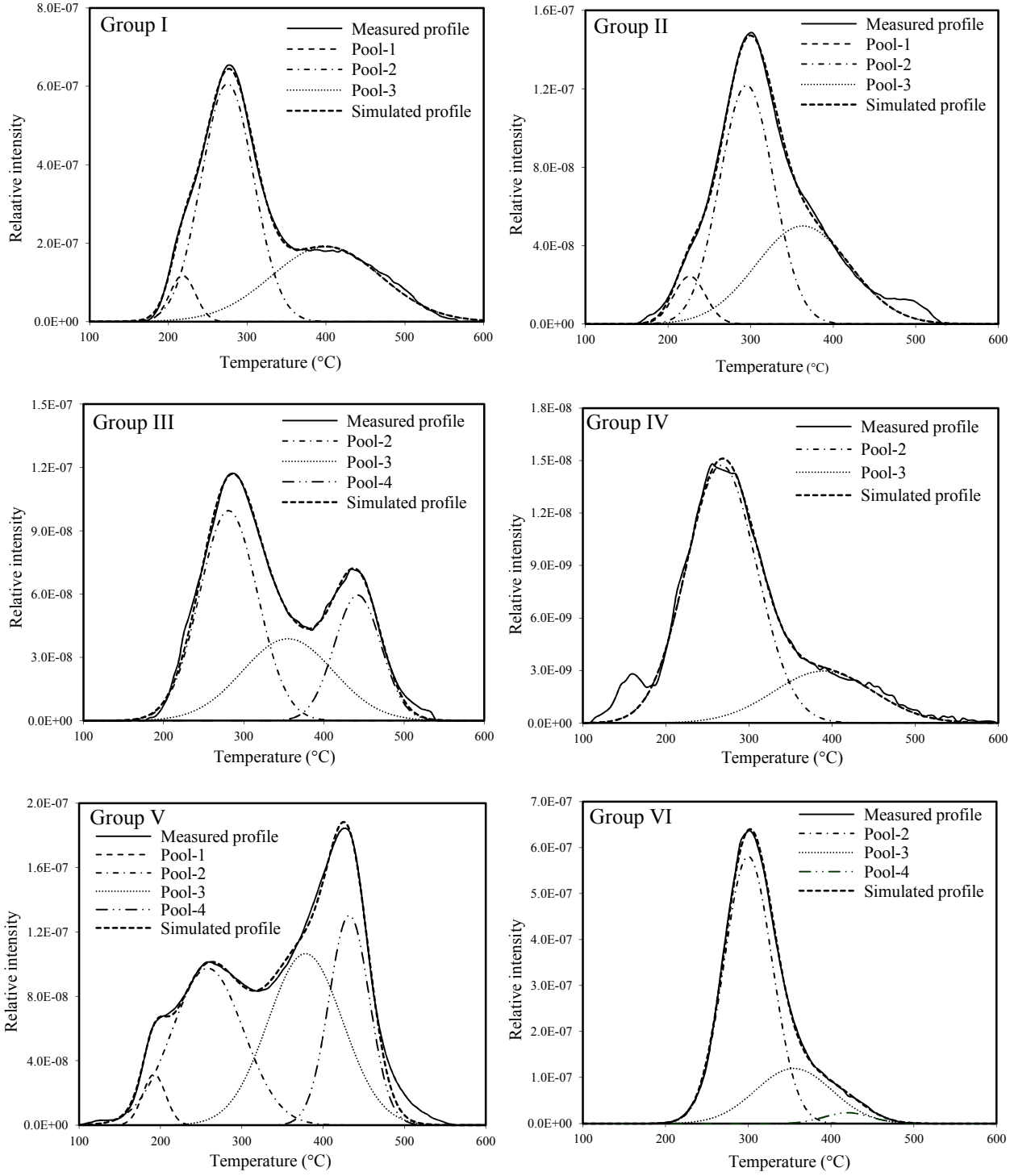

Fig. 8.6 The Gaussian distribution curves fitted for the evolved gas profiles (Group I-VI) of the thermal decomposition at 5°C/min

8.7 The kinetic evaluation of evolved gas profiles

By assuming independent, parallel, *n*th-order reactions for various products, the kinetic parameters for every partial reaction are evaluated by computationally direct model fitting method. The process was carried out in MATLAB software which was written for the purpose of this work (see Appendix D2) by following the evaluation concept explained in section 8.2. This programme allows to find a minimum value of deviation from three input data (apparent activation energy, pre-exponential factor and apparent reaction order) and the reaction order was varied between n = 1-4 for every reaction.

The kinetic parameters for every pool at different heating rates are given in table 8.1. The corresponding reactions of the different pools are numbered as 1, 2, 3, and 4. There are six lumped gas products listed in this table, out of which four (GI, GII, GIII, and GVI) were found to evolve as three peaks, one as two peaks (GIV) and one as four peaks (GV). This corresponds to 18 equations which describe the devolatilization of *Chlorella vulgaris*.

Table 8.1 Kinetic parameters for every partial reactions of *Chlorella vulgaris* pyrolysis from three heating rates (5, 10, 20°C/min)

Groups	Heating rate (°C/min)	Pool	E_a (kJ/mol)	log$A$ (min^{-1})	n	RMSE*
I	5	1	172	17.95	1.63	0.0032
		2	95	8.30	1.47	0.0039
		3	66	4.09	1.47	0.0057
	10	1	171	18.00	1.79	0.0030
		2	94	8.18	1.47	0.0036
		3	61	3.60	1.32	0.0036
	20	1	173	18.30	1.47	0.0049
		2	91	7.91	1.47	0.0037
		3	58	3.45	1.32	0.0036
II	5	1	162	16.70	1.79	0.0036
		2	105	8.95	1.47	0.0044
		3	66	4.36	1.32	0.0056
	10	1	169	17.14	1.63	0.0033
		2	107	8.91	1.32	0.0061
		3	70	4.64	1.32	0.0043
	20	1	172	17.48	1.47	0.0036
		2	102	8.30	1.47	0.0040
		3	69	4.46	1.47	0.0045

III	5	1	89	7.59	1.47	0.0037
		2	71	4.91	1.47	0.0038
		3	214	15.08	1.79	0.0049
	10	1	90	7.46	1.32	0.0056
		2	70	4.53	1.47	0.0047
		3	221	14.85	1.95	0.0062
	20	1	94	7.80	1.47	0.0038
		2	72	4.78	1.47	0.0044
		3	223	14.67	1.95	0.0064
IV	5	1	73	6.29	1.47	0.0045
		2	73	4.73	1.47	0.0058
	10	1	78	6.58	1.47	0.0034
		2	68	4.46	1.47	0.0050
	20	1	78	6.95	1.63	0.0047
		2	69	4.67	1.47	0.0043
V	5	1	163	18.00	1.47	0.0052
		2	66	5.70	1.47	0.0041
		3	96	6.86	1.47	0.0041
		4	223	15.95	1.47	0.0057
	10	1	164	17.76	1.79	0.0037
		2	78	6.70	1.47	0.0041
		3	82	5.59	1.32	0.0056
		4	192	13.70	1.92	0.0076
	20	1	164	18.10	1.95	0.0041
		2	80	7.00	1.47	0.0039
		3	81	5.65	1.47	0.0038
		4	214	15.33	1.95	0.0062
VI	5	1	124	10.66	1.47	0.0043
		2	88	6.46	1.47	0.0040
		3	212	15.48	1.79	0.0057
	10	1	113	9.37	1.47	0.0049
		2	77	5.60	1.47	0.0047
		3	221	15.78	1.79	0.0040
	20	1	117	9.97	1.47	0.0055
		2	82	5.93	1.47	0.0041
		3	226	15.70	1.79	0.0046

** RMSE: Root Mean Square Error (equation (8.6))*

The compensation effect was also observed from this study which is shown in Fig.8.7. A small valley of evaluation shows the presence of the relationship between apparent activation energy and pre-exponential factor to give the small deviation values. To facilitate the calculation of E_a, A and n value, the optimization was focused only around the valley.

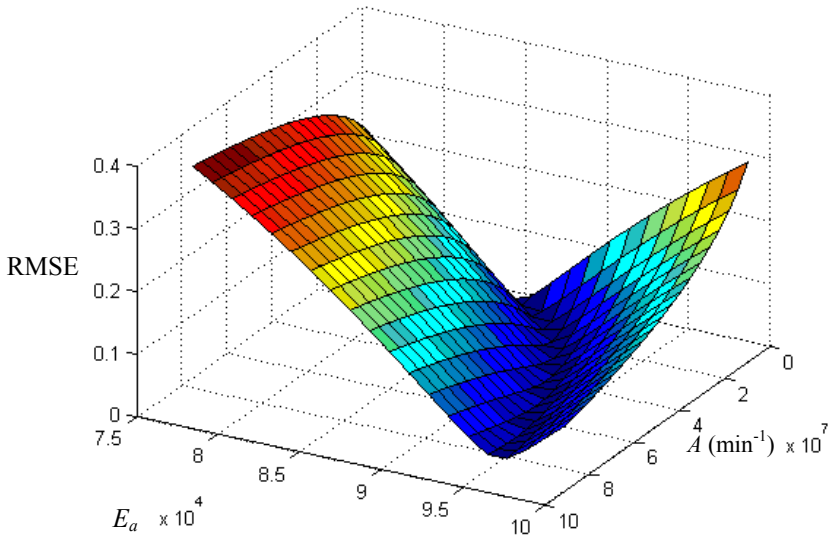

Fig. 8.7 The deviation (RMSE) for the evaluation of kinetic parameters (E_a and A)

The obtained kinetic parameters spread in a wide range which the apparent activation energies are 58-226 kJ/mol and the pre-exponential factors are 3.45-18.30 min^{-1}, while apparent reaction orders lie in a narrow range between 1.32-1.95. The variation of the kinetic parameter for different heating rates can be observed that they increase as the heating rate increases. The apparent activation energies in table 8.1 can be categorized into four ranges which are (1) E_a = 162-173 kJ/mol and log$A$ = 16.70 – 18.30 min^{-1}; (2) E_a = 66-124 kJ/mol and log$A$ = 5.70 – 10.66 min^{-1}; (3) E_a = 58 – 96 kJ/mol and log$A$ = 3.45 – 6.86 min^{-1}; (4) E_a = 192-226 kJ/mol and log$A$ = 13.70 – 15.95 min^{-1}.

The four ranges of kinetic parameters of evolved gas profiles, together with the peak temperature and decomposition temperature range of each pool in figure 8.6, it is assumed that there are four pseudo-components in thermal decomposition of *Chlorella vulgaris*. Each pseudo-component is pyrolyzed at different temperature range and different thermal behaviour. Also their decomposition peaks overlap each other, thus it is better to call 'pseudo-component' instead of component. The pseudo-component 1, 2, 3, 4 degrade around 180-250, 200-400,200-500 and 380-500°C, respectively.

Microalgae can be regarded as mixtures of protein, polysaccharides, lipid and minor components. To identify the materials presenting for each pseudo-component, the

information of gaseous evolution, the presence of functional groups in solid residue and the published literature are investigated.

FTIR spectra of solid residue which are produced from pyrolysis at different temperatures from 300 to 600°C by thermogravimetry technique are shown in Fig.8.8.

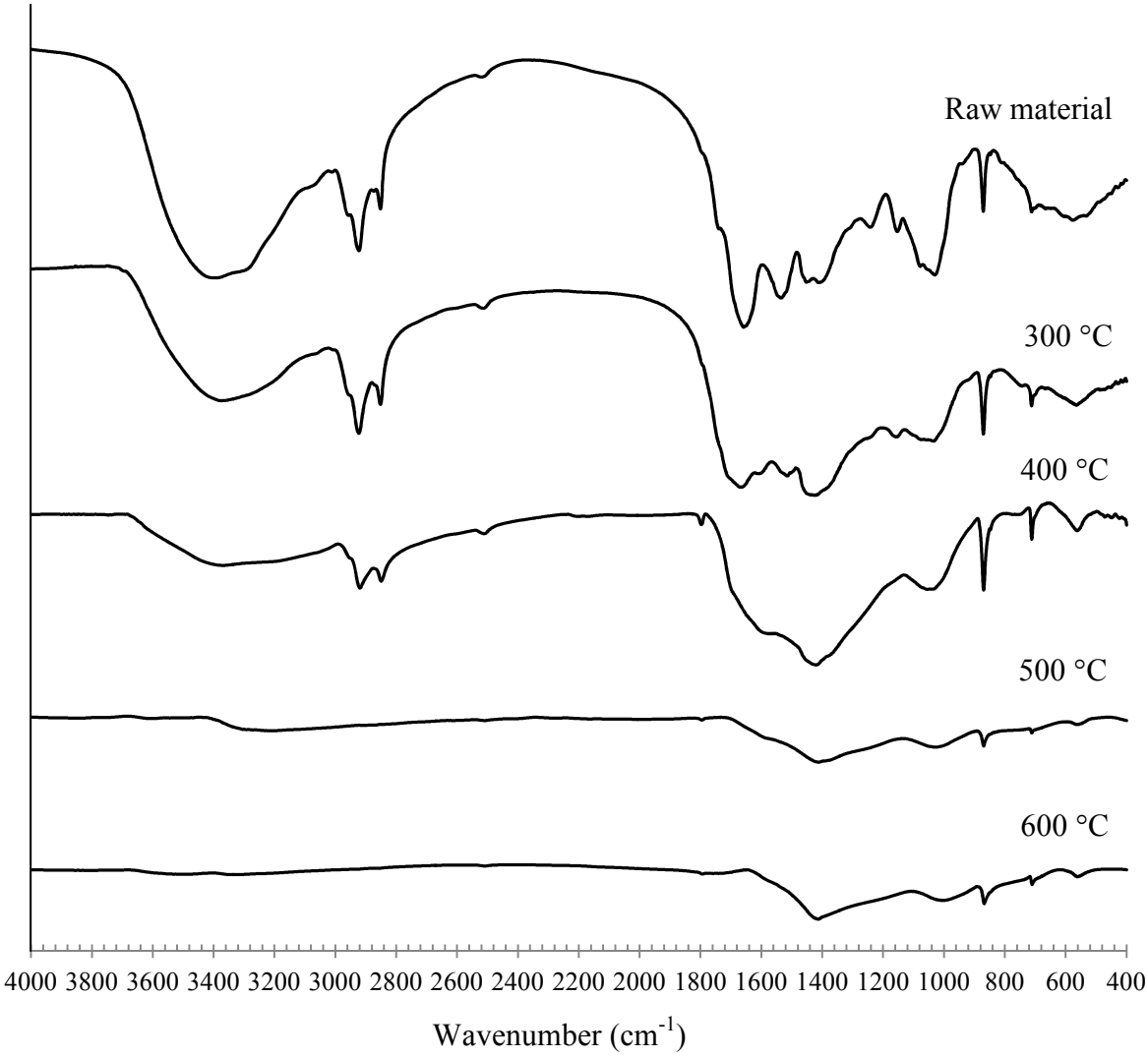

Fig. 8.8 FTIR spectrum of solid residue from pyrolysis of *Chlorella vulgaris* at different temperatures comparing to the spectrum of original biomass

From Fig.8.8, at temperatures up to 300°C, the 3000-2800 cm^{-1} peaks representing the lipid did not show any decomposition but the peak at 3400, 1700-1500 and 1000 cm^{-1} which are assigned to protein band I, II and III, and polysaccharides are reduced (the detail on FTIR assignment presented in chapter 5 previously). The solid residue at 500°C does not show the lipid peak anymore which can be said that the decomposition of lipid take place after

300°C and finish before 500°C. On the other hand, protein and polysaccharides (i.e. cellulose and starch) start the decomposition at a low temperature before 300°C and their process occur in a wide range of temperature up to 500°C. At temperature 500-600°C, there are no significant degradations.

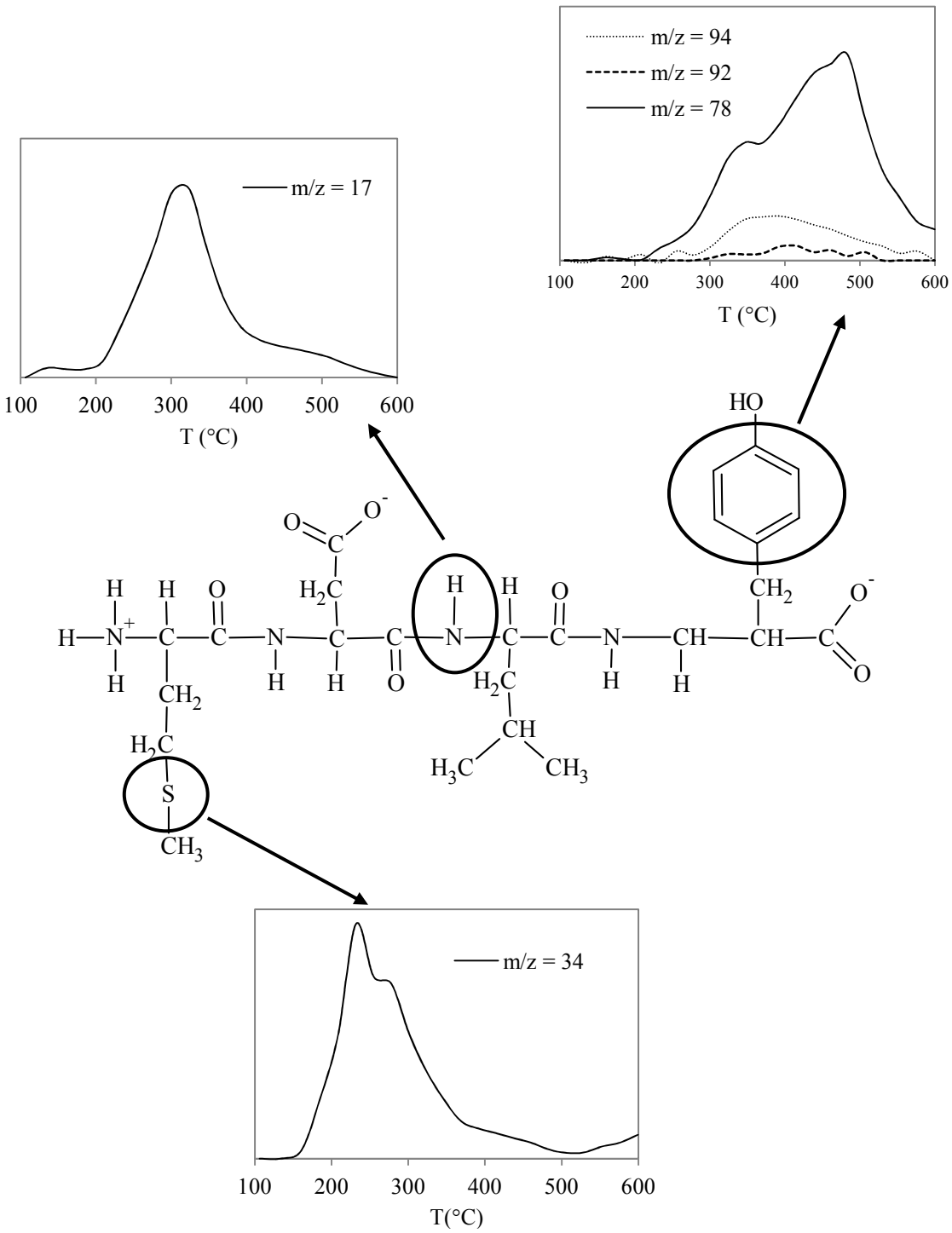

Fig. 8.9 A polypeptide chain and the evolved gas profiles related to the decomposition of some fractions of protein

Some important fractions presented in protein structure are highlighted by circles in Fig.8.9. The evolved gas profile of NH_3 (*m/z* = 17) and H_2S (*m/z* = 34) are produced mainly at 200-400°C. The groups of aromatic products such as benzene (*m/z* = 78), toluene (*m/z* = 92) and phenol (*m/z* = 94) evolve at wide temperature range from 200°C to 550°C. Although protein produces a high amount of gas products at 200-400°C, it can distribute to the degradation at higher temperature region for aromatic fractions. Thus, protein is considered to decompose in two different peaks by assuming that two different protein compositions decompose at different temperature region. These multiple steps of protein from the thermal decomposition process were also reported before [344-346].

The main polysaccharides presented in *Chlorella vulgaris* are cellulose from the cell wall and starch which both are decomposed at temperatures around 300-400°C [347-349]. The thermal behaviour of cellulose also reported in this work previously. Moreover, some publications reported the decomposition of protein and carbohydrates at low temperature, while lipid decomposition occurs at higher temperature on the thermal decomposition of algae [296, 298].

To summarize, from all information above it leads to the identification of each pseudo-component that pseudo-component 2 (200-400°C) comprises of protein component and pseudo-component 3 (200-500°C) consists of polysaccharides and some protein fractions. Pseudo-component 4 (380-500°C) represents the lipid component, while pseudo-component 1 represents the extractive or adsorbed molecules which are evolved at low temperatures.

8.8 Multi-component model

A multi-component model which consists of four independent, parallel reactions is applied in this study to described the devolatilization of *Chlorella vulgaris*. It is pointed out that there are four pseudo-components presenting in the *Chlorella vulgaris*. Each pseudo-component (M_i) decomposes in different temperature ranges independently.

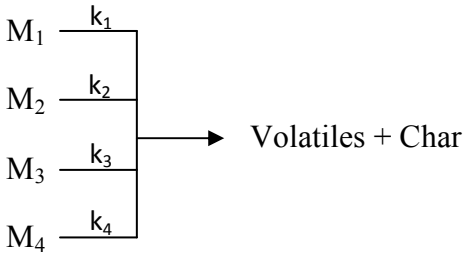

The rate expression in non-isothermal condition for each single reaction is shown in equation 8.4. The formal kinetic parameters of each pseudo-component are evaluated by direct model fitting by minimizing the root mean square error (RMSE). The parameter ranges (E_a, A and n) are similar to those applied for the pools of evolved gas profiles. The apparent kinetic parameters of four pseudo-components at three heating rates are listed in table 8.2.

The average apparent activation energies from three heating rates are in a range of 147, 88, 73 and 207 kJ/mol for pseudo-component 1, 2, 3 and 4, respectively. The apparent orders of reaction for every pseudo-component are between n =1 and n =2, excepting the pseudo-component 4 which gives the apparent order of reaction more than 2.0. The accuracy of the model can be affected by the size of value step, especially the pre-exponential factor. If small step is applied, more accuracy can be obtained but more time is required for the computation. The variation of the kinetic parameters for different heating rates can be observed that the apparent activation energy trends to increase when the heating rate increases. However the deviation of apparent activation energies is in the range of 1-5 kJ/mol which indicates a small influence of heat transfer.

Table 8.2 The formal kinetic parameters of four pseudo-component decompositions at heating rates 5, 10, 20°C/min

Pseudo-component	Heating rate (°C/min)	E_a (kJ/mol)	log$A$ (min^{-1})	n	RMSE*
1	5	144	15.05	1.63	0.0029
	10	148	15.43	1.63	0.0030
	20	150	15.95	1.79	0.0034
	average	147 ± 3	15.63 ± 0.45	1.68 ± 0.09	0.0031
2	5	86	7.21	1.32	0.0024
	10	88	7.30	1.32	0.0042
	20	89	7.38	1.32	0.0021
	average	88 ± 2	7.30 ± 0.09	1.32 ± 0.0	0.0029
3	5	73	4.93	1.63	0.0045
	10	73	4.99	1.79	0.0067
	20	74	5.08	1.47	0.0047
	average	73 ± 1	5.00 ± 0.08	1.63 ± 0.16	0.0053
4	5	209	14.85	1.63	0.0045
	10	201	14.21	2.26	0.0088
	20	210	14.66	2.11	0.0051
	average	207 ± 5	14.57 ± 0.33	2.00 ± 0.33	0.0061

** RMSE: Root Mean Square Error (equation (8.6))*

Fig.8.10 (a-c) shows the comparison between the experimental results and the models for *Chlorella vulgaris* pyrolysis, together with the individual rates of the four pseudo-component peaks at different heating rates (5, 10 and 20°C/min). When the dotted plots present the measured data from Thermogravimetry in form of DTG and the solid line plots present the calculated data or the model plots which are obtained from the summation of the apparent kinetic parameters of each pseudo-component (in Table 8.2). While the sub-curves plots present the evolution profiles of each pseudo-component obtained from their calculated apparent kinetic parameters (Table 8.2).

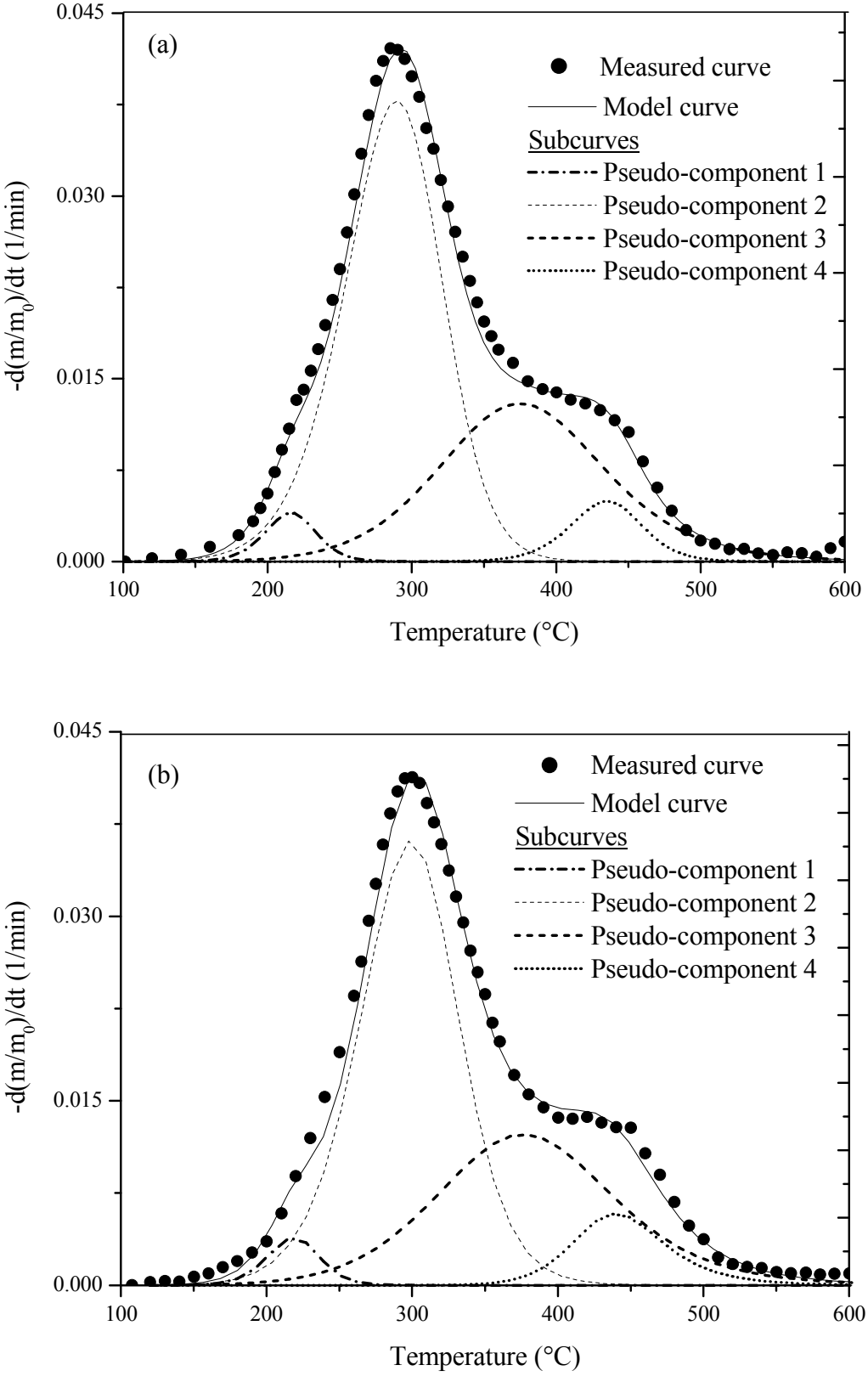

Fig. 8.10 Thermal decomposition rates, together with their individual component curves and the model plots at heating rates (a) 5, (b) 10, and (c) 20°C/min

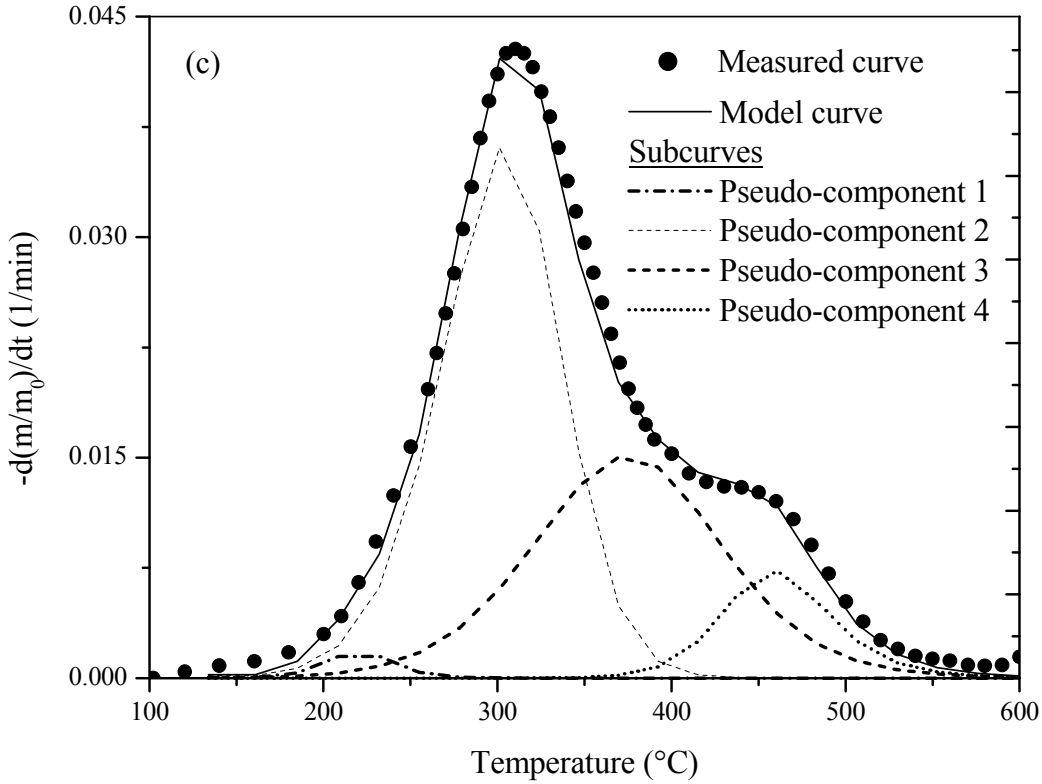

Fig. 8.10 Thermal decomposition rates, together with their individual component curves and the model plots at heating rates (a) 5, (b) 10, and (c) 20 °C/min (continued)

The good fitting between the model plots and the measured data can be observed in every heating rate. Deviation of model prediction was found to be less than RMSE = 0.01 for all condition. Thus, this four-component model suffices for the description of the thermal decomposition of *Chlorella vulgaris*.

8.9 Summary of non-isothermal kinetic analysis

In this work, the kinetic parameters for the thermal decomposition of *Chlorella vulgaris* have been derived from evolved gas profiles obtained from mass spectrometry by multi-product and multi-component approach. Thermogravimetry-Mass Spectrometry (TG-MS) technique was applied to these non-isothermal kinetic measurements. When the rate of pyrolysis can be monitored by thermobalance, the evolution of produced gases is detected by MS detector in the relationship with time. The potential of TG-MS data for the evaluation of kinetic parameters have been successful presented in this work.

Evolved gas analysis not only provides more detail on thermal decomposition mechanism, but also is shown to be very useful in discriminating between the thermal decomposition of the major components in term of 'pseudo-component'. This is especially true in the case of unknown mechanisms, where the characteristic of gas profiles can be used to identify the decomposition rate of materials in samples. Also in the case of the main components of sample cannot be identified to some specific chemicals or these chemicals cannot be extracted from sample without chemical change.

The evolved gas profiles from TG-MS have been influenced from the characteristics of the instrument and the experimental conditions. Thus, the data treatment is necessary to proceed before further evaluation of kinetics. The cold spot and the change in volumetric flow are the critical effects in this kinetic study.

The problem to identify the degree of conversion range of overlapping peaks or shoulders can be overcome by the deconvolution procedure with Gaussian distribution. Also this individual peak/shoulder represents the decomposition of the pseudo-components which are related to the presence of protein, polysaccharides and lipid contents in *Chlorella vulgaris* sample. The small peak around 180-250°C can be implied that it is from the decomposition of extractives or the evolution of adsorbed molecules. The main peak around 200-400°C is involved the decomposition of protein and another main peak around 200-500°C represents the decomposition of polysaccharides and also another fraction of protein. The last peak around 380-500°C is related to the degradation of lipid.

The pyrolysis of *Chlorella vulgaris* is successfully modelled by a kinetic scheme consisting of four independent *n*th-order reactions for four different pseudo-components. The direct evaluation of the derivation between the simulated rate expression and the evolved gas profiles was employed in this work. The apparent activation energies for the pseudo-components representing protein and polysaccharides are lower than 100 kJ/mol, while those of the peaks representing adsorbed molecules and lipid are higher, especially the lipid decomposition with apparent activation energy (~207 kJ/mol). The apparent orders of reaction of every pseudo-component are around 1.0-2.0 excepting the fourth pseudo-component for lipid which is higher than $n = 2.0$. In addition, the compensation effect can be observed during the kinetic evaluation, while the heat transfer influence can be determined as a small level.

Numerous studies on the thermal decomposition of biomass have focused on the estimation of kinetic equations by means of a global model from non-isothermal measurement at a single or many heating rates. The single global model gives only a set of kinetic parameters which represent the overall decomposition. However biomass consists of many components varying from species to species and also the pyrolysis process of biomass is complex. This detailed reaction model consists of several steps for each of the main components and the understanding of the evolution of volatile species during pyrolysis are important in term of the improved product design and improved product evaluation in the industry.

8.10 Comparison between isothermal and non-isothermal kinetic analysis

In this work, the isothermal data had been obtained from the experiment by Pyrolysis coupled with Mass Spectrometry (Py-MS) technique. Several measurements at different temperatures were carried out with a small sample size and the short experimental time need. The formal kinetic parameters from isothermal condition are categorized into three sections, low, middle and high temperature regions, due to the clearly observed of the change in mechanism at 430 and 500°C.

In the case of non-isothermal condition, measurements were carried out with constant heating rates (5, 10 and 20°C/min) to gain data in a wide range temperature. Thermogravimetry coupled with Mass Spectrometry (TG-MS) have been applied in non-isothermal pyrolysis. The kinetic parameters are evaluated from the evolution of volatile products. These evolved gas analysis gives more detail on the pyrolysis process and lead to the multi-component model reported in this work.

To validate the formal kinetic parameters from non-isothermal measurements, the comparison with data from isothermal measurements are necessary [28]. The summaries of isothermal and non-isothermal kinetic parameters from this study are listed in table 8.3.

For non-isothermal pyrolysis, pseudo-component 2 and pseudo-component 3 are the main decomposition peaks in the whole pyrolysis. Also protein and polysaccharides are the first and the second high content of *Chlorella vulgaris* sample. Thus, their apparent activation

energies are dominant over the others. The apparent activation energies and pre-exponential factors of pseudo-component 2 and 3 are relative low. Although these values are higher than the isothermal kinetic parameters, these values are still trend to be in a low level similarly. The pseudo-component 1 and 4 have the high apparent activation energy and pre-exponential factor but due to their small contribution, these high values might not influence the global parameters at different temperature of isothermal condition.

Table 8.3 Summarized isothermal and non-isothermal kinetic parameters of this work

Approach	**Identification**	***T* (°C)**	**E_a (kJ/mol)**	**log*A* (min^{-1})**	***n***
Isothermal	Low temperature region	250 - 430	57 ± 3	5.32 ± 0.55	1.21–1.45
	Middle temperature region	430 - 500	9 ± 9	1.75 ± 1.52	1.45
	High temperature region	500 - 600	40 ± 5	3.88 ± 0.78	1.45–1.15
Non-isothermal*	Pseudo-component 1 (extractives)	180 - 250	147 ± 3	15.63 ± 0.45	1.68 ± 0.09
	Pseudo-component 2 (protein)	200 - 400	88 ± 2	7.30 ± 0.09	1.32 ± 0.00
	Pseudo-component 3 (polysaccharides and protein)	200 - 500	73 ± 1	5.00 ± 0.08	1.63 ± 0.16
	Pseudo-component 4 (lipid)	380 - 500	207 ± 5	14.57 ± 0.33	2.00 ± 0.33

* average values from data at three heating rates at 5, 10 and 20°C/min

Isothermal apparent activation energies at reaction temperatures below 430°C are higher than those at above 430°C. Like isothermal data, at temperature lower than 400°C of non-isothermal condition, it is dominant by pseudo-component 2 with apparent activation energy 88 kJ/mol which is higher than the dominant apparent activation energy (73 kJ/mol) for pseudo-component 3 at high temperature region. The same trend also applies for the pre-exponential factor values. Moreover, both isothermal and non-isothermal condition provide the apparent orders of reaction in the range of n =1.0-2.0.

In addition, the order model equation is widely applied for isothermal and non-isothermal experiments. The low apparent activation energy and pre-exponential factor values in isothermal and some fractions in non-isothermal analysis suggest that another model rate equation should be studied in the future for the decomposition of this sample.

The kinetic data reported in Table 8.3 shows the difference between isothermal and non-isothermal kinetic data which can be caused by

1. Thermal decomposition in the solid state usually involves multiple steps that contribute to the overall reaction rate that is measured in thermal analysis experiments. The contribution of each step with different activation energies to the overall reaction rate will vary with both temperature and extent of conversion.
2. Isothermal and non-isothermal experiments are carried out at different temperature ranges. The isothermal experiments are measured in narrower temperature ranges than the non-isothermal ones which cover the wide range of temperature. The identical values of the kinetic parameters from isothermal and non-isothermal experiments cannot be obtained from the different conducted temperature region [350].
3. At very low range of the reaction extent (α), the isothermal data is influenced by the induction period when the sample is heated from outside to inside of particles. Also at very high range of the reaction extent (α), the change of high degree of conversion needs a long duration. The determination of the small mass changes over a long period of time is less accuracy because of the limited stability of detected ion current from MS detector [351].
4. The sample amount used in non-isothermal measurements is larger than those for isothermal measurement up to 20 times. The non-stationary heating of dynamic condition may cause the temperature gradient in the sample. The difficulty to measure the real sample temperature and real heating rate is the important problem in non-isothermal measurement. Although, in this experiment, the sample temperature sensor locates beneath the crucible holder, the small error in the real sample temperature reading can affect the evaluation of kinetic parameters.

The thermal decomposition involves multi-step reactions which can be observed from the kinetic data. Thus, it seems clear that a single kinetic parameter set is not enough to characterize any solid state reactions. Moreover, the similarity of kinetic parameters from isothermal and non-isothermal experiments is shown here. However the identical values cannot be obtained due to the unavoidable experimental factors.

Chapter 9

Conclusion and Recommendation

9.1 Research conclusion

Chlorella vulgaris, green freshwater algae, was selected for pyrolysis process in this study due to its high productivity and easy to cultivate. The characteristics of these algae showed promising properties which are comparable to those of plant biomass; although, the high ash content can be removed by pre-treatment. Main components of this microalgae sample are protein (43%), polysaccharides (22%), lipid (12%), moisture and mineral matter. These proportions agreed with the peak areas of DTG data which link to the main peak for the decomposition of protein and soluble polysaccharides and the shoulder at higher temperature for lipid and insoluble polysaccharides. Protein is the major component and it is the source of nitrogen-containing and aromatic products. The wide range of products can be observed from the condensed pyrolysis oil obtained from both analytical pyrolysis and pilot-scale pyrolysis of *Chlorella vulgaris*. Gaseous products mainly included water, ammonia, carbon dioxide, carbon monoxide and hydrogen but hydrogen seem to evolve after the devolatilization step at high temperature.

A preliminary pyrolysis carried out in the pilot-scale intermediate pyrolysis reactor, called Pyroformer was performed to basically assess the applicability of *Chlorella vulgaris* as a biomass feed in an existing reactor. *Chlorella vulgaris* produced a reasonable liquid product yield and the organic phase can be separated from aqueous phase easily. This benefit led to a low water content remaining in the pyrolysis oil. Moreover, the lower density, lower oxygen content and higher heating value showed the comparable properties over lignocellulosic pyrolysis oil. However, the aspects on the high ash content and high nitrogen content need to be further studied. In addition, pyrolysis oil from *Chlorella vulgaris* has potential to be a source of chemicals. Bio-char from this intermediate pyrolysis was dry, brittle and containing high mineral content which was suggested for fertilizer utilisation.

The kinetic analysis for pyrolysis process was explored in this work for both isothermal and non-isothermal conditions. The drawbacks of isothermal measurements were taken into account in the seeking of a suitable instrument set-up and operating conditions. Pyrolysis-Mass Spectrometry was selected for isothermal studies since it benefit from short time duration for analysis and requires a small amount of sample. Also, sample is heated up without temperature overshooting because the temperature is well controlled over the very small reactor and this instrument allowed the sample to be inserted into the reactor when the temperature reached a set point and remained constant. Thus, pyrolysis process was monitored from the starting point of its decomposition. The induction period could be observed in evolution data detected by mass spectrometric detector but this period was relative short compared to the duration of the whole measurement.

Firstly, polyethylene, a well-known polymer, was used to check the potential of Pyrolysis-Mass Spectrometry for isothermal evaluation. The result showed that polyethylene pyrolysis has apparent activation energy of 216 ± 9 kJ/mol; a pre-exponential factor of 14.89 ± 1.34 min^{-1}; and an apparent order of reaction between 0.7 and 1.6. These results were compared with reported values in literature and were found to be in good agreement. The melting process of polyethylene was taken into account of the deviation between measured data and calculated data. Moreover the benefit of isothermal measurement that it can detect the change of mechanism was observed in this work.

Furthermore, lignocellulosic materials, cellulose, hemicellulose and lignin were also analysed under isothermal conditions to evaluate the potential of the new developed instrument and the kinetic evaluation procedure on typical biomass materials. Cellulose and hemicellulose could be described by a single reaction with the set of apparent activation energy, pre-exponential factor and reaction order at 131 ± 6 kJ/mol, 10.89 ± 1.19 min^{-1} , 1.06 and 125 ± 5 kJ/mol, 11.53 ± 0.93 min^{-1}, 1.1, respectively. The thermogram of cellulose showed the narrow decomposition curve in the temperature range 350-400°C, while that of hemicellulose lay between 280 and 340°C. Lignin was determined as the main source of char production and it decomposed in a wide range of temperature from 320 to 500°C. Its kinetic parameters were E_a = 72 ± 4 kJ/mol, log$A$ = 6.51 ± 0.73 min^{-1} and n = 1.64-1.88. The good agreement between the kinetic parameters obtained from this study and the reported data was presented. Also, the obtained kinetic parameters can be applied to measured data up to 95% degree of conversion.

Unlike isothermal measurements, the pyrolysis temperatures increase with a constant heating rate during non-isothermal measurements. To gain more information on the evolution of products and reaction mechanism, evolved gas analysis was also applied to the non-isothermal study. Thermogravimetry-Mass Spectrometry was the technique to evaluate kinetic parameter from non-isothermal conditions. The evolution data for individual gas product was presented in the relationship of ion current with time. In this study, the utilization of TG-MS data procedure was successfully developed for kinetic evaluation based on the evolution profile of volatile species relevant to biomass pyrolysis. Due to the influence from the systematic error, data treatment of evolved gas profiles obtained from mass spectrometer was suggested to be the necessary process to gain the comparable data to the weight loss results. Moreover, the deconvolution method in the form of Gaussian distribution was well applicable to evolution data of volatile products. This deconvolution method allowed the kinetic evaluation can be applied for every single reaction, which their decomposition peaks are overlapping each other. The step-by-step procedure to employ raw TG-MS data for kinetic evaluation was demonstrated in this thesis in the case of *Chlorella vulgaris* pyrolysis. For the unknown mechanism, the evolved gas analysis technique proved to provide more understanding in thermal behaviour and reaction mechanism.

This thesis reported some new results for the kinetics of the thermal decomposition of *Chlorella vulgaris* as derived from isothermal and non-isothermal measurements in the Pyrolysis-Mass Spectrometry and Thermogravimetry-Mass Spectrometry, respectively. From analysis of isothermal data, it was found that pyrolysis proceeds in three distinct temperature zones with a transition around 430°C and 500°C. The reaction orders were found to increase from 1.21 to 1.45 in the lower temperature zone and constant at 1.45 within 430-500°C, then decrease from 1.45 to 1.15 in the higher temperature zone. At temperature from 250 to 430°C, *Chlorella vulgaris* pyrolysis was described by apparent activation energy of 57 ± 3 kJ/mol and log of pre-exponential factor of 5.32 ± 0.55 min^{-1}, while at temperature 500-600°C, the apparent activation energy was 40 ± 5 kJ/mol and log of pre-exponential factor was 3.88 ± 0.78 min^{-1}. In the middle temperature region (430-500°C), the apparent activation energy (9 ± 9 kJ/mol) and pre-exponential factor (1.75 ± 1.52 min^{-1}) are low.

In addition, for non-isothermal conditions, the pyrolysis of *Chlorella vulgaris* was successfully modelled by a kinetic scheme consisting of four independent, parallel *n*th-order reactions for four pseudo-components. The first pseudo-component corresponded to the fractions of extractives and adsorbed molecules which are reactive at low temperatures. The second pseudo-component represented the protein fraction and the third included polysaccharides and the remaining fractions of the protein. The fourth pseudo-component corresponded to the lipid fraction. These four categories for pseudo-components were derived from the temperature range of single peaks or/and shoulders of lumped evolved-gas profiles, together with kinetic data from individual deconvoluted peaks. Protein and polysaccharides were identified as the main influence of *Chlorella vulgaris* pyrolysis and their decompositions represented by pseudo-component 2 and 3 peaks, respectively. The kinetic parameters for pseudo-component 2 were E_a = 88 ± 2 kJ/mol, log$A$ = 7.30 ± 0.09 min^{-1}, and n = 1.32, while those for pseudo-component 3 were E_a = 73 ± 1 kJ/mol, log$A$ = 5.00 ± 0.08 min^{-1}, and n = 1.63. The decomposition of active compounds and the desorption process were described by the peak of pseudo-component 1 with E_a = 147 ± 3 kJ/mol, log$A$ = 15.63 ± 0.45 min^{-1}, and n = 1.68. Lipid decomposition (pseudo-component 4) showed the kinetic parameters at E_a = 207 ± 5 kJ/mol, log$A$ = 14.57 ± 0.33 min^{-1}, and n = 2.0.

Both isothermal and non-isothermal kinetic results were found to present satisfactorily in the pyrolysis data; despite, the detection of compensation effects in this work, especially for non-isothermal measurements. The heat transfer effect reflected the kinetic parameters at different heating rates. The kinetic parameters obtained from isothermal experiments were found to be correlative with those obtained from non-isothermal experiments. Both isothermal and non-isothermal analysis (main peaks) gave the low activation energies. The discrepancy in kinetic results caused from simplifications in the reaction mechanism, the difficulty to measure the real non-isothermal temperatures or heating rates, and heat transfer effect.

This work gives some new alternative ways for studying kinetics of biomass and new results on the kinetics of microalgae pyrolysis. First, this work showed and demonstrated the new developed instrument for isothermal kinetic analysis which provided good quality results. This instrument can be used with not only polymeric materials, but also biomass materials (both lignocellulosic and microalgal samples). Second, this work reported results of kinetics of microalgae pyrolysis which still has limited information nowadays. Third,

the deconvolution process by Gaussian distribution was applied to non-isothermal analysis aiming to suggest the alternative way to analysis the complex process of thermal decomposition.

The complementary use of the two approaches (isothermal and non-isothermal) can provide valuable information but it needs to be considered the shortcomings and limitations of each approach. Isothermal thermograms were found to be simpler to interpret than non-isothermal ones in the case of complex reaction scheme and this method is suitable for chemically fundamental studies. On the other hand, the rapidity of non-isothermal measurements leads to the application of this method on practical processes which are operated at similar conditions as non-isothermal experiment. However, the combination of non-isothermal measurement with evolved gas analysis gives useful information on released volatiles during decomposition. Moreover, together with the deconvolution technique with Gaussian distribution suggests the further application of this technique for samples with or without knowledge of their identified main compositions.

9.2 Recommendations

Following the studies undertaken in this thesis, some recommendations have been suggested for continuation of this work.

1. Microalgae compositions depend on the species and cultivation conditions. Lipid is the most promising content which is suitable for biodiesel application and leads to high qualities of pyrolysis oil with high aliphatic and low nitrogen-containing compounds. The selection of microalgae species should be determined together with the possibility of cultivation to increase lipid content.

2. The present study was focused only on the *n*th-order reaction model. The accuracy of kinetic parameters also depends on the model of reaction. The meaning of the 'best model' should be critically considered because of the lack of alternatives. Due to the low activation energies obtained from this work in some conditions, the other reaction models should be taken into account for future works.

3. Due to the computational needs, a great amount of time was spent in the development and application of the written programmes. Several studies can be carried out to evaluate

kinetic data regarding the different kinds of biomass and different pyrolysis conditions in future works. These attempts demand the modification in the programme code with certain computer software knowledge.

4. Since the non-isothermal kinetic procedure reported in this thesis is new for microalgae study, more experiments need to be performed for other biomass or different kinds of microalgae and under different conditions. Also to investigate the heating rate influence on kinetic parameters, more experiments at several different heating rates should be added into non-isothermal study.

5. To minimize the catalytic effect from ash content in microalgae, pre-treatment to remove mineral matter from biomass before applying the pyrolysis process is recommended in the case of the acceptable reduction of the economic efficiency.

6. The systematic errors influenced the pyrolysis characteristic and kinetic evaluation. Thus, the improvement of analytical instrument can enhance the accuracy of analysis. For example, the capillary connected between TG and MS detector should be changed to a metal tube which can withstand higher temperatures.

7. For the attempt to apply microalgae to the existing pyrolysis reactors, the feed form of microalgae is an important point that they should be pelletized before introducing into the reactor. This is because the powder form of this microalgae feed could cause blockages inside the feeding line and also to other parts of system.

8. To extend the use of kinetic parameters, the combination of chemical kinetic data with heat and mass transfer concepts will aid in reactor design and process control.

LIST OF REFERENCES

1. United Nations Framework Convention on Climate Change. [2012]. *Kyoto Protocol [online]*. Available from: **http://unfccc.int/kyoto protocol/items/2830.php** [Accessed 28 Mar 2012].

2. U.S. Energy Information Administration (EIA). (2011). *Trends in Renewable Energy Consumption and Electricity 2009 [online]*. Washington, DC: U.S. Department of Energy. Available from: **http://www.eia.gov/renewable/annual/trends/** [Accessed 28 Mar 2012].

3. Doran, M. (2009). Feedstocks for thermal conversion. IN: Bridgwater, T, et al. (eds.) *Thermal Biomass Conversion*. United Kingdom: CPL Scientific Publishing Services Ltd., 129-156.

4. German Solar Energy Society (DGS) and Ecofys (2005). *Planning and installing bioenergy systems: a guide for installers, architects and engineers*. London: James & James.

5. Envirolink Northwest (2010). *Biomass Strategy for England's Northwest: Summary Report 2010 [online]*. Available from: **http://www.alexandradockproject.co.uk/media/18004/Envirolink%20Northwest%20100727%20Biomass%20Summary%20Report.pdf** [Accessed 25 Nov 2011].

6. Harteveld, M., Godfroij, P., Neeft, J., Filip, A. and Rogulska, M. (2008). *Biofuel Projects and Activities in the EU version 2, July 2008 Biofuel Cited Reports & Recommendations [online]*. Available from: **http://www.biofuelstp.eu/downloads/biofuels_cities_project_activities_report_2.pdf** [Accessed 25 Nov 2011].

7. Jha, A. (2008). *UK announces world's largest algal biofuel project [online]*. Available from: **http://www.guardian.co.uk/environment/2008/oct/23/biofuels-energy** [Accessed 25 Nov 2011].

8. U.S. Department of Energy. Biomass Program [online]. Available from: **http://www1.eere.energy.gov/biomass/** [Accessed 25 Nov 2011].

9. Müller-Hagedorn, M., Bockhorn, H., Krebs, L., and Müller, U. (2003). A comparative kinetic study on the pyrolysis of three different wood species. *Journal of Analytical and Applied Pyrolysis*, 68-69, p.231-249.

10. Ganesh, A. and Raveendran, K. (2001). Biomass Selection Criteria for Pyrolytic Conversion Processes. IN: Bridgwater A.V. (ed) *Progress in thermochemical biomass conversion.* Oxford: Blackwell Science Ltd, 1025-1033.

11. Raveendran, K., Ganesh, A., and Khilar, K.C. (1996). Pyrolysis characteristics of biomass and biomass components. *Fuel*, 75(8), p.987-998.

12. Chakrabortty, A. (2008). *Secret report: biofuel caused food crisis [online]*. Available from: **http://www.guardian.co.uk/environment/2008/jul/03/biofules.renewableenergy** [Accessed 25 Nov 2011].

13. Holmes, S. (2008). *Bioenergy: Fuelling the food crisis? [online]*. Available from: **http://news.bbc.co.uk/1/hi/world/europe/7435439.stm** [Accessed 25 Nov 2011].

14. Case, M. (2008). *Food before fuel [online]*. Available from: **http://www.guardian.co.uk/commentisfree/2008/jul/11/biofuels.food?INTCMP=ILCNETTXT3487** [Accessed 25 Nov 2011].

15. Rice, T. (2011). *Biofuels are driving food prices higher [online]*. Available from: **http://www.guardian.co.uk/global-development/poverty-matters/2011/jun/01/biofuels-driving-food-prices-higher** [Accessed 25 Nov 2011].

16. Evans, A. (2011). *Global food crisis: Counting the real cost of biofuels [online]*. Available from: **http://www.guardian.co.uk/global-development/poverty-matters/2011/may/31/global-food-crisis-real-cost-biofuels?INTCMP=ILCNETTXT3487** [Accessed 25 Nov 2011].

17. Miao, X., Wu, Q and Yang, C. (2004). Fast pyrolysis of microalgae to produce renewable fuels. *Journal of Analytical and Applied Pyrolysis*, 71(2), p.855-863.

18. Miao, X. and Wu, Q. (2004). High yield bio-oil production from fast pyrolysis by metabolic controlling of Chlorella protothecoides. *Journal of Biotechnology*, 110(1), p.85-93.

19. Pan, P., Hu, C., Yang, W., Li, Y., Dong, L., Zhu, L., Tong, D., Qing, R. and Fan, Y. (2010). The direct pyrolysis and catalytic pyrolysis of Nannochloropsis sp. Residue for renewable bio-oils. *Bioresource Technology*, 101(12), p.4593-4599.

20. White, J.E., Catallo, W.J. and Legendre, B.L. (2011). Biomass Pyrolysis kinetics: A comparative critical review with relevant agricultural residue case studies. *Journal of Analytical and Applied Pyrolysis*, 91(1), p.1-33.

21. Koufopanos, C.A., Lucchesi, A. and Maschio, G. (1989). Kinetic modeling of the pyrolysis of biomass and biomass components. *The Canadian Journal of Chemical Engineering*, 67(1), p.75-84.

22. Orfão, J.J.M., Antunes, F.J.A., and Figueiredo, J.L. (1999). Pyrolysis kinetics of lignocellulosic materials-three independent reactions model. *Fuel*, 78(3), p.349-358.

23. Di Blasi, C., Modeling chemical and physical processes of wood and biomass pyrolysis. *Progress in Energy and Combustion Science*, 34(1), p.47-90.

24. Órfão, J.J.M. and Figueiredo, J.L. (2001). A simplified method for determination of lignocellulosic materials pyrolysis kinetics from isothermal thermogravimetric experiments. *Thermochimical Acta*, 380(1), p.67-78.

25. Antal, M.J., Jr. and Varhegyi, G. (1995). Cellulose Pyrolysis Kinetics: The Current State of Knowledge. *Industrial & Engineering Chemistry Research*, 34(3), P.703-717.

26. Reina, J., Velo, E. and Puigjaner, L. (1998). Kinetic Study of the Pyrolysis of Waste Wood. *Industrial & Engineering Chemistry Research*, 37(11), p.4290-4295.

27. Ward, S.M. and Braslaw, J. (1985). Experimental weight loss kinetics of wood pyrolysis under vacuum. *Combustion and Flame*, 61(3), p.261-269.

28. Bockhorn, H., Hornung, A. and Hornung, U. (1999). Mechanisms and kinetics of thermal decomposition of plastics from isothermal and dynamic measurements. *Journal of Analytical and Applied Pyrolysis*, 50(2), p.77-101.

29. Bockhorn, H., Hornung, A., Horning, U. and Jakobströer, P. (1999). Modelling of isothermal and dynamic pyrolysis of plastics considering non-homogeneous temperature distribution and detailed degradation mechanism. *Journal of Analytical and Applied Pyrolysis*, 49(1-2), p.53-74.

30. Bockhorn, H., Hornung, A., Hornung, U. and Schawaller, D. (1999). Kinetic study on the thermal degradation of polypropylene and polyethylene. *Journal of Analytical and Applied Pyrolysis*, 48(2), p.93-109.

31. Dahiya, J.B., Kumar, K., Muller-Hagedorn, M. and Bockhorn, H. (2008). Kinetics of isothermal and non-isothermal degradation of cellulose: model-based and model-free methods. *Polymer International*, 57(5), p.722-729.

32. Flynn, J.H., Brown, M. and Sestak, J. (1987). Report on the workshop: Current problems of kinetic data reliability evaluated by thermal analysis. *Thermochimical Acta*, 110, p.101-112.

33. Basu, P. (2010). Biomass Characterisitics. IN:*Biomass Gasification Design Handbook.* Boston: Academic press, 27-63.

34. Sims, R.E.H. (2004). *Bioenergy options for a cleaner environment: in developed and developing countries*. UK: Elsevier Ltd.

35. Balat, M. (2008). Mechanisms of Thermochemical Biomass Conversion Processes. Part1: Reactions of Pyrolysis. *Energy Sources, Part A: Recovery, Utilization, and Environmental Effects*, 30(7), p.620-635.

36. Sharypov, V.I., Marin, N., Beregovtsova, N.G., Baryshnikov, S.V., Kuznetsov, B.N, Cebolla, V.L. and Weber, J.V. (2002). Co-pyrolysis of wood biomass and synthetic polymer mixtures. Part I: influence of experimental conditions on the evolution of solids, liquids and gases. *Journal of Analytical and Applied Pyrolysis*, 64(1), p.15-28.

37. Demirbas, A. (1997). Calculation of higher heating values of biomass fuels. *Fuel*, 76(5), p.431-434.

38. Moldoveanu, S.C. (1998). *Analytical pyrolysis of natural organic polymers*. Techniques and Instrumentation in Analytical Chemistry. Vol. 20. Amsterdam: Elsevier Science B.V.

39. Cheng, J. (2010). *Biomass to Renewable Energy Processes*. US.:CRC Press.

40. Brown, R.C. (2003). *Biorenewable resources: Engineering New Products from Agriculture*. Iowa: Blackwell Publishing.

41. Clasen, C. and Kulicke, W.M. (2001). Determination of viscoelastic and rheo-optical material functions of water-soluble cellulose derivatives. *Progress in Polymer Science*, 26(9), p.1839-1919.

42. Demirbas, A. (2000). Mechanisms of liquefaction and pyrolysis reactions of biomass. *Energy Conversion and Management*, 41(6), p.633-646.

43. Yaman, S. (2004). Pyrolysis of Biomass to Produce Fuels and Chemical Feedstocks. *Energy Conversion and Mangement*, 45(5), p.651-671.

44. Faravelli, T., Frassoldati, A., Migliavacca, G. and Ranzi, E. (2010). Detailed kinetic modeling of the thermal degradation of lignins. *Biomass and Bioenergy*, 34(3), p.290-301.

45. Sharma, R.K., Wooten, J.B, Baliga, V.L., Lin, X., Geoffrey, C.W. and Hajaligol, M.R. (2004). Characterization of chars from pyrolysis of lignin. *Fuel*, 83(11-12), p.1469-1482.

46. Mitsuhashi, S., Kishimoto, T., Uraki, Y., Okamoto, T. and Ubukata, M. (2008). Low molecular weight lignin suppresses activation of NF-κB and HIV-1 promoter. *Bioorganic & Medicinal Chemistry*, 16(5), p.2645-2650.

47. Britt, P.F., Buchanan, A.C., Thomas, K.B. and Lee, S.-K. (1995). Pyrolysis mechanisms of lignin: surface-immobilized model compound investigation of acid-catalyzed and free-radical reaction pathways. *Journal of Analytical and Applied Pyrolysis*, 33, p.1-19.

48. Dorrestijn, E., Laarhoven, L.J.J., Arends, I.W.C.E. and Mulder, P. (2000). The occurrence and reactivity of phenoxyl linkages in lignin and low rank coal. *Journal of Analytical and Applied Pyrolysis*, 54(1-2), p.153-192.

49. Jiang, G., Nowakowski, D.J. and Bridgwater, A.V. (2010). A systematic study of the kinetics of lignin pyrolysis. *Thermochimica Acta*, 498(1-2), p.61-66.

50. Tomaselli, L. (2004). The Microalgal cell. IN: Richmond, A. (ed) *Handbook of Microalgal Culture: Biotechnology and Applied Phycology*. Oxford: Blackwell Science Ltd.

51. Darley, W.M. (1982). *Algal Biology: A physiological approach*. Basic Microbiology Vol.9. Oxford: Blackwell Scientific.

52. Graham, L.E., Graham, J.M. and Wilcox, L.W. (2009). *Algae*. 2nd ed. US:Pearson Benjamin Cummings.

53. Khan, S.A., Rashmi, Hussain, M.Z., Prasad, S. and Banerjee, U.C. (2009). Prospects of biodiesel production from microalgae in India. *Renewable and Sustainable Energy Reviews*, 13(9), p.2361-2372.

54. Tokuşoglu, Ö. and Üunal, M.K. (2003). Biomass Nutrient Profiles of Three Microalgae: Spirulina platensis, Chlorella vulgaris, and Isochrisis galbana. *Journal of Food Science*, 64(4), p.1144-1148.

55. Rebolloso-Fuentes, M.M., Navarro-Pérez, A., Garcia-Camacho, F., Ramos-Miras, J.J. and Guil-Guerrero, J.L. (2001). Biomass Nutrient Profiles of the Microalga Nannochloropsis. *Journal of Agricultural and Food Chemistry*, 49(6), p. 2966-2972.

56. Rebolloso-Fuentes, M.M., Navarro-Pérez, A., Ramos-Miras, J.J. and Guil-Guerrero, J.L. (2001). Biomass Nutrient Profiles of the Microalga Phaeodactylum Tricornutum. *Journal of Food Biochemistry*, 25(1), p.57-76.

57. Rebolloso Fuentes, M.M., Acién Fernández, G. G., Sánchez Pérez, J. A. and Guil Guerrero, J. L. (2000). Biomass nutrient profiles of the microalga Porphyridium cruentum. *Food Chemistry*, 70(3), p.345-353.

58. Zou, S., Wu, Y., Yang, M., Li, C. and Tong, J. (2009). Thermochemical Catalytic Liquefaction of the Marine Microalgae Dunaliella tertiolecta and Characterization of Bio-oils. *Energy & Fuels*, 23(7), p.3753-3758.

59. Pacheco-Vega, J.M. and Sánchez-Saavedra, M.D.P. (2009). The Biochemical Composition of Chaetoceros muelleri (Lemmermann Grown) with an Agricultural Fertilizer. *Journal of the World Aquaculture Society*, 40(4), p.556-560.

60. Bellinger, E.G. (1992). *A key to common algae: Freshwater estuarine and some coastal species.* London: The Institution of Water and Environmental Management.

61. Becker, E.W. (2008). *Microalgae: Biotechnology and Microbiology*. New York: Cambridge University Press.

62. Lewin, R.A. (1962). *Physiology and Biochemistry of Algae*. London: Academic Press.

63. Siddhanta, A.K., Chhatbar, M.U., Mehta, G.K., Sanandiya, N.D., Kumar, S., Oza, M.D. Prasad, K. and Meena, R. (2011). The cellulose contents of Indian seaweeds. *Journal of Applied Phycology*, 23(5), p.919-923.

64. Siddhanta, A.K., Prasad, K., Meena, R., Prasad, G., Mehta, G.K., Chhatbar, M.U., Oza, M.D., Kumar, S. and Sanandiya, N.D. (2009). Profiling of cellulose content in Indian seaweed species. *Bioresource Technology*, 100(24). P.6669-6673.

65. Wang, J. and Chen, C. (2009). Biosorbents for heavy metals removal and their future. *Biotechnology Advances*, 27(2), p.195-226.

66. Davis, T.A., Volesky, B. and Mucci, A. (2003). A review of the biochemistry of heavy metal biosorption by brown algae. *Water Research*, 37(18), p.4311-4330.

67. Turvey, J.R. and Griffiths, L.M., Mucilage from a fresh-water red alga of the genus Batrachospermum. *Phytochemistry*, 12(12), p.2901-2907.

68. Malcolm R, B. (1991). The amino-acid and sugar composition of 16 species of microalgae used in mariculture. *Journal of Experimental Marine Biology and Ecology*, 145(1), p.79-99.

69. Anastasakis, K., Ross, A.B. and Jones, J.M. (2011). Pyrolysis behaviour of the main carbohydrates of brown macro-algae. *Fuel*, 90(2), p. 598-607.

70. Zemke-White, W.L. and Clements, K.D. (1999). Chlorophyte and rhodophyte starches as factors in diet choice by marine herbivorous fish. *Journal of Experimental Marine Biology and Ecology*, 240(1), p.137-149.

71. Nichols, B.W., James, A.T. and Breuer, J. (1967). Interrelationships between fatty acid biosynthesis and acyl-lipid synthesis in Chlorella vulgaris. *The Biochemical Journal*, 104(2), p.486-496.

72. Petkov, G. and Garcia, G. (2007). Which are fatty acids of the green alga Chlorella? *Biochemical Systematics and Ecology*, 35(5), p. 281-285.

73. Converti, A., Casazza, A.A., Ortiz, E.Y., Perego, P. and Del Borghi, M. (2009). Effect of temperature and nitrogen concentration on the growth and lipid content of Nannochloropsis oculata and Chlorella vulgaris for biodiesel production. *Chemical Engineering and Processing: Process Intensification*, 48(6), p.1146-1151.

74. Yoo, C., Jun, S.-Y., Lee, J.-Y., Ahn, C.-Y. and Oh, H.-M. (2010). Selection of microalgae for lipid production under high levels carbon dioxide. *Bioresource Technology*, 101(1, Supplement), p.S71-S74.

75. Mcardle, R.N., Lasekan, J., Engel, R. and Behrens, P. (1994). Protein and Amino Acid Content of Selected Microalgae Species. *LWT - Food Science and Technology*, 27(3), p.249-252.

76. González López, C.V., Garcia, M.C.C., Fernández, F.G.A., Bustos, G.S., Chisti, Y. and Sevilla, J.M.F. (2010). Protein measurements of microalgal and cyanobacterial biomass. *Bioresource Technology*, 101(19), p.7587-7591.

77. Muller-Feuga, A., Le Guédes, R., Hervé, A. and Durand, P. (1998). Comparison of artificial light photobioreactors and other production systems using Porphyridium cruentum. *Journal of Applied Phycology*, 10(1), p.83-90.

78. Richmond, A. (2007). H*andbook of Microalgal Culture Biotechnology and Applied Phycology*. UK: Blackwell Publishing.

79. Wang, B., Li, Y., Wu, N. and Lan, C. (2008). CO_2 bio-mitigation using microalgae. *Applied Microbiology and Biotechnology*, 79(5), p.707-718.

80. Suh, I. and Lee, C.-G. (2003). Photobioreactor engineering: Design and performance. *Biotechnology and Bioprocess Engineering*, 8(6), p.313-321.

81. Moreno, J., Vargas, M.A., Rodriguez, H., Rivas, J. and Guerrero, M.G. (2003). Outdoor cultivation of a nitrogen-fixing marine cyanobacterium, Anabaena sp. ATCC 33047. *Biomolecular Engineering*, 20(4-6), p.191-197.

82. Hsieh, C.-H. and Wu, W.-T. (2009). Cultivation of microalgae for oil production with a cultivation strategy of urea limitation. *Bioresource Technology*, 100(17), p.3921-3926.

83. Stehfest, K., Toepel, J. and Wilhelm, C. (2005). The application of micro-FTIR spectroscopy to analyze nutrient stress-related changes in biomass composition of phytoplankton algae. *Plant Physiology and Biochemistry*, 43(7), p.717-726.

84. Tran, N.-P., Park, J.-K. and Lee, C.-G. (2009). Proteomics analysis of proteins in green alga Haematococcus lacustris (Chlorophyceae) expressed under combined stress of nitrogen starvation and high irradiance. *Enzyme and Microbial Technology*, 45(4), p.241-246.

85. Schenk, P., Thomas-Hall, S., Stephens, E., Marx, U., Mussgnug, J., Posten, C. Kruse, O. and Hankamer, B. (2008). Second Generation Biofuels: High-Efficiency Microalgae for Biodiesel Production. *BioEnergy Research*, 1(1), p.20-43.

86. Rodolfi, L., Chini Zittelli, G., Bassi, N., Padovani, G., Biondi, N., Bonini, G. and Tredici, M.R. (2009). Microalgae for oil: Strain selection, induction of lipid synthesis and outdoor mass cultivation in a low-cost photobioreactor. *Biotechnology and Bioengineering*, 102(1), p.100-112.

87. Ugwu, C.U., Aoyagi, H. and Uchiyama, H. (2008). Photobioreactors for mass cultivation of algae. *Bioresource Technology*, 99(10), p.4021-4028.

88. Demirbas, M.F., (2011). Biofuels from algae for sustainable development. *Applied Energy*, 88, p.3473-3480.

89. Singh, R.N. and Sharma, S. (2012). Development of suitable photobioreactor for algae production-A review. *Renewable and Sustainable Energy Reviews*, 16, p.2347-2353.

90. Benemann, J.R. (1997). CO_2 mitigation with microalgae systems. *Energy Conversion and Management*, 38(Supplement 1), p.S475-S479.

91. Brennan, L. and Owende, P. (2010). Biofuels from microalgae--A review of technologies for production, processing, and extractions of biofuels and co-products. *Renewable and Sustainable Energy Reviews*, 14(2), p.557-577.

92. Kosaric, N., Nguyen, H.T. and Bergougnoum, M.A. (1974). Growth of Spirulina maxima algae in effluents from secondary waste-water treatment plants. *Biotechnology and Bioengineering*, 16(7), p.881-896.

93. Markou, G. and Georgakakis, D. (2011). Cultivation of filamentous cyanobacteria (blue-green algae) in agro-industrial wastes and wastewaters: A review. *Applied Energy*, 88(10), p.3389-3401.

94. Gouveia, L. and Oliveira A. (2009). Microalgae as a raw material for biofuels production. *Journal of Industrial Microbiology & Biotechnology*, 36(2), p.269-274.

95. Posten, C. and Schaub, G. (2009). Microalgae and terrestrial biomass as source for fuels-A process view. *Journal of Biotechnology*, 142(1), p.64-69.

96. Dismukes, G.C., Carrieri, D., Bennette, N., Ananyev, G.M. and Posewitz, M.C. (2008). Aquatic phototrophs: efficient alternatives to land-based crops for biofuels. *Current Opinion in Biotechnology*, 19(3), p.235-240.

97. Singh, J. and Gu, S. (2010). Commercialization potential of microalgae for biofuels production. *Renewable and Sustainable Energy Reviews*, 14(9), p.2596-2610.

98. Amin, S. (2009). Review on biofuel oil and gas production processes from microalgae. *Energy Conversion and Management*, 50(7), p.1834-1840.

99. Chisti, Y. (2007). Biodiesel from microalgae. *Biotechnology Advances*, 25(3), p.294-306.

100. Fernández F.G, A., Fernández-Sevilla, J.M. and Grima, E.M. (2009). Challenges in microalgae biofuels. *New Biotechnology*, 25(Supplement 1), p.S268-S268.

101. Spolaore, P., Joannis-Cassan, C., Duran, E. and Isambert, A. (2006). Commercial applications of microalgae. *Journal of Bioscience and Bioengineering,* 101(2), p.87-96.

102. Demirbas, A. and Faith Demirbas, M. (2011). Importance of algae oil as a source of biodiesel. *Energy Conversion and Management*, 52(1), p.163-170.

103. Hirano, A., Ueda, R., Hirayama, S. and Ogushi, Y. (1997). CO2 fixation and ethanol production with microalgal photosynthesis and intracellular anaerobic fermentation. *Energy*, 22(2-3), p.137-142.

104. Vergara-Fernández, A., Vargas, G., Alarcón, N. and Velasco, A. (2008). Evaluation of marine algae as a source of biogas in a two-stage anaerobic reactor system. *Biomass and Bioenergy*, 32(4), p.338-344.

105. Ghirardi, M.L, Zhang, L., Lee, J.W., Flynn, T., Seibert, M., Greenbaum, E. and Melis, A. (2000). Microalgae: a green source of renewable H_2. *Trends in Biotechnology*, 18(12), p.506-511.

106. Hornung, A. and Apfelbacher. (2008). *Biomass Processing*. GB patent application GB0808740.5

107. Hornung, A., Apfelbacher, A. and Sagi, S. (2011). Intermediate pyrolysis: A sustainable biomass-to-energy concept - Biothermal valorisation of biomass (BtVB) process. *Journal of Scientific & Industrial Research*, 70, p.664-667.

108. Belcher, H. and Swale, E. (1976). *A beginner's guide to Freshwater Algae*. London: Her Majesty's Stationery Office.

109. Higashiyama, T. (1967). 'Gigantism' of chlorella vulgaris II. mechanism of induction of cigantism. *Plant & Cell Physiol*., 8, p. 581-593.

110. Phycology research group, Charles University in Prague. Czech Republic, (2006). *Determinační praktikum – galerie [online]*. Available from: **http://botany.natur.cuni.cz/algo/determin.html** [Accessed 25 Jun 2011].

111. Alyabyev, A.J, Loseva, N.L, Gordon, L.K., Andreyeva, I.N., Rachimova, G.G., Tribunskih, V.I., Ponomareva, A.A. and Kemp, R.B. (2007). The effect of changes in salinity on the energy yielding processes of Chlorella vulgaris and Dunaliella maritima cells. *Thermochimica Acta*, 458(1-2), p.65-70.

112. Liang, Y., Sarkany, N. and Cui, Y. (2009). Biomass and lipid productivities of Chlorella vulgaris under autotrophic, heterotrophic and mixotrophic growth conditions. *Biotechnology Letters*, 31(7), p.1043-1049.

113 Widjaja, A., Chien, C.-C. and Ju, Y.-H. (2009). Study of increasing lipid production from fresh water microalgae Chlorella vulgaris. *Journal of the Taiwan Institute of Chemical Engineers*, 40(1), p.13-20.

114. Aksu, Z. and Dönmez, G. (2006). Binary biosorption of cadmium(II) and nickel(II) onto dried Chlorella vulgaris: Co-ion effect on mono-component isotherm parameters. *Process Biochemistry*, 41(4), p.860-868.

115. Aksu, Z. (2001). Equilibrium and kinetic modelling of cadmium(II) biosorption by C. vulgaris in a batch system: effect of temperature. *Separation and Purification Technology*, 21(3), p.285-294.

116. Aksu, Z. and Açikel, Ü. (2000). Modelling of a single-staged bioseparation process for simultaneous removal of iron(III) and chromium(VI) by using Chlorella vulgaris. *Biochemical Engineering Journal*, 4(3), p.229-238.

117. Aksu, Z. (2002). Determination of the equilibrium, kinetic and thermodynamic parameters of the batch biosorption of nickel(II) ions onto Chlorella vulgaris. *Process Biochemistry*, 38(1), p.89-99.

118. Ferreira, L.S., Rodrigues, M.S., De Carvalho, J.C.M., Lodi, A., Finocchio, E., Perego, P. and Converti, A. (2011). Adsorption of Ni^{2+}, Zn^{2+} and Pb^{2+} onto dry biomass of Arthrospira (Spirulina) platensis and Chlorella vulgaris. I. Single metal systems. *Chemical Engineering Journal,* 173(2), p.326-333.

119. Gokhale, S.V., Jyoti, K.K. and Lele, S.S. (2008). Kinetic and equilibrium modeling of chromium (VI) biosorption on fresh and spent Spirulina platensis/Chlorella vulgaris biomass. *Bioresource Technology*, 99(9), p.3600-3608.

120. Wong, J.P.K., Wong, Y.S. and Tam, N.F.Y. (2000). Nickel biosorption by two chlorella species, C. Vulgaris (a commercial species) and C. Miniata (a local isolate). *Bioresource Technology*, 73(2), p.133-137.

121. Çetinkaya Dönmez, G., Aksu, Z., Öztürk, A. and Kutsal, T. (1999). A comparative study on heavy metal biosorption characteristics of some algae. *Process Biochemistry*, 34(9), p.885-892.

122. Lau, P.S., Tam, N.F.Y. and Wong, Y.S. (1998). Operational optimization of batchwise nutrient removal from wastewater by Carrageenan immobilized Chlorella vulgaris. *Water Science and Technology*, 38(1), p.185-192.

123. González, L.E., Cañizares, R.O. and Baena, S. (1997). Efficiency of ammonia and phosphorus removal from a colombian agroindustrial wastewater by the microalgae Chlorella vulgaris and Scenedesmus dimorphus. *Bioresource Technology*, 60(3), p.259-262.

124. Kim, J., Lingaraju, B.P., Rheaume, R., Lee, J.-Y. and Siddiqui, K.F. (2010). Removal of Ammonia from Wastewater Effluent by Chlorella Vulgaris. *Tsinghua Science & Technology*, 15(4), p.391-396.

125. Bich, N.N., Yaziz, M.I. and Bakti, N.A.K. (1999). Combination of Chlorella vulgaris and Eichhornia crassipes for wastewater nitrogen removal. *Water Research*, 33(10), p.2357-2362.

126. Lim, S.-L., Chu, W.-L. and Phang, S.-M. (2010). Use of Chlorella vulgaris for bioremediation of textile wastewater. *Bioresource Technology*, 101(19), p.7314-7322.

127. Aksu, Z. and Tezer, S. (2005). Biosorption of reactive dyes on the green alga Chlorella vulgaris. *Process Biochemistry*, 40(3-4), p.1347-1361.

128. McEvoy, E., Wright, P.C. and Bustard, M.T. (2004). The effect of high concentration isopropanol on the growth of a solvent-tolerant strain of Chlorella vulgaris. *Enzyme and Microbial Technology*, 35(2-3), p.140-146.

129. Rai, L.C., Rai, P.K. and Mallick, N. (1996). Regulation of heavy metal toxicity in acid-tolerant Chlorella: Physiological and biochemical approaches. *Environmental and Experimental Botany*, 36(1), p.99-109.

130. Bhola, V., Desikan, R., Santosh, S.K., Subburamu, K. Sanniyasi, E. and Bux, F. (2011). Effects of parameters affecting biomass yield and thermal behaviour of Chlorella vulgaris. *Journal of Bioscience and Bioengineering*, 111(3), p.377-382.

131. Bridgwater, A.V. (2003) Renewable fuels and chemicals by thermal processing of biomass. *Chemical Engineering Journal*, 91(2-3), p.87-102.

132. Bridgwater, A.V., Meier, D. and Radlein, D. (1999). An overview of fast pyrolysis of biomass. *Organic Geochemistry*, 30(12), p.1479-1493.

133. Van de Velden, M., Baeyens, J., Brems, A., Janssens, B. and Dewil, R. (2010). Fundamentals, kinetics and endothermicity of the biomass pyrolysis reaction. *Renewable Energy*, 35(1), p.232-242.

134. Hornung, A. and Apfelbacher, A. (2008). *Thermal treatment of biomass*. GB patent application GB 0808739.7

135. Hornung, A., Apfelbacher, A. and Sagi, S. (2009). High Integrative, CO_2 Negative, high Efficient Power generation (ICONE POWER) from ash rich biomass coupled with production of algae based bio oils as well as biochar at Hainhaus/Odenwald (BtVB). IN: *17th European Biomass Conference and Exhibition*. 2009. Hamburg, Germany.

136. Di Blasi, C. (1998) mparison of semi-global mechanisms for primary pyrolysis of lignocellulosic fuels. *Journal of Analytical and Applied Pyrolysis*, 47(1), p.43-64.

137. Dupont, C., Chen, L., Cances, J., Commandre, J.-M., Cuoci, A., Pierucci, S. and Ranzi, E. (2009). Biomass pyrolysis: Kinetic modelling and experimental validation under high temperature and flash heating rate conditions. *Journal of Analytical and Applied Pyrolysis*, 85(1-2), p.260-267.

138. Thurner, F. and Mann, U. (1981). Kinetic investigation of wood pyrolysis. *Industrial & Engineering Chemistry Process Design and Development*, 20(3), p.482-488.

139. Williams, P.T. and Besler, S. (1994). Thermogravimetric analysis of the components of biomass. IN: Bridgwater, A.V. (ed). *Advances in Thermochemical Biomass Conversion*. London: Chapman & Hall, 771-783.

140. Hosoya, T., Kawamoto, H. and Saka, S. (2007). Cellulose–hemicellulose and cellulose–lignin interactions in wood pyrolysis at gasification temperature. *Journal of Analytical and Applied Pyrolysis*, 80(1), p.118-125.

141. Morf, P., Hasler, P. and Nussbaumer, T. (2002). Mechanisms and kinetics of homogeneous secondary reactions of tar from continuous pyrolysis of wood chips. *Fuel*, 81(7), p.843-853.

142. Gilbert, P., Ryu, C., Sharifi, V. and Swithenbank, J. (2009). Tar reduction in pyrolysis vapours from biomass over a hot char bed. *Bioresource Technology*, 100(23), p.6045-6051.

143. Zaror, C.A, Hutchings, I.S., Pyle, D.L., Stiles, H.N. and Kandiyoti, R. (1985). Secondary char formation in the catalytic pyrolysis of biomass. *Fuel*, 64(7), p.990-994.

144. Boroson, M.L., Howard, J.B., Longwell, J.P. and Peters, W.A. (1989). Product yields and kinetics from the vapor phase cracking of wood pyrolysis tars. *AIChE Journal*, 35(1), p.120-128.

145. Neves, D., Thunman, H., Matos, A., Tarelho, L. and Gómez-Barea, A. (2011). Characterization and prediction of biomass pyrolysis products. *Progress in Energy and Combustion Science*, 37(5), p.611-630.

146. Bradbury, A.G.W., Sakai, Y. and Shafizadeh, F. (1979). A kinetic model for pyrolysis of cellulose. *Journal of Applied Polymer Science*, 23(11), p.3271-3280.

147. Mamleev, V., Bourbigot, S. and Yvon, J. (2007). Kinetic analysis of the thermal decomposition of cellulose: The change of the rate limitation. *Journal of Analytical and Applied Pyrolysis*, 80(1), p.141-150.

148. Agrawal, R.K. (1988). Kinetics of reactions involved in pvrolvsis of cellulose II. The modified kilzer-bioid model. *The Canadian Journal of Chemical Engineering*, 66(3), p.413-418.

149. Banyasz, J.L., Li, S., Lyons-Hart, J.L. and Shafer, K.H. (2001). Cellulose pyrolysis: the kinetics of hydroxyacetaldehyde evolution. *Journal of Analytical and Applied Pyrolysis*, 57(2), p.223-248.

150. Geoffrey N, R. (1987). Glycolaldehyde from pyrolysis of cellulose. *Journal of Analytical and Applied Pyrolysis*, 10(3), p.251-255.

151. Piskorz, J., Radlein, D. and Scott, D.S. (1986). On the mechanism of the rapid pyrolysis of cellulose. *Journal of Analytical and Applied Pyrolysis*, 9(2), p.121-137.

152. Banyasz, J.L., Li, S., Lyons-Hart, J. and Shafer, K.H. (2001). Gas evolution and the mechanism of cellulose pyrolysis. *Fuel*, 80(12), p.1757-1763.

153. Šimkovic, I., Varhegyi, G., Antal, M.J., Ebringerová, A., Szekely, T. and Szabo, P. (1988). Thermogravimetric/mass spectrometric characterization of the thermal decomposition of (4-O-methyl-D-glucurono)-D-xylan. *Journal of Applied Polymer Science*, 36(3), p.721-728.

154. Varhegyi, G., Antal, M.J., Szekely, T. and Szabo, P. (1989). Kinetics of the thermal decomposition of cellulose, hemicellulose, and sugarcane bagasse. *Energy & Fuels*, 3(3), p.329-335.

155. Di Blasi, C. and Lanzetta, M. (1997). Intrinsic kinetics of isothermal xylan degradation in inert atmosphere. *Journal of Analytical and Applied Pyrolysis*, 40-41(0), p.287-303.

156. Shen, D.K., Gu, S. and Bridgwater, A.V. (2010). Study on the pyrolytic behaviour of xylan-based hemicellulose using TG–FTIR and Py–GC–FTIR. *Journal of Analytical and Applied Pyrolysis*, 87(2), p.199-206.

157. Jegers, H.E. and Klein, M.T. (1985). Primary and secondary lignin pyrolysis reaction pathways. *Industrial & Engineering Chemistry Process Design and Development*, 24(1), p.173-183.

158. Hosoya, T., Kawamoto, H. and Saka, S. (2008). Secondary reactions of lignin-derived primary tar components. *Journal of Analytical and Applied Pyrolysis*, 83(1), p.78-87.

159. Nunn, T.R., Howard, J.B., Longwell, J.P. and Peters, W.A. (1985). Product compositions and kinetics in the rapid pyrolysis of sweet gum hardwood. *Industrial & Engineering Chemistry Process Design and Development*, 24(3), p.836-844.

160. Williams, P.T. and Besler, S. (1996). The influence of temperature and heating rate on the slow pyrolysis of biomass. *Renewable Energy*, 7(3), p.233-250.

161. González, J.F., Encinar, J.M., Canito, J.L., Sabio, E. and Chacón, M. (2003). Pyrolysis of cherry stones: energy uses of the different fractions and kinetic study. *Journal of Analytical and Applied Pyrolysis*, 67(1), p.165-190.

162. Ingram, L., Mohan, D., Bricka, M., Steele, P., Strobel, D., Crocker, D., Mitchell, B., Mohammad, J., Cantrell, K. and Pittman, C.U. (2007). Pyrolysis of Wood and Bark in an Auger Reactor: Physical Properties and Chemical Analysis of the Produced Bio-oils. *Energy & Fuels*, 22(1), p.614-625.

163. Czernik, S. and Bridgwater, A.V. (2004). Overview of Applications of Biomass Fast Pyrolysis Oil. *Energy & Fuels*, 18(2), p.590-598.

164. Barth, T. and Kleinert, M. (2008). Motor Fuels From Biomass Pyrolysis. *Chemical Engineering & Technology*, 31(5), p.773-781.

165. Mohan, D., Pittman, C.U. and Steele, P.H. (2006). Pyrolysis of Wood/Biomass for Bio-oil: A Critical Review. *Energy & Fuels*, 20(3), p.848-889.

166. Oasmaa, A. and Czernik, S. (1999). Fuel Oil Quality of Biomass Pyrolysis OilsState of the Art for the End Users. *Energy & Fuels*, 13(4), p.914-921.

167. Beis, S.H., Onay, Ö. and Koçkar, Ö.M. (2002). Fixed-bed pyrolysis of safflower seed: influence of pyrolysis parameters on product yields and compositions. *Renewable Energy*, 26(1), p.21-32.

168. Sensöz, S. and Kaynar, I. (2006). Bio-oil production from soybean (Glycine max L.); fuel properties of Bio-oil. *Industrial Crops and Products*, 23(1), p.99-105.

169. Bridgwater, A.V. (1999). Principles and practice of biomass fast pyrolysis processes for liquids. *Journal of Analytical and Applied Pyrolysis*, 51(1-2), p.3-22.

170. Zhang, Q., Chang, J., Wang, T. and Xu, Y. (2007). Review of biomass pyrolysis oil properties and upgrading research. *Energy Conversion and Management*, 48(1), p.87-92.

171. Demirbas, A. (2004). Effects of temperature and particle size on bio-char yield from pyrolysis of agricultural residues. *Journal of Analytical and Applied Pyrolysis*, 72(2), p.243-248.

172. Omar, S., Girgis, B. and Taha, F. (2003). Carbonaceous materials from seed hulls for bleaching of vegetable oils. *Food Research International*, 36(1), p.11-17.

173. Mohan, D., Pittman Jr., C.U., Bricka, M., Smith, F., Yancey, B. Mohammad, J. Steele, P.H., Alexandre-Franco, M.F., Gómez-Serrano, V. and Gong, H. (2007). Sorption of arsenic, cadmium, and lead by chars produced from fast pyrolysis of wood and bark during bio-oil production. *Journal of Colloid and Interface Science*, 310(1), p.57-73.

174. Tennant, M.F. and Mazyck, D.W. (2003). Steam-pyrolysis activation of wood char for superior odorant removal. *Carbon*, 41(12), p.2195-2202.

175. Demirbas, A. (2006). Production and Characterization of Bio-Chars from Biomass via Pyrolysis. *Energy Sources, Part A: Recovery, Utilization, and Environmental Effects*, 28(5), p.413-422.

176. Boateng, A.A., Cooke, P.H. and Hicks, K.B. (2007). Microstructure development of chars derived from high-temperature pyrolysis of barley (Hordeum vulgare L.) hulls. *Fuel*, 86(5-6), p.735-742.

177. Garcia, A.N., Font, R. and Marcilla, A. (1995). Gas Production by Pyrolysis of Municipal Solid Waste at High Temperature in a Fluidized Bed Reactor. *Energy & Fuels*, 9(4), p.648-658.

178. Pillng, M.J. and Seakins, P.W. (2007). *Reaction Kinetics*. New York: Oxford University Press Inc.

179. Metiu, H. (2006). *Physical Chemistry: Kinetics*. UK: Taylor & Francis Group.

180. Burnham, A.K. and Braun, R.L. (1999). Global Kinetic Analysis of Complex Materials. *Energy & Fuels*, 13(1), p.1-22.

181. Vyazovkin, S. and Wight, C.A. (1998). Isothermal and non-isothermal kinetics of thermally stimulated reactions of solids. *International Reviews in Physical Chemistry*, 17(3), p.407-433.

182. Branca, C. and Di Blasi, C. (2003). Kinetics of the isothermal degradation of wood in the temperature range 528–708 K. *Journal of Analytical and Applied Pyrolysis*, 67(2), p.207-219.

183. Hornung, U., Hornung, A. and Bockhorn, H. (1998). Investigation of Thermal Degradation of Solids in an Isothermal, Gradient Free Reactor. *Chemical Engineering & Technology*, 21(4), p.332-337.

184. Bahng, M.-K., Mukarakate, C., Robichaud, D.J. and Nimlos, M.R. (2009). Current technologies for analysis of biomass thermochemical processing: A review. *Analytica Chimica Acta*, 651(2), p.117-138.

185. Freeman, E.S. and Carroll, B. (1958). The Application of Thermoanalytical Techniques to Reaction Kinetics: The Thermogravimetric Evaluation of the Kinetics of the Decomposition of Calcium Oxalate Monohydrate. *The Journal of Physical Chemistry*, 62(4), p.394-397.

186. Coats, A.W. and Redfern, J.P. (1964). Kinetic Parameters from Thermogravimetric data. *Nature*, 201(4914), p.68-69.

187. Friedman, H.L. (1964). Kinetics of thermal degradation of char-forming plastics from thermogravimetry. Application to phenolic plastic. *Journal of Polymer Science*, 6C, p.183-195.

188. Conesa, J.A., Marcilla, A., Caballero, J.A. and Font, R. (2001). Comments on the validity and utility of the different methods for kinetic analysis of thermogravimetric data. *Journal of Analytical and Applied Pyrolysis*, 58-59, p.617-633.

189. Höhne, G.W.H., Hemminger, W.F. and Flammersheim, H.-J. (2003). *Differential scanning calorimetry*. Germany: Springer-Verlag Berlin Heidelberg.

190. Devasia, R., Nair, C.P.R., Sivadasan, P., Katherine, B.K and Ninan, K.N. (2003). Cyclization reaction in poly(acrylonitrile/itaconic acid) copolymer: An isothermal differential scanning calorimetry kinetic study. *Journal of Applied Polymer Science*, 88(4), p.915-920.

191. Toda, A., Oda, T., Hikosaka, M. and Saruyama, Y. (1997). A new method of analysing transformation kinetics with temperature modulated differential scanning calorimetry: application to polymer crystal growth. *Polymer*, 38(1), p.231-233.

192. Sbirrazzuoli, N., Girault, Y. and Elégant, L. (1997). Simulations for evaluation of kinetic methods in differential scanning calorimetry. Part 3 — Peak maximum evolution methods and isoconversional methods. *Thermochimica Acta*, 293(1-2), p.25-37.

193. Materazzi, S., Gentili, A. and Curini, R. (2006). Applications of evolved gas analysis: Part 2: EGA by mass spectrometry. *Talanta*, 69(4), p.781-794.

194. Materazzi, S. and Curini, R. (2001). The coupling of mass spectrometry with thermoanalytical instruments: Applications of evolved gas analysis. *Applied spectroscopy Reviews*, 36(2-3), p. 169-180.

195. Materazzi, S. and Curini, R. (2001). On-line evolved gas analysis by infrared spectroscopy coupled to thermoanalytical instruments. *Applied Spectroscopy Reviews*, 36(1), p.1-9.

196. Materazzi, S., Gentili, A. and Curini, R. (2006). Applications of evolved gas analysis: Part 1: EGA by infrared spectroscopy. *Talanta*, 68(3), p.489-496.

197. Tao, L., Zhao, G.B., Qian, J. and Qin, Y.K. (2010). TG-FTIR characterization of pyrolysis of waste mixtures of paint and tar slag. *Journal of Hazardous Materials*, 175(1-3), p.754-761.

198. Yang, H., Yan, R., Chen, H., Lee, D.H. and Zheng, C. (2007). Characteristics of hemicellulose, cellulose and lignin pyrolysis. *Fuel*, 86(12-13), p.1781-1788.

199. Khelfa, A., Finqueneisel, G., Auber, M. and Weber, J. (2008). Influence of some minerals on the cellulose thermal degradation mechanisms. *Journal of Thermal Analysis and Calorimetry*, 92(3), p.795-799.

200. Huang, Y.F., Kuan, W.H., Chiueh, P.T. and Lo, S.L. (2011). Pyrolysis of biomass by thermal analysis-mass spectrometry (TA-MS). *Bioresource Technology*, 102(3), p.3527-3534.

201. Ischia, M., Perazzolli, C., Dal Maschio, R. and Campostrini, R. (2007). Pyrolysis study of sewage sludge by TG-MS and TG-GC-MS coupled analyses. *Journal of Thermal Analysis and Calorimetry*, 87(2), p.567-574.

202. Azeez, A.M., Meier, D., Odermatt, J. and Willner, T. (2010). Fast Pyrolysis of African and European Lignocellulosic Biomasses Using Py-GC/MS and Fluidized Bed Reactor. *Energy & Fuels*, 24(3), p.2078-2085.

203. Radmanesh, R., Courbariaux, Y., Chaouki, J. and Guy, C. (2006). A unified lumped approach in kinetic modeling of biomass pyrolysis. *Fuel*, 85(9), p.1211-1220.

204. Tsamba, A.J., Yang, W., Blasiak, W. and Wójtowicz, M. A. (2007). Cashew Nut Shells Pyrolysis: Individual Gas Evolution Rates and Yields. *Energy & Fuels*, 21(4), p.2357-2362.

205. De Jong, W., Pirone, A. and Wójtowicz, M.A. (2003). Pyrolysis of Miscanthus Giganteus and wood pellets: TG-FTIR analysis and reaction kinetics. *Fuel*, 82(9), p.1139-1147.

206. Holstein, A., Bassilakis, R., Wójtowicz, M.A. and Serio, M.A. (2005). Kinetics of methane and tar evolution during coal pyrolysis. *Proceedings of the Combustion Institute*, 30(2), p.2177-2185.

207. Bassilakis, R., Carangelo, R.M. and Wójtowicz, M.A. (2001). TG-FTIR analysis of biomass pyrolysis. *Fuel*, 80(12), p.1765-1786.

208. Müller-Hagedorn, M., Bockhorn, H., Krebs, L. and Müller, U. (2003). A comparative kinetic study on the pyrolysis of three different wood species. *Journal of Analytical and Applied Pyrolysis*, 68-69, p.231-249.

209. Rostami, A.A., Hajaligol, M.R. and Wrenn, S.E. (2004). A biomass pyrolysis sub-model for CFD applications. *Fuel*, 83(11-12), p.1519-1525.

210. Várhegyi, G., Szabó, P. and Antal, M.J. (2002). Kinetics of Charcoal Devolatilization. *Energy & Fuels*, 16(3), p.724-731.

211. Mühlen, H.J. and Sowa, F. (1995). Factors influencing the ignition of coal particles studies with a pressurized heated-grid apparatus. *Fuel*, 74(11), p.1551-1554.

212. Di Nola, G., de Jong, W. and Spliethoff, H. (2009). The fate of main gaseous and nitrogen species during fast heating rate devolatilization of coal and secondary fuels using a heated wire mesh reactor. *Fuel Processing Technology*, 90(3), p.388-395.

213. Stubington, J.F. and Aiman, S. (1994). Pyrolysis kinetics of bagasse at high heating rates. *Energy & Fuels*, 8(1), p.194-203.

214. Prins, M.J., Lindén, J., Li, Z. S.,Bastiaans, R. J. M., van Oijen, J. A., Aldén, M. and De Goey, L. P. H. (2009). Visualization of Biomass Pyrolysis and Temperature Imaging in a Heated-Grid Reactor. *Energy & Fuels*, 23(2), p.993-1006.

215. Prins, M. J., Li, Z. S., Bastiaans, R. J. M., van Oijen, J. A., Aldén, M. and De Goey, L. P. H. (2011). Biomass pyrolysis in a heated-grid reactor: Visualization of carbon monoxide and formaldehyde using Laser-Induced Fluorescence. *Journal of Analytical and Applied Pyrolysis*, 92(2), p.280-286.

216. Man, C.K., Gibbins, J.R., Witkamp, J.G. and Zhang, J. (2005). Coal characterisation for NOx prediction in air-staged combustion of pulverised coals. *Fuel*, 84(17), p.2190-2195.

217. Zhang, Y., Kajitani, S., Ashizawa, M. and Oki, Y. (2010). Tar destruction and coke formation during rapid pyrolysis and gasification of biomass in a drop-tube furnace. *Fuel*, 89(2), p.302-309.

218. Zhang, Y., Kajitani, S., Ashizawa, M. and Miura, K. (2006). Peculiarities of Rapid Pyrolysis of Biomass Covering Medium- and High-Temperature Ranges. *Energy & Fuels*, 20(6), p.2705-2712.

219. Luan, J., Sun, R., Wu, S., Lu, J. and Yao, N. (2009). Experimental Studies on Reburning of Biomasses for Reducing NOx in a Drop Tube Furnace. *Energy & Fuels*, 23(3), p.1412-1421.

220. Kajitani, S., Hara, S. and Matsuda, H. (2002). Gasification rate analysis of coal char with a pressurized drop tube furnace. *Fuel*, 81(5), p.539-546.

221. Biagini, E., Cioni, M. and Tognotti, L. (2005). Development and characterization of a lab-scale entrained flow reactor for testing biomass fuels. *Fuel*, 84(12-13), p.1524-1534.

222. Yasunaga, K., Gillespie, F., Simmie, J.M., Curran, H.J., Kuraguchi, Y., Hoshikawa, H., Yamane, M. and Hidaka, Y. (2010). A Multiple Shock Tube and Chemical Kinetic Modeling Study of Diethyl Ether Pyrolysis and Oxidation. *The Journal of Physical Chemistry A*, 114(34), p.9098-9109.

223. Bhaskaran, K.A. and Roth, P. (2002). The shock tube as wave reactor for kinetic studies and material systems. *Progress in Energy and Combustion Science*, 28(2), p.151-192.

224. Saleh, H.E. (2011). The preparation and shock tube investigation of comparative ignition delays using blends of diesel fuel with bio-diesel of cottonseed oil. *Fuel*, 90(1), p.421-429.

225. Ngo, T.-A., Kim, J. and Kim, S.-S. (2011). Fast pyrolysis of palm kernel cake in a closed-tubular reactor: Product compositions and kinetic model. *Bioresource Technology*, 102(5), p.4273-4276.

226. Mani, T., Mahinpey, N. and Murugan, P. (2011). Reaction kinetics and mass transfer studies of biomass char gasification with CO2. *Chemical Engineering Science*, 66(1), p.36-41.

227. Minami, E. and Saka, S. (2006). Kinetics of hydrolysis and methyl esterification for biodiesel production in two-step supercritical methanol process. *Fuel*, 85(17-18), p.2479-2483.

228. Schmieder, H., Abeln, J., Boukis, N., Dinjus, E., Kruse, A., Kluth, M., Petrich, G., Sadri, E. and Schacht, M. (2000). Hydrothermal gasification of biomass and organic wastes. *The Journal of Supercritical Fluids*, 17(2), p.145-153.

229. Stuhler, S. and Wyman, C. (2003). Estimation of temperature transients for biomass pretreatment in tubular batch reactors and impact on xylan hydrolysis kinetics. *Applied Biochemistry and Biotechnology*, 105(1), p.101-114.

230. Kruse, A., Maniam, P. and Spieler, F. (2006). Influence of Proteins on the Hydrothermal Gasification and Liquefaction of Biomass. 2. Model Compounds. *Industrial & Engineering Chemistry Research*, 46(1), p.87-96.

231. Hansson, K.-M., Samuelsson, J., Tullin, C. and Amand, L.-E. (2004). Formation of HNCO, HCN, and NH_3 from the pyrolysis of bark and nitrogen-containing model compounds. *Combustion and Flame*, 137(3), p.265-277.

232. Shuangning, X., Weiming, Y. and Li, B. (2005). Flash pyrolysis of agricultural residues using a plasma heated laminar entrained flow reactor. *Biomass and Bioenergy*, 29(2), p.135-141.

233. Brown, A.L., Dayton, D.C., Nimlos, M.R. and Daily, J.W. (2001). Design and Characterization of an Entrained Flow Reactor for the Study of Biomass Pyrolysis Chemistry at High Heating Rates. *Energy & Fuels*, 15(5), p.1276-1285.

234. Jarvis, M.W., Haas, T.J., Donohoe, B.S., Dailay, J.W., Gaston, K.R., Frederick, W.J. and Nimlos, M.R. (2010). Elucidation of Biomass Pyrolysis Products Using a Laminar Entrained Flow Reactor and Char Particle Imaging. *Energy & Fuels*, 25(1), p.324-336.

235. Huang, H. and Tang, L. (2007). Treatment of organic waste using thermal plasma pyrolysis technology. *Energy Conversion and Management*, 48(4), p.1331-1337.

236. Fincke, J.R., Anderson, R.P., Hyde, T.A. and Detering, B.A (2002). Plasma Pyrolysis of Methane to Hydrogen and Carbon Black. *Industrial & Engineering Chemistry Research*, 41(6), p.1425-1435.

237. Koufopanos, C.A., Papayannakos, N., Maschio, G. and Lucchesi, A. (1991). Modelling of the pyrolysis of biomass particles. Studies on kinetics, thermal and heat transfer effects. *The Canadian Journal of Chemical Engineering*, 69(4), p.907-915.

238. Larfeldt, J., Leckner, B. and Melaaen, M.C. (2000). Modelling and measurements of the pyrolysis of large wood particles. *Fuel*, 79(13), p.1637-1643.

239. Hagge, M.J. and Bryden, K.M. (2002). Modeling the impact of shrinkage on the pyrolysis of dry biomass. *Chemical Engineering Science*, 57(14), p.2811-2823.

240. Benkoussas, B., Consalvi, J.L., Porterie, B., Sardoy, N. and Loraud, J.C. (2007). Modelling thermal degradation of woody fuel particles. *International Journal of Thermal Sciences*, 46(4), p.319-327.

241. Babu, B.V. and Chaurasia, A.S. (2004). Pyrolysis of biomass: improved models for simultaneous kinetics and transport of heat, mass and momentum. *Energy Conversion and Management*, 45(9-10), p.1297-1327.

242. Janse, A.M.C., Westerhout, R.W.J. and Prins, W. (2000). Modelling of flash pyrolysis of a single wood particle. *Chemical Engineering and Processing: Process Intensification*, 39(3), p.239-252.

243. Biagini, E., Fantei, A. and Tognotti, L. (2008). Effect of the heating rate on the devolatilization of biomass residues. *Thermochimica Acta*, 472(1-2), p.55-63.

244. Haykiri-Acma, H., Yaman, S. and Kucukbayrak, S. (2006). Effect of heating rate on the pyrolysis yields of rapeseed. *Renewable Energy*, 31(6), p.803-810.

245. Jalan, R.K. and Srivastava, V.K. (1999). Studies on pyrolysis of a single biomass cylindrical pellet—kinetic and heat transfer effects. *Energy Conversion and Management*, 40(5), p.467-494.

246. Luo, S., Xiao, B., Hu, Z. and Liu, S. (2010). Effect of particle size on pyrolysis of single-component municipal solid waste in fixed bed reactor. *International Journal of Hydrogen Energy*, 35(1), p.93-97.

247. Papadikis, K., Gu, S. and Bridgwater, A.V. (2010). Computational modelling of the impact of particle size to the heat transfer coefficient between biomass particles and a fluidised bed. *Fuel Processing Technology*, 91(1), p.68-79.

248. Raveendran, K., Ganesh, A. and Khilar, K.C. (1995). Influence of mineral matter on biomass pyrolysis characteristics. *Fuel*, 74(12), p.1812-1822.

249. Fahmi, R., Bridgwater, A.V., Bridgwater, Donnison, I., Yates, N. and Jones, J.M. (2008). The effect of alkali metals on combustion and pyrolysis of Lolium and Festuca grasses, switchgrass and willow. *Fuel*, 86(10-11), p.1560-1569.

250. Yang, H., Yan, R., Chen, H., Zheng, C., Lee, D.H. and Liang, D.T. (2006). Influence of mineral matter on pyrolysis of palm oil wastes. *Combustion and Flame*, 146(4), p.605-611.

251. Doğan, G.(2003). Effect of Catalyst on Yield of Liquid Products from Biomass via Pyrolysis. *Energy Sources*, 25(8), p.753-765.

252. Ayhan, D. (2002). Gaseous products from biomass by pyrolysis and gasification: effects of catalyst on hydrogen yield. *Energy Conversion and Management*, 43(7), p.897-909.

253. Blasi, C.D., Branca, C. and D'Errico, G. (2000). Degradation characteristics of straw and washed straw. *Thermochimica Acta*, 364(1-2), p.133-142.

254. Galway, A.K. and Brown, M.E. (1997). Arrhenius parameters and compensation behaviour in solid-state decomposition. *Thermochimica Acta*, 300, p.107-115.

255. Marcilla, A., Gomez, A., Menargues, S. and Garcia-Quesada, J.C. (2007). New Approach To Elucidate Compensation Effect between Kinetic Parameters in Thermogravimetric Data. *Industrial & Engineering Chemistry Research*, 46(13), p.4382-4389.

256. Flynn, J.H. (1990). Temperature dependence of the rate of reaction in thermal analysis. *Journal of Thermal Analysis and Calorimetry*, 36(4), p. 1579-1593.

257. Agrawal, R.K. (1992). Analysis of non-isothermal reaction kinetics. Part 1. Simple reactions. *Thermochimica Acta*, 203(C), P.93-110.

258. Narayan, R. and Antal, M.J. (1996). Thermal Lag, Fusion, and the Compensation Effect during Biomass Pyrolysis. *Industrial & Engineering Chemistry Research*, 35(5), p.1711-1721.

259. Wang, S., Jiang, X.M., Wang, N., Yu, L.J., Li, Z. and He, P.M. (2007). Research on Pyrolysis Characteristics of Seaweed. *Energy & Fuels*, 21(6), p.3723-3729.

260. Várhegyi, G., Bobály, B., Jakab, E. and Chen, H. (2010). Thermogravimetric Study of Biomass Pyrolysis Kinetics. A Distributed Activation Energy Model with Prediction Tests. *Energy & Fuels*, 25(1), p.24-32.

261. De Jong, W., Di Nola, G, Venneker, B.C.H., Spliethoff, H. and Wójtowicz, M. A. (2007). TG-FTIR pyrolysis of coal and secondary biomass fuels: Determination of pyrolysis kinetic parameters for main species and NO_x precursors. *Fuel*, 86(15), p.2367-2376.

262. Açıkalın, K. (2011) Thermogravimetric analysis of walnut shell as pyrolysis feedstock. *Journal of Thermal Analysis and Calorimetry*, 105(1), p.145-150.

263. Antal, M.J. and Várhegyi, G. (1997) Impact of Systematic Errors on the Determination of Cellulose Pyrolysis Kinetics. *Energy & Fuels*, 11(6), p.1309-1310.

264. Antal, M.J., Várhegyi, G. and Jakab, E. (1998) Cellulose Pyrolysis Kinetics: Revisited. *Industrial & Engineering Chemistry Research*, 37(4), p.1267-1275.

265. Grønli, M., Antal, M.J. and Várhegyi, G. (1999). A Round-Robin Study of Cellulose Pyrolysis Kinetics by Thermogravimetry. *Industrial & Engineering Chemistry Research*, 38(6), p.2238-2244.

266. Zhang, X., Li, J., Yang, W. and Blasiak, W. (2011). Formation Mechanism of Levoglucosan and Formaldehyde during Cellulose Pyrolysis. *Energy & Fuels*, 25(8), p.3739-3746.

267. Patwardhan, P.R., Dalluge, D.L., Shanks, B.H. and Brown, R.C. (2011). Distinguishing primary and secondary reactions of cellulose pyrolysis. *Bioresource Technology*, 102(8), p.5265-5269.

268. Cabrales, L. and Abidi, N. (2010). On the thermal degradation of cellulose in cotton fibers. *Journal of Thermal Analysis and Calorimetry*, 102(2), p.485-491.

269. Shen, D.K. and Gu, S. (2009). The mechanism for thermal decomposition of cellulose and its main products. *Bioresource Technology*, 100(24), p.6496-6504.

270. Lin, Y.-C, Cho, J., Tompsett, G.A., Westmoreland, P.R. and Huber, G.W. (2009). Kinetics and Mechanism of Cellulose Pyrolysis. *The Journal of Physical Chemistry C*, 113(46), p.20097-20107.

271. Mamleev, V., Bourbigot, S. and Yvon, J. (2007). Kinetic analysis of the thermal decomposition of cellulose: The main step of mass loss. *Journal of Analytical and Applied Pyrolysis*, 80(1), p.151-165.

272. Luo, Wang, Liao and Cen (2004). Mechanism Study of Cellulose Rapid Pyrolysis. *Industrial & Engineering Chemistry Research*, 43(18), p.5605-5610.

273. Capart, R., Khezami, L. and Burnham, A.K. (2004). Assessment of various kinetic models for the pyrolysis of a microgranular cellulose. *Thermochimica Acta*, 417(1), p.79-89.

274. Li, S., Lyon-Hart, J., Banyasz, J. and Shafer, K. (2001). Real-time evolved gas analysis by FTIR method: an experimental study of cellulose pyrolysis. *Fuel*, 80(12), p.1809-1817.

275. Alves, S.S. and Figueiredo, J.L. (1989). Kinetics of cellulose pyrolysis modelled by three consecutive first-order reactions. *Journal of Analytical and Applied Pyrolysis*, 17(1), p.37-46.

276. Milosavljevic, I. and Suuberg, E.M. (1995). Cellulose Thermal Decomposition Kinetics: Global Mass Loss Kinetics. *Industrial & Engineering Chemistry Research*, 34(4), p.1081-1091.

277. Suuberg, E.M., Milosavljevic, I. and Oja, V. (1996). Two-regime global kinetics of cellulose pyrolysis: The role of tar evaporation. *Symposium (International) on Combustion*, 26(1), p.1515-1521.

278. Milosavljevic, I., Oja, V. and Suuberg, E.M. (1996). Thermal Effects in Cellulose Pyrolysis: Relationship to Char Formation Processes. *Industrial & Engineering Chemistry Research,* 35(3), p.653-662.

279. Rao, T.R. and Sharma, A. (1998). Pyrolysis rates of biomass materials. *Energy*, 23(11), p.973-978.

280. Yang, P. and Kokot, S. (1996). Thermal analysis of different cellulosic fabrics. *Journal of Applied Polymer Science*, 60(8), p.1137-1146.

281. Reynolds, J.G. and Burnham, A.K. (1997). Pyrolysis Decomposition Kinetics of Cellulose-Based Materials by Constant Heating Rate Micropyrolysis. *Energy & Fuels*, 11(1), p.88-97.

282. Teng, H. and Wei, Y.-C. (1998). Thermogravimetric Studies on the Kinetics of Rice Hull Pyrolysis and the Influence of Water Treatment. *Industrial & Engineering Chemistry Research*, 37(10), p.3806-3811.

283. Várhegyi, G., Antal Jr, M.J., Jakab, E. and Szabó, P. (1997). Kinetic modelling of biomass pyrolysis. *Journal of Analytical and Applied Pyrolysis*, 42(1), p.73-87.

284. Cozzani, V., Lucchesi, A., Stoppato, G. and Maschio, G. (1997). A new method to determine the composition of biomass by thermogravimetric analysis. *The Canadian Journal of Chemical Engineering*, 75(1), p.127-133.

285. Manyà, J.J., Velo, E. and Puigjaner, L. (2002). Kinetics of Biomass Pyrolysis: a Reformulated Three-Parallel-Reactions Model. *Industrial & Engineering Chemistry Research,* 42(3), p.434-441.

286. Fisher, T., Hajaligol, M., Waymack, B. and Kellogg, Diane (2002). Pyrolysis behavior and kinetics of biomass derived materials. *Journal of Analytical and Applied Pyrolysis,* 62(2), p.331-349.

287. Orfão, J.J.M., Antunes, F.J.A. and Figueiredo, J.L. (1999) Pyrolysis kinetics of lignocellulosic materials—three independent reactions model. *Fuel*, 78(3), p.349-358.

288. Ferdous, D., Dalai, A.K., Bej, S.K. and Thring, R.W. (2002). Pyrolysis of Lignins: Experimental and Kinetics Studies. *Energy & Fuels*, 16(6), p.1405-1412.

289. Murugan, P., Mahinpey, N., Johnson, K.E. and Wilson, M. (2008). Kinetics of the Pyrolysis of Lignin Using Thermogravimetric and Differential Scanning Calorimetry Methods. *Energy & Fuels*, 22(4), p.2720-2724.

290. Pasquali, C.E.L. and Herrera, H. (1997). Pyrolysis of lignin and IR analysis of residues. *Thermochimica Acta*, 293(1-2), p.39-46.

291. Dominguez, J.C., Oliet, M., Alonso, M.V., Gilarranz, M.A. and Rodriguez, F. (2008). Thermal stability and pyrolysis kinetics of organosolv lignins obtained from Eucalyptus globulus. *Industrial Crops and Products*, 27(2), p.150-156.

292. Mani, T., Murugan, P. and Mahinpey, N. (2008). Determination of Distributed Activation Energy Model Kinetic Parameters Using Simulated Annealing Optimization Method for Nonisothermal Pyrolysis of Lignin. *Industrial & Engineering Chemistry Research*, 48(3), p.1464-1467.

293. Nunn, T.R., Howard, J.B., Longwell, J.P. and Peters, W.A. (1985). Product compositions and kinetics in the rapid pyrolysis of milled wood lignin. *Industrial & Engineering Chemistry Process Design and Development*, 24(3), p.844-852.

294. Svenson, J., Pettersson, J.B.C. and Davidsson, K.O. (2004). Fast pyrolysis of the main components of birch wood. *Combustion Science and Technology*, 176(5-6), p.977-990.

295. Chan, R.W.-C. and Krieger, B.B. (1981). Kinetics of dielectric-loss microwave degradation of polymers: Lignin. *Journal of Applied Polymer Science*, 26(5), p.1533-1553.

296. Peng, W., Wu, Q. and Tu, P. (2001). Pyrolytic characteristics of heterotrophic Chlorella protothecoides for renewable bio-fuel production. *Journal of Applied Phycology*, 13(1), p.5-12.

297. Peng, W., Wu, Q., Tu, P. and Zhao, N. (2001). Pyrolytic characteristics of microalgae as renewable energy source determined by thermogravimetric analysis. *Bioresource Technology*, 80(1), p.1-7.

298. Shuping, Z., Yulong, W., Mingde, Y., Chun, L. and Junmao, T. (2010). Pyrolysis characteristics and kinetics of the marine microalgae Dunaliella tertiolecta using thermogravimetric analyzer. *Bioresource Technology*, 101(1), p.359-365.

299. Li, D., Chen, L., Zhang, X. Ye, N. and Xing, F. (2011). Pyrolytic characteristics and kinetic studies of three kinds of red algae. *Biomass and Bioenergy*, 35(5), p.1765-1772.

300. Li, D., Chen, L., Zhao, J., Zhang, X., Wang, Q., Wang, H. and Ye, N. (2010). Evaluation of the pyrolytic and kinetic characteristics of Enteromorpha prolifera as a source of renewable bio-fuel from the Yellow Sea of China. *Chemical Engineering Research and Design*, 88(5-6), p.647-652.

301. Li, D., Chen, L., Yi, X., Zhang, X. and Ye, N. (2010). Pyrolytic characteristics and kinetics of two brown algae and sodium alginate. *Bioresource Technology*, 101(18), p.7131-7136.

302. Hui, Z., Huaxiao, Y., Mengmeng, Z. and Song, Q. (2010). Pyrolysis characteristics and kinetics of macroalgae biomass using thermogravimetric analyzer. *Proceedings of World Academy of Science, Engineering and Technology,* 65, p.1161-1166.

303. Kirtania, K. and Bhattacharya, S. (2012). Application of the distributed activation energy model to the kinetic study of pyrolysis of the fresh water algae Chlorococcum humicola. *Bioresource Technology*, 107(0), p.476-481.

304. Fushimi, C., Katayama, S. and Tsutsumi, A. (2009). Elucidation of interaction among cellulose, lignin and xylan during tar and gas evolution in steam gasification. *Journal of Analytical and Applied Pyrolysis*, 86(1), p.82-89.

305. Cozzani, V., Lucchesi, A., Stoppato, G. and Maschio, G. (1997). A new method to determine the composition of biomass by thermogravimetric analysis. *Canadian Journal of Chemical Engineering*, 75(1), p.127-133.

306. The Culture Collection of Algae, The University of Texas at Austin. *Media list [online]*. Available from: **http://www.sbs.utexas.edu/utex/media.aspx**. [Accessed 13 Jan 2012].

307. Ross, A.B., Jones, J.M., Kubacki, M.L. and Bridgeman, T. (2008). Classification of macroalgae as fuel and its thermochemical behaviour. *Bioresource Technology*, 99(14), p.6494-6504.

308. Peter, M. (2002). Energy production from biomass (part 1): overview of biomass. *Bioresource Technology*, 83(1), p.37-46.

309. Telmo, C., Lousada, J. and Moreira, N. (2010). Proximate analysis, backwards stepwise regression between gross calorific value, ultimate and chemical analysis of wood. *Bioresource Technology*, 101(11), p.3808-3815.

310. Smedes, F. and Thomasen, T.K. (1996). Evaluation of the Bligh & Dyer lipid determination method. *Marine Pollution Bulletin*, 32(8-9), p.681-688.

311. Ayhan, D. (2010). Use of algae as biofuel sources. *Energy Conversion and Management*, 51(12), p.2738-2749.

312. Babich, I.V., Van der Hulst, M., Lefferts, L., Moulijin, J.A., O'Connor, P. and Seshan, K. (2011). Catalytic pyrolysis of microalgae to high-quality liquid bio-fuels. *Biomass and Bioenergy*, 35(7), p.3199-3207.

313. Socrates, G. (1980). *Infrared characteristic group frequencies*. Chichester: Wiley.

314. Giordano, M., Kansiz, M., Heraud, P., Beardall, J., Wood, B. and McNaughton, D. (2001). Fourier transform infrared spectroscopy as a novel tool to investigate changes in intracellular macromolecular pools in the marine microalga Chaetoceros muellerii (Bacillariophyceae). *Journal of Phycology*, 37(2), p.271-279.

315. Mecozzi, M., Pietroletti, M. and Tornambè, A. (2011). Molecular and structural characteristics in toxic algae cultures of Ostreopsis ovata and Ostreopsis spp. evidenced by FTIR and FTNIR spectroscopy. *Spectrochimica Acta Part A: Molecular and Biomolecular Spectroscopy*, 78(5), p.1572-1580.

316. Delwiche, C.F., Graham, L.E. and Thomson, N. (1989). Lignin-like compounds and sporopollenin in Coleochaete, an algal model for land plant ancestry. *Science*, 245(4916),p.399-401.

317. Mark A., R. (1984). Fucus 'lignin': A reassessment. *Phytochemistry*, 23(9), p.2029-2032.

318. Martone, P.T., Estevez, J.M., Lu, F., Ruel, K., Denny, M.W., Somerville, C. and Ralph, J. (2009). Discovery of Lignin in Seaweed Reveals Convergent Evolution of Cell-Wall Architecture. *Current Biology*, 19(2), p.169-175.

319. Grierson, S., Strezov, V., Ellem, G., McGregor, R. and Herbertson, J. (2009). Thermal characterisation of microalgae under slow pyrolysis conditions. *Journal of Analytical and Applied Pyrolysis*, 85(1-2), p.118-123.

320. Qiang, L., Wen-zhi, L., Dong, Z. and Xi-feng, Z. (2009). Analytical pyrolysis–gas chromatography/mass spectrometry (Py–GC/MS) of sawdust with Al/SBA-15 catalysts. *Journal of Analytical and Applied Pyrolysis*, 84(2), p.131-138.

321. Ribechini, E., Zanaboni, M., Raspolli Galletti, A.M., Antonetti, C., Nassi o Di Nasso, N., Bonari, E. and Colombini, M.P. (2012). Py-GC/MS characterization of a wild and a selected clone of Arundo donax, and of its residues after catalytic hydrothermal conversion to high added-value products. *Journal of Analytical and Applied Pyrolysis*, 94, p.223-229.

322. Hossain, M.K., Strezov, V., Chan, K.Y., Ziolkowski, A. and Nelson, P.F. (2011). Influence of pyrolysis temperature on production and nutrient properties of wastewater sludge biochar. *Journal of Environmental Management*, 92(1), p.223-228.

323. Kim, S. and Kim, Y.-C. (2005). Using isothermal kinetic results to estimate the kinetic triplet of the pyrolysis of high density polyethylene. *Journal of Analytical and Applied Pyrolysis*, 73(1), p.117-121.

324. Ceamanos, J., Mastral, J.F., Millera, A. and Aldea, M.E. (2002). Kinetics of pyrolysis of high density polyethylene. Comparison of isothermal and dynamic experiments. *Journal of Analytical and Applied Pyrolysis*, 65(2), p.93-110.

325. Westerhout, R.W.J., Waanders, J., Kuipers, J.A.M and Van Swaaij, W.P.M. (1997). Kinetics of the Low-Temperature Pyrolysis of Polyethene, Polypropene, and Polystyrene Modeling, Experimental Determination, and Comparison with Literature Models and Data. *Industrial & Engineering Chemistry Research*, 36(6), p.1955-1964.

326. Sinfrônio, F.S.M., Santos, J.C.O., Pereira, L.G., Souza, A.G., Concei, M.M., Fernandes, Jr., V.J. and Fonseca, V.M. (2005). Kinetic of thermal degradation of low-density and high-density polyethylene by non-isothermal thermogravimetry. *Journal of Thermal Analysis and Calorimetry*, 79(2), p.393-399.

327. Conesa, J.A., Caballero, J., Marcilla, A. and Font, R. (1995). Analysis of different kinetic models in the dynamic pyrolysis of cellulose. *Thermochimica Acta*, 254, p.175-192.

328. Dollimore, D. and Holt, B. (1973). Thermal degradation of cellulose in nitrogen. *Journal of Polymer Science: Polymer Physics Edition*, 11(9), p.1703-1711.

329. Zhao, H., Yan, H., Dong, S., Zhang, Y., Sun, B. Zhang, C., Ai, Y., Chen, B., Liu, Q., Sui, T. and Qin, S. (2011). Thermogravimetry study of the pyrolytic characteristics and kinetics of macro-algae Macrocystis pyrifera residue. *Journal of Thermal Analysis and Calorimetry*, p.1-6.

330. Wilburn, F.W. (1999). The determination of kinetic parameters from DTG curves — fact or fiction? *Thermochimica Acta*, 340-341, p.77-87.

331. Statheropoulos, M., Kyriakou, S. and Tzamtzis, N. (1998). Performance evaluation of a TG/MS system. *Thermochimica Acta*, 322(2), p.167-173.

332. Garcia, R., Arenillas, A., Crespo, J.L., Pis, J.J. and Moinelo, S.R. (2002). A Comparative Tg-Ms Study of the Carbonization Behavior of Different Pitches. *Energy & Fuels*, 16(4), p.935-943.

333. Statheropoulos, M. and Kyriakou, S.A. (2000). Quantitative thermogravimetric-mass spectrometric analysis for monitoring the effects of fire retardants on cellulose pyrolysis. *Analytica Chimica Acta*, 409(1-2), p.203-214.

334. Hatton, P. and Southward, B. (2003). Optimisation of the connection between TA-MS systems together with improved data interpretation for TA-MS applications. *Journal of Thermal Analysis and Calorimetry*, 72(1), p.83-92.

335. Andrew R, M. (1994). Simultaneous thermogravimetry—differential thermal analysis—mass spectrometry (TG—DTA—MS) using a heated capillary interface. *Thermochimica Acta*, 234, p.21-29.

336. Hoffmann, S., Schmidt, M., Scharsach, S. and Kniep, R. (2012). TG–MS of air-sensitive compounds in argon. *Thermochimica Acta*, 527, p.204-210.

337. Varhegyi, G., Antal, M.J., Szekely, T., Till, F. and Jakab, E. (1988). Simultaneous thermogravimetric-mass spectrometric studies of the thermal decomposition of biopolymers. 1. Avicel cellulose in the presence and absence of catalysts. *Energy & Fuels*, 2(3), p.267-272.

338. Selck, D.A., Woodfield, B.F., Boerio-Goates, J. and Austin, D.E. (2012). Simple, inexpensive mass spectrometric analyzer for thermogravimetry. Rapid Communications in Mass Spectrometry, 26(1), p.78-82.

339. Ale Ebrahim, H. and Jamshidi, E. (2004). Synthesis gas production by zinc oxide reaction with methane: elimination of greenhouse gas emission from a metallurgical plant. *Energy Conversion and Management*, 45(3), p.345-363.

340. Baugh, P.J. (1993). *Gas Chromatography: A Practical Approach*. Oxford: Oxford University Press.

341. Roduit, B., Baldyga, J., Maciejewski, M. and Baiker, A. (1997). Influence of mass transfer on interaction between thermoanalytical and mass spectrometric curves measured in combined thermoanalyser-mass spectrometer systems. *Thermochimica Acta*, 295(1-2), p.59-71.

342. Young, D.M. and Crowell, A.D. (1962). *Physical adsorption of gases*. London: Butterworths.

343. Oscik, J. (1982). *Adsorption*. England: Ellis Horwood Limited.

344. Soares, R.M.D., Scremin, F.F. and Soldi, V. (2005). Thermal Stability of Biodegradable Films Based on Soy Protein and Corn Starch. *Macromolecular Symposia*, 229(1), p.258-265.

345. Swain, S.N., Rao, K.K. and Nayak, P.L. (2004). Biodegradable polymers. III. Spectral, thermal, mechanical, and morphological properties of cross-linked furfural–soy protein concentrate. *Journal of Applied Polymer Science*, 93(6), p.2590-2596.

346. Cieśla, K. and Vansant, E. (2010). Physico-chemical changes taking place in gamma irradiated bovine globulins studied by thermal analysis. *Journal of Thermal Analysis and Calorimetry*, 99(1), p.315-324.

347. Guinesi, L.S., da Róz, A.L., Corradini, E., Mattoso, L.H.C., Teixeira, E.M. and Curvelo, A.A.S. (2006). Kinetics of thermal degradation applied to starches from different botanical origins by non-isothermal procedures. *Thermochimica Acta*, 447(2), p.190-196.

348. Liu, X., Yu, L., Xie, F., Li, M., Chen, L. and Li, X. (2010). Kinetics and mechanism of thermal decomposition of cornstarches with different amylose/amylopectin ratios. *Starch - Stärke*, 62(3-4), p.139-146.

349. Liu, X., Yu, L., Liu, H., Chen, L. and Li, L. (2008). In situ thermal decomposition of starch with constant moisture in a sealed system. *Polymer Degradation and Stability*, 93(1), p.260-262.

350. Vyazovkin, S. (2000). Computational aspects of kinetic analysis.: Part C. The ICTAC Kinetics Project — the light at the end of the tunnel? *Thermochimica Acta*, 355(1-2), p.155-163.

351. Maciejewski, M. (2000). Computational aspects of kinetic analysis.: Part B: The ICTAC Kinetics Project — the decomposition kinetics of calcium carbonate revisited, or some tips on survival in the kinetic minefield. *Thermochimica Acta*, 355(1-2), p.145-154.

352. Kaisersberger, E. and Post, E. (1997). Practical aspects for the coupling of gas analytical methods with thermal-analysis instruments. *Thermochimica Acta*, 295(1-2), p.73-93.

353. Maciejewski, M. and Baiker, A. (1997). Quantitative calibration of mass spectrometric signals measured in coupled TA-MS system. *Thermochimica Acta*, 295(1-2), p.95-105.

354. Kamruddin, M, Ajikumar, P.K., Dash, S., Tyagi, A.K. and Raj, B. (2003). Thermogravimetry-evolved gas analysis-mass spectrometry system for materials research. *Bulletin of Materials Science*, 26(4), p.449-460.

Appendix A: Evaluation of TG-MS system

The in-house built TG-MS is a coupling of a thermogravimetric analyser (TG/DSC 1 Mettler Toledo) with a Quadrapole Mass Spectrometry (ThermoStarTM Pfeiffer vacuum with QMS200). The performance of TG and MS was evaluated by calcium oxalate monohydrate ($CaC_2O_4 \cdot H_2O$) which present a well-known stoichiometric thermal decomposition reaction.

$$CaC_2O_4 \cdot H_2O \rightarrow CaC_2O_4 + H_2O$$

$$CaC_2O_4 \rightarrow CaCO_3 + CO$$

$$CaCO_3 \rightarrow CaO + CO_2$$

Calcium oxalate monohydrate 10 mg was heated in TG under helium atmosphere. Temperature ramp started from ambient temperature to 850°C with heating rate 20°C/min. Produced gases were transferred to a deactivated capillary which was kept at 300°C to mass spectrometric detector. Simultaneous measurement between weight loss in TG and the gas evolution from MS was controlled by two synchronized software which start and stop measuring at the same time.

A1. TG-MS design

The TG furnace has a horizontal configuration with a horizontal purge gas flow. A quartz capillary minimizes the memory effect [331]. When evolved gases are purged out of the TG chamber, their temperature decreases rapidly, this can cause the condensation. Thus the transfer line is kept at 300°C. This TG-MS system has a simple construction and low cost; however, the capillary is suggested to be replaced 2-3 times per year depending on how often of use due to the unavoidable condensation at a cold spot. This cold spot cannot eliminate because of the fixed feature of the commercial TG.

The pressure of the MS inlet is kept in a high vacuum ($1\text{-}5\times10^{-5}$ mbar) to minimize the interference between the residual gas in the system and the analysed gases [352]. Total pressure is controlled by the length and inner diameter of inlet capillary, the temperature of transfer line and the purge gas flow. These factors will be constant throughout the measurements to maintain a stable total pressure.

A2. Influence of carrier gas flow rate

The evolved gases produced in TG chamber are mixed with the carrier gas and transferred to MS detector. Thus the ratio between analysed and carrier gas depends on the flow rate of carrier gas. The fluctuation of the flow rate will change the intensity of the MS signal. Two concerns for the setting of flow rate are the dilution of the analysed gases and back diffusion phenomena [353]. The analysed gases should be diluted as small as possible to increase the MS sensitivity but too low flow rate can lead to long transfer time and the back diffusion which causes the shifting towards higher temperatures and the broadened peaks. At low flow rate, the laminar flow of the purge gas can be disturbed by a convection flow; while less heat exchange occurred in high flow rate leads to a temperature gradient and low sensitivity in MS signal [352, 354]. Therefore the stability of carrier gas flow and the flow rate are important for the MS signal.

Figure A1 shows the evolved gas intensities of H_2O, CO and CO_2 at different helium flow rate (50, 100 and 150 ml/min). The intensity of three gases is reduced as the helium flow rate increase. At 50 ml/min rate, there is a small shift toward longer time due to an increased holding time and the peak area of evolved gases at low flow rate. Flow rate at 100 ml/min does not show a shift or broaden peak and give high intensity than 150 ml/min.

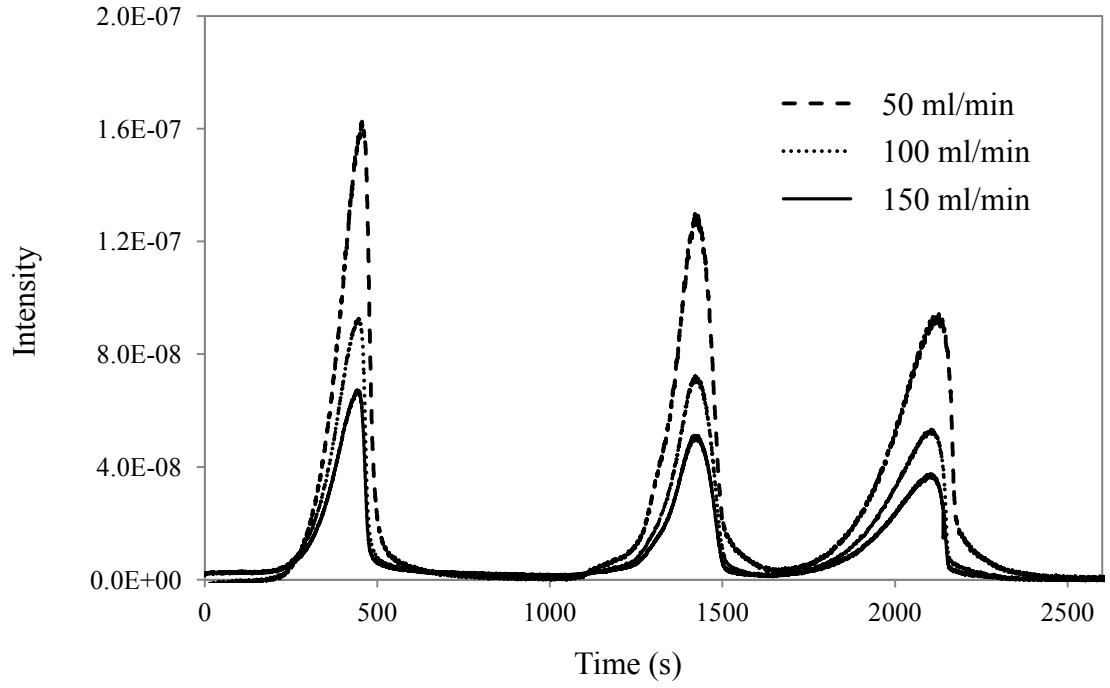

Fig. A1 Intensity change of the mass spectrometric signals resulting from decomposition of calcium oxalate monohydrate at helium flow rate 50, 100 and 150 ml/min.

A3. Transfer time delay

Transfer time is a total time of which evolved gases take to transfer from TG sample crucible to MS detector. Both high dead volumes of the TG chamber and a long distance in capillary lead to the greater transfer time. Moreover, the influence from the physical interaction or condensation at cold spot also cause a longer holding time in the system.

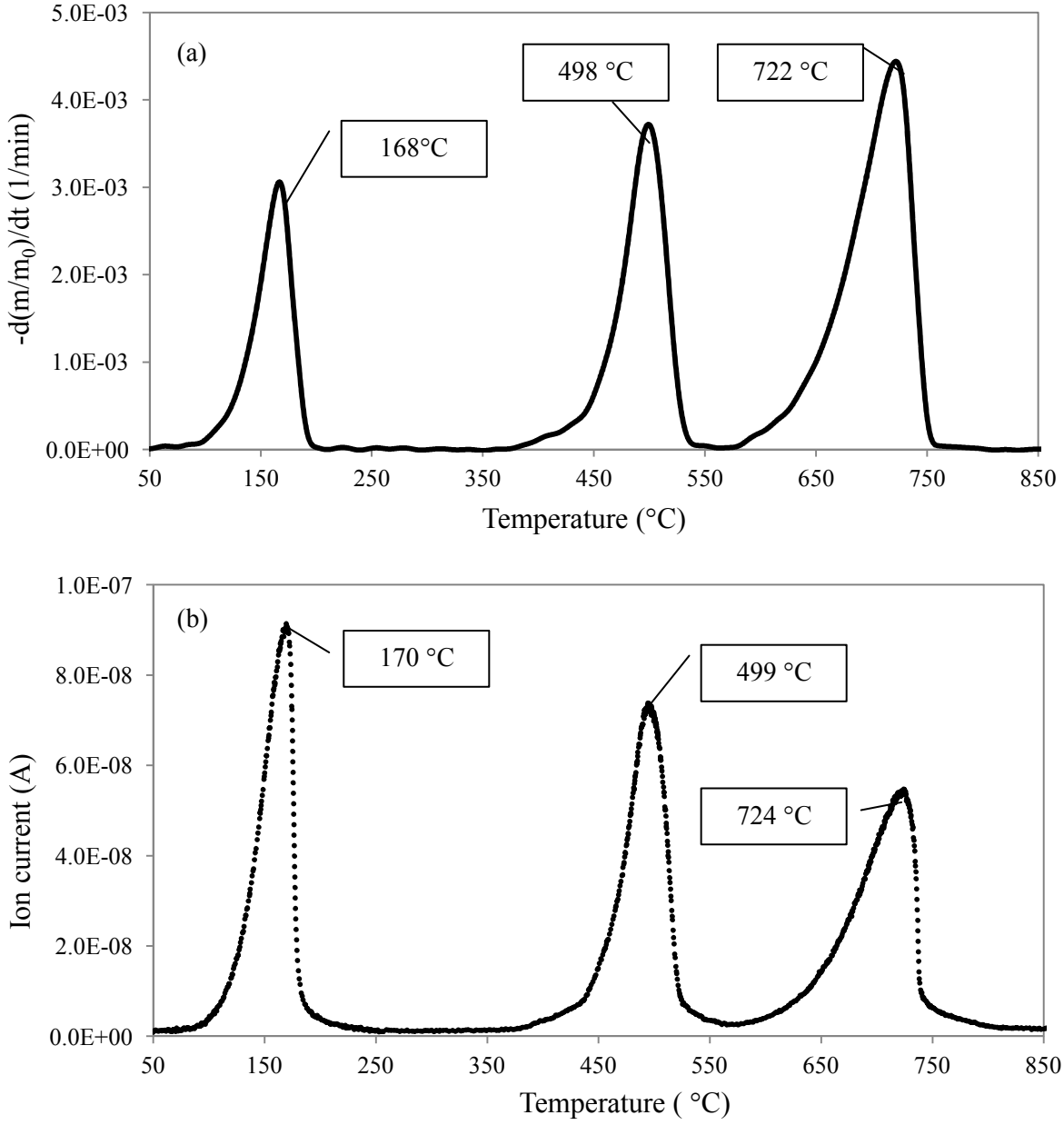

Fig. A2 The peak temperatures of H_2O, CO and CO_2 production from (a) DTG and from (b) the evolved gas profile

From figure A2, the difference peak temperature for H_2O, CO and CO_2 are 2, 1 and 2°C, respectively which can be converted to the transfer time at 6, 3 and 6 s by the heating rate value. Thus the average transfer time is 5 seconds. The hydrocarbons can take longer time in the capillary due to their higher interaction between gas and solid phase by adsorption process.

Appendix B: Selected evolution profile of isothermal measurements of polyethylene

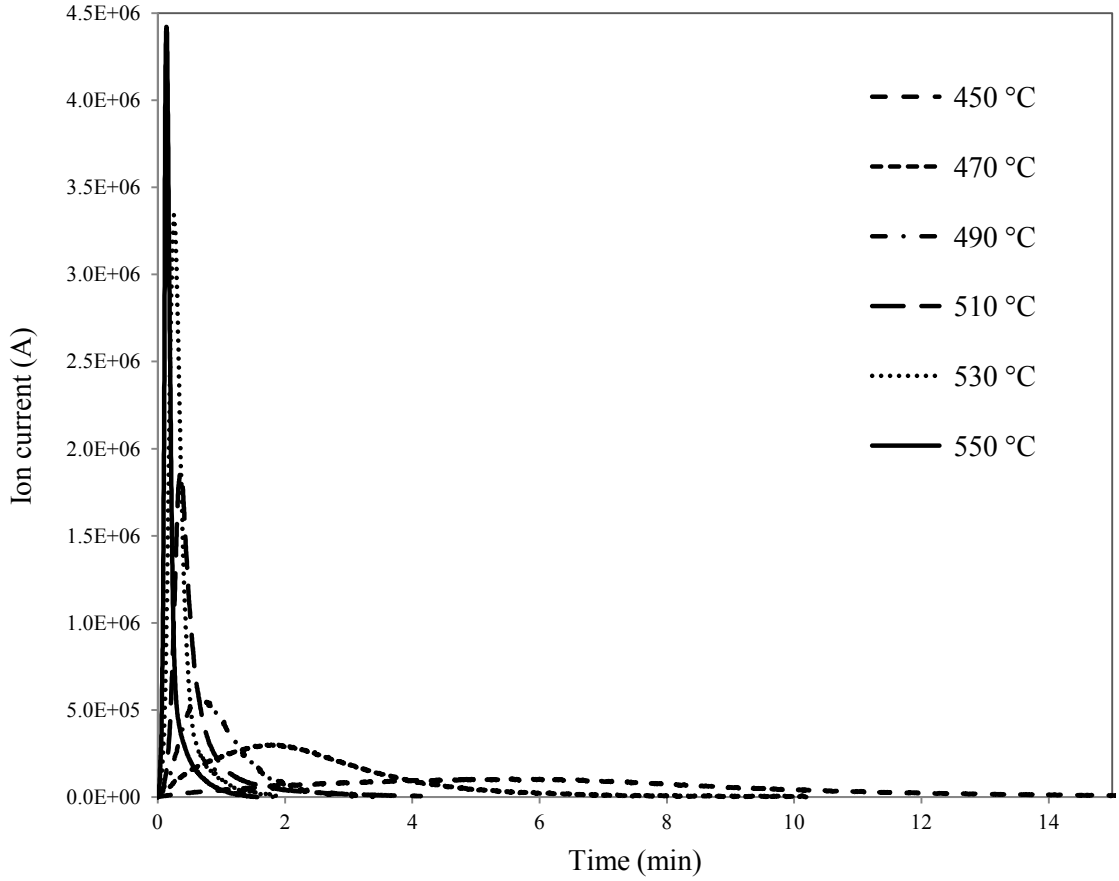

Fig. B1 Evolution profiles in relationship with time (min) of polyethylene pyrolysis under isothermal condition at selected temperatures

Appendix C: The optimal parameters for Gaussian distribution curves of each evolved gas profile at 95% confidence interval

Table C1. The Gaussian parameters of the evolved gas profiles of pyrolysis at 5°C/min

Groups	Pool	T_{max} (°C)	*s*	*H*	R^2	RMSE
I	1	218	23	1.1740e-7	0.9987	7.18e-9
	2	275	47	6.0630e-7		
	3	400	98	1.910e-7		
II	1	226	27	2.438e-8	0.9961	2.95e-9
	2	295	46	1.218e-7		
	3	363	80	5.005e-8		
III	1	281	51	9.955e-8	0.9971	2.11e-9
	2	355	80	3.883e-8		
	3	442	41	5.954e-8		
IV	1	267	60	1.474e-8	0.9849	5.81e-10
	2	390	85	2.961e-9		
V	1	192	20	3.143e-8	0.9947	4.38e-9
	2	258	62	9.745e-8		
	3	378	65	1.066e-7		
	4	432	35	1.3030e-7		
VI	1	300	41	5.8040e-7	0.9995	4.58e-9
	2	355	65	1.196e-7		
	3	420	40	2.3240e-8		

Table C2. The Gaussian parameters of the evolved gas profiles of pyrolysis at 10°C/min

Groups	Pool	T_{max} (°C)	*s*	*H*	R^2	RMSE
I	1	219	25	3.1730e-7	0.9975	2.93e-8
	2	284	49	1.6690e-6		
	3	408	100	5.9730e-7		
II	1	235	25	3.4960e-8	0.9991	4.7070e-9
	2	309	45	3.7270e-7		
	3	375	80	1.4810e-7		
III	1	298	50	2.2670e-7	0.9983	3.4100e-9
	2	390	90	5.8530e-8		
	3	482	48	1.1150e-7		

IV	1	279	57	1.4680e-8	0.9701	8.6460e-10
	2	384	90	3.0290e-9		
V	1	207	25	8.3950e-8	0.9982	7.3990e-9
	2	271	57	1.9720e-7		
	3	380	70	1.9290e-7		
	4	436	50	3.8000e-7		
VI	1	313	45	1.5160e-6	0.9960	4.3260e-8
	2	345	70	5.3730e-7		
	3	440	40	1.1180e-7		

Table C3. The Gaussian parameters of the evolved gas profiles of pyrolysis at 20 °C/min

Groups	**Pool**	T_{max} **(°C)**	***s***	***H***	$\mathbf{R^2}$	**RMSE**
I	1	220	23	5.78e-7	0.9978	5.396e-8
	2	285	50	2.77e-6		
	3	400	100	4.252e-7		
II	1	240	25	1.277e-7	0.9976	1.59e-8
	2	322	51	6.323e-7		
	3	390	90	2.667e-7		
III	1	309	53	4.500e-7	0.9963	1.23e-8
	2	390	85	1.557e-7		
	3	502	50	2.287e-7		
IV	1	263	57	8.026e-8	0.9970	1.678e-9
	2	368	85	9.958e-9		
V	1	205	27	1.517e-7	0.9973	1.790e-8
	2	275	55	4.619e-7		
	3	380	75	3.375e-7		
	4	445	45	5.394e-7		
VI	1	309	42	3.799e-6	0.9979	9.485e-8
	2	365	70	2.269e-6		
	3	462	43	9.016e-7		

Appendix D:Computational scripts for kinetic evaluation

D1. Main computational script for isothermal kinetic evaluation for application in C++ programme (provided by Professor Andreas Hornung)

```
/*    Beginnend mit Nullzeitpunkt
      bis das Ende der Datei erreicht ist ... */

      time = ZeroScan.T;
      mass = 0.0;
      n = ScanCnt - ZeroScan.Nr;

      for (i = 0; i < n; i++)
      {
            if (Scan( &s) == 0)
            {

/* Bestimme mittlere Masse; Integriere auf mit Trapezregel*/

                  data[i].T = s.T;
                  data[i].M = 0.0;

                  for (j = 0; j<MassCnt; j++)
                        data[i].M += ( (s.MIC[j] - ZeroScan.MIC[j])
* HeadScan.MIC[j] );

                  IntVal += (s.T - time) * (data[i].M + mass) / 2.0;
                  data[i].I = IntVal;

/*                printf( "%4d\t%6.3f\t%12.7g\t%12.7g\n", s.Nr, s.T,
data[i].M, IntVal);*/
                  time = s.T;
                  mass = data[i].M;
            }
            else
            {
                  printf( "\n*** Fehler beim Einlesen von Scan #
%d", i+1+ZeroScan.Nr);
                  return 1;
            };
      };

/*************************************
********** Raten bestimmen *************
*************************************/

/* Ausgabedatei öffnen, Alpharaten für alle Scans bestimmen,
Ergebnisse ausgeben */

      printf( "\nDatenausgabe läuft ...");

      if ((Out = fopen( FileName, "wt")) == NULL)
```

```
      {
            printf("\n*** Fehler beim Öffnen der Ausgabedatei:
ScanCalc()");
            return 1;
      };

      fprintf( Out, "Nr\tTime\tMasse\tAlpha");

      for (i = 0; i < n; i++)
      {
            alpha = (data[i].I*DV + data[i].M*VR) / IntVal / DV;
            fprintf( Out, "%c%d\t%f\t%g\t%g", 13, i+ZeroScan.Nr+1,
data[i].T,
                              data[i].M, alpha);
      };

      fclose( Out);

      return 0;
}
```

D2. Main computational script for non-isothermalkinetic evaluation for application in MATLAB programme (developed in this work)

```
function
[errorTotal,bestval,bestEind,bestKind,bestNind,bestEval,bestKval] =
compute
%% main simulation function
%  called by function run
%  returns : errorTotal: total average error for a given set of
parameters
%            bestval   : best (minimal) value of error in current
simulations
%            bestEind  : index in Egrid for which best error is achieved
%            bestKind  : index in Kgrid for which best error is achieved
%            bestNind  : index in Ngrid for which best error I s achieved
%            bestEval  : best Ea value
%            bestKval  : best k0 value

app = getUD;

% set minimum and maximum values of n and number of points in the Ngrid
n1 = app.MinN;
n2 = app.MaxN;
NumN = app.NumN;
n = linspace(n1,n2,NumN); % Ngrid

% axes 'ax1' : (Ea,k0) plot
ax1 = findobj('Tag','ax1');
axes(ax1); hold on;
hCurrentPoint = plot(app.Egridrun(1),app.Kgridrun(1),'rd'); % displays
current simulation on a (Ea,k0) plot as a red diamond
```

```
% axes 'ax2' : initialisation in (temperature,intensity) plot of hIntn -
simulated curve, hBest - best simulated curve
ax2 = findobj('Tag','ax2');
axes(ax2); hold on; grid on;
hIntn = plot(0,0,'r.'); hold on;
hBest = plot(0,0,'w-');

% axes 'ax3' : initialisation in Error plot of hError - deviation between
experimental and simulated curves
ax3 = findobj('Tag','ax3');
axes(ax3); hold on;grid on;
hError = semilogy(0,1,'w.');
set(ax3,'Color',[0.6 0.6 0.6]);

% find a handle of 'Log' listbox
lbxInfo = findobj('Tag','lbxInfo');

% set gas constant
R = app.R;

% initialise iteration variable
iter = 1;

% initialise matrix of errors (3 dimensional (Ea,k0,n))
errorTotal = ones(length(app.Egridrun),length(app.Kgridrun),NumN);

% func = inline('exp(-E./(R*p))','p','E','R'); - old version Matlab 5.3

% loop for Ea
for iEa = 1:length(app.Egridrun)
% create a function for integration
func = @(t) exp(-app.Egridrun(iEa)./(R*t)); % t - is a temperature

% loop for k0
for ik0 = 1:length(app.Kgridrun)
% loop for n
for iN = 1:length(n)

% initilase error vector for one set of (Ea,k0,n)
error = zeros(1,3);

for i=3:-1:1 % do it for all sets of experimental data

% integrate intensity
                y = zeros(size(app.data(i).intn));
y(1) = 0;
for jj=2:length(app.data(i).intn)
%                     intg =
%
quadl(func,app.data(i).temp(1),app.data(i).temp(jj),[],[],app.Egridrun(iE
a),R);
%                     % need to change to f = @(t) - old vesion Matlab
5.3
intg = quadl(func,app.data(i).temp(1),app.data(i).temp(jj));
if (n(iN)==1)
% if n==1
y(jj) = 1 - exp(-(app.Kgridrun(ik0)/app.data(i).beta)*intg);
else
% if n<>1
```

```
                        y(jj) = 1 - (1+(n(iN)-
1)*(app.Kgridrun(ik0)/app.data(i).beta)*intg)^(1/(1-n(iN)));
end
end

% compute error for each experimental set
error(i) = sqrt(sum((y-app.data(i).intn).^2)/(length(y)-1));

end
% averaging error for one set of (Ea,k0,n)
errorTotal(iEa,ik0,iN) = mean(error);

% searching for optimal point
if (iter==1) % initialisation of return parameters
bestval = errorTotal(iEa,ik0,iN);
                bestEind = 1;
                bestKind = 1;
                bestNind = 1;
                bestEval = app.Egridrun(bestEind);
bestKval = app.Kgridrun(bestKind);
bestcurve = y;
                app.bestcurve = y;
setUD(app);
else
if errorTotal(iEa,ik0,iN)<bestval
bestval = errorTotal(iEa,ik0,iN);
                    bestEind = iEa;
                    bestKind = ik0;
                    bestNind = iN;
                    bestEval = app.Egridrun(bestEind);
bestKval = app.Kgridrun(bestKind);
bestcurve = y;
                    app.bestcurve = y;
setUD(app);
end
end

% plot current point on (Ea,k0) plot
axes(ax1); hold on;
delete(hCurrentPoint);
hCurrentPoint = plot(app.Egridrun(iEa),app.Kgridrun(ik0),'rd');
set(hCurrentPoint,'Tag','CurrentPoint');

% plot simulated curve (red) and best simulated curve (white) on
(temperature,intensity) plot
axes(ax2); hold on; grid on;
delete(hIntn);
hIntn = plot(app.data(1).temp,y,'r-'); hold on; %
set(hIntn,'Tag','intn');
delete(hBest);
hBest = plot(app.data(1).temp,bestcurve,'w-');
set(hBest,'Tag','bestCurve');

% plot error on the Error plot
axes(ax3); %hold on;
hError = semilogy(iter,mean(error),'w.'); hold on;
set(hError,'Tag','error');

% to let matlab update figure
pause(0.00001);
```

```
% update iterator
iter = iter+1;

% add results of simulation to 'Log' text box
str  = ['Error=',num2str(errorTotal(iEa,ik0,iN))];
            strbest = ['best:
Ea(',num2str(bestEind),')=',num2str(app.Egridrun(bestEind)),'
k0(',num2str(bestKind),') = ',num2str(app.Kgridrun(bestKind)),'
n(',num2str(bestNind),') = ',num2str(n(bestNind)),'
Error=',num2str(errorTotal(bestEind,bestKind,bestNind))];
val = get(lbxInfo,'Value');
info = get(lbxInfo,'String');
info = strvcat(info,[str,strbest]);
set(lbxInfo,'String',info);
set(lbxInfo,'Value',val+1);
end% end of loop for n

app=getUD;

% checks to stop simulation
if (app.stoprun)
            app.stoprun = 0;
setUD(app);
return;
end

% cheks to skip simulation(s)
if (app.skiprun)
            app.skiprun = 0;
setUD(app);
break;
end
end% end of loop for k0
end% end of loop for Ea

setUD(app);
```